ENGINEERING EVALUATION OF THERMAL SHIELD REPAIR

Prepared for

SOUTHERN CALIFORNIA EDISON COMPANY
San Clemente, California

July 1990

Prepared by

Jan S. Porowski
Manu L. Badlani
Evan L. Westermann
Joseph J. Vasalani

SMC O'DONNELL INC.
ENGINEERING DESIGN & ANALYSIS SERVICES

241 CURRY HOLLOW ROAD
PITTSBURGH, PENNSYLVANIA 15236
(412) 655-1200
FAX: (412) 655-2928

ENGINEERING EVALUATION OF THERMAL SHIELD REPAIR

TABLE OF CONTENTS

		Pages
1.0	INTRODUCTION	1
2.0	DESCRIPTION OF EXISTING SUPPORT SYSTEM	3
3.0	MODIFIED SUPPORT SYSTEM	13
4.0	HISTORY OF THERMAL SHIELD PERFORMANCE	28
5.0	METHOD OF ANALYSIS	29
6.0	FINITE ELEMENT MODELS	34
7.0	TURBULENT FORCING FUNCTION	57
8.0	MODAL ANALYSIS	61
9.0	RANDOM VIBRATION ANALYSIS	71
10.0	THERMAL TRANSIENTS	74
11.0	SEISMIC ANALYSIS	78
12.0	FATIGUE ANALYSIS	84
13.0	STRESS CONCENTRATION FACTORS FOR FATIGUE ANALYSIS	91
14.0	MODEL QUALIFICATION	92
15.0	RESULTS	95
16.0	SUMMARY OF RESULTS	132
17.0	CONCLUSIONS	134
18.0	REFERENCES	135
	APPENDIX A & B	

ENGINEERING EVALUATION OF THERMAL SHIELD REPAIR

1.0 INTRODUCTION

Flow-induced vibration due to coolant flow through the annular passages between the reactor vessel and internal components such as core barrel or thermal shield in a PWR is a complex phenomenon and can cause excessive vibratory motion and fatigue failure. There have been several instances of thermal shield failures due to flow-induced vibration, References [1, 2, 3]. Excitation from turbulent fluid loading has been the cause of the flow induced vibration and inadequate thermal shield support has usually been blamed for these failures [4]. In case of SONGS Unit 1, the flow-induced vibration has resulted in failure of the thermal shield supporting structure [3]. The excessive vibration of the thermal shield was sufficient to cause broken bolts in the bottom supports, to back dowel pins out of position, to produce excessive wear at motion limiter keys and to result in failure of the upper support flexures.

SMC O'Donnell performed an independent analysis and evaluation of the thermal shield supporting structure failure and proposed repair. The purpose of this analysis was to assure that the redesigned support system, once implemented, will maintain its integrity for at least one cycle and its functionality for presumably the remaining expected life of the reactor.

The support system was redesigned by Westinghouse. The modified supports are to be installed during the 1990 outage by Kraftwerk Union.

The scope of work includes the following:

1) Evaluation of flow-induced dynamics of thermal shield and core barrel for existing and modified designs.

2) Participation in development and evaluation of alternate thermal shield support modifications

3) Design review and quantitative evaluation of thermal shield support modifications established by Westinghouse for implementation by Bechtel-KWU Alliance.

In order to understand the failure mechanism and quantify the failure modes, the initial investigation included a detailed review and evaluation of the existing data and inspection results for the San Onofre thermal shield, as well as those obtained from the literature and discussions on other plants. The results of this investigation showed that the thermal shield support failure was caused by turbulence induced random vibration.

This report contains a description of the random flow-induced vibration analysis of the thermal shield supporting structure performed to determine the loads and stresses in the lower support block bolts and dowels as well as the upper flexures. Fatigue and failure analysis of the fasteners, bottom blocks and flexures are also presented herein. Both the existing support design and proposed repair design were analyzed and compared to evaluate the increased safety margins. These calculations also include a scoping evaluation of thermal and seismic load effects on fatigue life of the support system.

2.0 DESCRIPTION OF EXISTING SUPPORT SYSTEM

The basic design of the thermal shield support system in the SONGS I Plant is diagrammatically explained in Figures 2-1 and 2-2 [3]. The assembly of the core barrel with thermal shield in the reactor pressure vessel is shown in Figures 2-3 and 2-4. Figure 2-4a defines the orientation of inlet and outlet nozzles. There are six block assemblies which support the bottom end of the shield and restrain the shield vertical and radial motion relative to the core barrel. These lower supports are fitted into a circumferential groove in the core barrel and are attached by a series of bolts and dowel pins. These supports are azimuthally located 60 degrees apart (0, 60, 120, 180, 240 and 300°). The block at location 0° has an additional key ensuring proper orientation of the thermal shield on the core barrel. Figures 2-5a and 2-5b show the details of the support block assemblies. A center bolt which clamps the top of the support block to the core barrel during initial assembly is 3/4" in diameter. Two long bolts, which are 7/8" diameter, clamp the thermal shield to the top of the block and the core barrel. At the bottom of the block, there are two 1/2" bolts which clamp the bottom of the block to the core barrel and two 3/4" dowel pins to limit the vertical motion between the block and the core barrel. In between the upper and lower fastener elevations, there are two 3/4" dowel pins which limit the relative vertical motion between the thermal shield and the core barrel. The bolts at SONGS are protected against rotation by a lockbar which fits into a groove in the bolt head and is welded to the thermal shield.

There are also four upper displacement limiters shown in Figure 2-6 which are located roughly 9.5 inches below the top of the shield. These displacement limiters are located 90 degrees apart (0, 90, 180, and 270°). Initially, these keys limited the lateral or tangential motion between the two components but had a large radial gap. The design was modified following evidence of large relative radial displacements during the initial hot functional test program in 1966. The improved design (at the beginning of plant operation) limited the relative radial motion between the barrel and thermal shield at the key locations to approximately 15 mils (0.015 inch) at normal operating conditions.

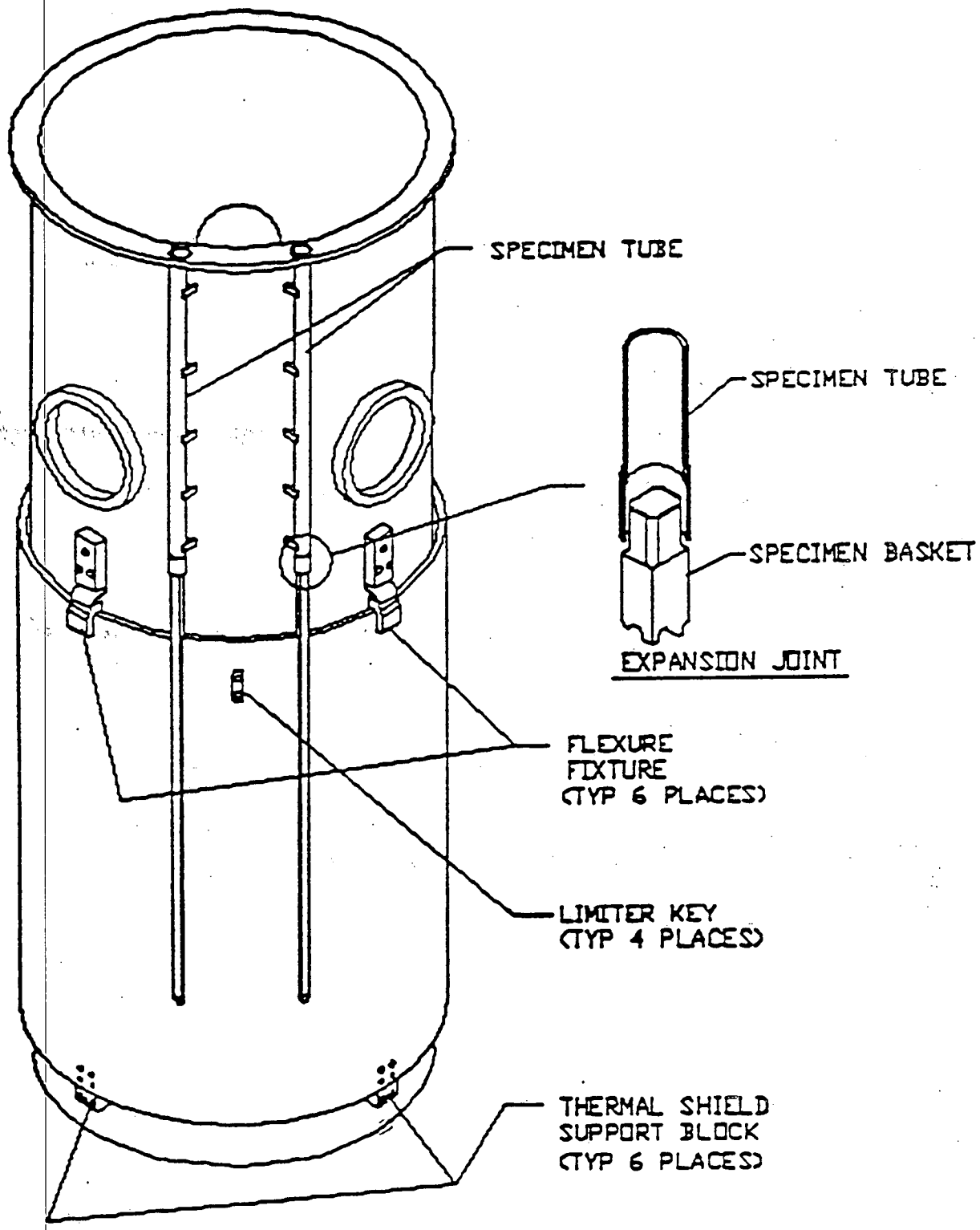

FIGURE 2-1 SCE THERMAL SHIELD SUPPORT

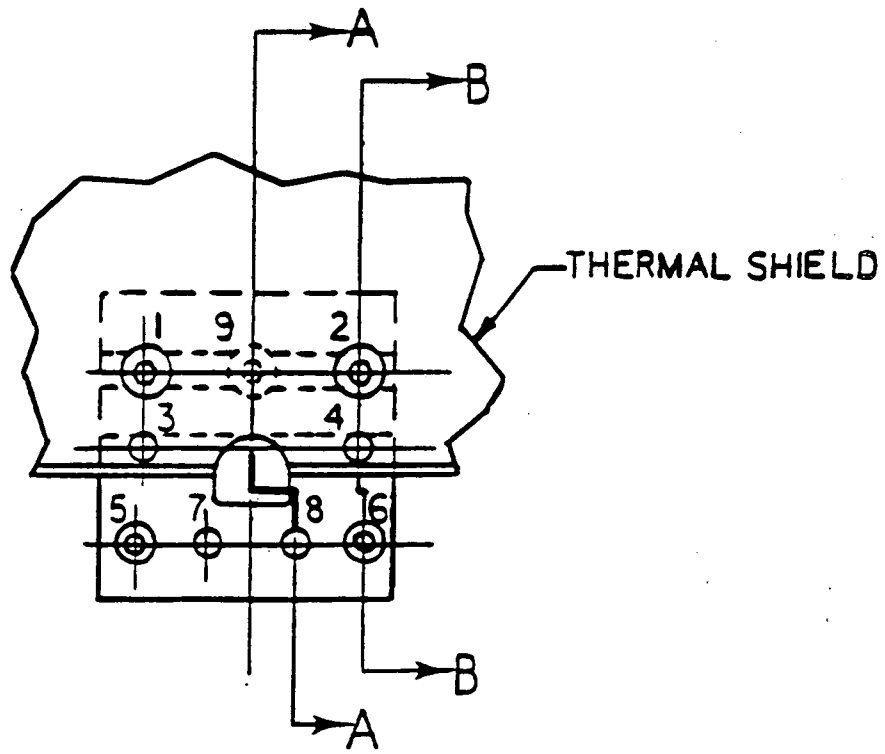

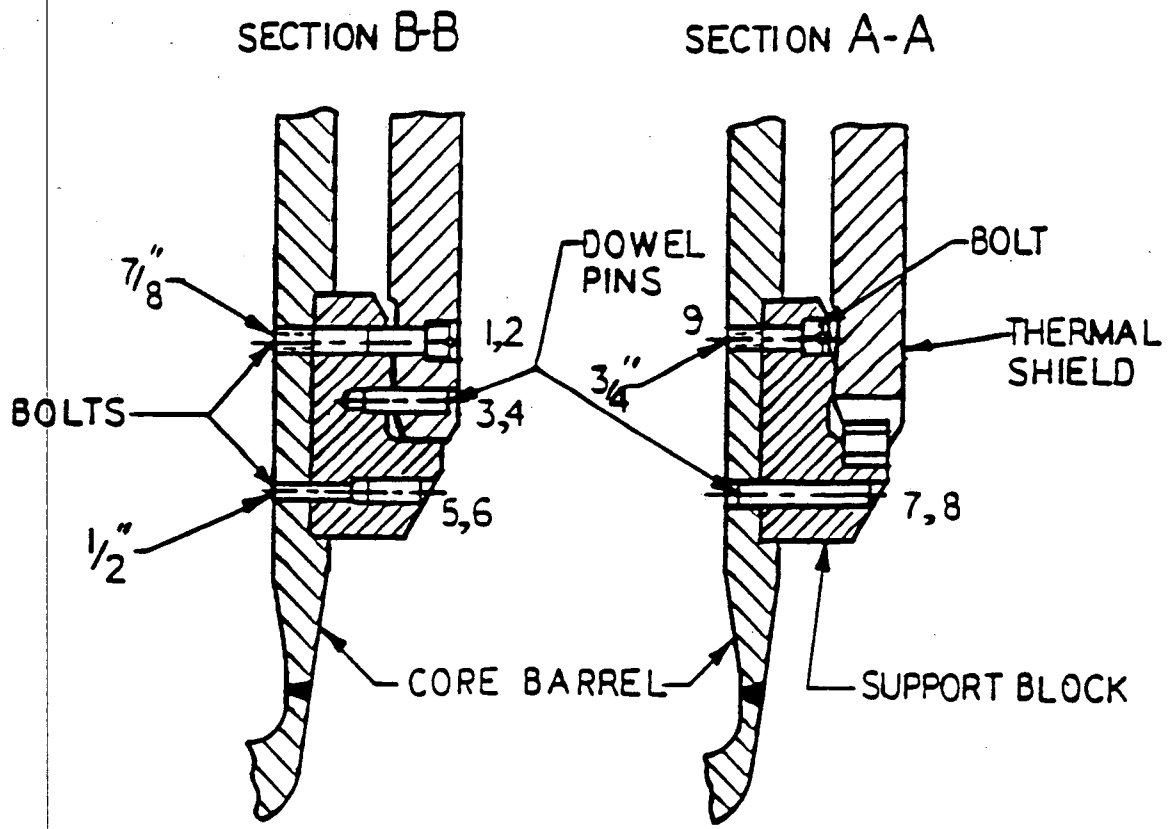

FIGURE 2-2 THERMAL SHIELD SUPPORT BLOCK DESIGN

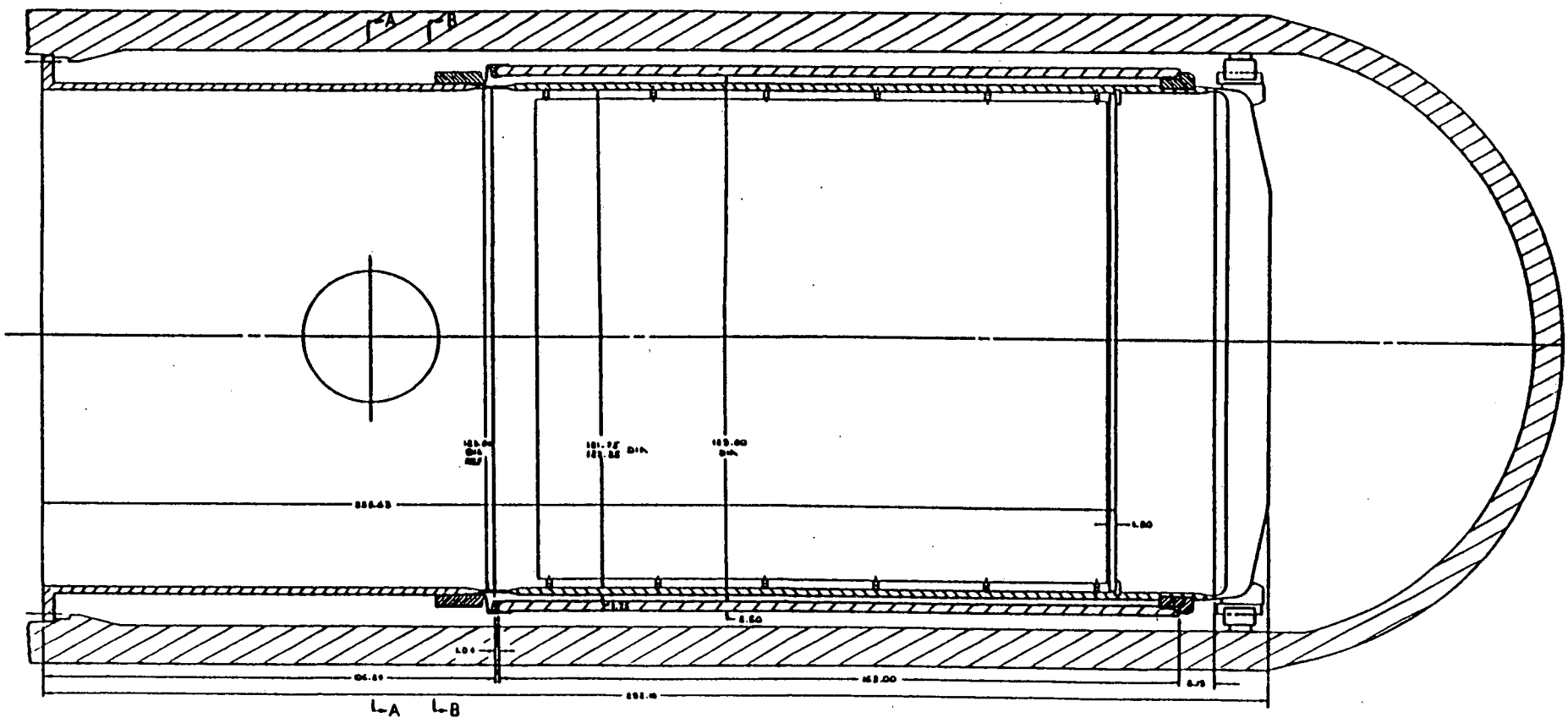

FIGURE 2-3 THERMAL SHIELD ASSEMBLY

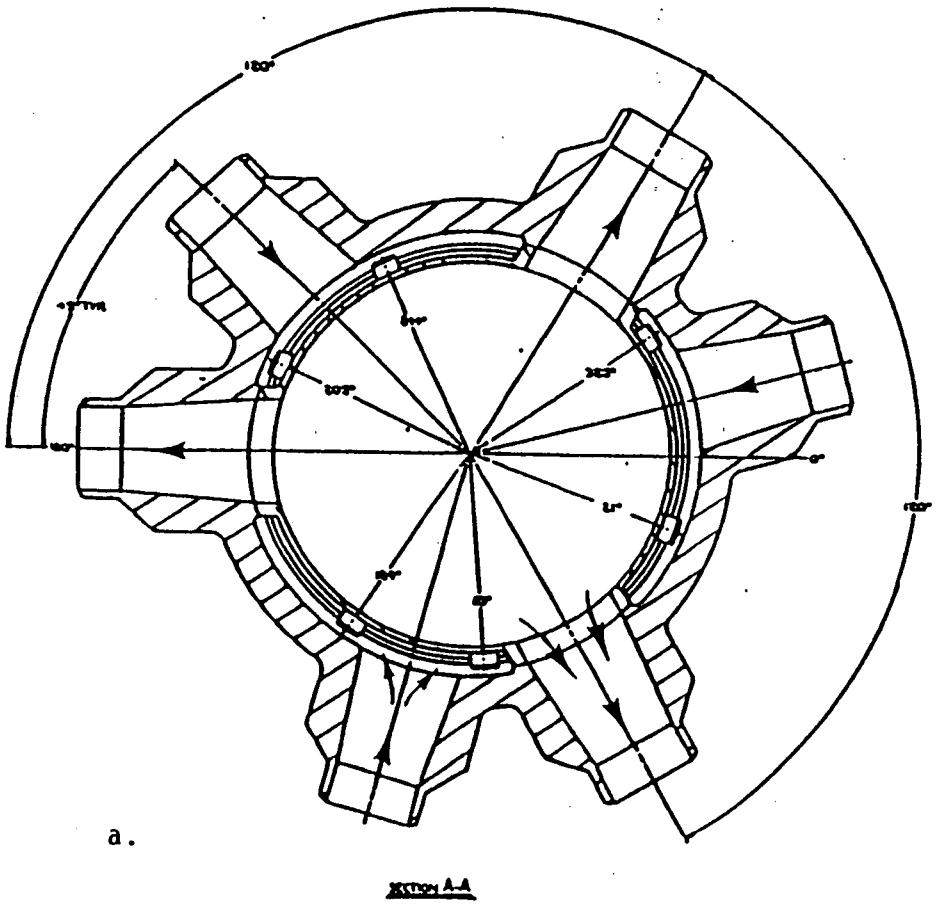

a.

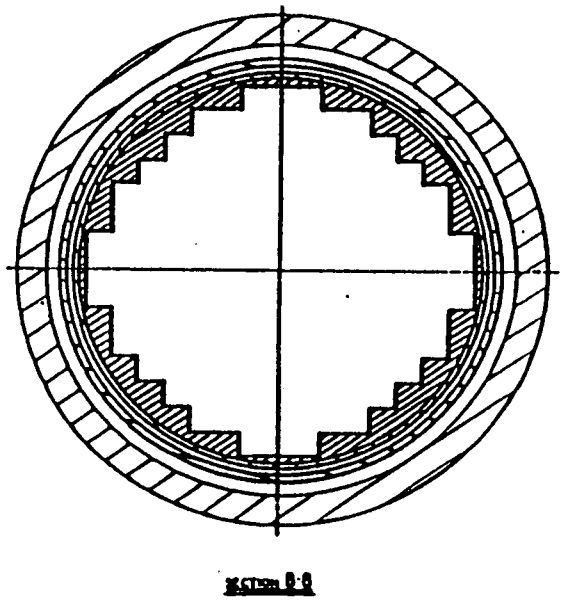

b.

FIGURE 2-4 NOZZLE ARRANGEMENT AND CORE LATERAL SUPPORT

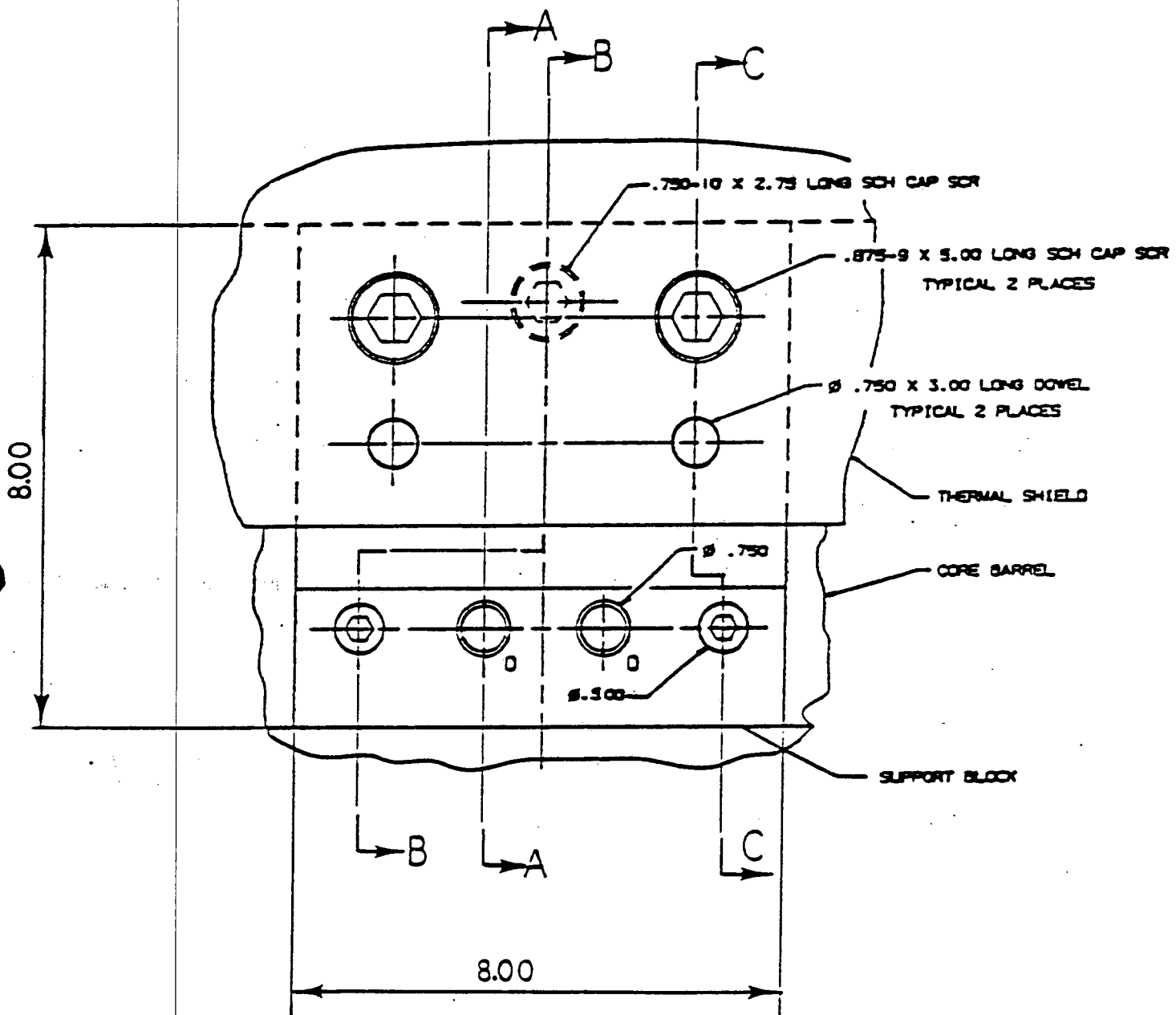

FIGURE 2-5a EXISTING LOWER SUPPORT BLOCK DESIGN

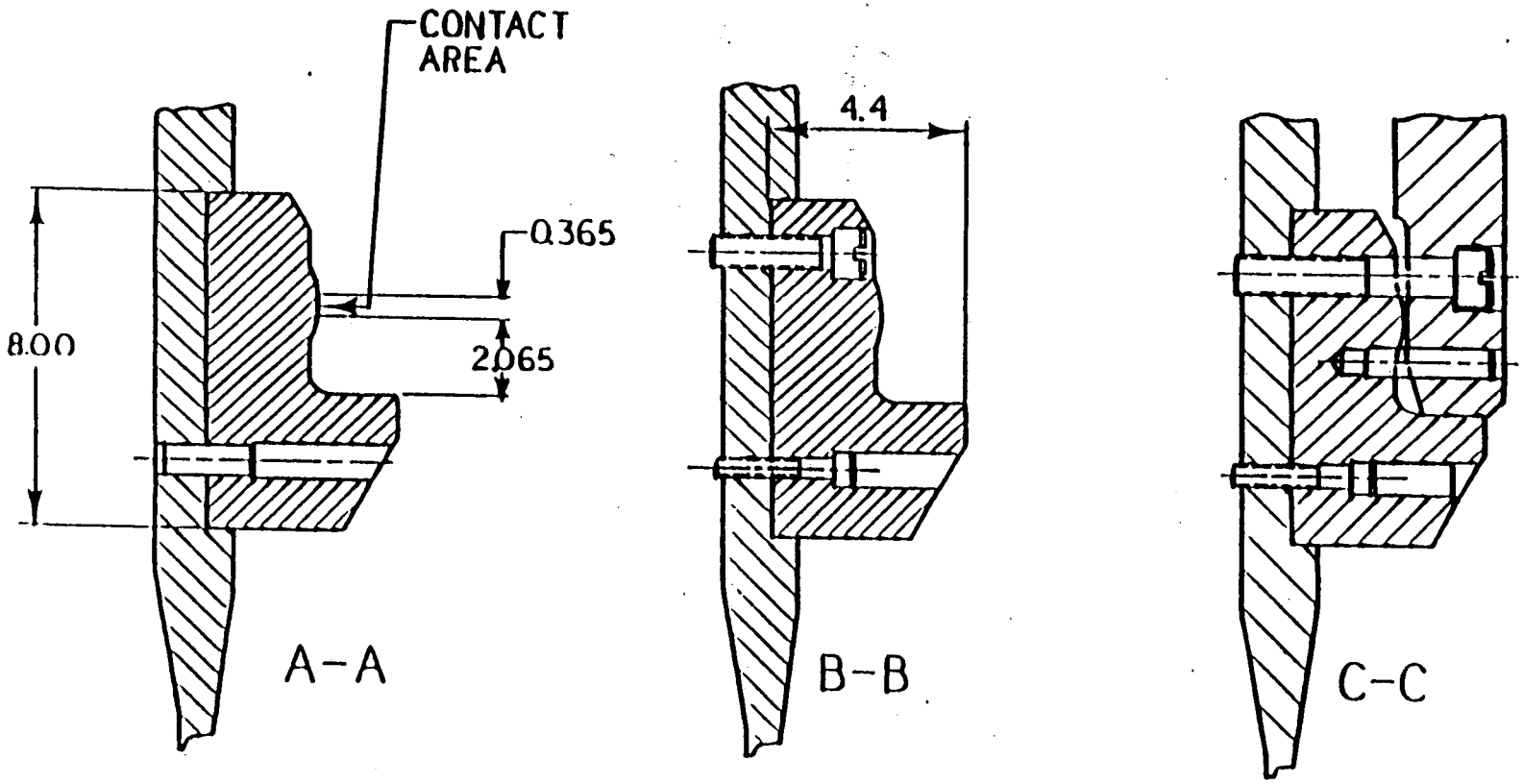

FIGURE 2-5b EXISTING LOWER SUPPORT BLOCK DESIGN

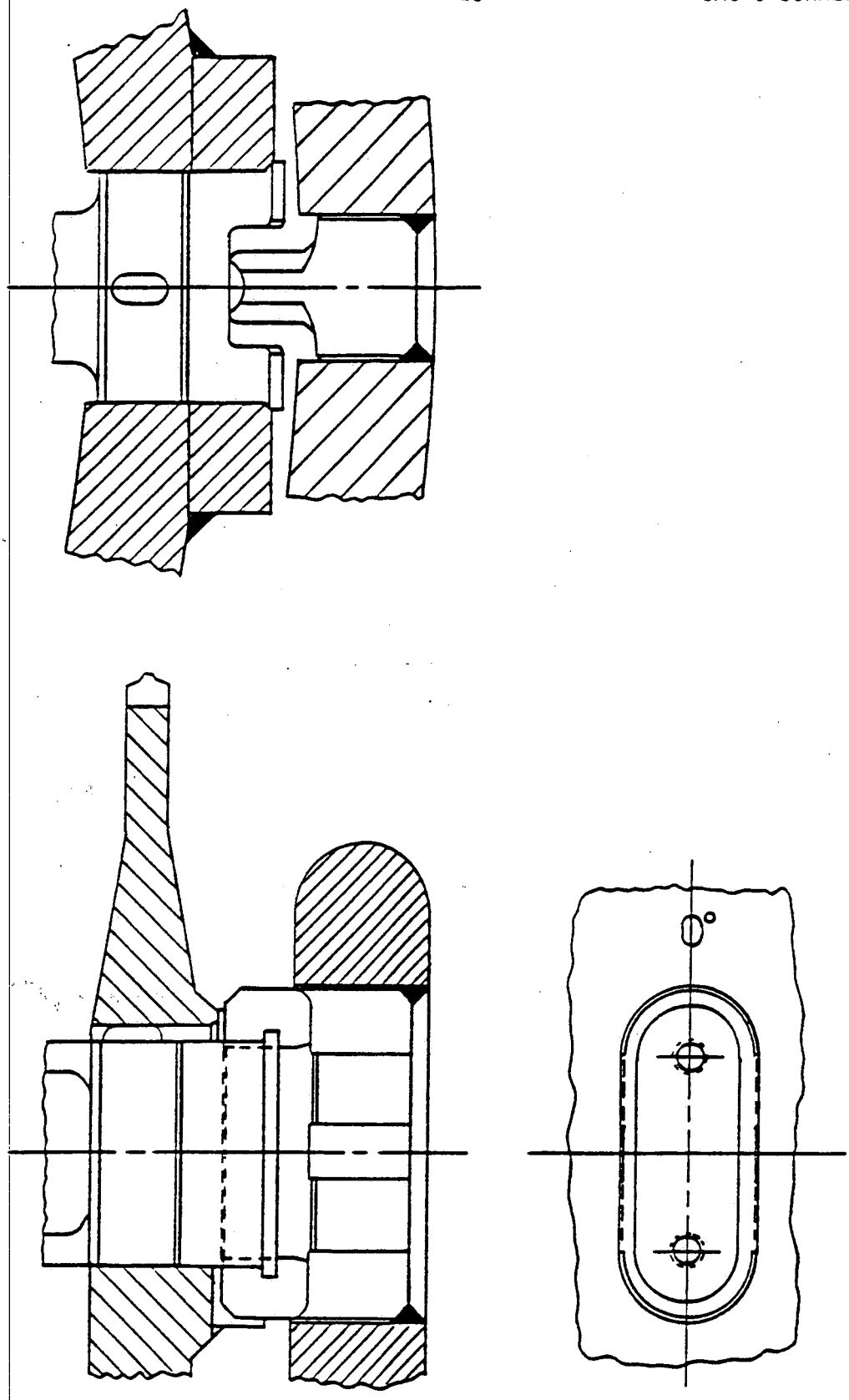

FIGURE 2-6 EXISTING UPPER DISPLACEMENT LIMITERS - KEYS

Another modification that was made after the SONGS hot functional test was to install six (6) flexure supports shown in Figure 2-7 between the top of the thermal shield and the core barrel. The flexures are located at 21°, 85°, 124°, 205°, 244° and 325°. The upper block of the flexure is bolted to the core barrel. The bottom section is welded to the top of the thermal shield. The upper block is connected to the bottom section by the web resisting radial and tangential motion of the shield but flexible in case of differential movement of the shield in the axial direction. Only one of the flexures has been fully functional. This is the 124° flexure and the last inspection confirmed that this flexure is still intact and functional. The remaining flexures were also inspected to the extent possible and they are still in place even though they are cracked or broken.

The nominal core barrel thickness at SONGS I is 1.75 inches and the thermal shield is 2.5 inches. The relative thickness of these two components influences the thermal lag that occurs during thermal transients. This may influence the low cycle fatigue loads experienced by the bolts. The temperatures of the core barrel and thermal shield are also affected by absorption of gamma radiation energy.

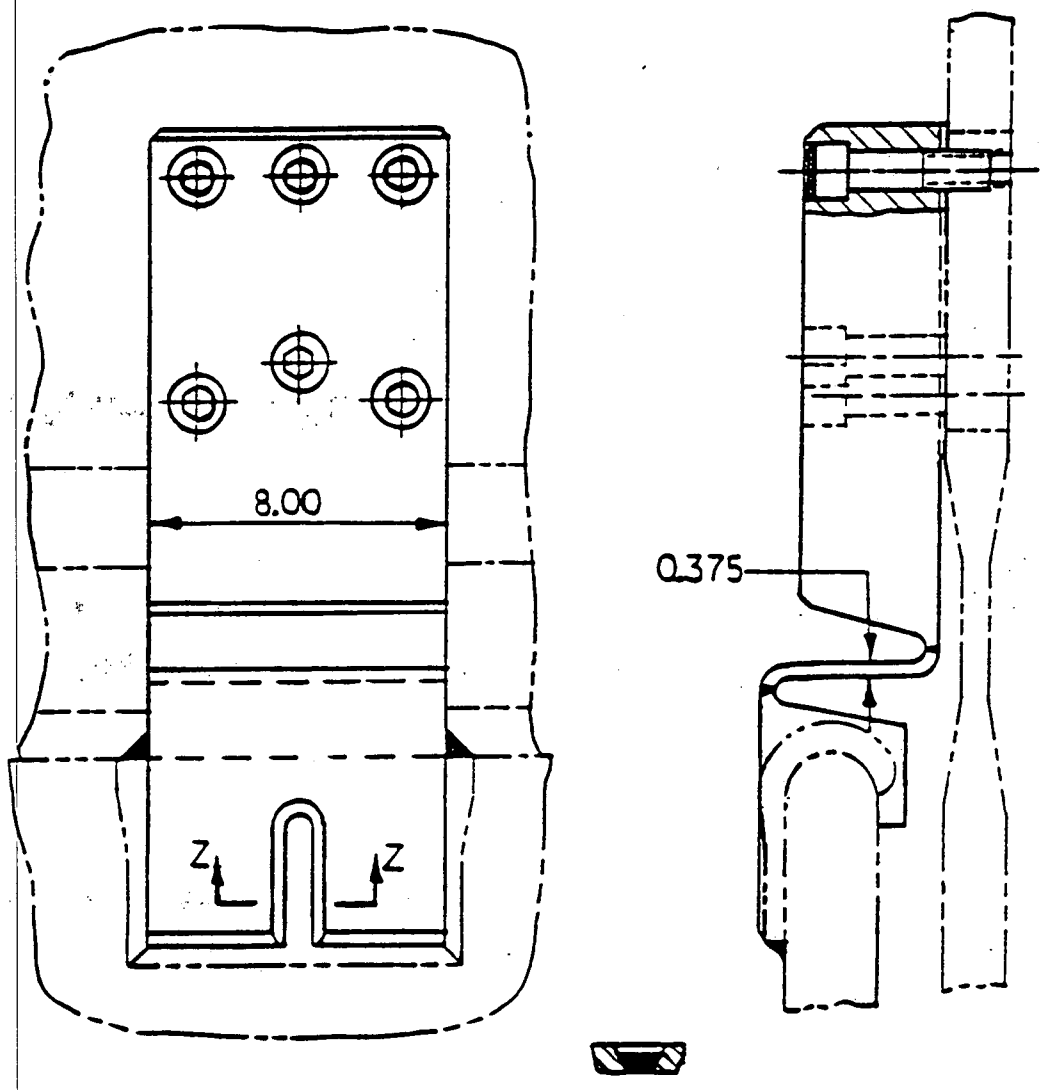

SECTION Z-Z

FIGURE 2-7 EXISTING UPPER FLEXURE

3.0 MODIFIED SUPPORT SYSTEM

The modified design of the bottom support block at azimuthal locations 60, 120, 180, 240 and 300° is shown in Figures 3-1a and b. Figures 3-2a and b show the bottom block at location 0°. This block includes the key which ensures proper orientation of the thermal shield with respect to the core barrel. The changes to the bottom supports are illustrated in Figure 3-3. The support was widened from 8 to 11 inches and the cross-sectional area of the bolts and dowel pins was increased. For example, three bolts of 1" diameter will be used to hold the thermal shield to the core barrel instead of the existing two bolts of 0.875" diameter. Three dowel pins penetrating the thermal shield will be used instead of two and their diameter is increased from 0.750 to 1.25 inch. An interference fit is used and the locking mechanism for bolts and pins is improved. Special KWU star heads are used for bolts. The pins are protected by secured locking nuts or starheads. A summary comparison of the new and old support block design is shown in Table 3-1.

The modified design of the keys is illustrated in Figures 3-4a and b and 3-5a and b for locations 0, 180, 270 and 90°, respectively.

The modified design of the flexures is shown in Figures 3-6a, b and c. The design was changed to reduce the local stress concentrations. Since the new flexures must be assembled under water, they are attached to the upper core barrel and the upper edge of the thermal shield by bolts and pins. XM-19 material of higher strength than previously applied 304 stainless steel is used. The weld at the web has been eliminated and the web geometry improved to maintain flexibility in the vertical direction with simultaneous reduction of stress ranges at web ends for vibratory loads. Table 3-2 gives a comparison of the new and old flexure designs.

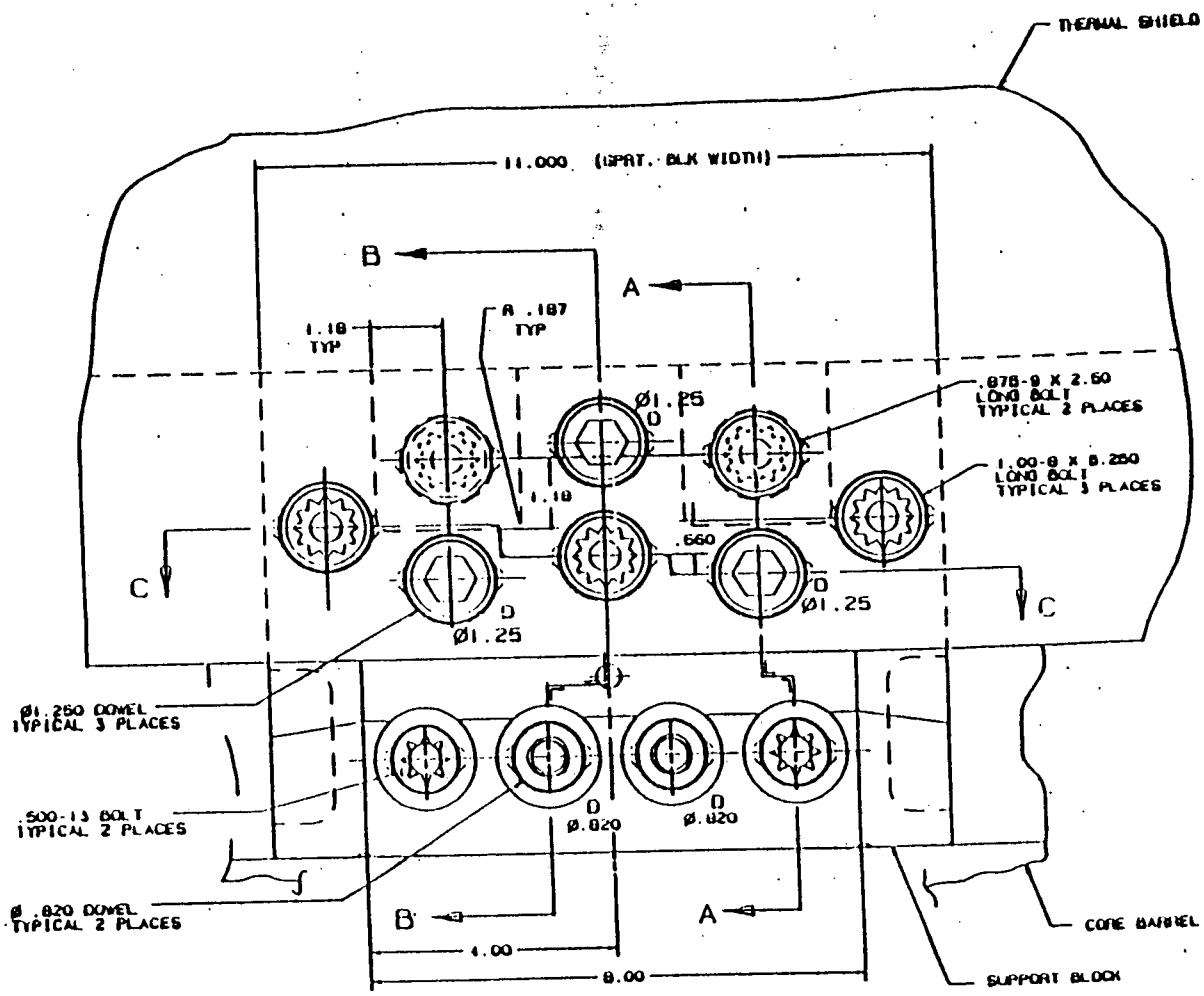

FIGURE 3-1a MODIFIED DESIGN OF SUPPORT BLOCK
AT LOCATIONS 60, 120, 180, 240, 300°

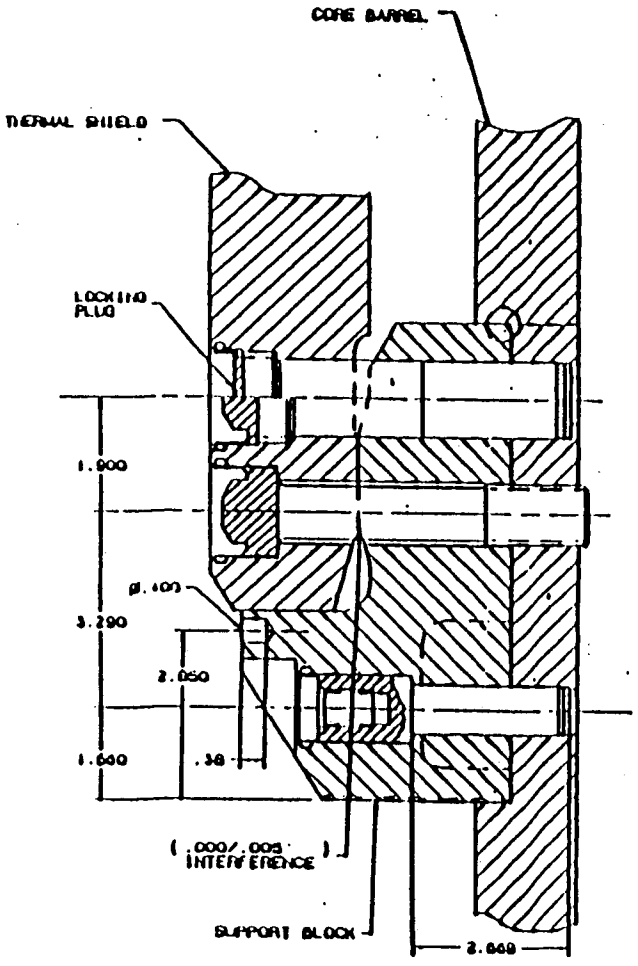

SECTION B-B

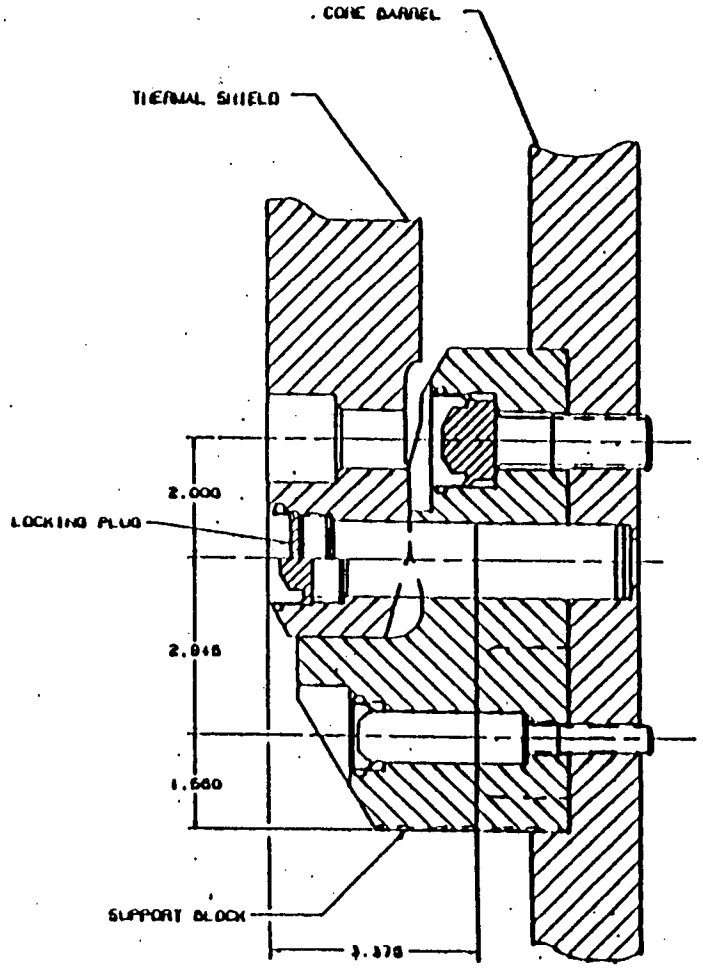

SECTION A-A

FIGURE 3-1b MODIFIED DESIGN OF SUPPORT BLOCK AT LOCATIONS 60, 120, 180, 240, 300°

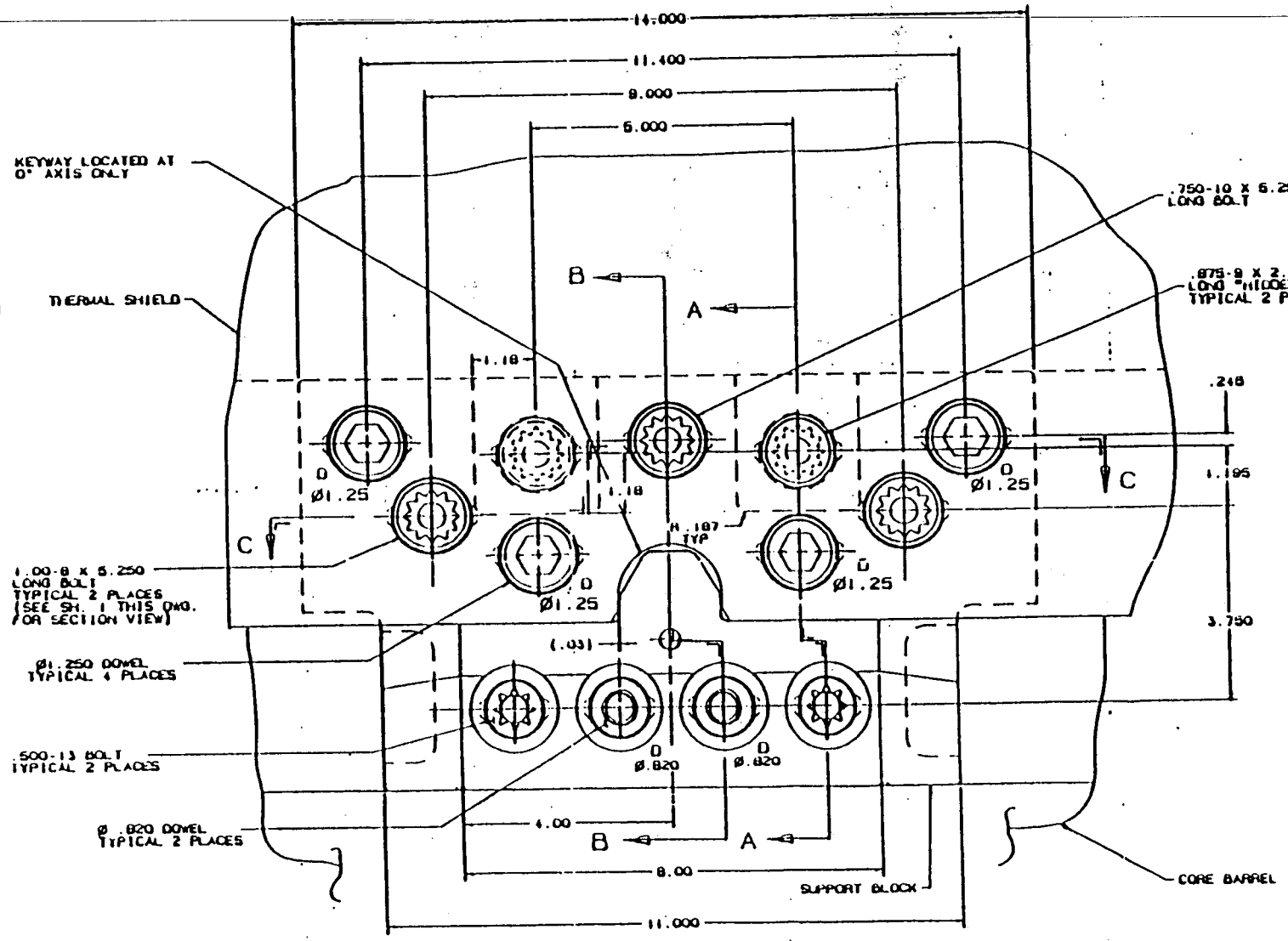

FIGURE 3-2a MODIFIED DESIGN OF SUPPORT BLOCK AT LOCATION 0°

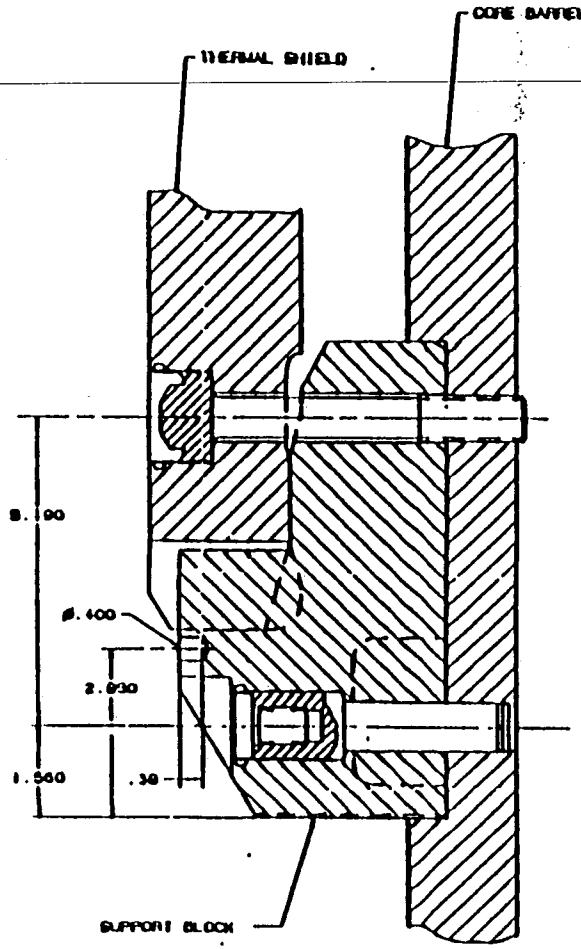

SECTION B-B

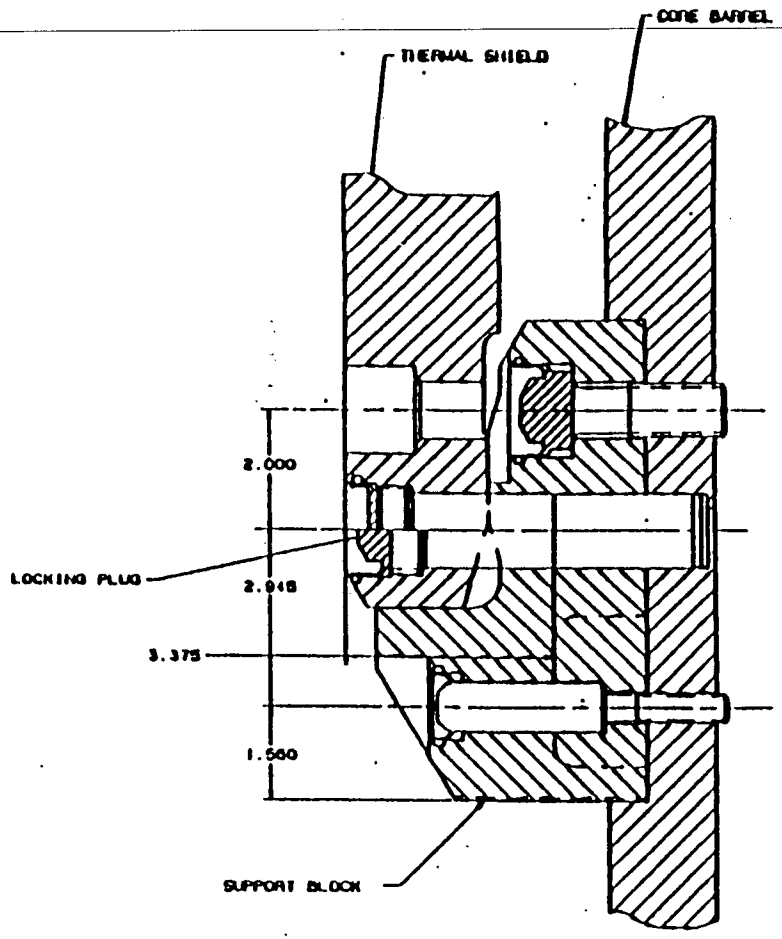

SECTION A-A

FIGURE 3-2b MODIFIED DESIGN OF SUPPORT BLOCK AT LOCATION 0°

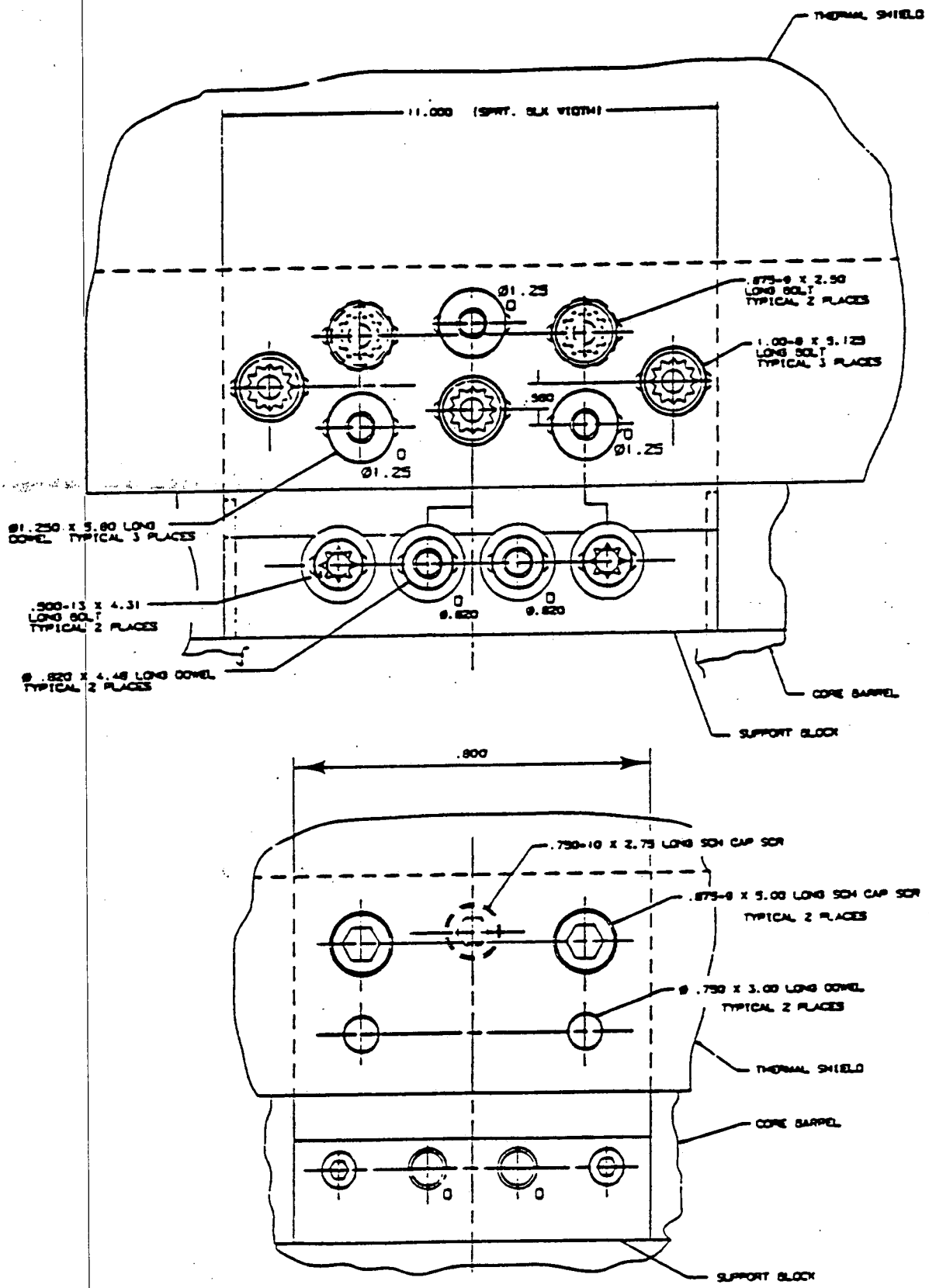

FIGURE 3-3 COMPARISON OF EXISTING AND MODIFIED SUPPORT BLOCKS

TABLE 3-1

COMPARISON OF LOWER SUPPORT BLOCKS

MODIFIED DESIGN	EXISTING DESIGN
• 11" wide	8" wide
• Contact area between the block and thermal shield increase to 12 sq inch	from 3 sq inch
• Number and area of bolts increased to:	from:
two ϕ .875 1.2 sq in.	one ϕ .750 0.44 sq in. (hidden bolt) BL*-CB
three ϕ 1.00 2.3 sq in.	two ϕ .875 1.2 sq in. (upper bolt) TS*-CB
two ϕ .5 0.4 sq in.	two ϕ .500 0.4 sq in. (lower bolt) BL*-CB
• Number and area of dowel pins increased to:	from:
two ϕ .820 1.06 sq in.	two ϕ .750 0.88 sq in. (lower pins) BL-CB
three ϕ 1.25 3.7 sq in.	two ϕ .750 0.88 sq in. (upper pins) TS-BL-CB
• Dowel pins designed for Interference Fit	Shrink Fit
• Bolts & dowel pins will be restrained by a locking nut or crimped head	Bolts - welded lock bar Dowels - welded

BL - Block
CB - Core Barrel
TS - Thermal Shield

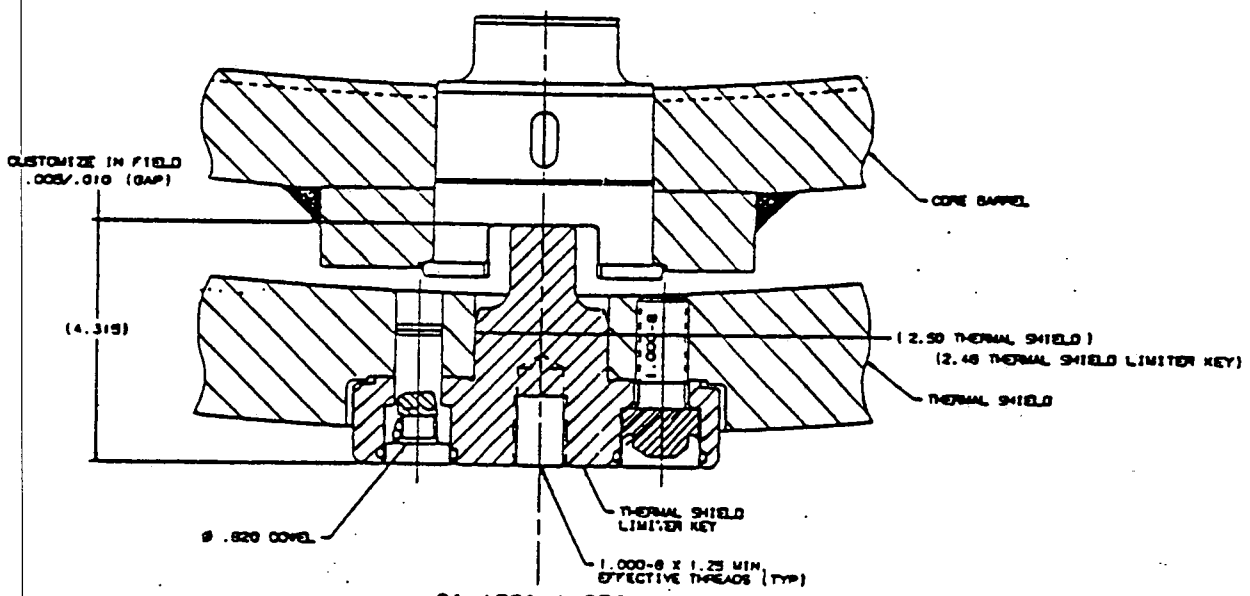

0°, 180° & 270°

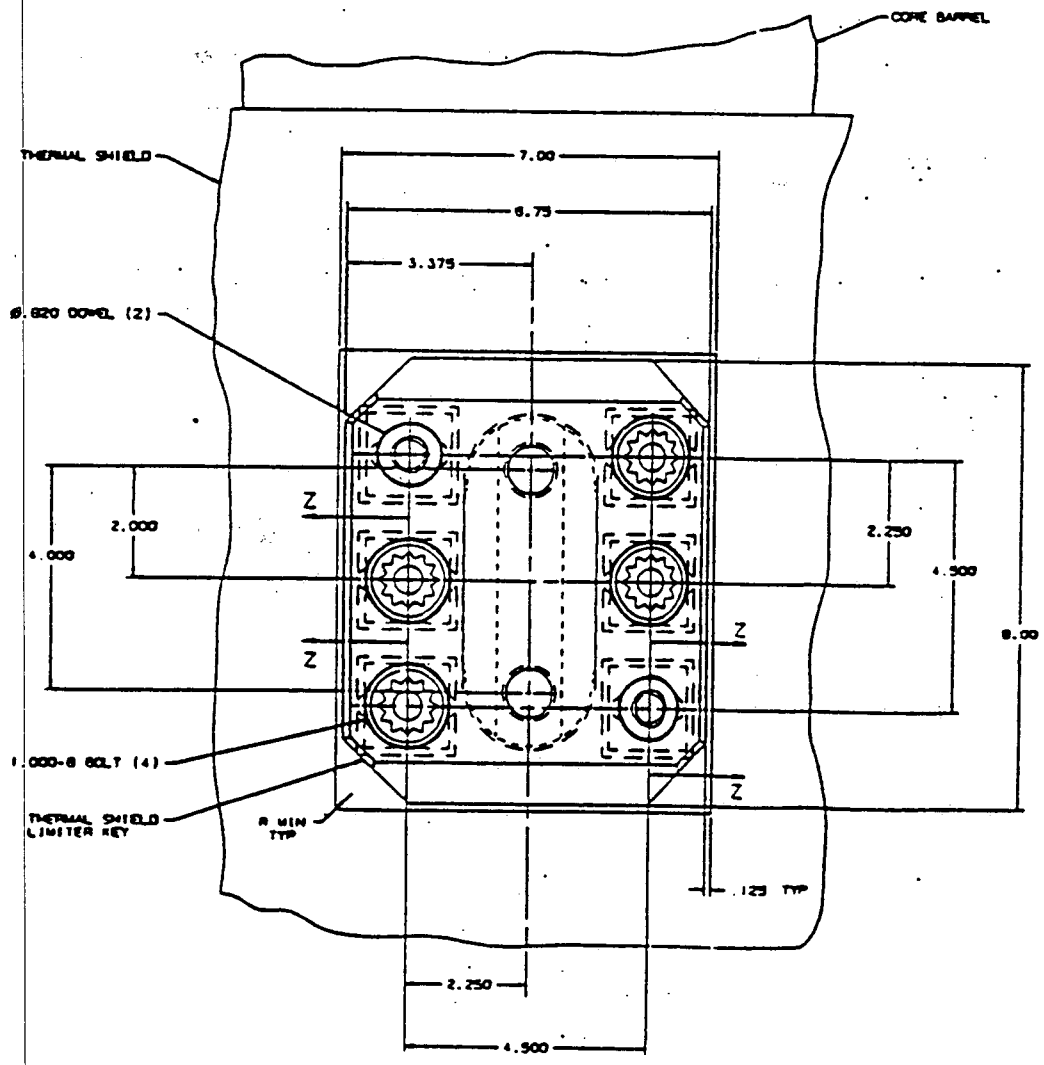

FIGURE 3-4a MODIFIED UPPER KEY DESIGN
AT LOCATION 0, 180, 270°

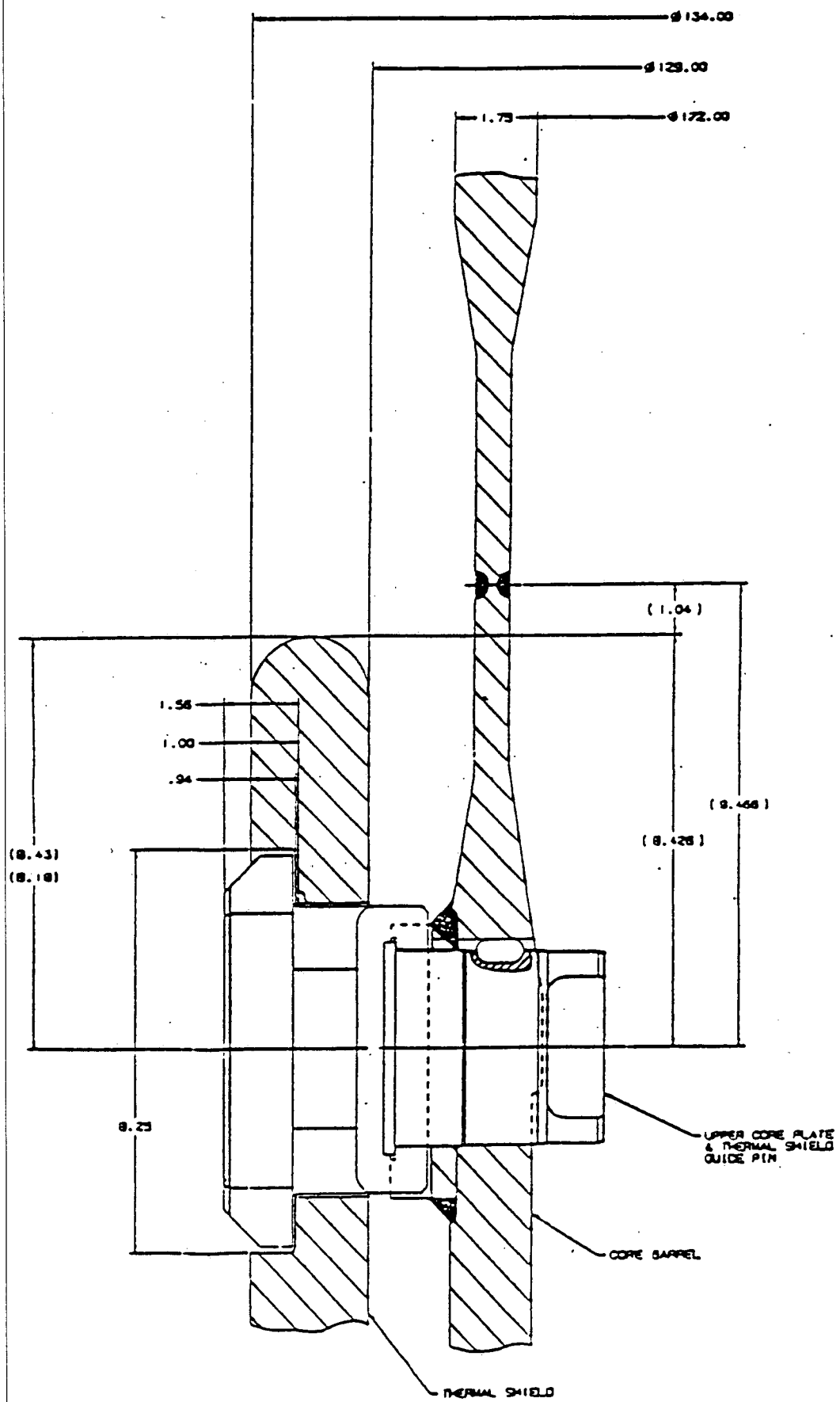

FIGURE 3-4b MODIFIED UPPER KEY DESIGN AT LOCATIONS 0, 180, 270°

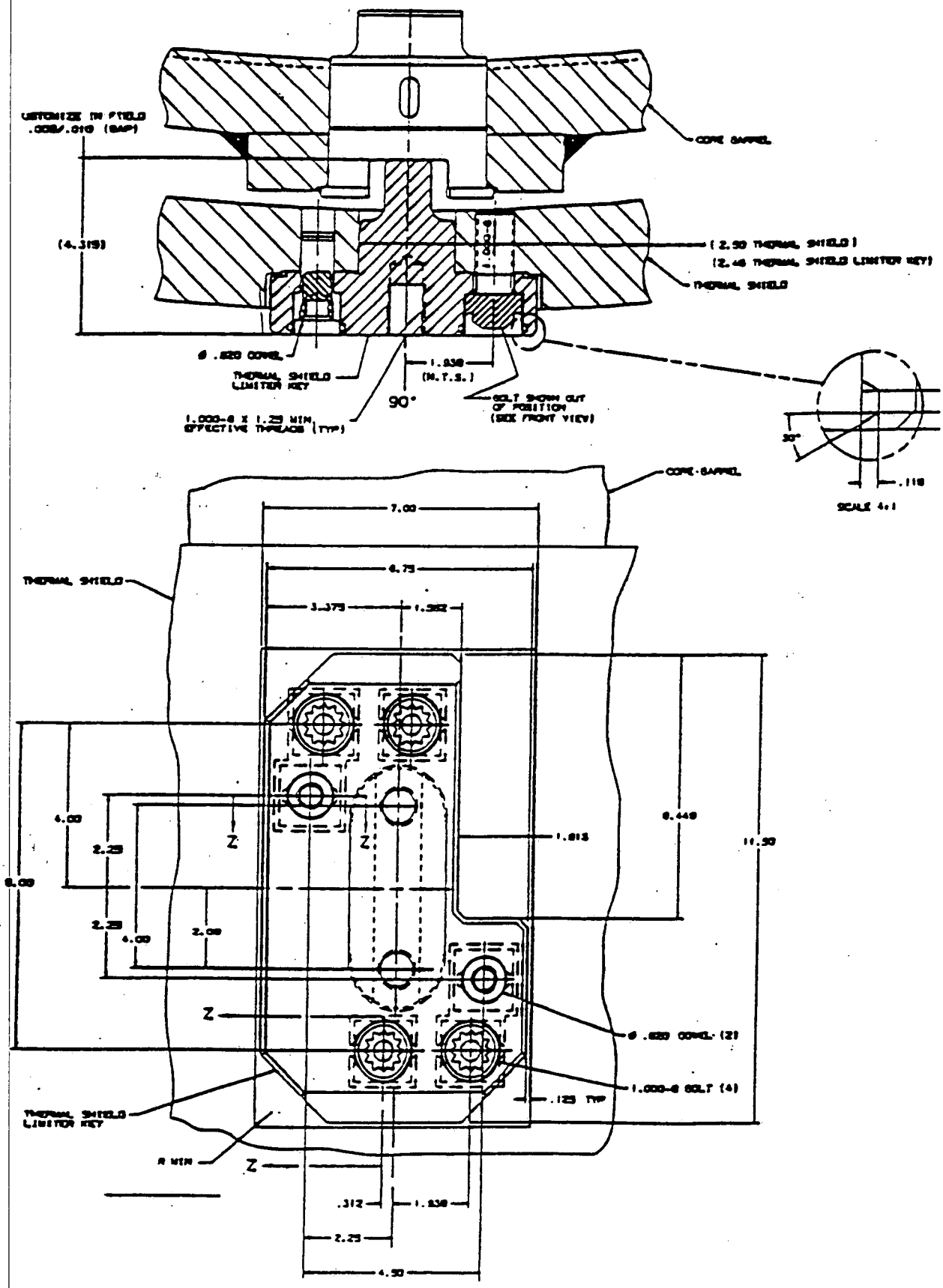

FIGURE 3-5a MODIFIED UPPER KEY DESIGN AT LOCATION 90°

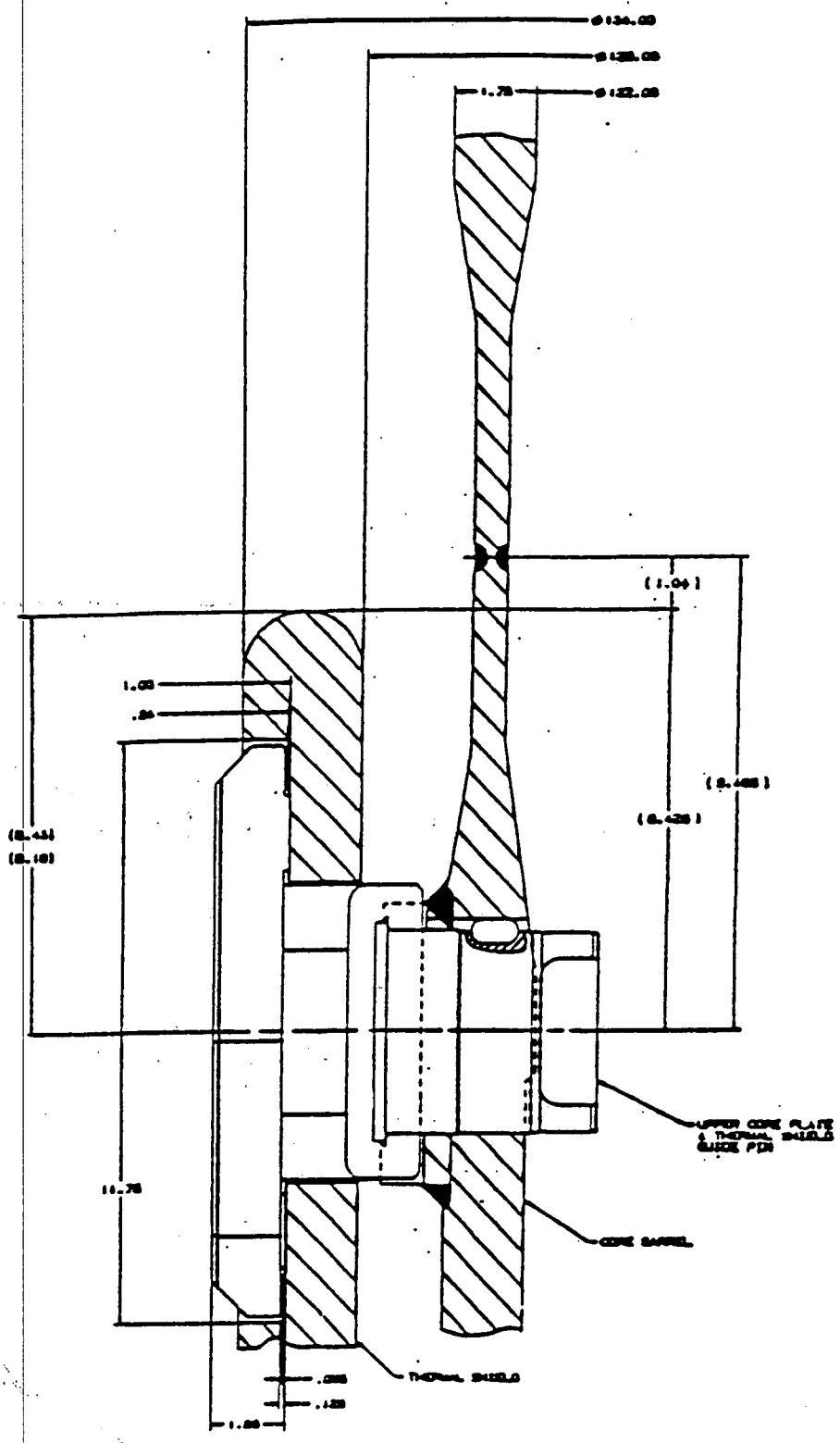

FIGURE 3-5b MODIFIED UPPER KEY DESIGN
AT LOCATION 90°

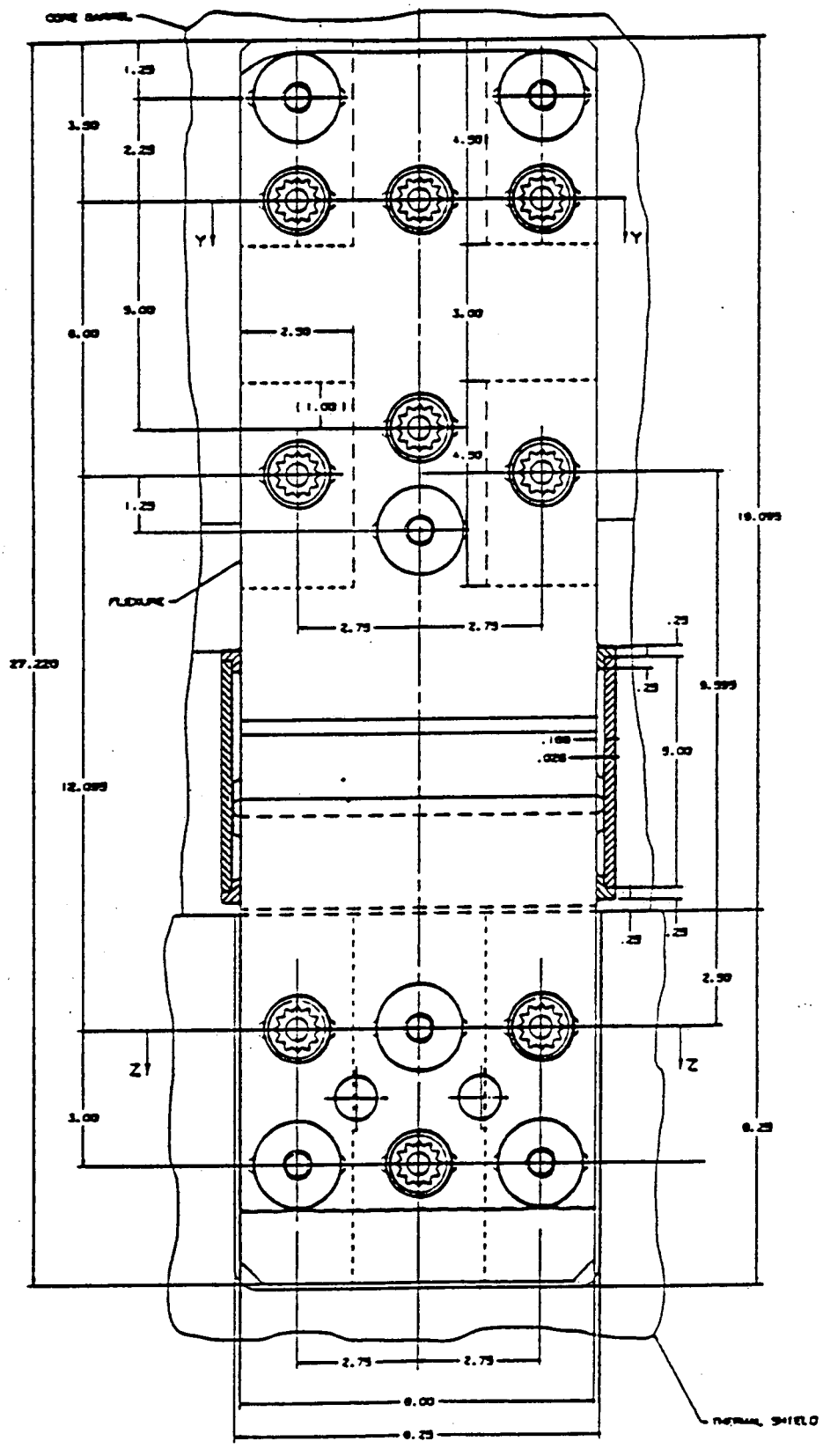

FIGURE 3-6a MODIFIED UPPER FLEXURE DESIGN

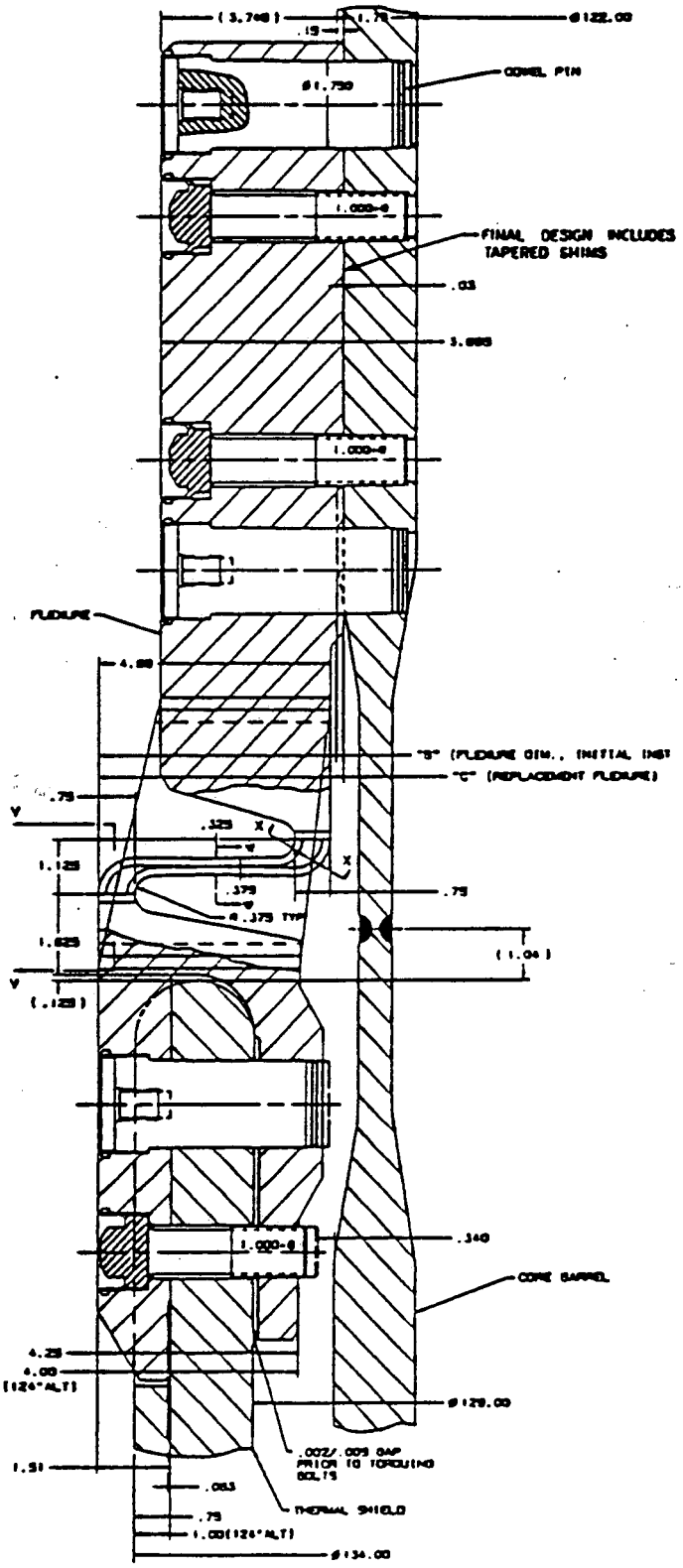

FIGURE 3-6b MODIFIED UPPER FLEXURE DESIGN

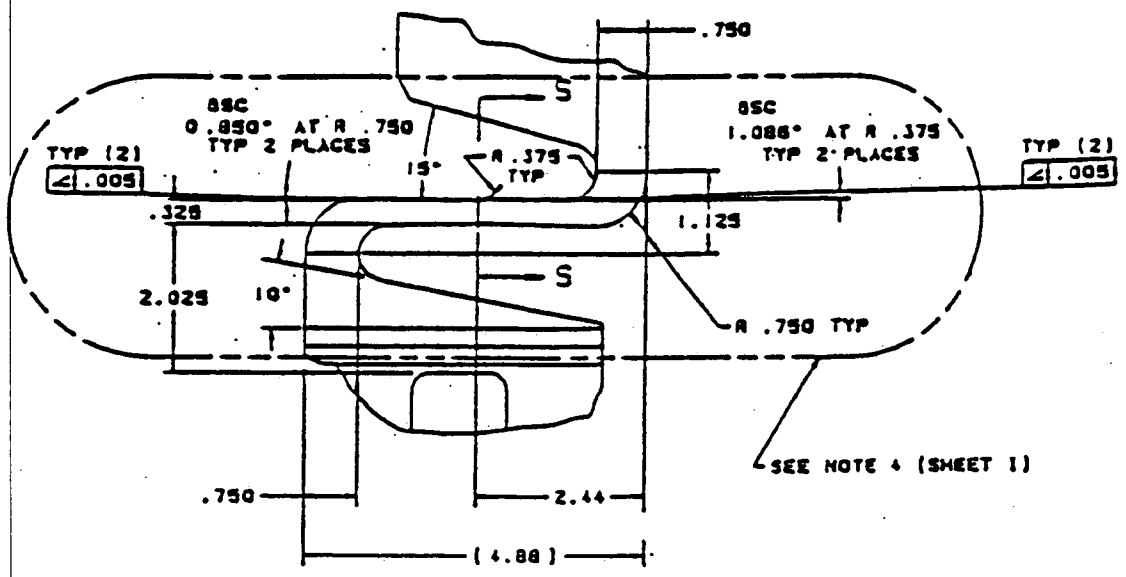

VIEW V-V
SCALE 1:1

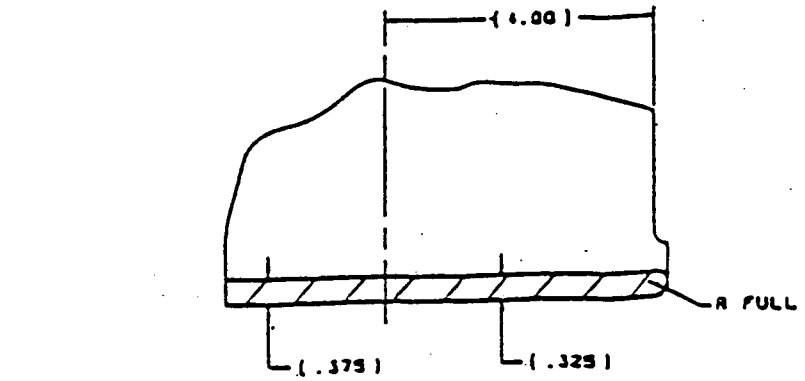

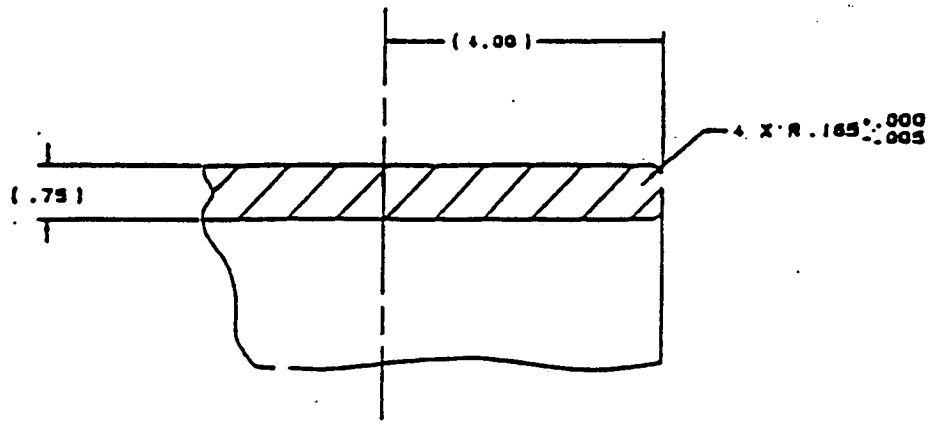

FIGURE 3-6c DETAILS OF MODIFIED UPPER FLEXURE LEAF

TABLE 3-2

COMPARISON OF FLEXURES

MODIFIED DESIGN	EXISTING DESIGN
• Material SA-479 XM-19 high alloy stainless steel (annealed) Tensile 100 ksi Yield 55 ksi Hardness 293 Brinell	ASTM A-276 type 304SS Tensile 75 ksi Yield 30 ksi Hardness 202 Brinell
• Flexure fabricated in one piece (no welds)	Welded in web area
• Preloaded flexure web area	No preload
• Web geometry improved to reduce stress concentration	--
• One flexure will be moved to reduce loading	--

4.0 HISTORY OF THERMAL SHIELD PERFORMANCE

The detailed chronological information concerning progressive degradation of the existing thermal shield support system is given elsewhere [3].

The analysis of the existing support, used herein to correlate results for the modified design, is based on the results of the 1972 inspection performed after 50 months (4.1 EFPY) of operation. This inspection confirmed that none of the flexures were broken.

The inspection in 1976 performed after 88 months (7.3 EFPY) indicated that two of the flexures were still intact.

The September 1978 inspection performed after 95.8 months (8 EFPY) showed that only the flexure at 124° was still not broken. The same result was obtained in December 1988.

The December 1988 inspection completed after 156 months (13 EFPY) revealed limited degradation of support blocks.

5.0 METHOD OF ANALYSIS

The overall technical approach and method of analysis used for this evaluation may be described as 'hybrid' in nature, utilizing a combination of the following programs:

1. Finite element code (ANSYS) - for the modal and stress analysis
2. Finite difference fluid dynamics code (FLOW3D) - for the flow analysis
3. SMC O'Donnell programs - for the random flow-induced vibration and fatigue analysis.

A flow chart showing the details of the various elements in the total analysis scheme is shown in Figure 5-1. The chart illustrates how these individual elements interact with each other and tie together in the overall picture.

The response of a linear, elastic damped structure to random loading has approximately a normal or Gaussian distribution [5, 6]. Since the turbulent flow-induced vibration of the thermal shield is random in nature, only a rms amplitude can be predicted. If the forcing function is known, the mean square response of a cylindrical shell excited by turbulence is given by [4, 6]:

$$\bar{y}^2 = \frac{AG(f)}{64\pi^3} \sum_{\alpha} \frac{\phi_\alpha^2 J_{\alpha\alpha}}{M_\alpha^2 f^3 \xi_\alpha} \qquad (1)$$

where,

$J_{\alpha\alpha}$ = joint acceptance

$G(f)$ = single-sided pressure power spectral density, $(psi)^2/Hz$

M_α = generalized surface mass density

ϕ_α = structural mode shape

ANALYSIS FLOW CHART

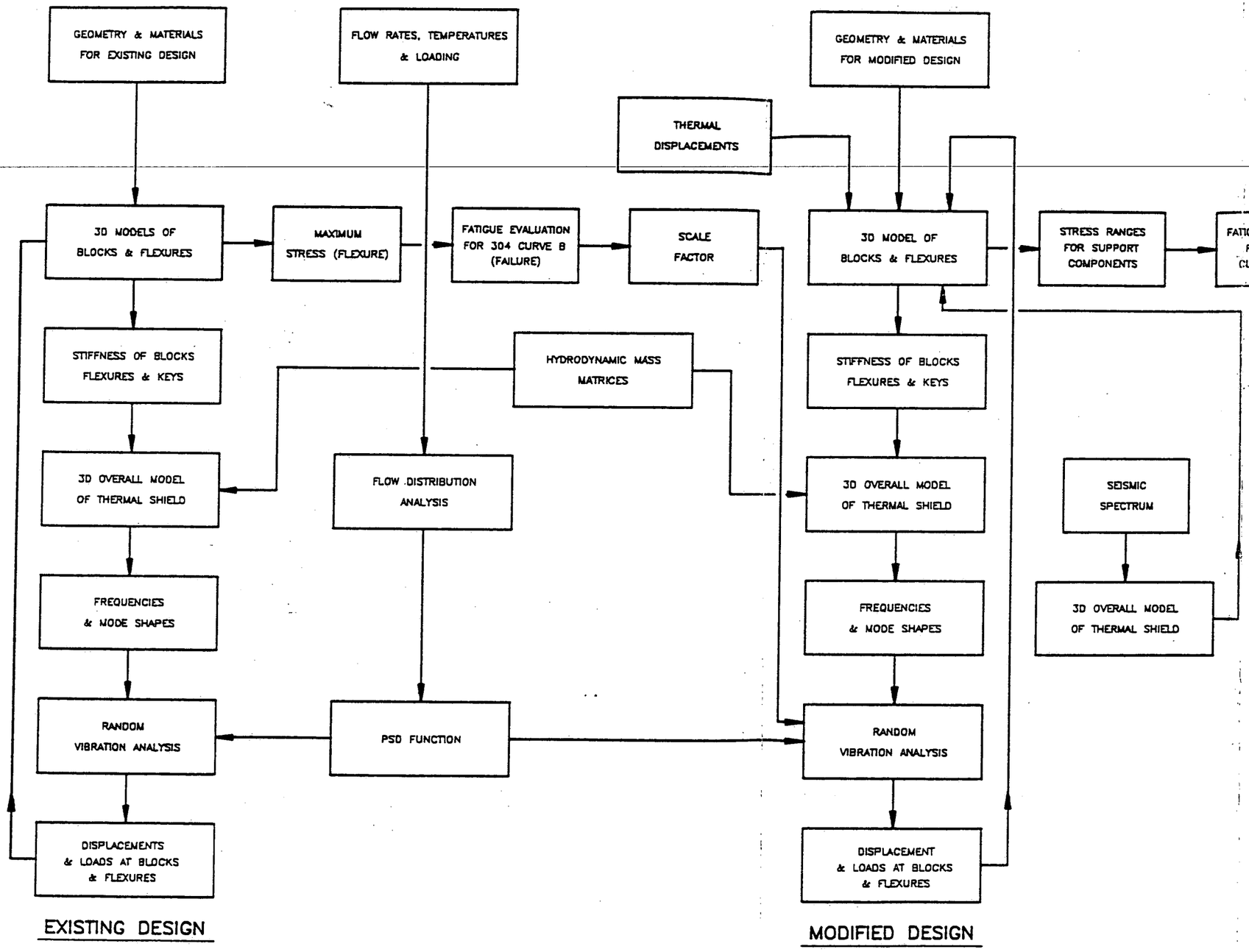

FIGURE 5-1 ANALYSIS CHART

A = area over which the force is applied

f_α = natural frequency, Hz

ξ_α = structural damping ratio (% critical)

α = modal index

Note that the mode shape function is normalized such that

$$\int_A \phi_\alpha^2 \, dA = 1 \qquad (2)$$

Equation (1) shows that the response of the thermal shield involves [7]:

1. Knowledge of the mode shapes, ϕ_α and natural frequencies, f_α.
2. Knowledge or evaluation of the joint acceptance.
3. Knowledge of the pressure spectral density, which is a measure of the forcing function as a function of frequency. The spatial distribution of the fluctuating pressure loading should also be known.

The dynamic characteristics of the thermal shield/core barrel in terms of their natural frequencies and mode shapes were evaluated using the ANSYS finite element program, [8].

The existing design was first analyzed to correlate the analytical model to field data. Based on the geometry and materials of the SONGS 1 design, an overall finite element model of the core barrel and thermal shield was developed for performing the modal analysis to determine the natural frequencies and mode shapes. The supporting blocks and flexures were modeled as springs in the overall model. The stiffnesses of these springs were determined from separate three-dimensional finite element models of the blocks and flexures. The effect of fluid was incorporated by inputting appropriate hydrodynamic mass matrices.

The joint acceptance of a mode is a measure of the degree to which the spatial distribution of pressure on the surface of the thermal shield is compatible with the structural mode shape. It is determined by spatial integrations over the surface of the thermal shield. The integrand of the joint acceptance involves the coherence (or correlation) function which is a function of separation distance and frequency and is related to the correlation length. Physically, the correlation length is approximately the distance beyond which properties of the flow field show little correlation. The parameters for defining the coherence function are usually based on field or laboratory data. Such data were not made available to SMC O'Donnell. However, an upper bound estimate of the response can be made by assuming the loading to be perfectly correlated. This approach gives results that are an order of magnitude higher. The actual value of J was then determined by comparing these results to field data.

In flow-induced random vibration, the forcing function is defined by the pressure spectral density and the coherence function, which are usually obtained by measurements on a laboratory model and then scaled up to the prototype, or by measurements on a prototype of the same design. As mentioned earlier, the pressure spectral density forcing function data were not made available to SMC O'Donnell. Hence, the pressure spectral density was established based on data available in the literature and the local fluid velocities obtained from a flow analysis performed for SONGS Unit 1.

The spatial variation of the fluctuating pressure field was determined from a three-dimensional flow model using the FLOW3D Code, [9]. The three-dimensional flow model was based on the actual flow rate and geometry of the SONGS 1 core barrel/thermal shield structure. This model provided the local fluid velocities in the gaps between the thermal shield and core barrel as well as between the core barrel and reactor vessel. The spatial variation of the fluctuating pressure field was determined from the local velocity vectors using a rms pressure coefficient. Having established the forcing function, Equation (1) was used with results from the ANSYS modal analysis to obtain the response for each mode. The total response was then obtained by combining the mean square responses for each mode. For closely spaced modes the grouping method given in the United States Nuclear Regulatory

Guide [18] was used to combine the modal responses. Note, that the random pressure loading acts on the inside and outside of the thermal shield. Separate analyses were run for each of these cases and the total response obtained by combining the mean square responses for the two loading cases using the SRSS method. A separate program was written to perform all these latter functions.

The RMS response obtained using the approach described was used as the input to the separate three-dimensional finite element models of the lower support blocks and upper flexures. The resulting loads and stresses obtained at the support block bolts and upper flexures were used to evaluate their fatigue life. For a Gaussian random process, such as turbulence-induced vibration the absolute value of zero to peak amplitude follows a Rayleigh distribution [10, 11]. Based on this distribution and the ASME fatigue curve, the fatigue life of the component can be evaluated. A separate program was written to perform this fatigue evaluation.

In order to predict fatigue damage, the analytical model developed was calibrated by benchmarking against the actual field data [3]. The operation history and inspection results, as presented in [3], indicate that the upper flexures broke sometime between 50 months and 88 months of operating time, while the lower blocks remained intact. It was thus assumed that the number of cycles for the flexures to reach their fatigue failure usage factor of 1.0 corresponded to 50 months of operation time. The analytical model was scaled to correlate the analytical results to this data. The adjusted model was then used for subsequent life prediction of the new design. The effects of thermal transients and seismic events were included in the evaluation of the new design.

A detailed description of this approach including details of the finite element and fatigue analyses are given in the sections that follow.

6.0 FINITE ELEMENT MODELS

The finite element method was used for performing the following parts of the overall analysis:

(i) Modal analysis - to evaluate the natural frequencies and mode shapes of the thermal shield and core barrel.

(ii) Structural analysis - to determine the stresses in the upper flexures and lower support block bolts for subsequent use in their fatigue evaluation. The structural analysis included thermal and seismic evaluations.

The ANSYS finite element program was used for both of these analyses. An overall core barrel/thermal shield finite element model was developed for performing the modal analysis. This overall model was also used for the seismic analysis. In addition to the overall model, separate three-dimensional finite element models of the upper flexures and lower support blocks were developed for determining their stiffnesses which were input into the overall model. These three-dimensional models were also used for determining the stresses in the flexures and bolts required for their fatigue evaluation. Models were made for both the old and new designs.

The finite element model developed for determining the natural frequencies and mode shapes for the old and new designs is shown in Figure 6-1. The components included in this model are the core barrel, the thermal shield, the lower support blocks, the flexures, and the radial limiter keys. The core barrel and thermal shield were modeled using three dimensional quadrilateral shell elements (STIF 63) while the radial, vertical, and tangential stiffnesses of the support block and radial limiters were simulated using a combination of uni-directional spring elements (STIF14).

The stiffnesses of the support blocks were obtained from solid element three dimensional finite element models for the old and new designs, Figures 6-2 and 6-3. Each model was subjected to unit deflections in the three principal directions. The resulting reaction forces at the imposed deflection nodes were then used to obtain the stiffnesses. The stiffnesses

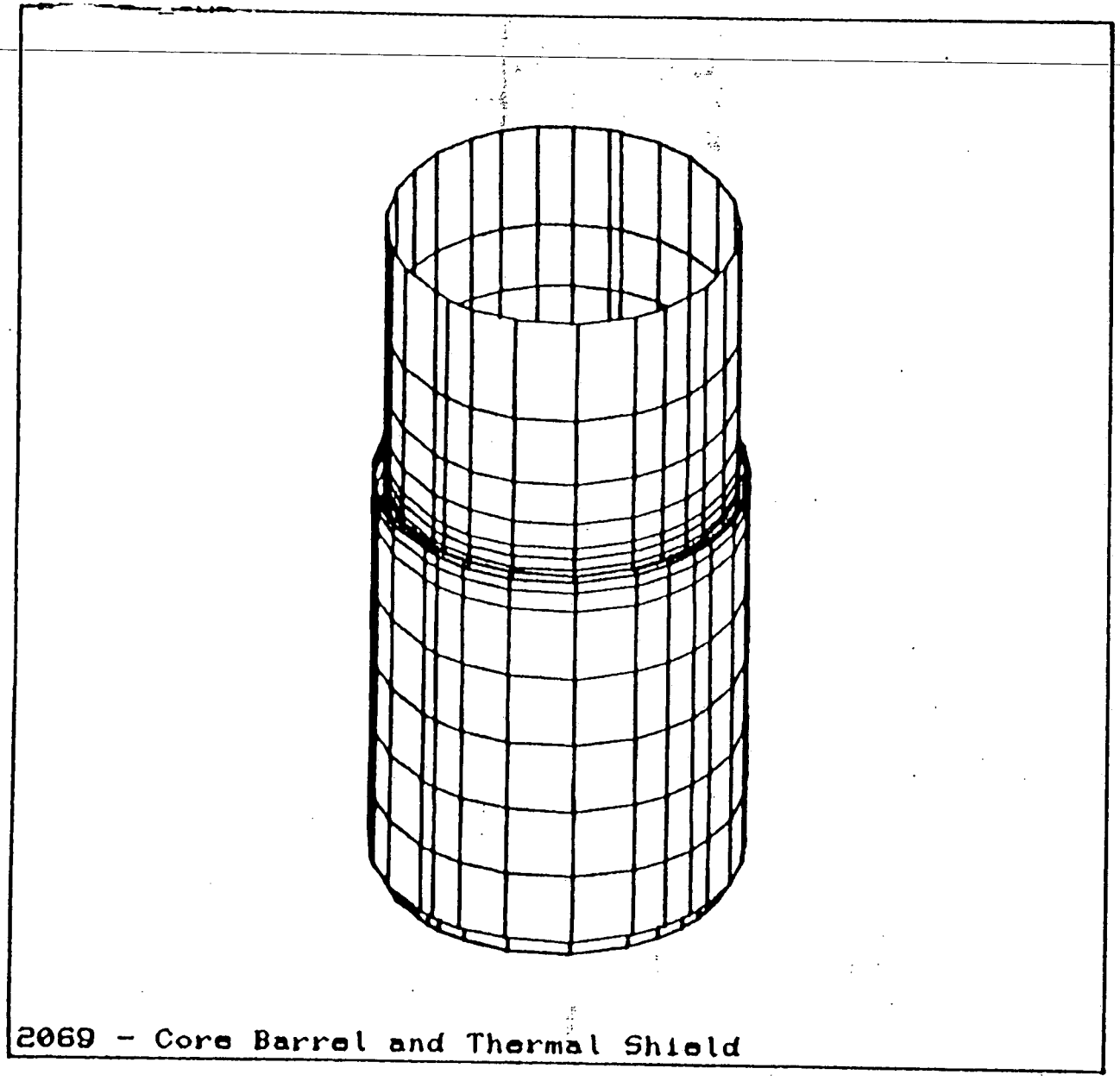

FIGURE 6-1 THERMAL SHIELD - CORE BARREL FINITE ELEMENT MODEL

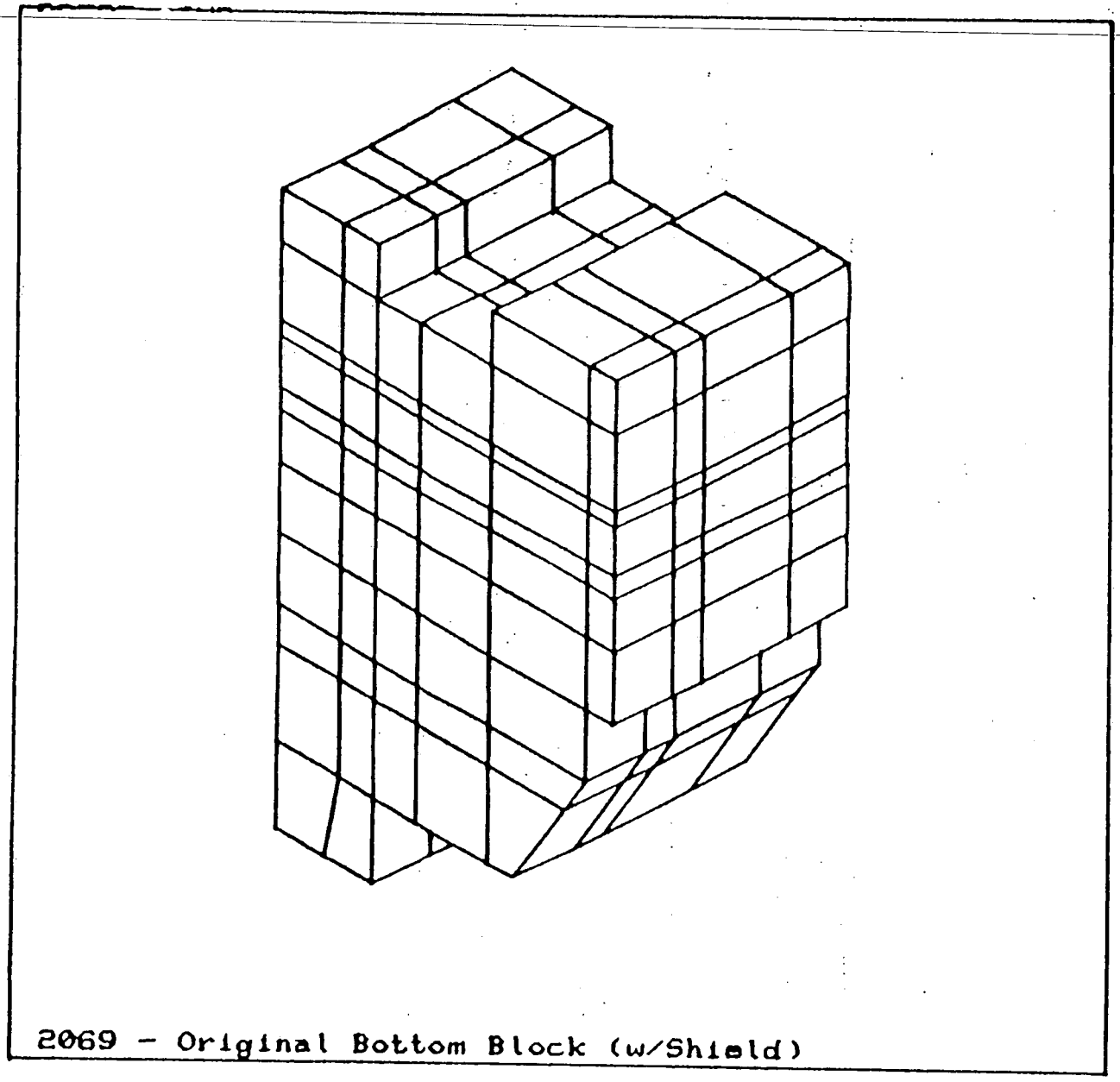

FIGURE 6-2 OLD SUPPORT BLOCK - FINITE ELEMENT MODEL

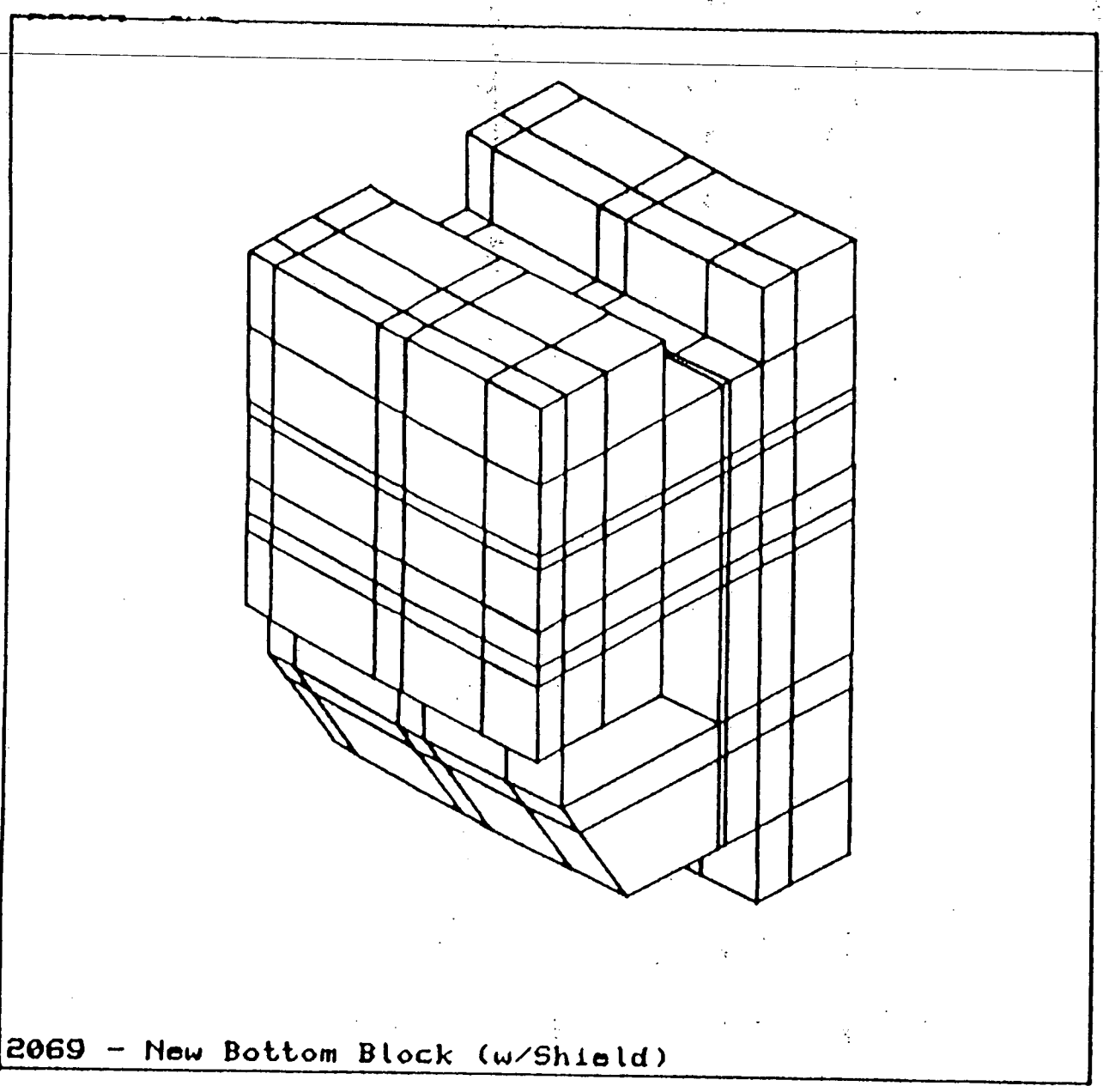

FIGURE 6-3 NEW SUPPORT BLOCK - FINITE ELEMENT MODEL

of the included portions of the thermal shield and core barrel shells were arbitrarily set to a very high value so that the computed stiffnesses do not include any contribution due to these shells.

The flexures were simulated using a stiffness matrix element (STIF 27) generated from the new and old flexure detail models. The matrix generated by this element is 12 x 12. It relates two nodal points each with six degrees of freedom per node. The solid element three-dimensional finite element models for the flexures are shown in Figures 6-4 and 6-5.

The stiffness of the radial limiter keys was computed by hand since these keys only resist motion in the radial direction and are of a simple geometry.

The original bottom block model is a three-dimensional model of the bottom block with a portion of the core barrel and thermal shield. The block, core barrel and thermal shield are made up of ANSYS STIF 45 elements. These are three-dimensional isoparametric solid elements. The bolts that attach the block to the core barrel and the thermal shield to the block and core barrel are modeled using ANSYS STIF 4 elements. These are three-dimensional elastic beam elements. These beam elements were given an initial strain to simulate preload. See Figure 6-6 for the dimensions used for this model.

Three-dimensional gap elements (ANSYS STIF 52) were used in the interfaces between the thermal shield bottom and the block ledge as well as between the thermal shield back and the block face. Gaps were also used between the block back and the core barrel. See Figure 6-7 for the gap locations and their initial status. The Young's Modulus of the core barrel was made artificially high because its shell flexibility was taken into account in the three-dimensional model of the entire core barrel and thermal shield.

The model uses a symmetry plane along the center of the block because only half of the block was modeled. The bottom of the core barrel was constrained in translation in all directions. All nodes on the top of the thermal shield are coupled in their radial and vertical translation. Fig.6-8

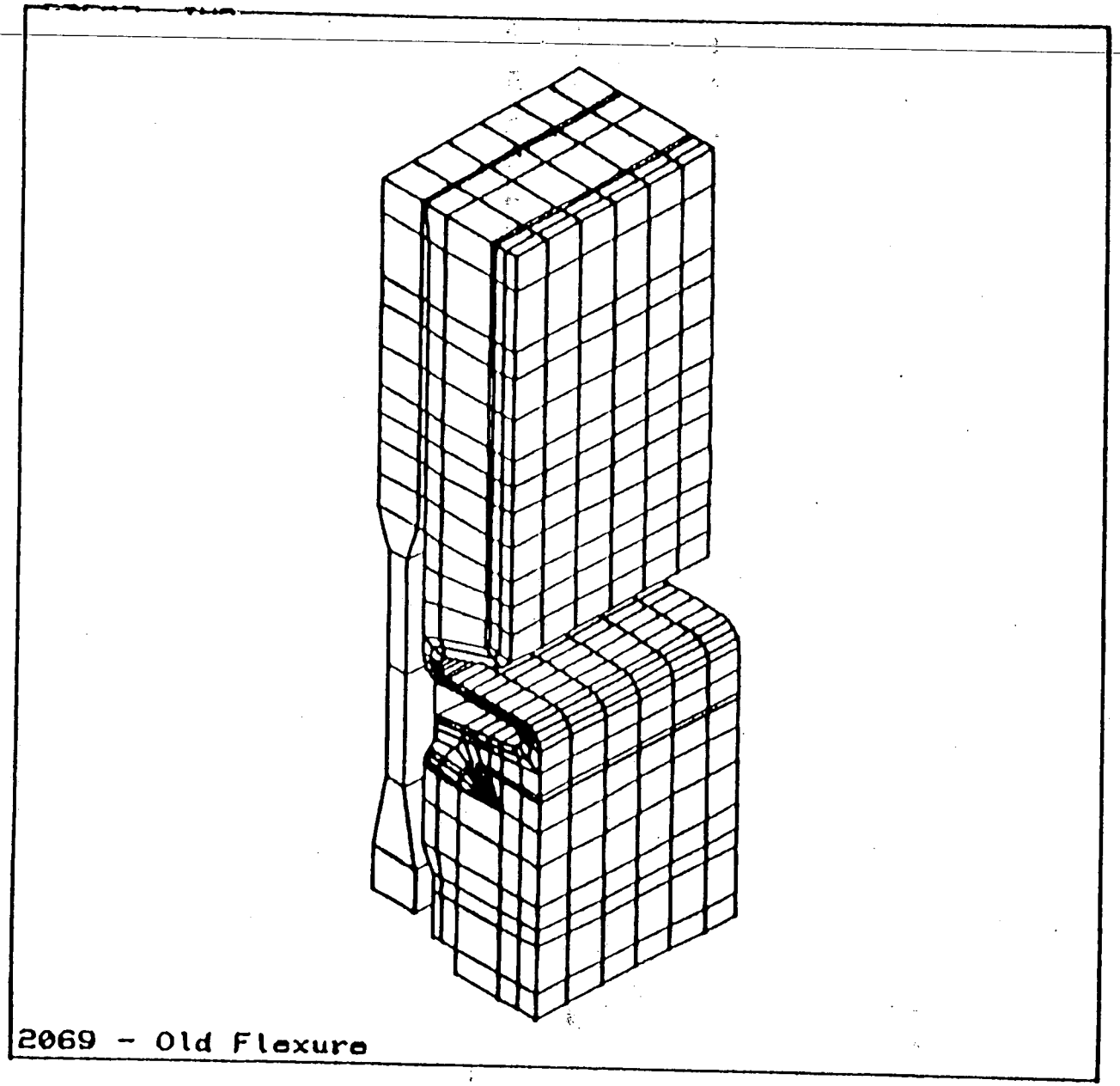

FIGURE 6-4 OLD FLEXURE - FINITE ELEMENT MODEL

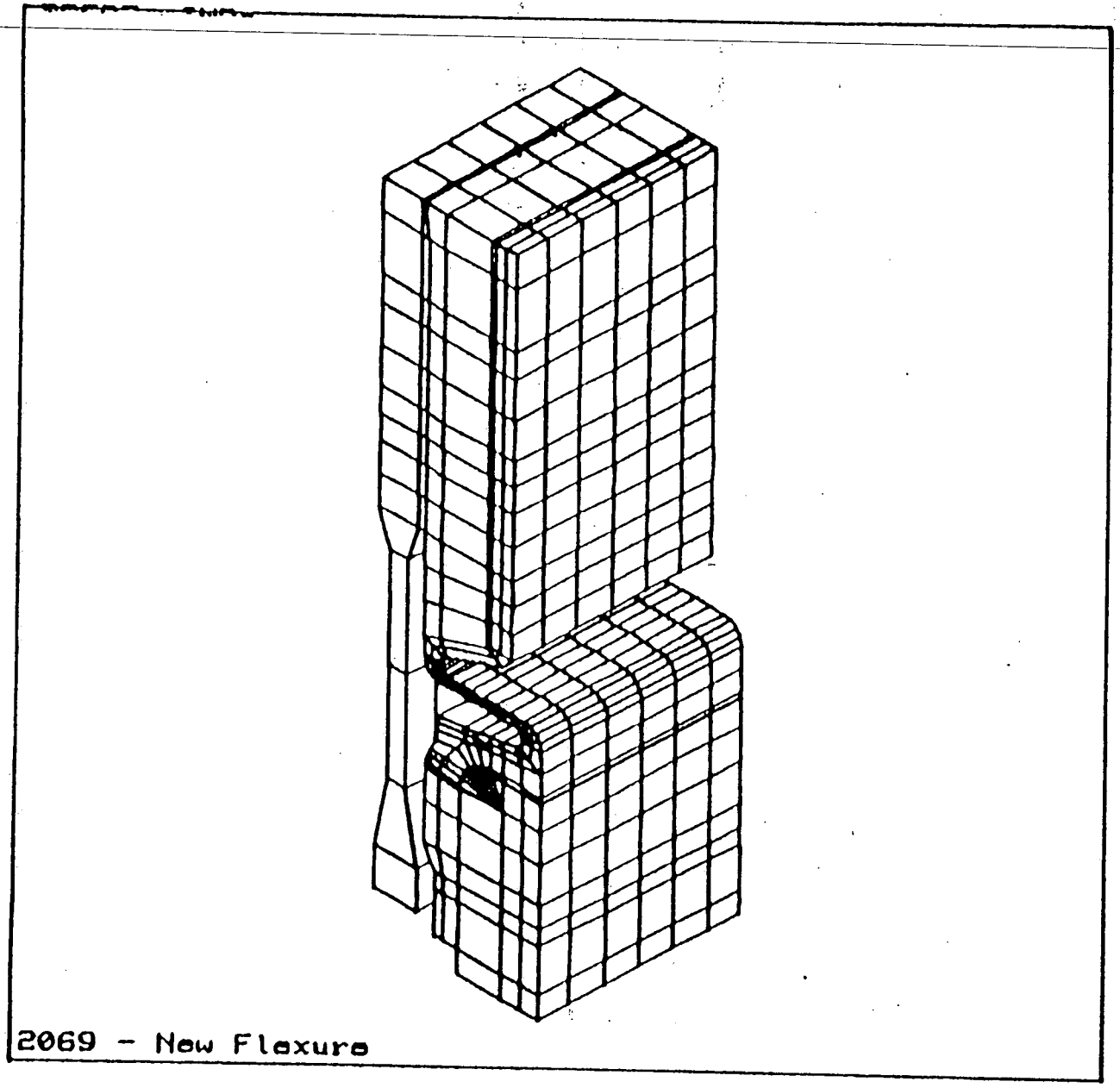

FIGURE 6-5 NEW FLEXURE - FINITE ELEMENT MODEL

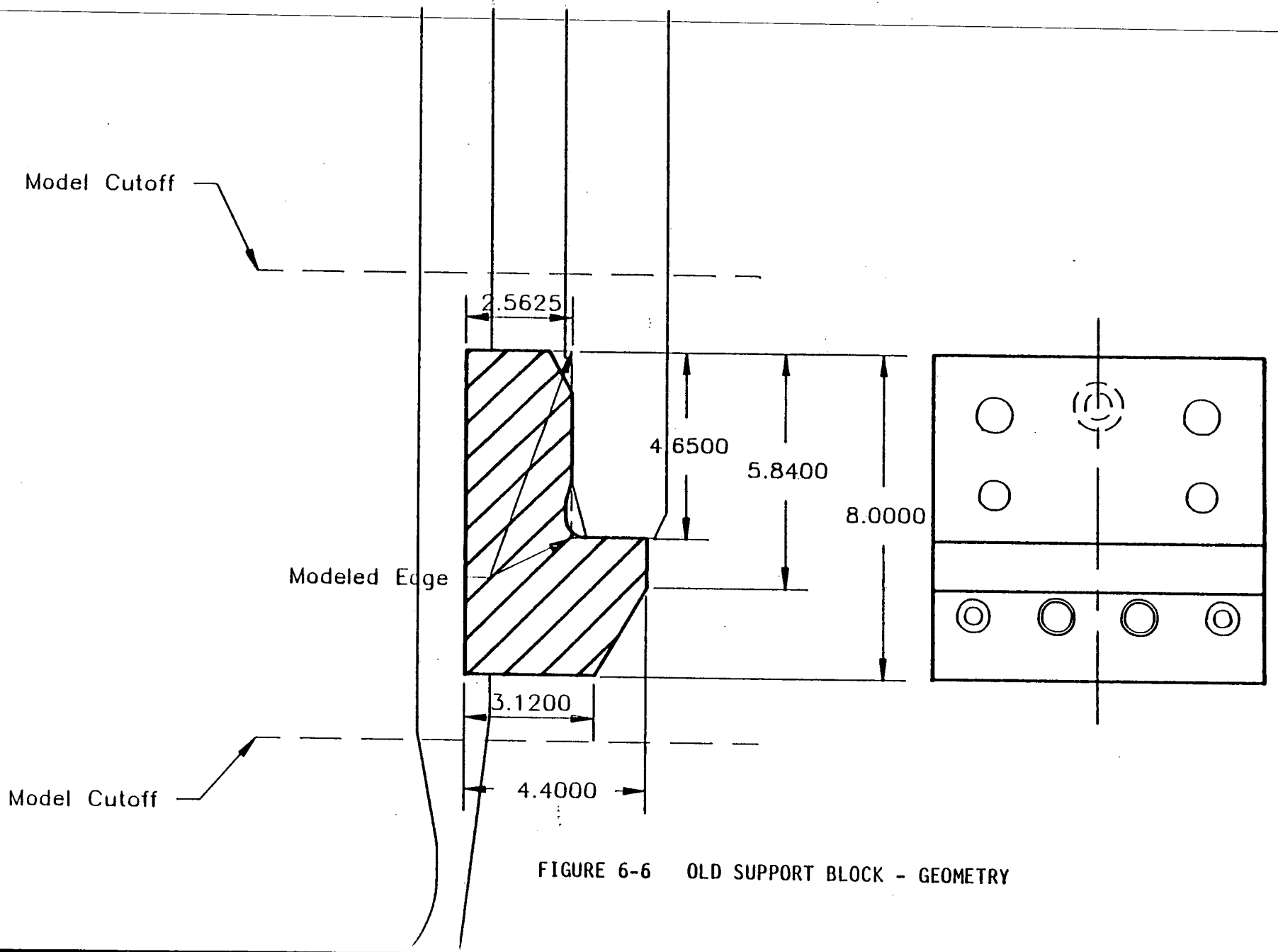

FIGURE 6-6 OLD SUPPORT BLOCK - GEOMETRY

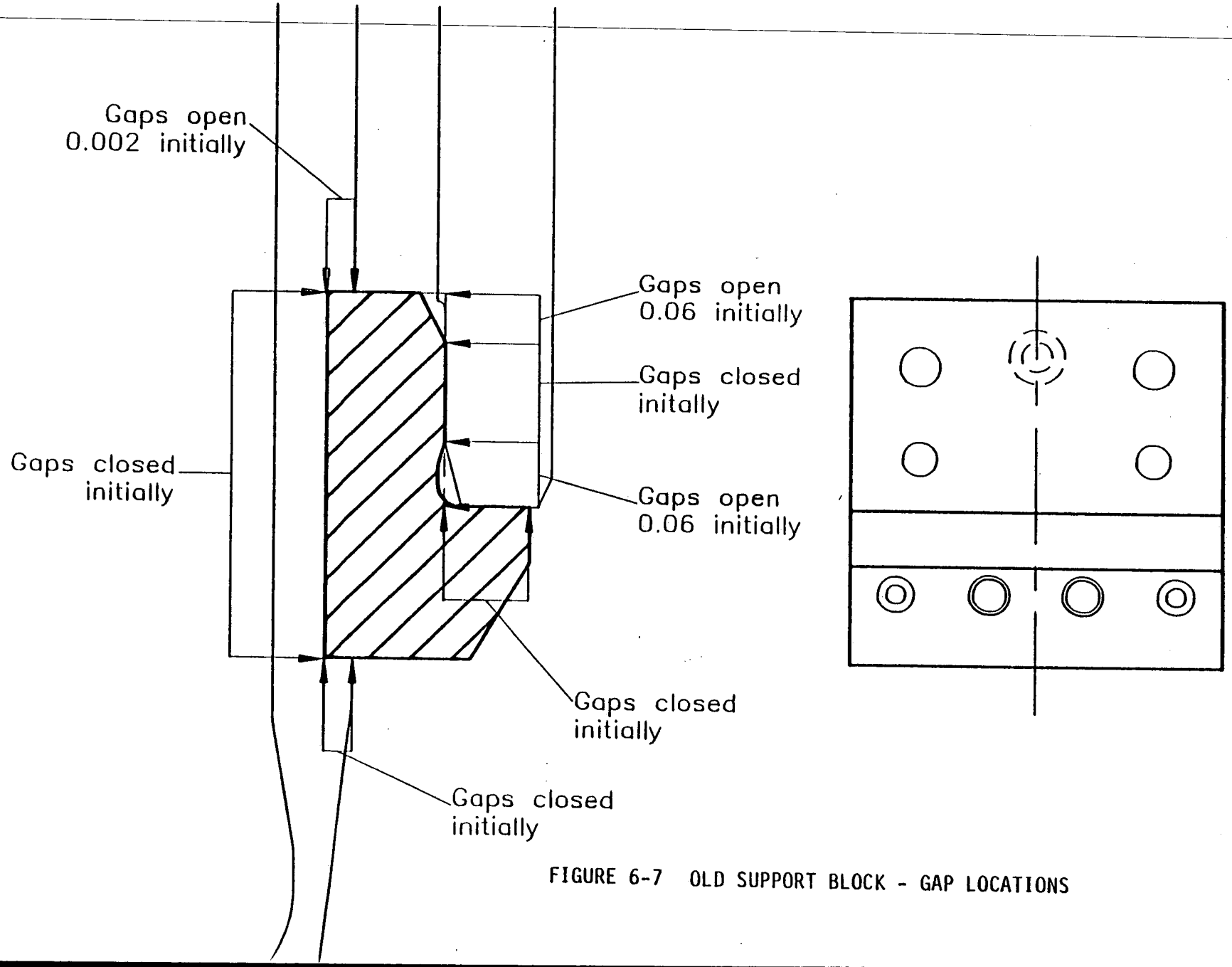

FIGURE 6-7 OLD SUPPORT BLOCK - GAP LOCATIONS

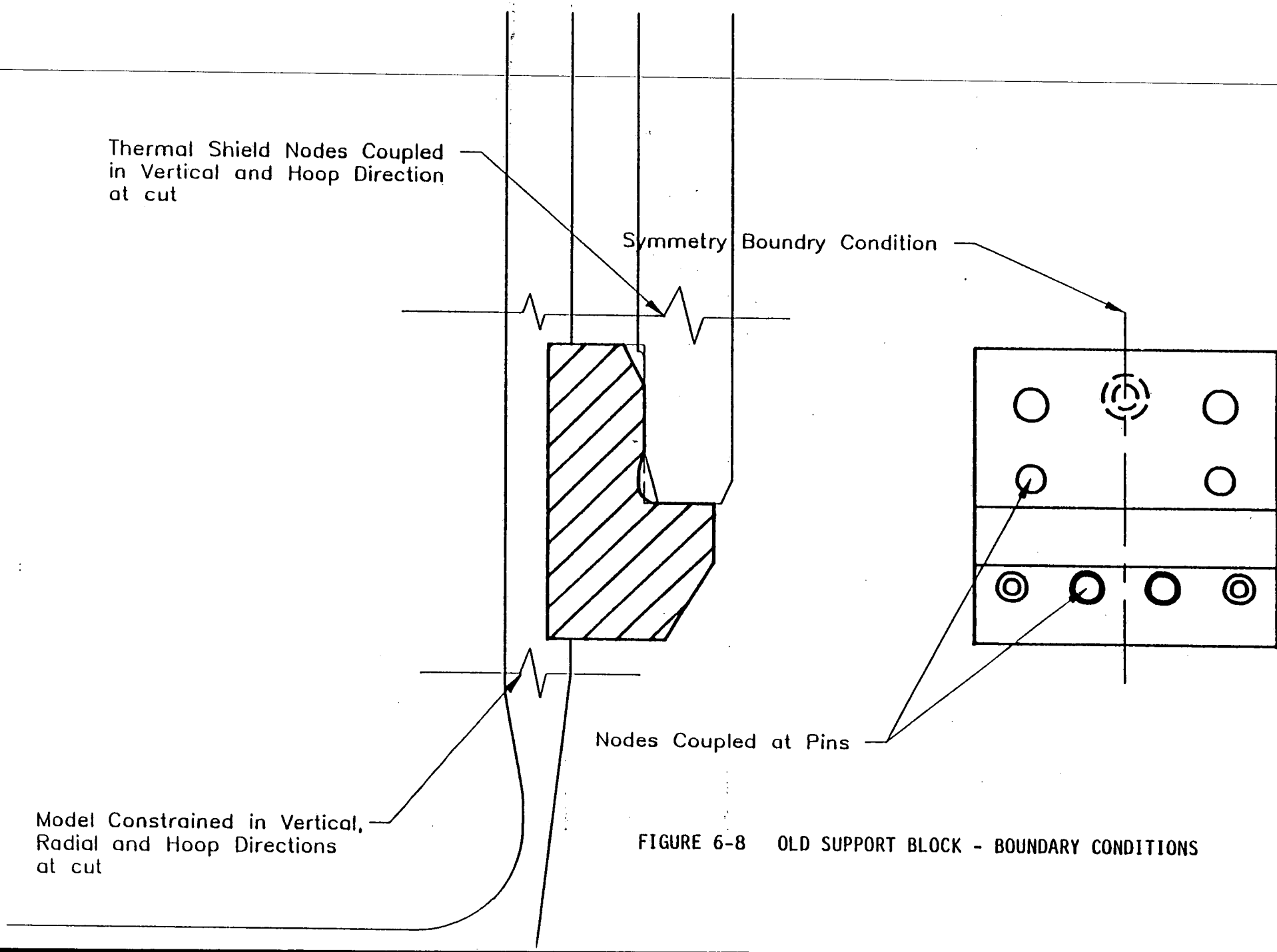

FIGURE 6-8 OLD SUPPORT BLOCK - BOUNDARY CONDITIONS

shows the boundary conditions used on the original bottom block model. The pins that secure the block to the core barrel and the shield to the block are represented by coupling the appropriate nodes in the vertical and hoop directions.

The model used to analyze the original upper flexure is a three-dimensional model of the upper flexure, core barrel and thermal shield. The upper flexure, core barrel and thermal shield are made up of ANSYS STIF 45 three-dimensional isoparametric elements. The bolts that attach the top of the flexure to the core barrel are represented by STIF 4 three-dimensional elastic beam elements. These elements are given an initial strain to simulate preload. Figures 6-9a and b contain the dimensions used for the upper flexure model.

Three-dimensional gap elements, STIF 52, are used in the interface between the flexure and the core barrel. See Figure 6-10 for the gap locations and initial status.

To make loading the model consistent with the overall three-dimensional model, a node was placed at the centroid of the bottom of the thermal shield. Rigid links connect this node to all other nodes on the bottom face of the thermal shield. ANSYS STIF 4 three-dimensional elastic beams were used as the rigid links. These beams were given high cross-sectional areas and moments of inertia.

The bottom of the core barrel in the submodel was constrained from translating in all directions. To simulate the pins that secure the flexure to the core barrel and the thermal shield to the flexure, the corresponding nodes were coupled in the vertical and hoop directions. See Figure 6-11 for the boundary conditions used in the existing design flexure model.

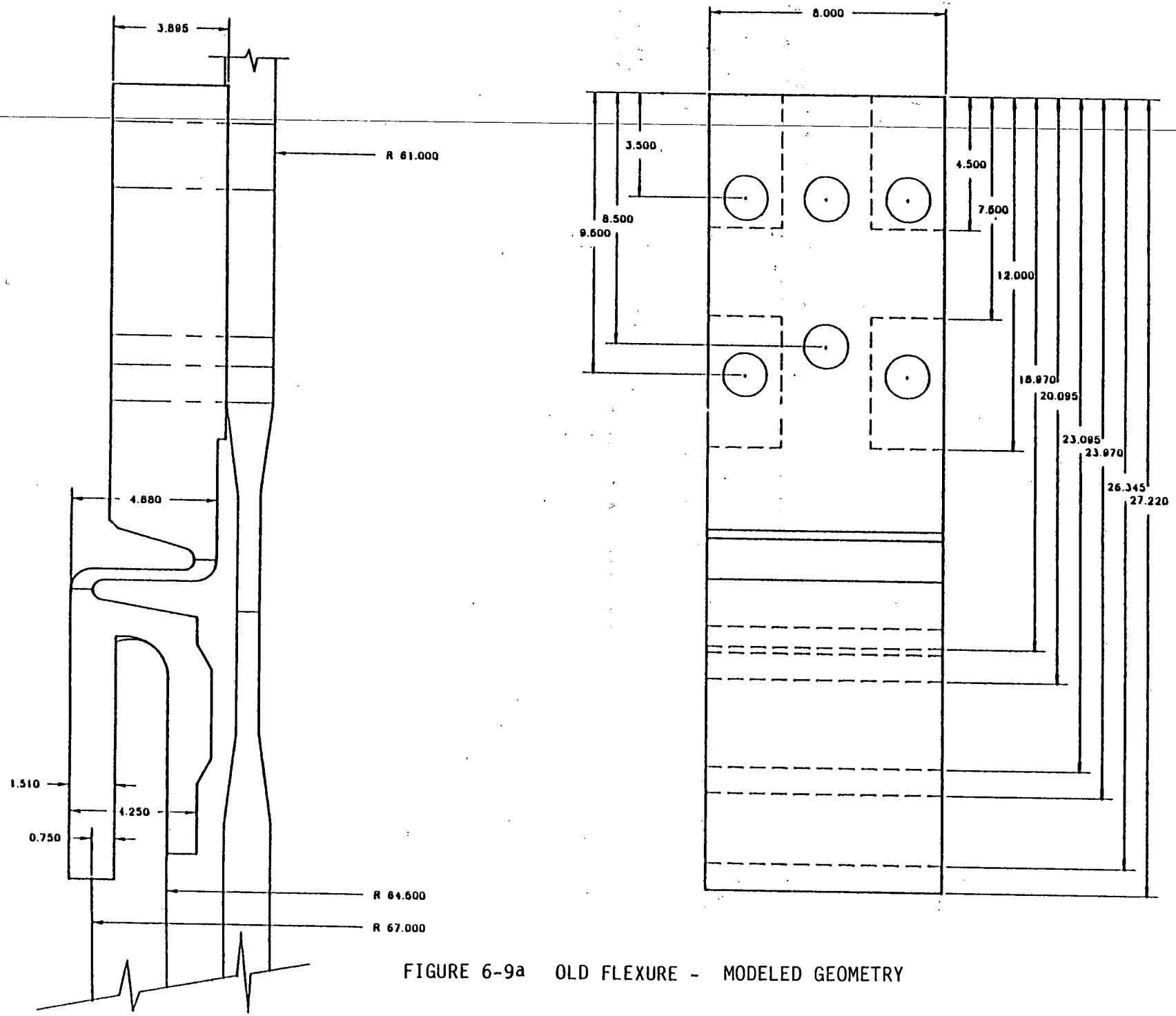

FIGURE 6-9a OLD FLEXURE - MODELED GEOMETRY

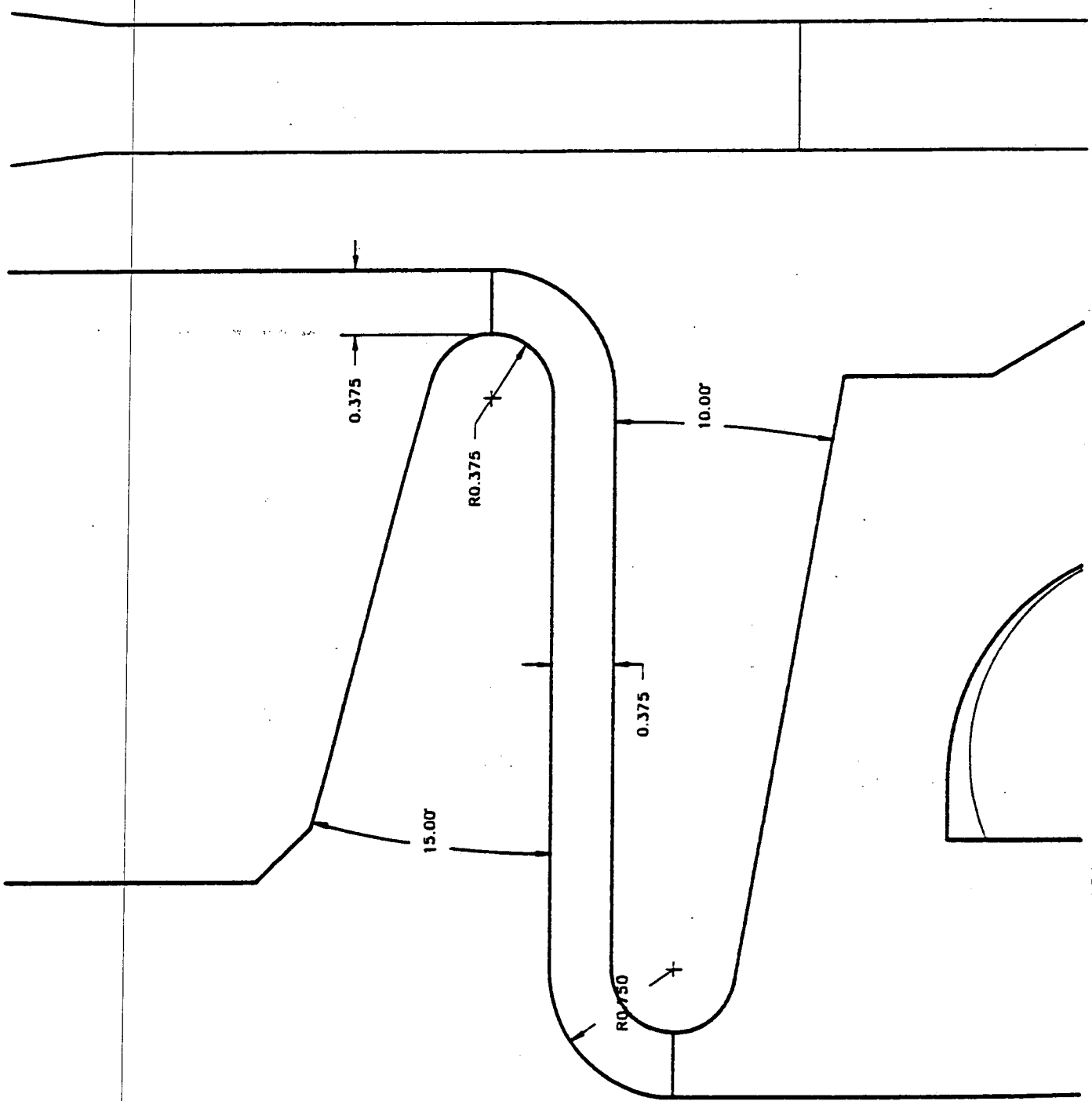

FIGURE 6-9b OLD FLEXURE - MODELED GEOMETRY OF FLEXURE WEB

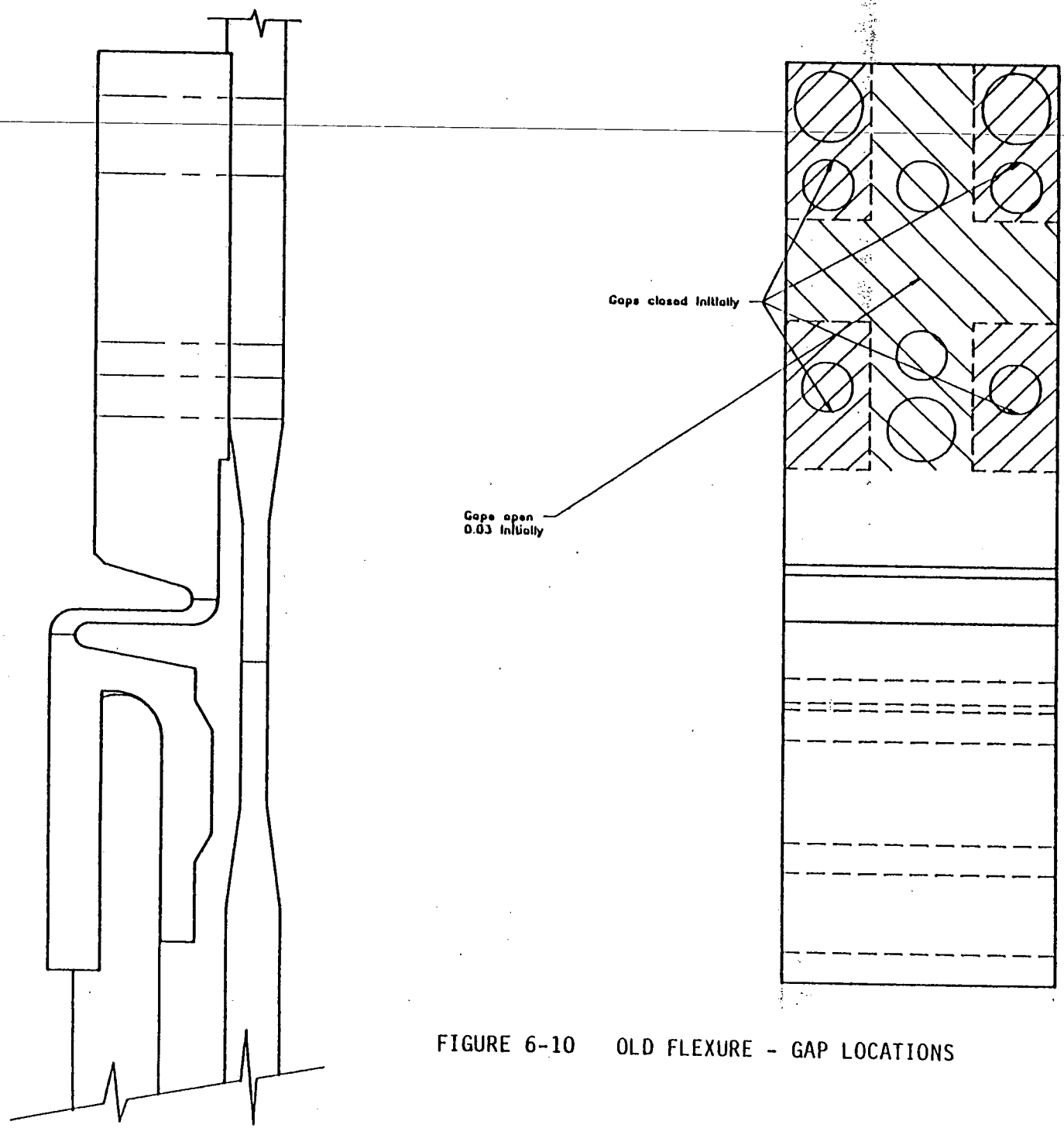

FIGURE 6-10 OLD FLEXURE - GAP LOCATIONS

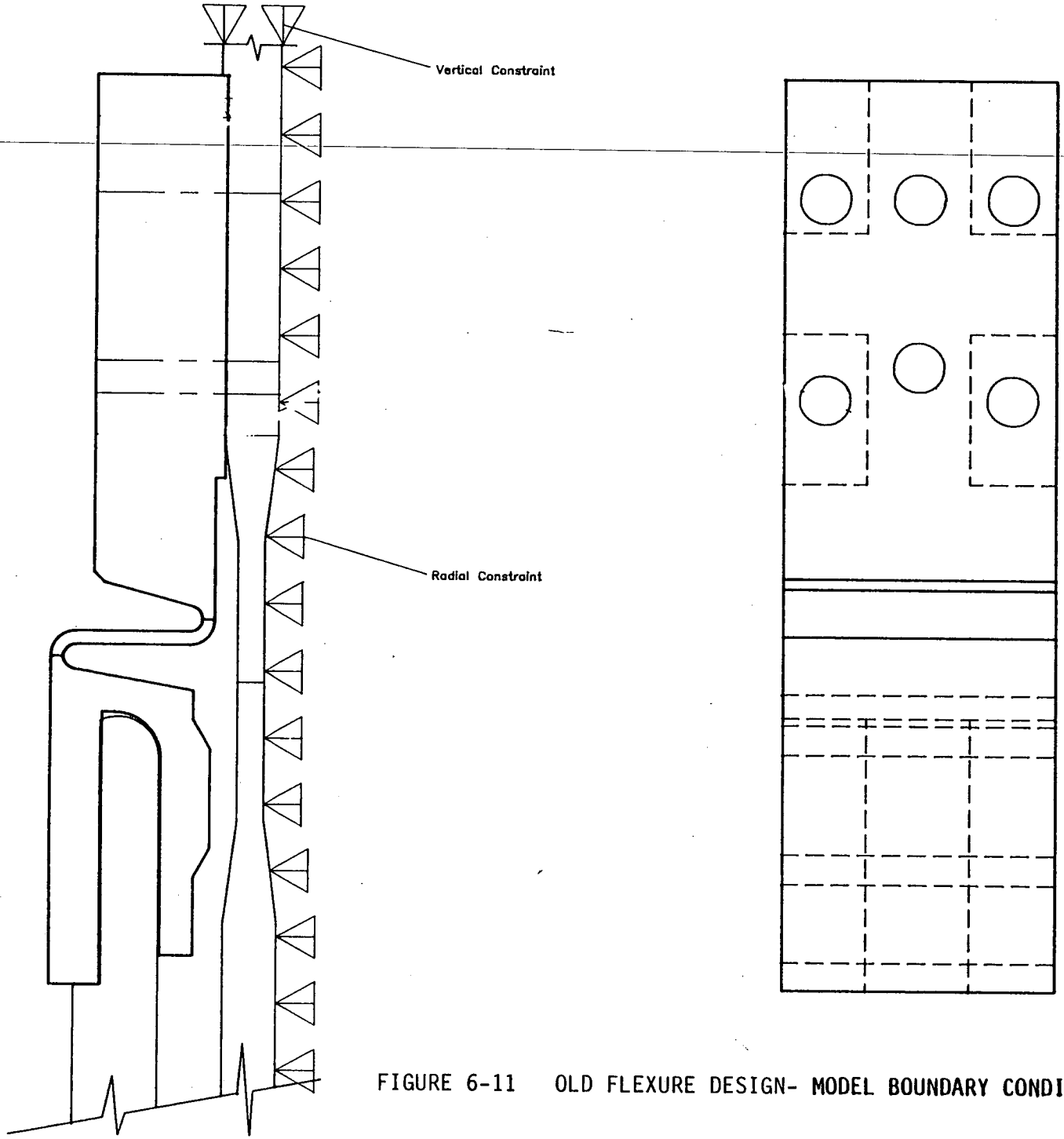

FIGURE 6-11 OLD FLEXURE DESIGN- MODEL BOUNDARY CONDITIONS

The new bottom block was modeled in a manner similar to the old block using the same type of ANSYS elements. Figure 6-12 shows the dimensions used for this model, while Figure 6-13 shows the gap locations and their initial status.

As before, the model uses a symmetry plane along the center of the block because only half of the block was modeled. Figure 6-14 shows the boundary conditions used on the new bottom block model.

The model used to analyze the new upper flexure is a three-dimensional model of the upper flexure, core barrel and thermal shield. The modeling was similar to that of the old design using the same type of ANSYS elements. Figures 6-15a and b contain the dimensions used for the upper flexure model. Figure 6-16 shows the gap locations and initial status, while Figure 6-17 shows the boundary conditions used in the new design flexure model.

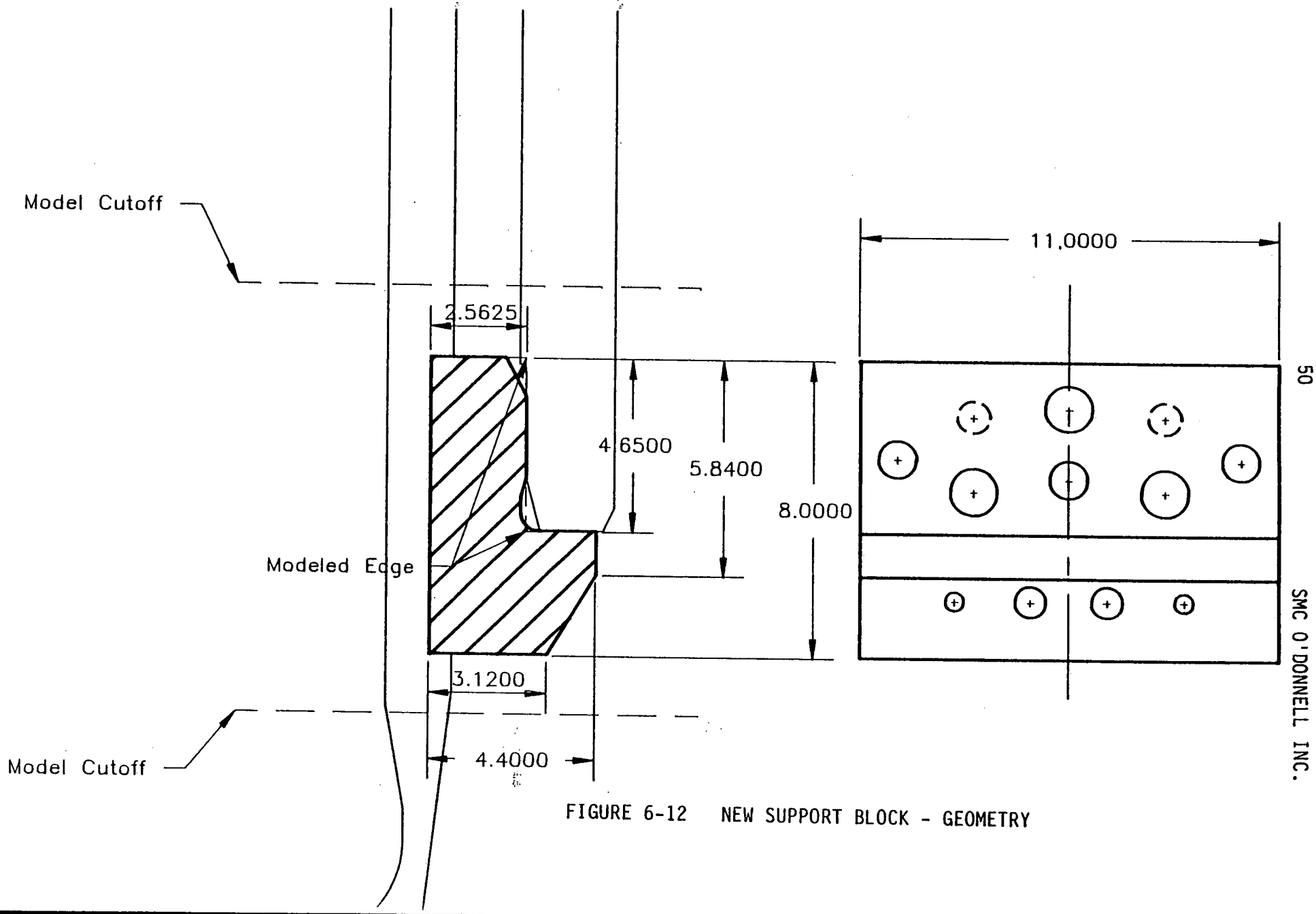

FIGURE 6-12 NEW SUPPORT BLOCK - GEOMETRY

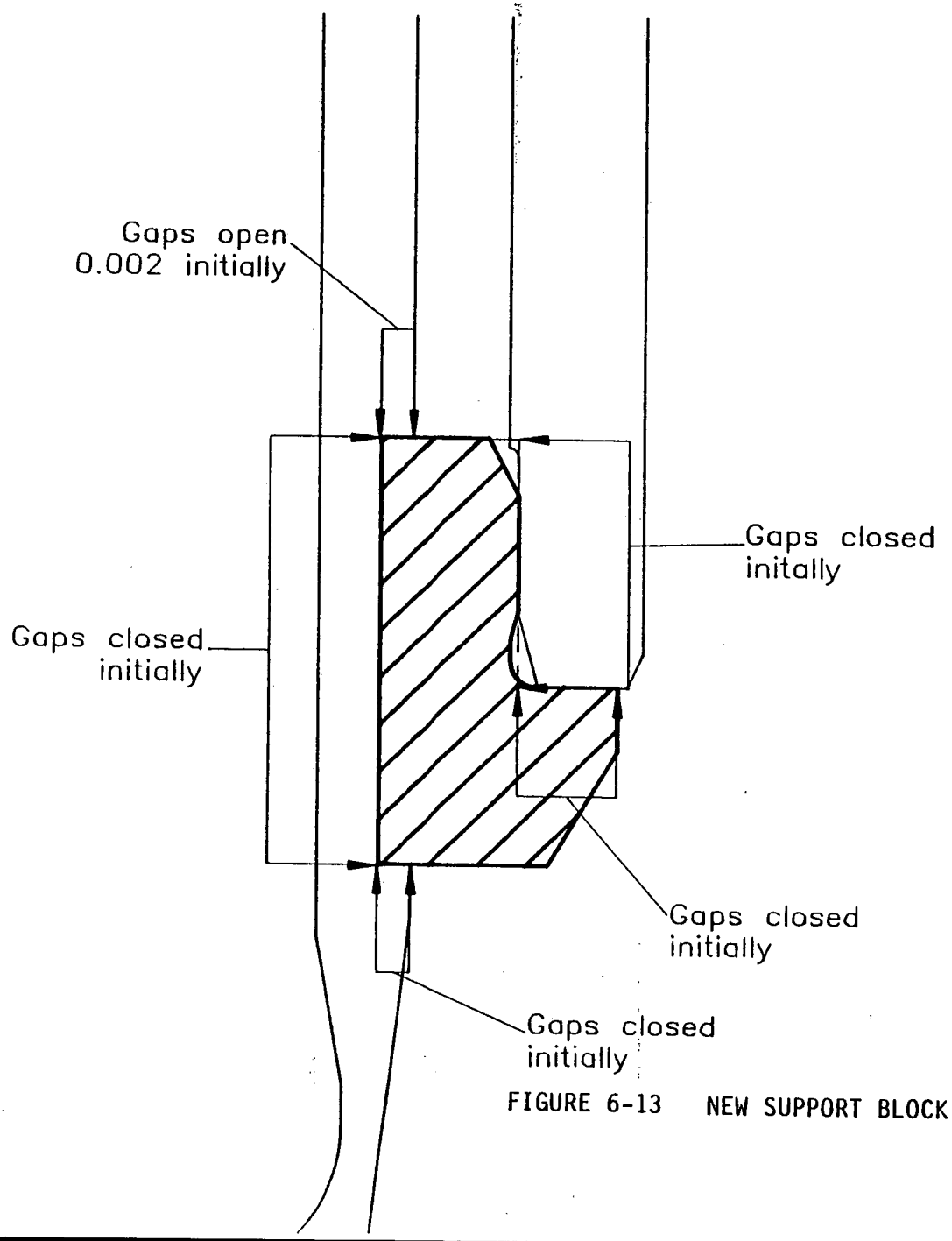

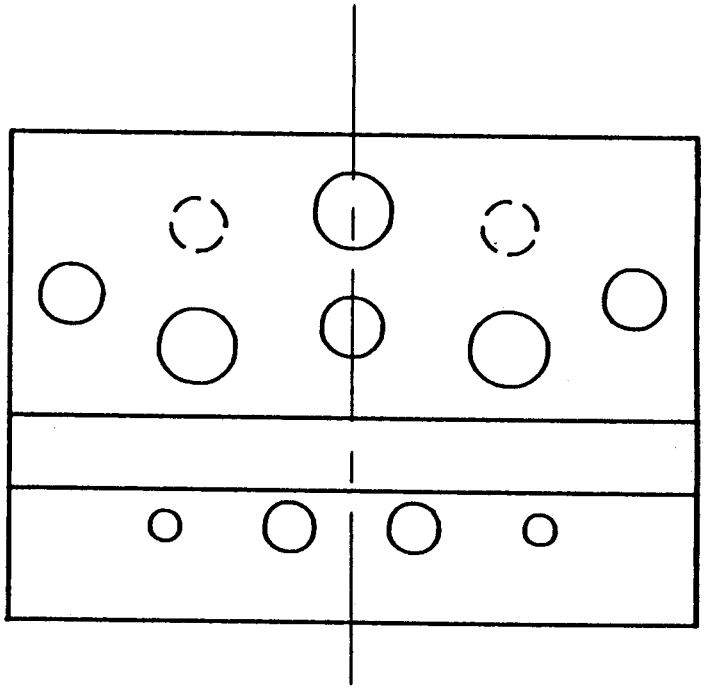

FIGURE 6-13 NEW SUPPORT BLOCK - GAP LOCATIONS

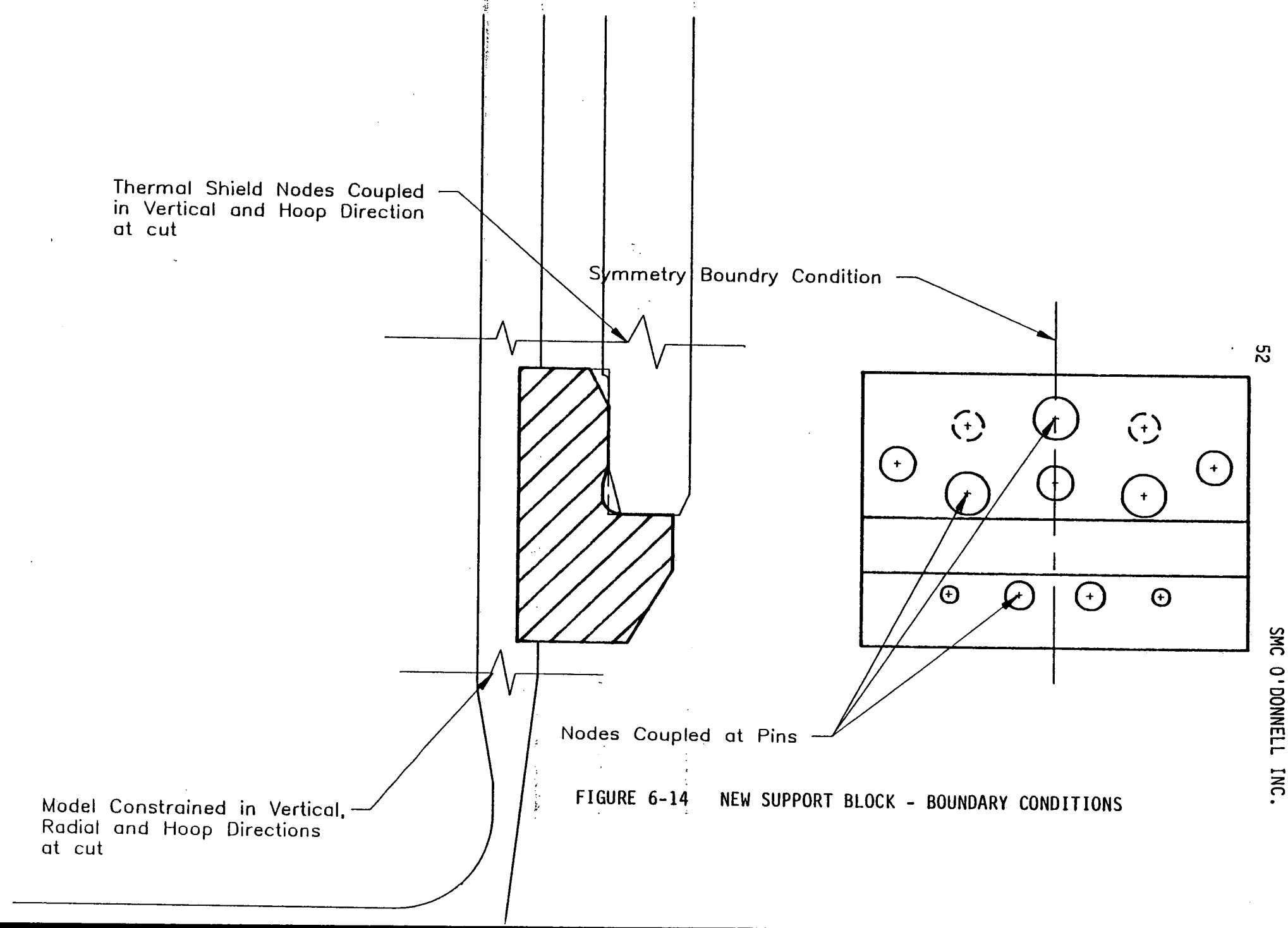

FIGURE 6-14 NEW SUPPORT BLOCK - BOUNDARY CONDITIONS

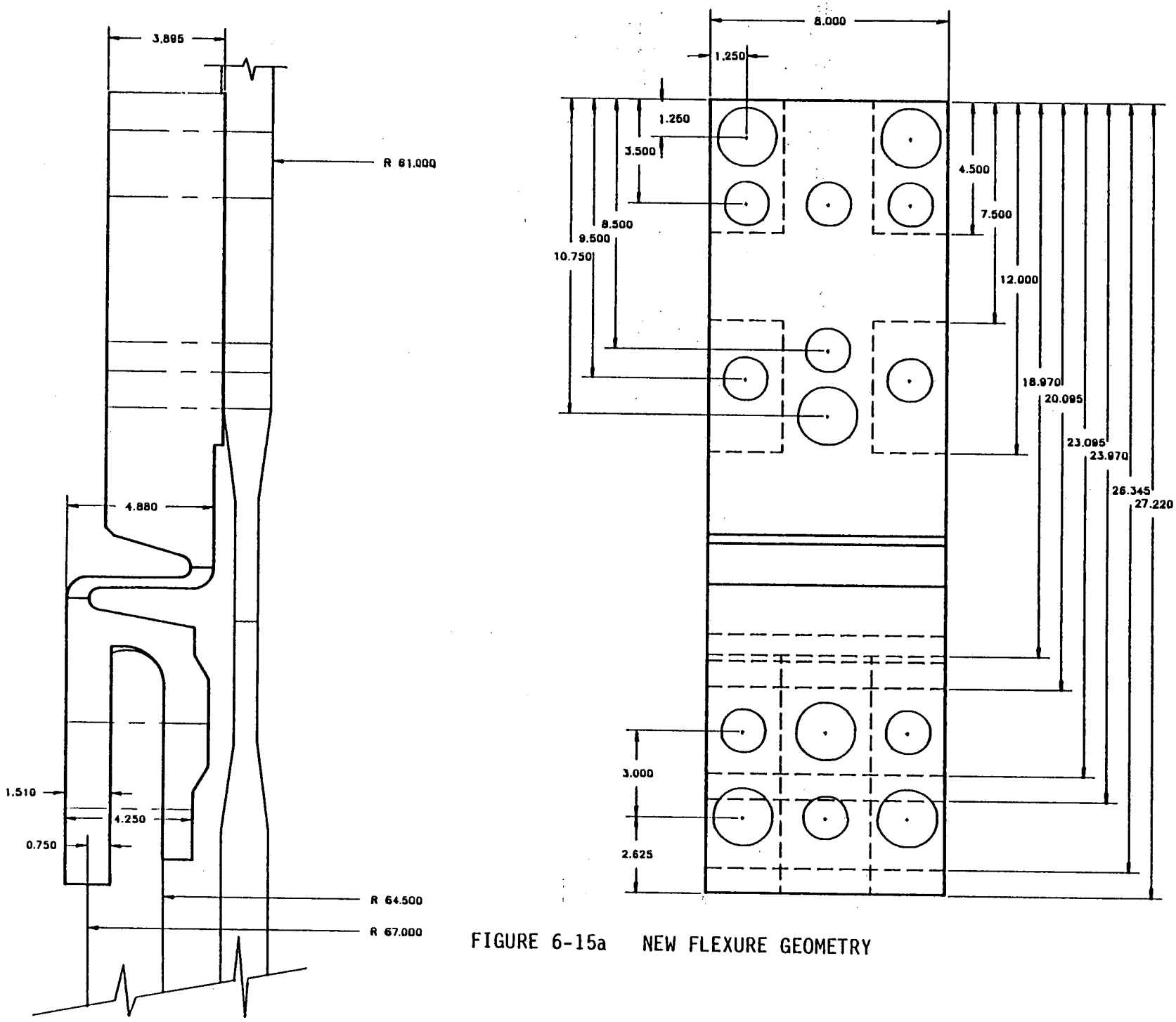

FIGURE 6-15a NEW FLEXURE GEOMETRY

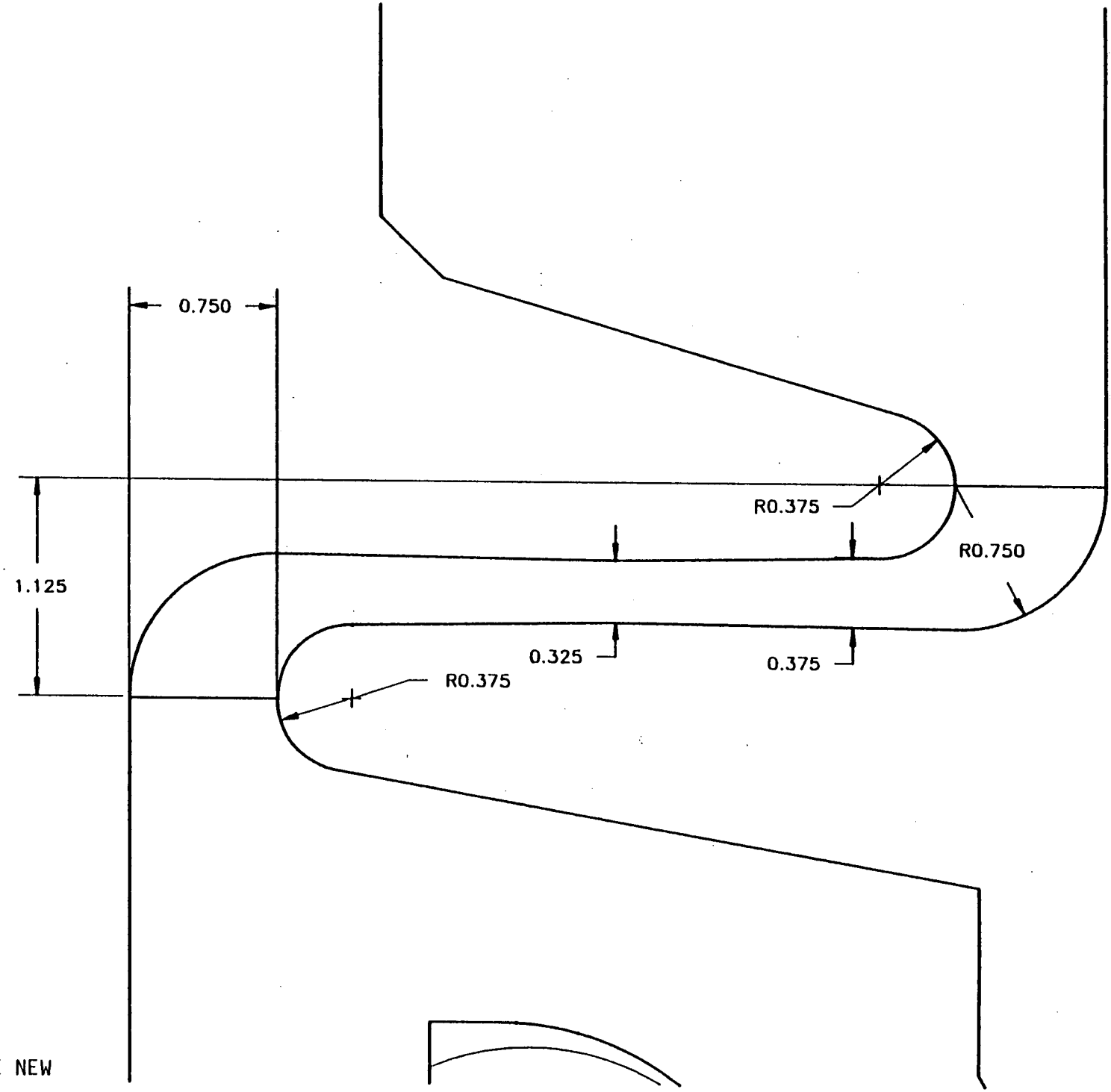

FIGURE 6-15b
GEOMETRY OF THE NEW
FLEXURE WEB

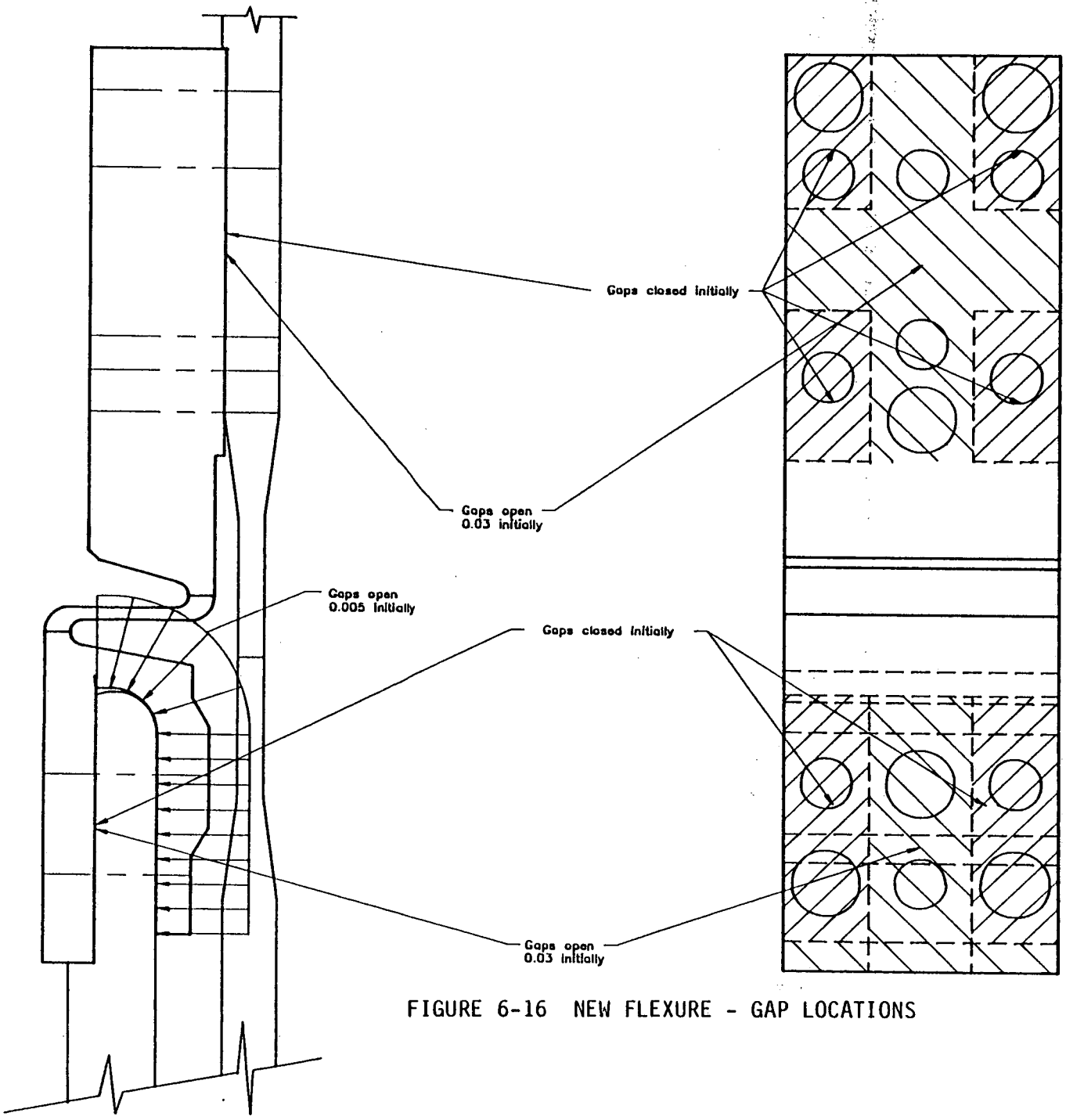

FIGURE 6-16 NEW FLEXURE - GAP LOCATIONS

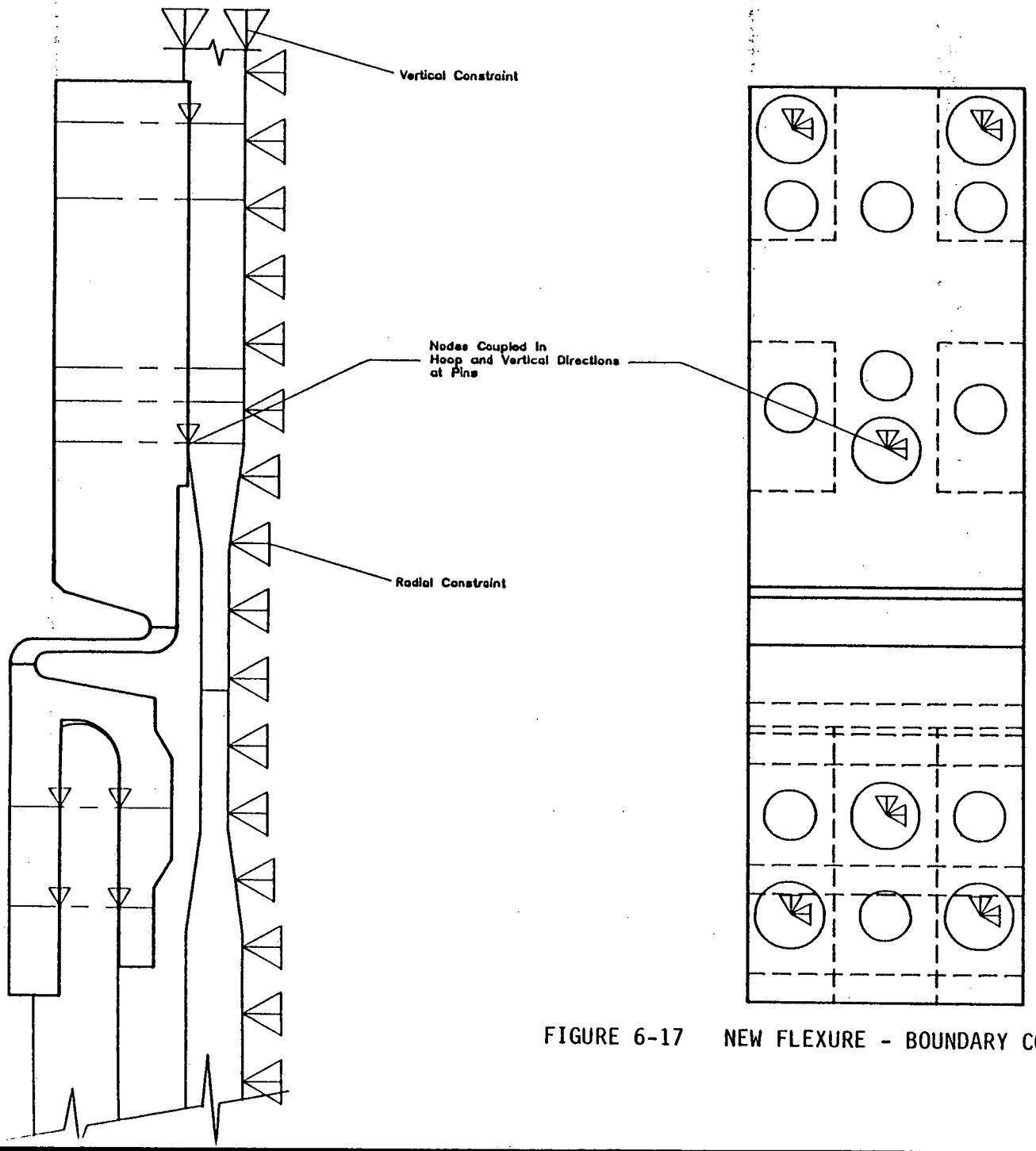

FIGURE 6-17 NEW FLEXURE - BOUNDARY CONDITIONS

7.0 TURBULENT FORCING FUNCTION

There are some data available in the literature on dynamic pressure measurements in the downcomer of a PWR [12, 13, 14]. The random pressure fluctuations were found to decrease as the frequency increased. The plot of the normalized pressure spectral density (PSD) data showed an exponentially decaying trend with increasing frequency [13]. The general empirical equation for the frequency range of interest here was given as:

$$x = Ae^{-BF} \tag{3}$$

where

$x = \frac{G(f)}{\rho^2 u^4 (\delta/u)}$ is the normalized PSD, and

$F = \frac{f\delta}{u}$ is the reduced frequency

Here,

ρ = density of the fluid
u = flow velocity in the annulus gap
δ = gap width of the downcomer
A,B = constants

Combining these equations, the pressure spectral density can be written as:

$$G(f) = K(\frac{\rho u^2}{2})^2 e^{-Cf} \tag{4}$$

where K and C are appropriately adjusted constants.

The dynamic pressure is related to the local fluid velocity as follows:

$$\bar{p} = C_p(\frac{1}{2} \rho u^2) \tag{5}$$

where

$\bar{p}$ = rms pressure
C_p = rms pressure coefficient

Equations (4) and (5) are used for evaluating the constants, since

$$\int_0^\infty G(f)\, df = \bar{p}^2 \tag{6}$$

Substituting from (4) and (5) gives:

$$K \int_0^\infty e^{-Cf}\, df = C_p^{\,2} \tag{7}$$

or

$$K = C\, C_p^{\,2} \tag{8}$$

Thus, the pressure PSD is given by:

$$G(f) = C\, C_p^{\,2} \left(\frac{\rho u^2}{2}\right)^2 e^{-Cf} \tag{9}$$

Based on the pressure measurements made in [13], the value of the rms pressure coefficient C_p was found to vary from 0.22 to 0.38 with a mean of 0.27. This mean value was used in the present analysis. Note that the effect of varying C_p would be to vary the pressure spectral density and hence the RMS response. However, since the model is qualified by correlating the analytically determined response to the actual operating data, this would only result in a different scale factor for use in evaluating the new design.

The value of C used in this analysis was also obtained from approximating the mean of the data given in [13]. The value of C was determined to be .048. The normalized PSD function $G(f)/(\rho\frac{u^2}{2})^2$ is plotted in Figure 7-1.

The local velocities for use in (9) were obtained from a three-dimensional flow model of the SONGS Unit 1 core barrel/thermal shield, using the FLOW3D Code. Static pressure cases were run for one-pump, two-pumps and three-pumps. Discussions with SCE and Westinghouse, however, indicated that only the three-pump case was realistic. Thus, the velocities were based on the three-pump case. A brief description of the FLOW3D model with the results of the three pump case is given in Appendix A.

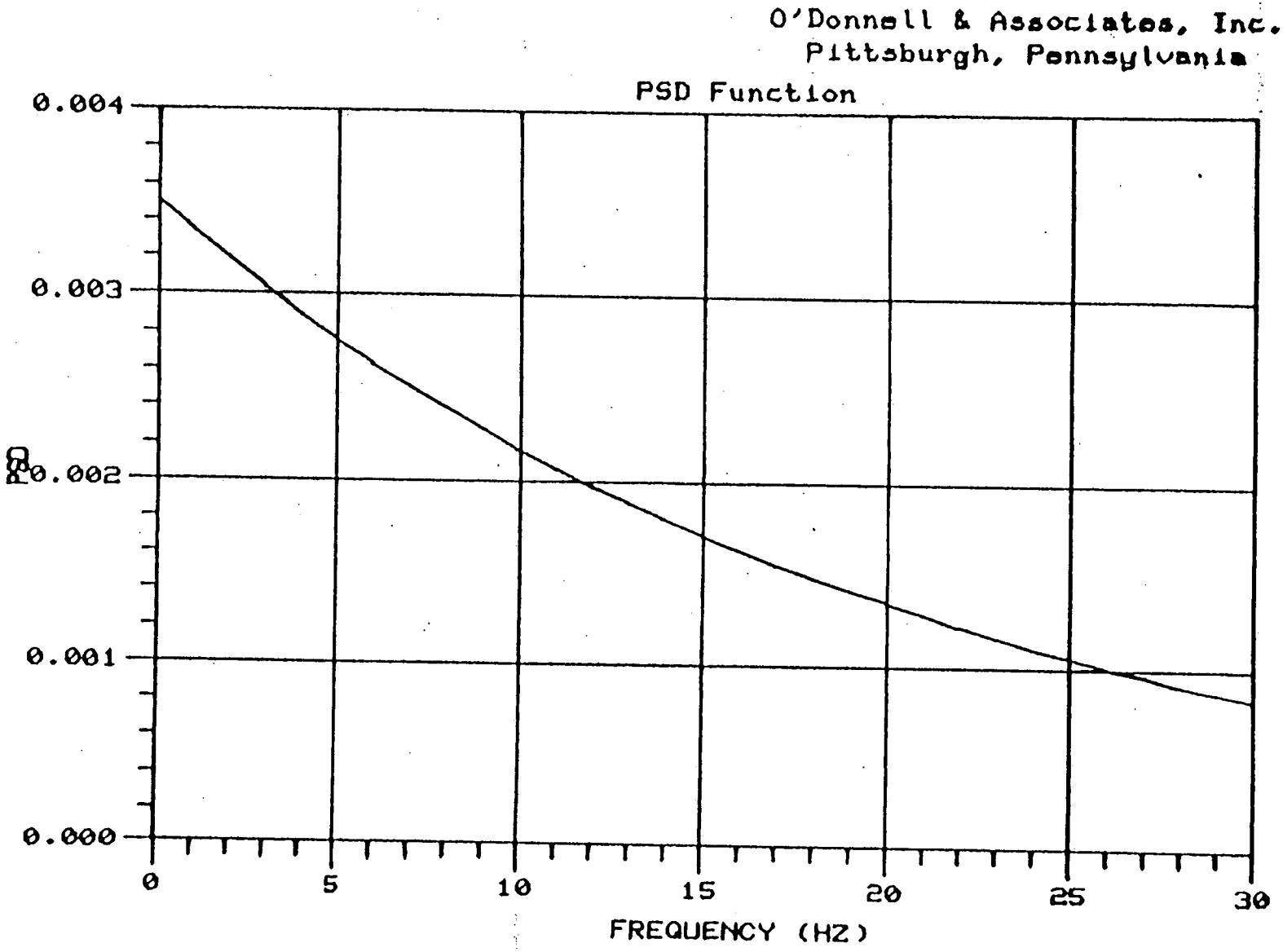

FIGURE 7-1 PSD FUNCTION

8.0 MODAL ANALYSIS

The ANSYS finite element program was used for performing the modal analysis of the thermal shield and core barrel. The finite element model used has been discussed in the previous section. Both the new support design as well as the old support design were analyzed.

Typical mode shapes and natural frequencies obtained from the modal analysis of the core barrel-thermal shield with the old support design are shown in Figures 8-1 through 8-4. The mode shapes that are of interest and are included in the subsequent random vibration analysis are the core barrel and thermal shield beam modes (n = 1) and the thermal shield shell modes corresponding to n = 2 and n = 3.

The natural frequencies corresponding to these mode shapes were correlated against the measured and analytical frequency data provided by Westinghouse [3].

For the beam mode, the effect of the added mass due to the water between the shells can be estimated from Fritz's equation [15, 16, 17].

$$h_a = \rho \frac{a^2}{b - a} \frac{1}{1 + 12a^2/\ell^2} \quad (10)$$

where

h_a = hydrodynamic mass per unit area

ρ = fluid mass density

a = radius of inner cylinder

b = radius of outer cylinder

ℓ = length of the shell

Alternately, the augmented mass approach where the density of the core barrel/thermal shield is adjusted to obtain the natural frequencies that correlate with the measured/analytical data can be used for the beam mode.

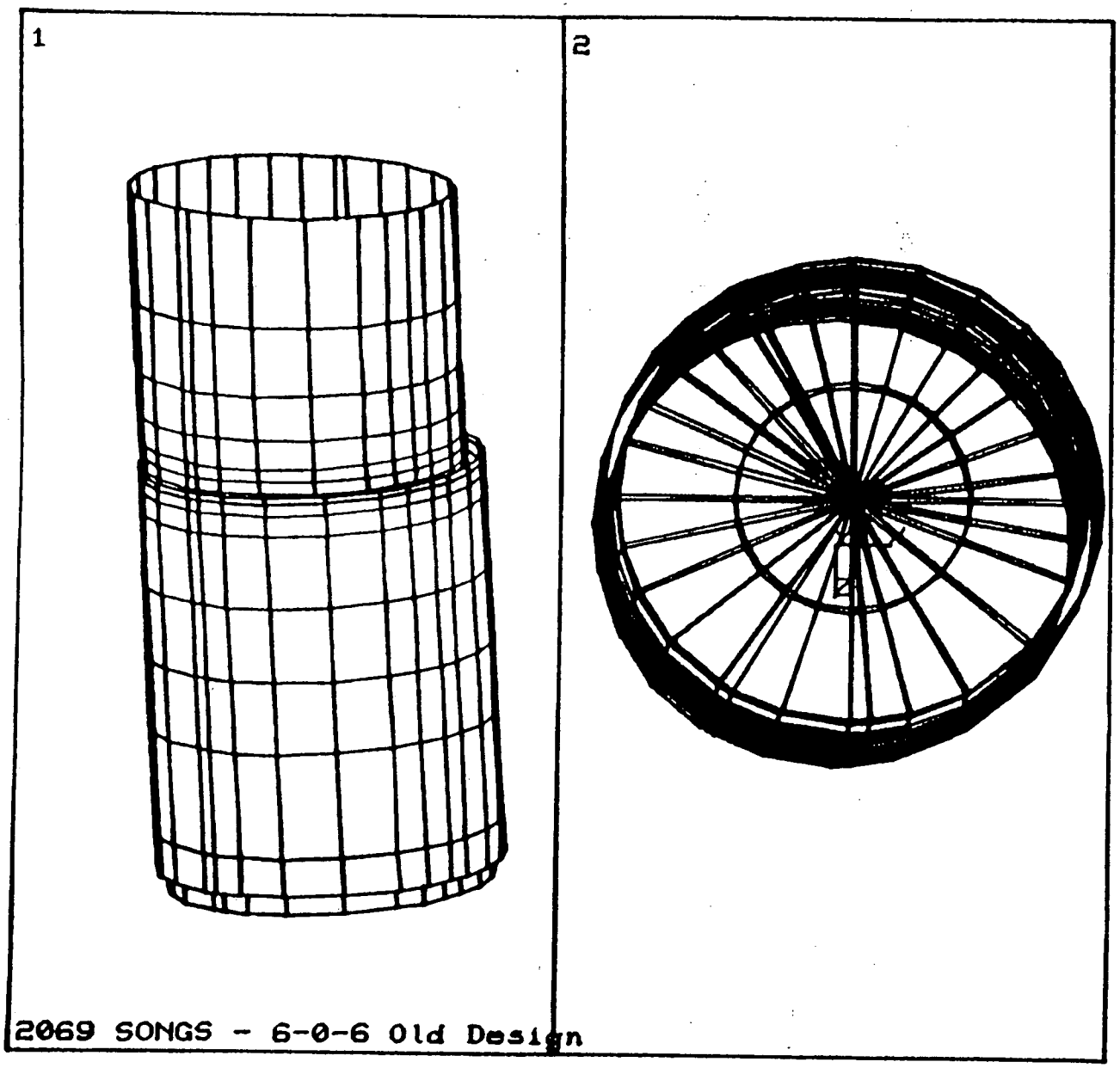

FIGURE 8-1 CORE BARREL BEAM MODE - OLD DESIGN

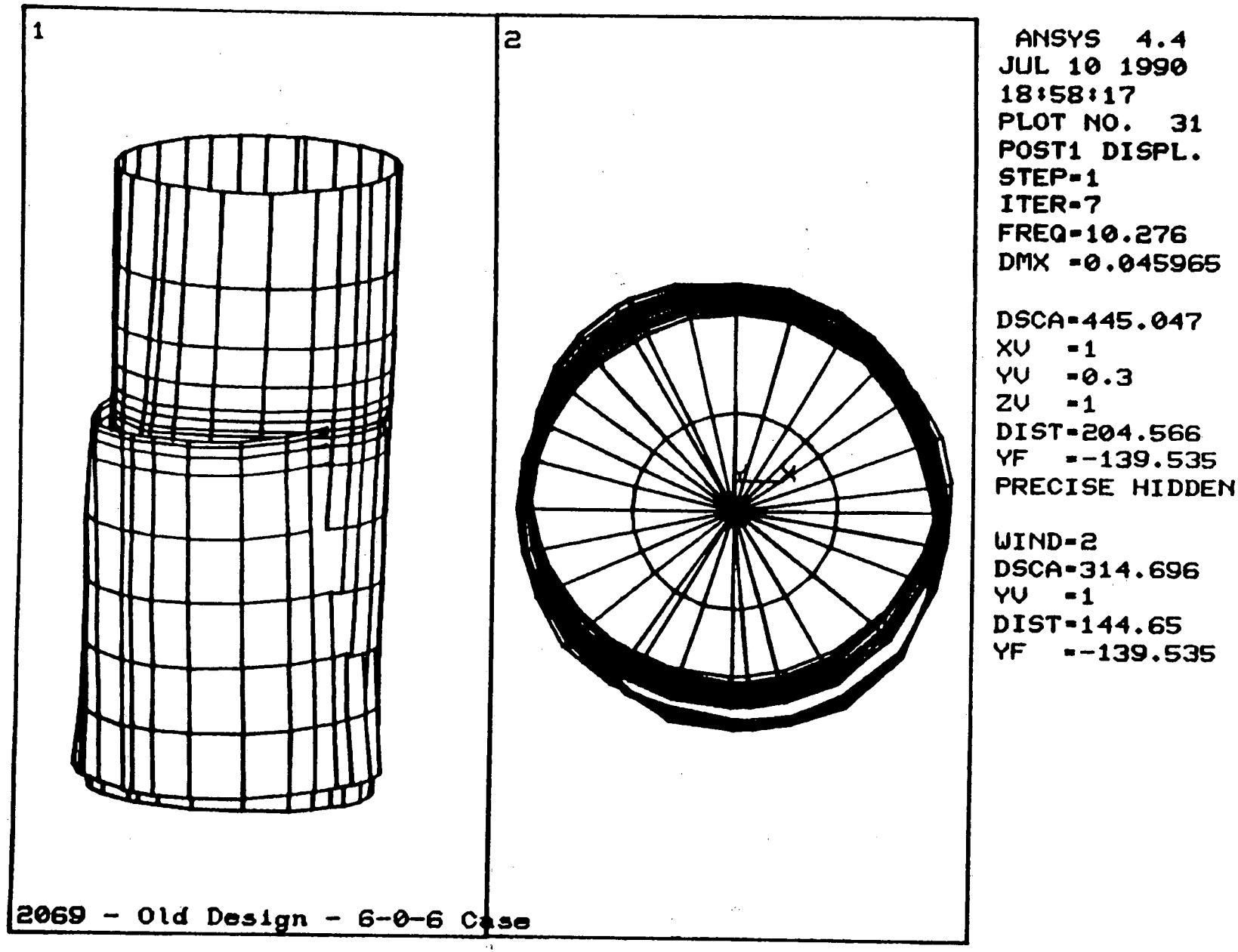

FIGURE 8-2 THERMAL SHIELD BEAM MODE - OLD DESIGN

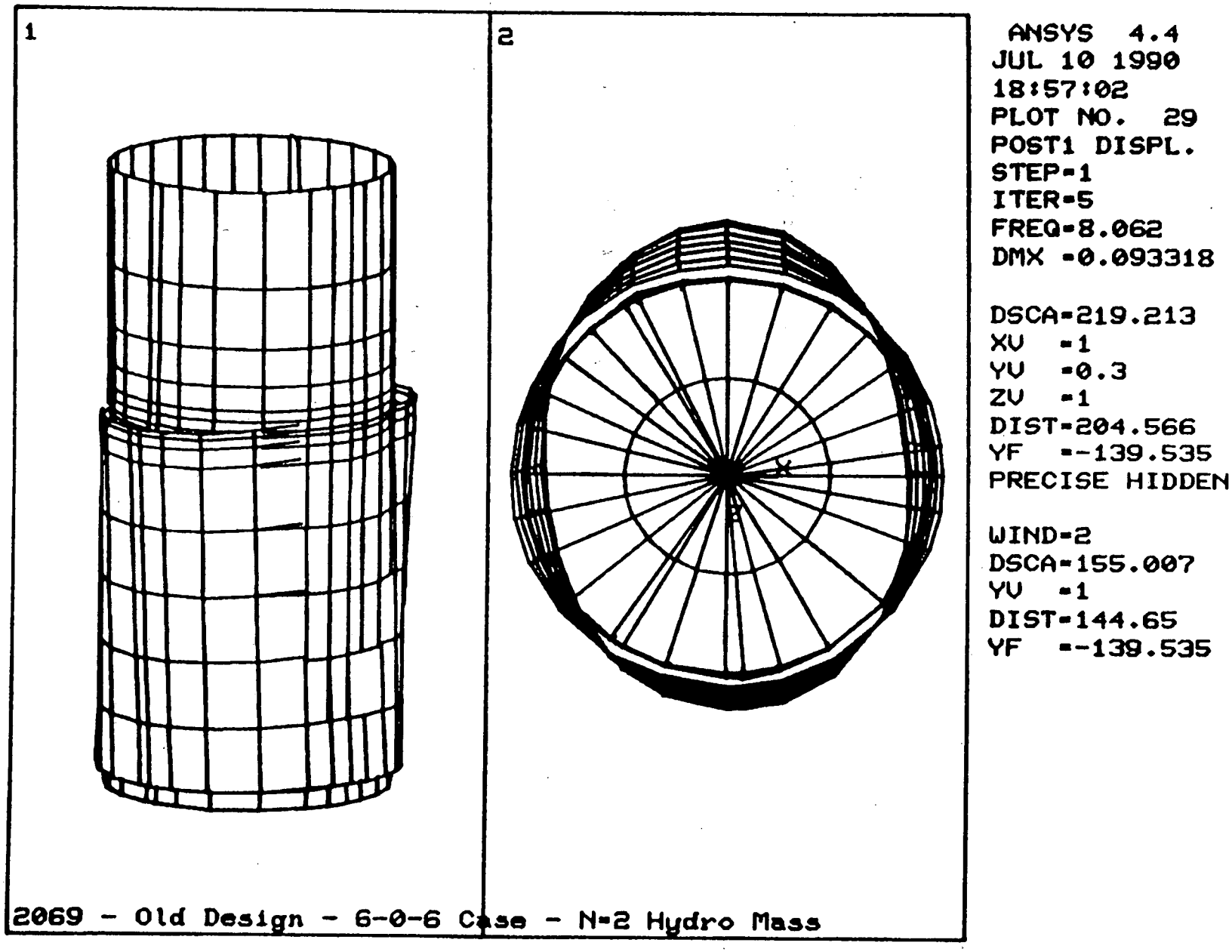

FIGURE 8-3 THERMAL SHIELD SHELL MODE (n = 2) OLD DESIGN

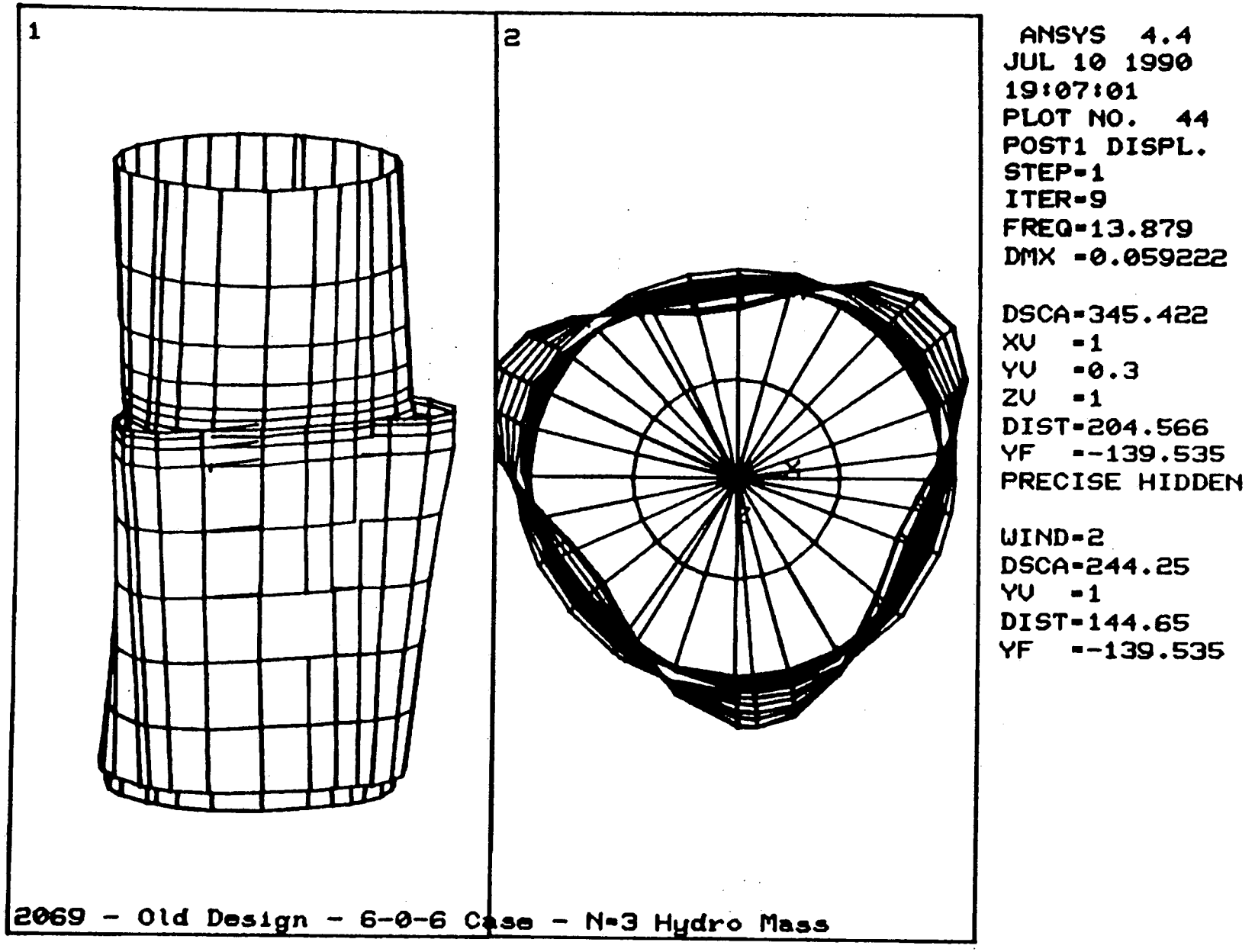

FIGURE 8-4 THERMAL SHIELD SHELL MODE (n = 3) OLD DESIGN

For the shell modes (n = 2 and n = 3) the hydrodynamic mass matrices per unit area were determined from [17]:

$$h_n^a = \frac{\rho a}{n} \frac{b^{2n} + a^{2n}}{b^{2n} - a^{2n}}$$

$$h_n^b = \frac{\rho b}{n} \frac{b^{2n} + a^{2n}}{b^{2n} - a^{2n}}$$

$$h_n^{ab} = \frac{2\rho b}{n} \frac{a^n b^n}{b^{2n} - a^{2n}} \qquad (11)$$

$$h_n^{ba} = \frac{2\rho a}{n} \frac{a^n b^n}{b^{2n} - a^{2n}}$$

where

n = circumferential mode number

The core barrel with its internals is relatively stiff compared to the thermal shield. It vibrates primarily in the beam mode. As a result, there is very little fluid cross-coupling between the core barrel and the thermal shield shell modes. Hence, the off-diagonal terms of the hydrodynamic mass matrices given by equation (11) for n = 2 and n = 3 were appropriately adjusted to give frequencies that were in approximate agreement with the measured frequencies.

The modal analysis for the new design was performed using the same hydrodynamic mass matrices. Typical beam and shell modes for the new design are illustrated in Figures 8-5 through 8-8.

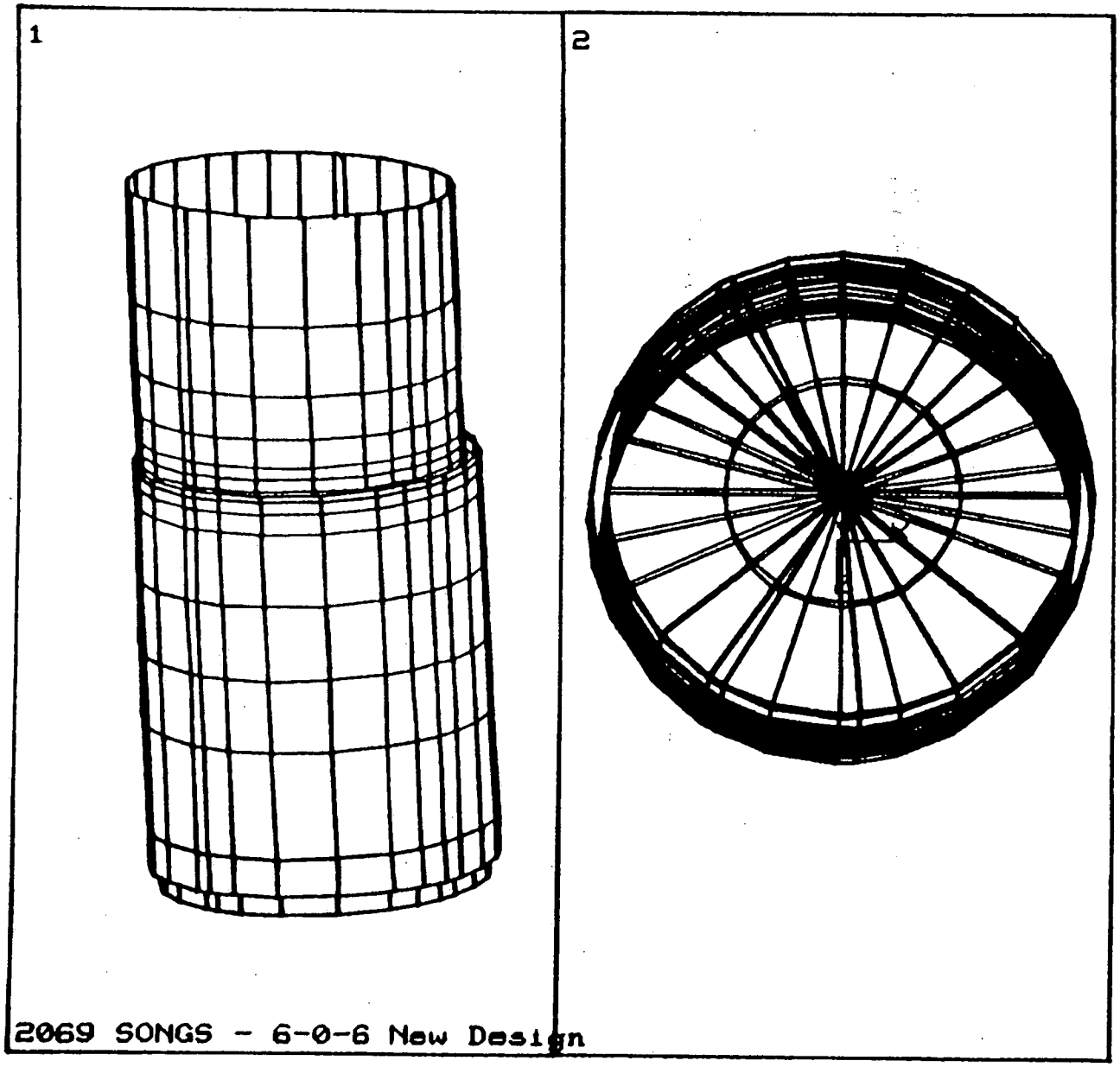

FIGURE 8-5 CORE BARREL BEAM MODE - NEW DESIGN

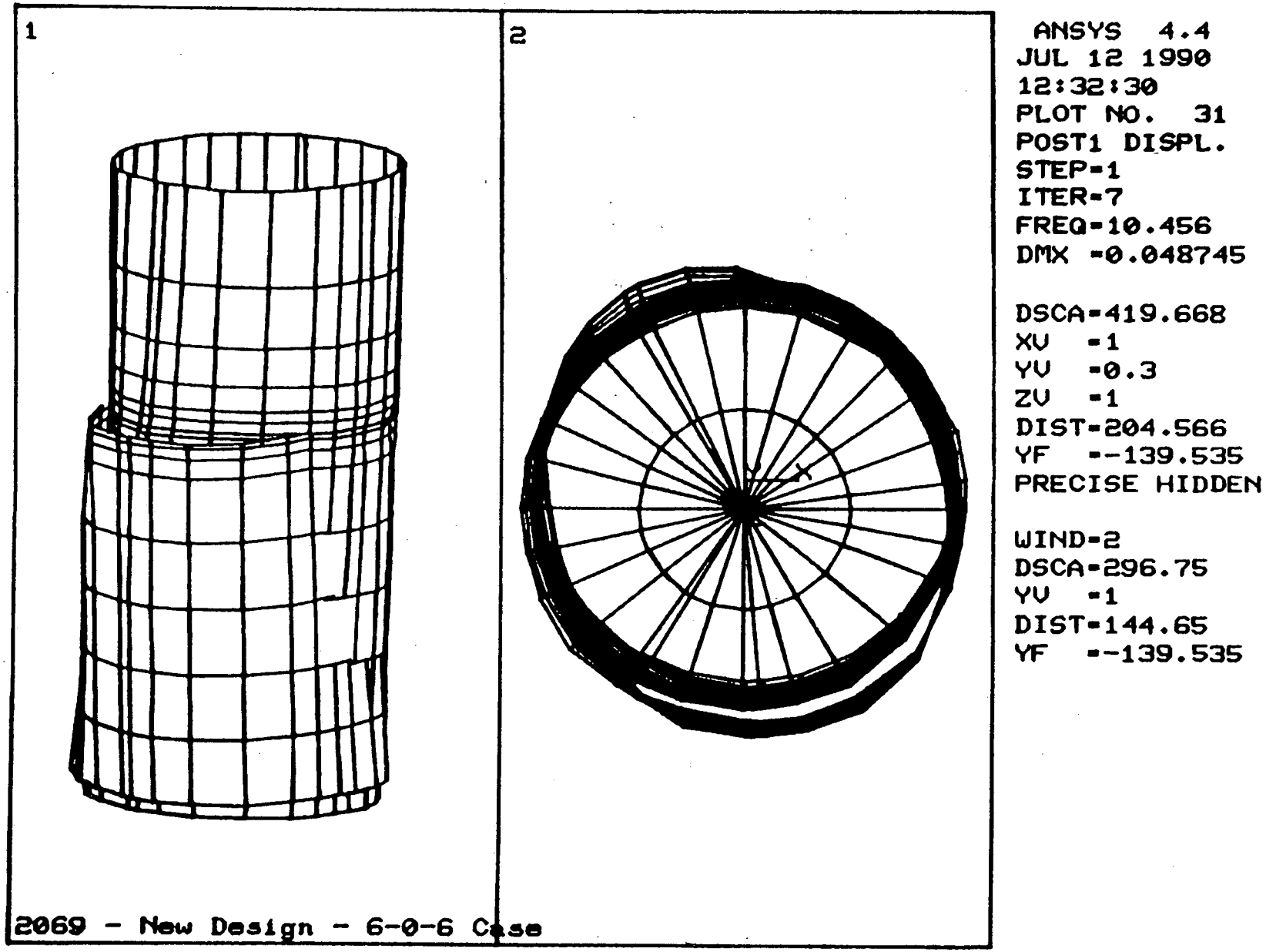

FIGURE 8-6 THERMAL SHIELD BEAM MODE - NEW DESIGN

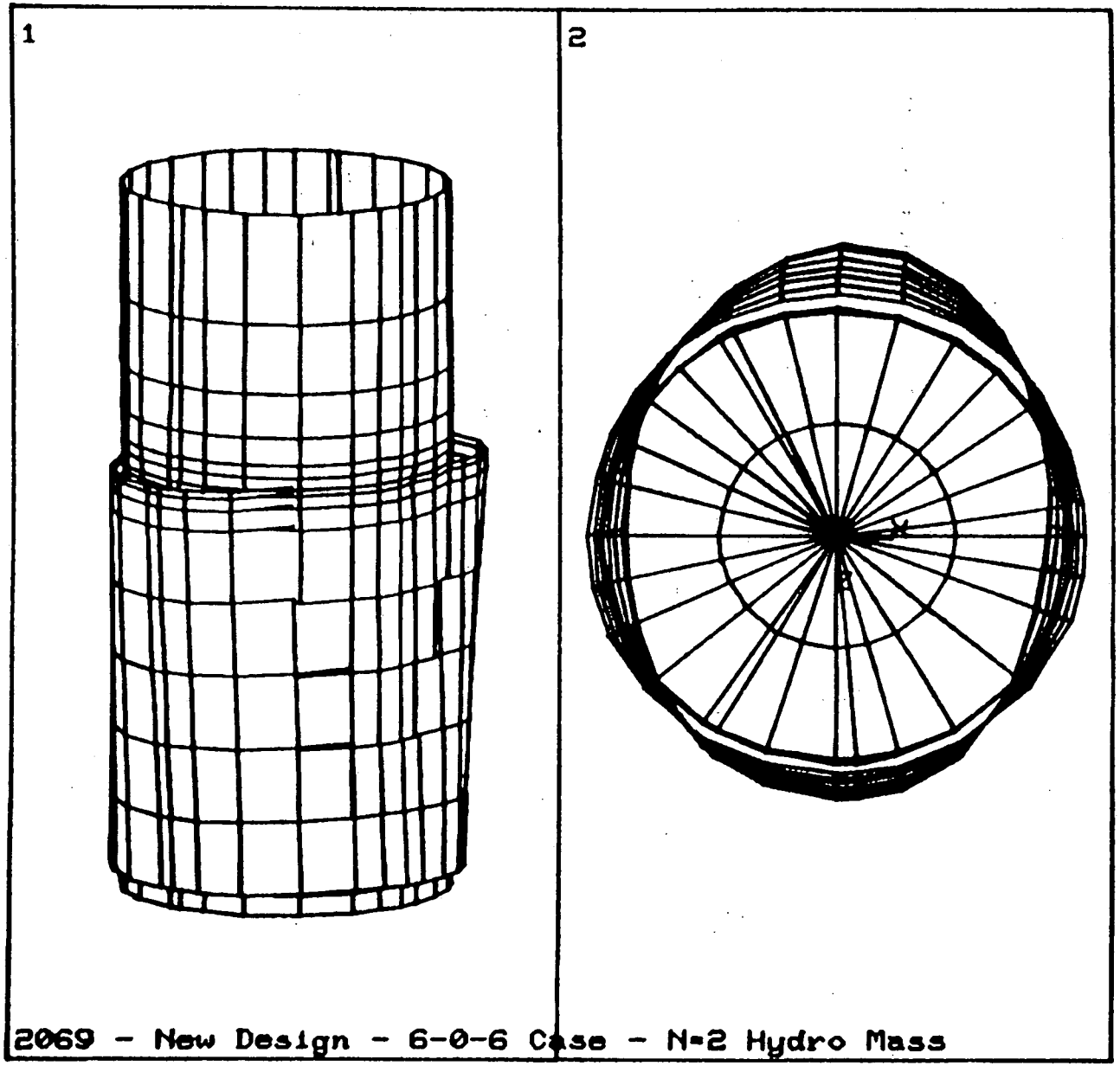

FIGURE 8-7 THERMAL SHIELD SHELL MODE (n = 2) NEW DESIGN

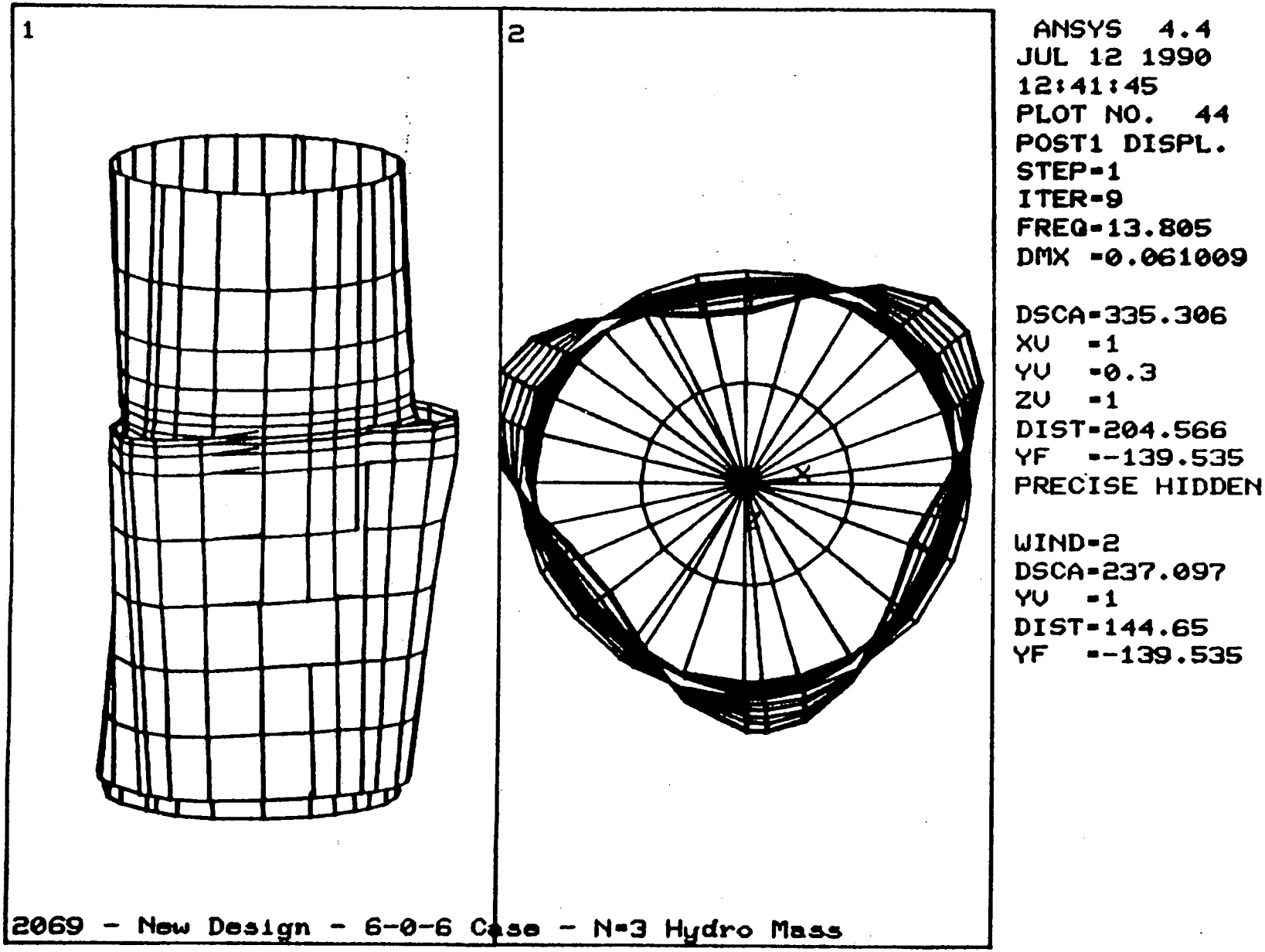

FIGURE 8-8 THERMAL SHIELD SHELL MODE (n = 3) NEW DESIGN

9.0 RANDOM VIBRATION ANALYSIS

The frequencies and mode shapes obtained from the ANSYS modal analysis and the PSD developed by Equation (9) are used in Equation (1) to determine the thermal shield response. Since the joint acceptance is a function of how the mode shape and the pressure loading match spatially, the mean square response for each mode in the discretized form is taken as:

$$\bar{y}^2 = \frac{K\,\phi^2(x)}{64\pi^3 M^2 f^3 \xi} \sum_{j=1}^{N} \phi_j^2\, G_j\, A_j^2 \qquad (12)$$

where N is the total number of elements, ϕ is normalized with respect to its maximum, M is the mass associated with the mode and K is a constant.

The turbulence-induced pressure loading acts on the inside and outside of the thermal shield. Separate analyses were performed for each case, as illustrated in Figures 9-1 and 9-2. The mean square response for each case is then given by:

$$\bar{y}_{in}^2 = \sum_i \bar{y}_i^2 \qquad \text{(for Figure 9-1)} \qquad (13)$$

and

$$\bar{y}_{out}^2 = \sum_i \bar{y}_i^2 \qquad \text{(for Figure 9-2)} \qquad (14)$$

where i is the modal index.

Note that the closely spaced modes are combined using the methodology of USNRC Regulatory Guide 1.92

The total RMS response is then obtained from:

$$\bar{y} = \sqrt{\bar{y}_{in}^2 + \bar{y}_{out}^2} \qquad (15)$$

The mean square response from (15) was correlated to the operational data for the old flexure/support design to obtain the actual value of the constant K, which was then used in the evaluation of the new flexure/support design.

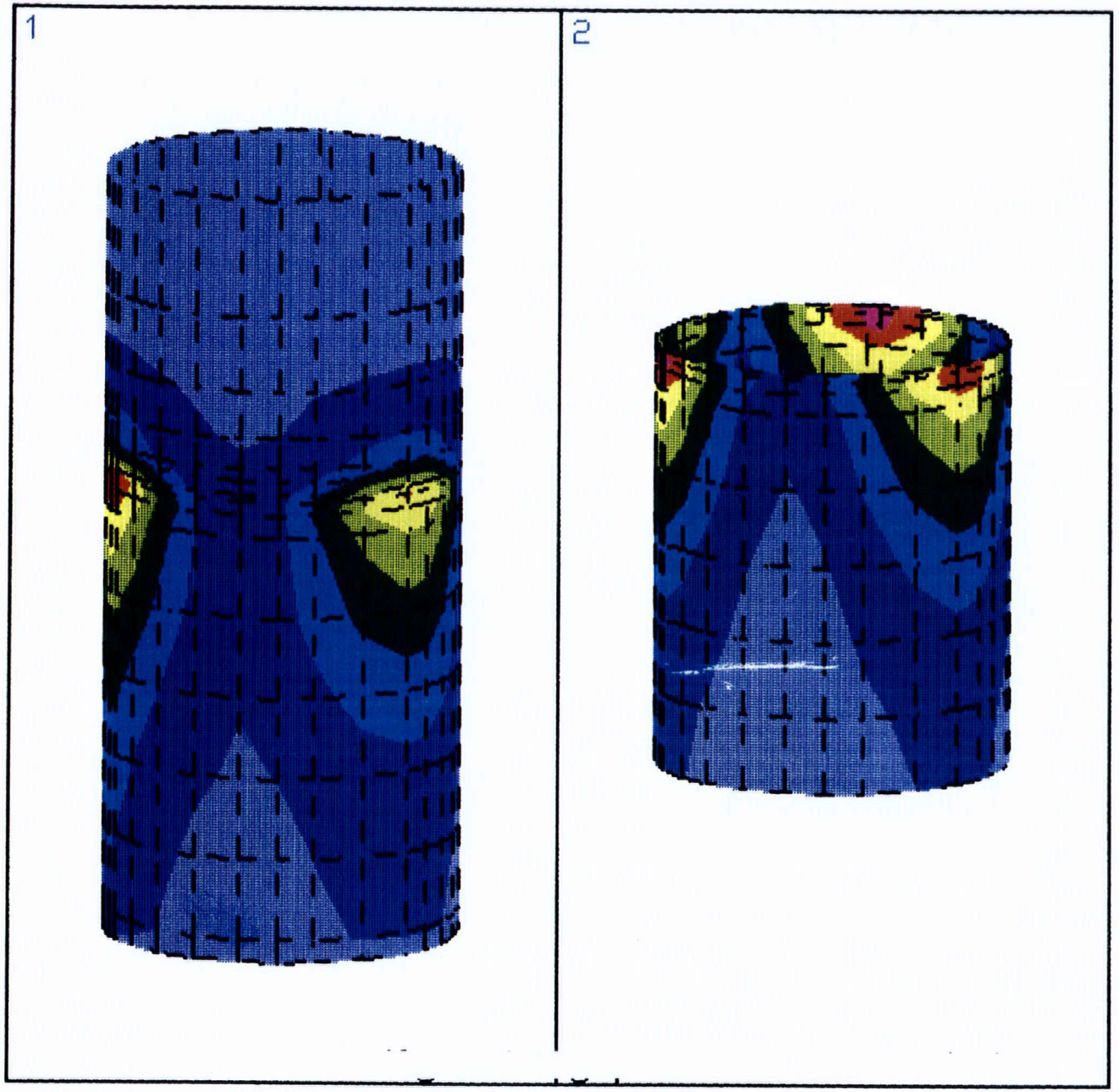

FIGURE 9-1 NORMALIZED INWARDLY ACTING PRESSURE DISTRIBUTION

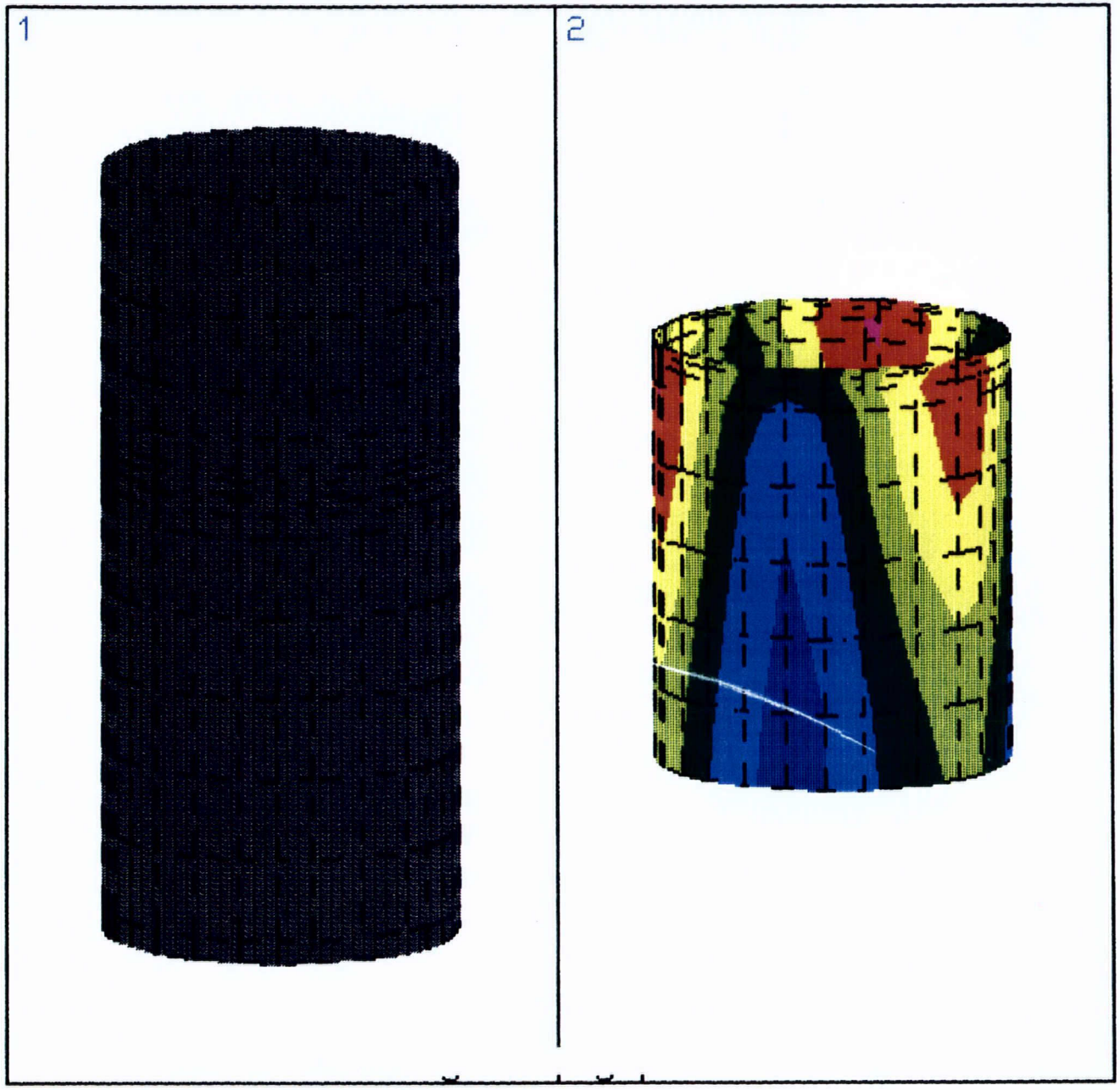

FIGURE 9-2 NORMALIZED OUTWARDLY ACTING PRESSURE DISTRIBUTION

10.0 THERMAL TRANSIENTS

The effect of thermal transients was included in the fatigue analysis by considering the thermal loads and displacements at the blocks and flexures due to these transients. Table 10-1 gives a summary of the block loads and flexure displacements for the various transients. Table 10-2 gives the rotations [Reference: Westinghouse--Due to the nonsymmetric core arrangement and the proprietary nature of the data that would be needed for the model constants required to perform the thermal transient analysis, the block loads and flexure displacements were directly provided by Westinghouse. It is believed that this data is good enough for assessing the fatigue damage due to the thermal transients in the evaluation of the new design.]. These loads and displacements were used as inputs to the three-dimensional block and flexure models to determine the stresses needed for the fatigue evaluation.

The fatigue-damage for the thermal transients was determined by considering the thermal cyclic history shown in Figure 10-1.

The bolt stresses due to thermal loads on the blocks were determined to result in insignificant fatigue damage.

TABLE 10-1*

Summary of SCE Thermal Shield Repair - Thermal Loads/Displacements

T ref = 70 F

	Block Loads (lbf)						Flexure Deflections (inch)					
Case	0	300	240	180	120	60	325	244	205	124	85	352
Steady St, 91.5%												
RAD	-3082	1114	968	-3259	1159	1249	-0.011	-0.013	-0.013	-0.011	-0.012	-0.012
VERT	2760	3588	4968	5520	2484	2208	[illegible]	[illegible]	[illegible]	[illegible]	[illegible]	[illegible]
TANG	-867	-7307	5993	766	-5508	6649	0.000	0.001	-0.001	0.000	0.000	0.000
Steady St, 100%												
RAD	-3390	1215	1039	-3565	1247	1362	-0.013	-0.015	-0.015	-0.013	-0.014	-0.014
VERT	3036	3864	5244	6072	2484	2208	[illegible]	[illegible]	[illegible]	[illegible]	[illegible]	[illegible]
TANG	-982	-7957	6594	863	-6025	7250	0.000	0.001	-0.001	0.000	0.000	0.000
Loss of Load												
RAD	-4749	-189	-317	-4967	-111	-41	-0.014	-0.015	-0.015	-0.014	-0.015	-0.014
VERT	4692	5796	6900	8004	4140	4140	0.028	0.027	0.027	0.028	0.026	0.026
TANG	-904	-8006	6643	794	-5940	7299	0.000	0.001	-0.001	0.000	0.000	0.000
Step Ld Decr												
RAD	-4251	323	179	-4455	387	472	-0.012	-0.014	-0.014	-0.013	-0.013	-0.013
VERT	3864	4692	6348	6900	3312	3036	0.024	0.023	0.023	0.024	0.022	0.022
TANG	-920	-8051	6519	817	-6034	7260	0.000	0.001	-0.001	0.000	0.000	0.000
Step Ld Decr(E)												
RAD	-2676	1637	1461	-2834	1661	1776	-0.011	-0.013	-0.013	-0.011	-0.012	-0.012
VERT	1932	3036	4692	4968	1932	1380	0.015	0.015	0.015	0.015	0.014	0.014
TANG	-943	-7444	6131	831	-5610	6835	0.000	0.001	-0.001	0.000	0.000	0.000
Reactor Trip												
RAD	-173	1469	1336	-177	1432	1535	0.004	0.003	0.003	0.004	0.003	0.003
VERT	-2760	-1104	-552	-1656	-1932	-1932	-0.008	-0.008	-0.008	-0.008	-0.008	-0.008
TANG	-556	-2710	2223	503	-2140	2709	0.000	0.000	0.000	0.000	0.000	0.000
Cool Down												
RAD	477	501	477	500	477	501	0.000	0.000	0.000	0.000	0.000	0.000
VERT	-552	-552	-828	-552	-552	-552	-0.003	-0.003	-0.003	-0.003	-0.003	-0.003
TANG	-47	-23	23	55	-24	22	0.000	0.000	0.000	0.000	0.000	0.000

*Reference: Westinghouse Electric Company

TABLE 10-2*

Summary of SCE Thermal Shield Repair - Thermal Displacements (Rotations)

T ref = 70 F

	Block Rotation (x 1000 RAD)						Flexure Rotations (x 1000 RAD)					
Case	0	300	240	180	120	60	325	244	205	124	85	352
Steady St, 91.5%												
RAD	0.000	0.005	-0.004	0.000	0.004	-0.004	-0.029	-0.025	0.028	0.026	0.000	0.000
VERT	0.001	0.016	-0.015	-0.001	0.015	-0.016	-0.054	-0.100	0.091	0.060	0.021	-0.021
TANG	-0.014	0.024	0.052	0.035	0.006	-0.006	-0.688	-0.688	-0.689	-0.687	-0.877	-0.879
Steady St, 1												
RAD	0.000	0.005	-0.005	0.000	0.005	-0.005	-0.032	-0.027	0.030	0.029	0.000	0.000
VERT	0.001	0.018	-0.017	-0.001	0.016	-0.017	-0.056	-0.112	0.103	0.062	0.026	-0.026
TANG	-0.020	0.022	0.052	0.034	0.001	-0.011	-0.789	-0.790	-0.791	-0.789	-0.996	-0.998
Loss of Load												
RAD	0.000	0.005	-0.005	0.000	0.005	-0.005	-0.033	-0.026	0.029	0.030	-0.001	0.001
VERT	0.001	0.018	-0.017	-0.001	0.016	-0.017	-0.032	-0.137	0.127	0.037	0.050	-0.051
TANG	-0.052	-0.010	0.018	0.001	-0.033	-0.044	-0.742	-0.743	-0.744	-0.741	-0.949	-0.951
Step Ld Decr												
RAD	0.000	0.005	-0.005	0.000	0.005	-0.005	-0.033	-0.026	0.030	0.030	-0.001	0.001
VERT	0.001	0.018	-0.017	-0.001	0.016	-0.017	-0.043	-0.125	0.116	0.049	0.039	-0.040
TANG	-0.036	0.006	0.035	0.017	-0.016	-0.027	-0.722	-0.722	-0.723	-0.721	-0.929	-0.931
Step Ld Decr(E)												
RAD	0.000	0.005	-0.004	0.000	0.004	-0.005	-0.030	-0.026	0.028	0.027	0.000	0.000
VERT	0.001	0.017	-0.016	-0.001	0.015	-0.016	-0.058	-0.105	0.097	0.064	0.022	-0.022
TANG	-0.005	0.036	0.064	0.046	0.016	0.004	-0.683	-0.683	-0.684	-0.682	-0.876	-0.877
Reactor Trip												
RAD	0.000	0.002	-0.002	0.000	0.002	-0.002	-0.011	-0.009	0.009	0.011	-0.001	0.001
VERT	0.001	0.006	-0.006	-0.001	0.006	-0.006	-0.050	-0.068	0.072	0.045	0.011	-0.013
TANG	-0.008	0.019	0.029	0.016	0.006	0.004	0.254	0.254	0.254	0.254	0.186	0.185
Cool Down												
RAD	0.000	0.000	0.000	0.000	0.000	0.000	0.000	0.000	0.000	0.000	0.000	0.000
VERT	0.000	0.000	0.000	0.000	0.000	0.000	-0.001	0.001	-0.001	0.001	-0.001	0.001
TANG	0.006	0.006	0.006	0.006	0.006	0.006	0.027	0.027	0.027	0.027	0.027	0.027

*Reference: Westinghouse Electric Company

CYCLES PER 15 YEARS:

X30 (1) LOSS OF LOAD

X750 (2) STEP LOAD DECREASE

X255 (3) REACTOR TRIP x 150
LOSS OF FLOW x 30
STEP LOAD DECREASE (E) x 75

X75 (4) COOL DOWN & HEAT UP

X7635 (5) UNIT LOADING x 6870
STEP LOAD INCREASED x 750
LOSS OF POWER x 15

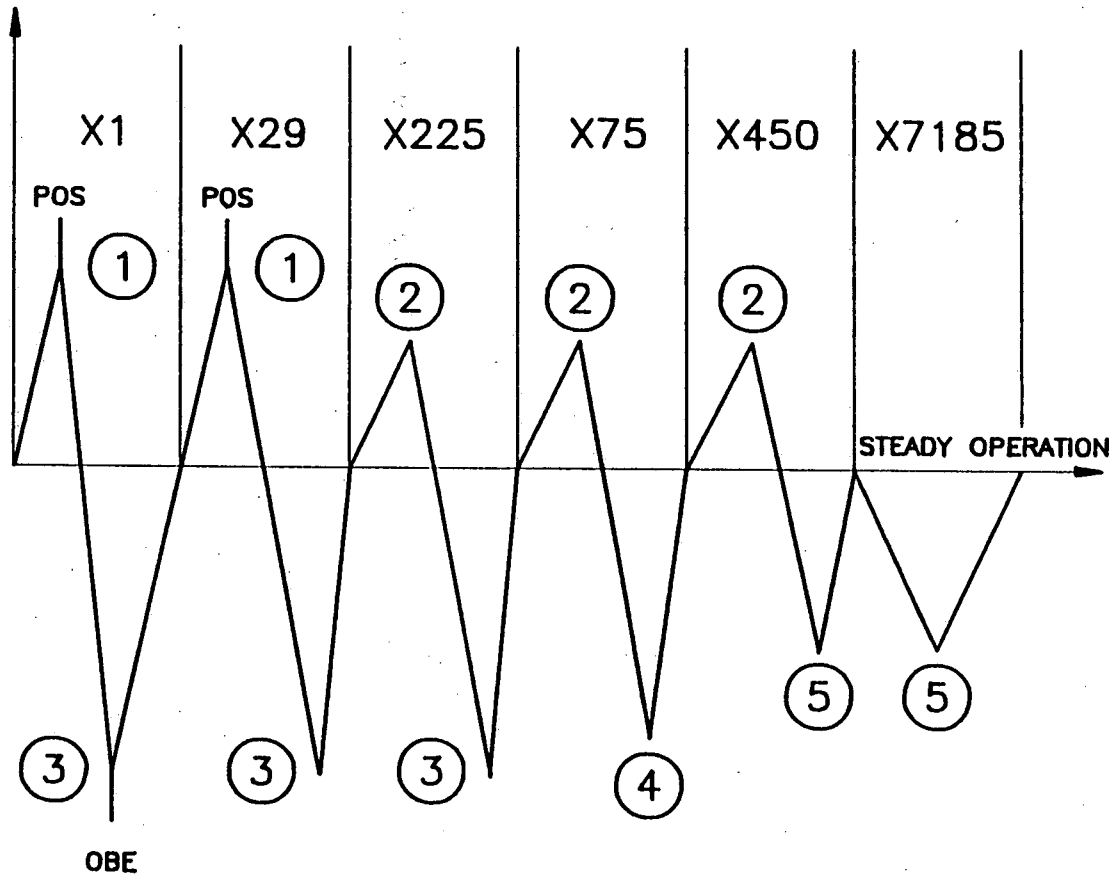

STRESS RANGE 2Sa (THERMAL ONLY)	61,740	61,740	56,970	53,410	36,650	29,990
USAGE FACTOR FOR THERMAL LOADS PLUS FIV 4 σ LOADS + (POS + OBE) CASE 6-0-6 NEW DESIGN	0.042	0.344	0.078	0.017	0.018	0.213

$\Sigma = 0.712$ (Design Curve A)

FIGURE 10-1 ASSUMED CYCLIC HISTORY OF THERMAL EXPANSION STRESS IN FLEXURES

11.0 SEISMIC ANALYSIS

An equivalent static 'g' seismic analysis of the core barrel/thermal shield structure was performed for the new support block/flexure design. The three-dimensional overall core barrel/thermal shield finite element model discussed earlier was used for the seismic analysis. The seismic spectra for the horizontal north-south, east-west and vertical directions are shown in Figures 11-1, 11-2 and 11-3.

The ANSYS finite element program was used to perform the seismic analysis. The same modes that were included in the flow-induced vibration analysis were considered for the seismic analysis. The total response was obtained by combining the individual responses using the SRSS method. For closely spaced modes the grouping method from USNRC Regulatory Guide 1.92 was used for combining the individual responses.

The response from the overall model was used as input to the three-dimensional block and flexure models to determine the stresses required for the fatigue analysis. The seismic streses are shown in Tables 11-4 and 11-5.

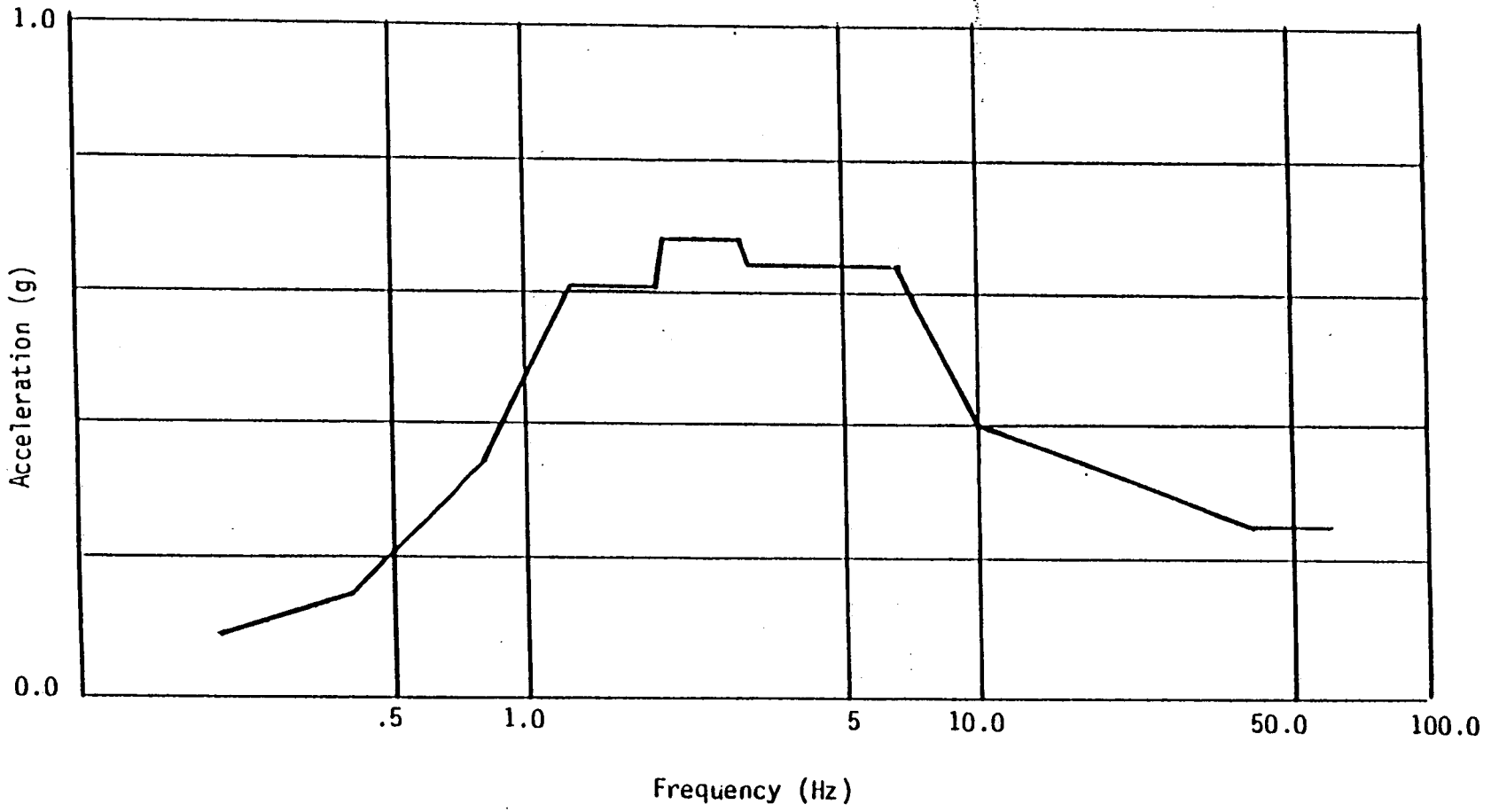

FIGURE 11-1 OBE SPECTRA (2% DAMPING) N-S (HORIZONTAL)

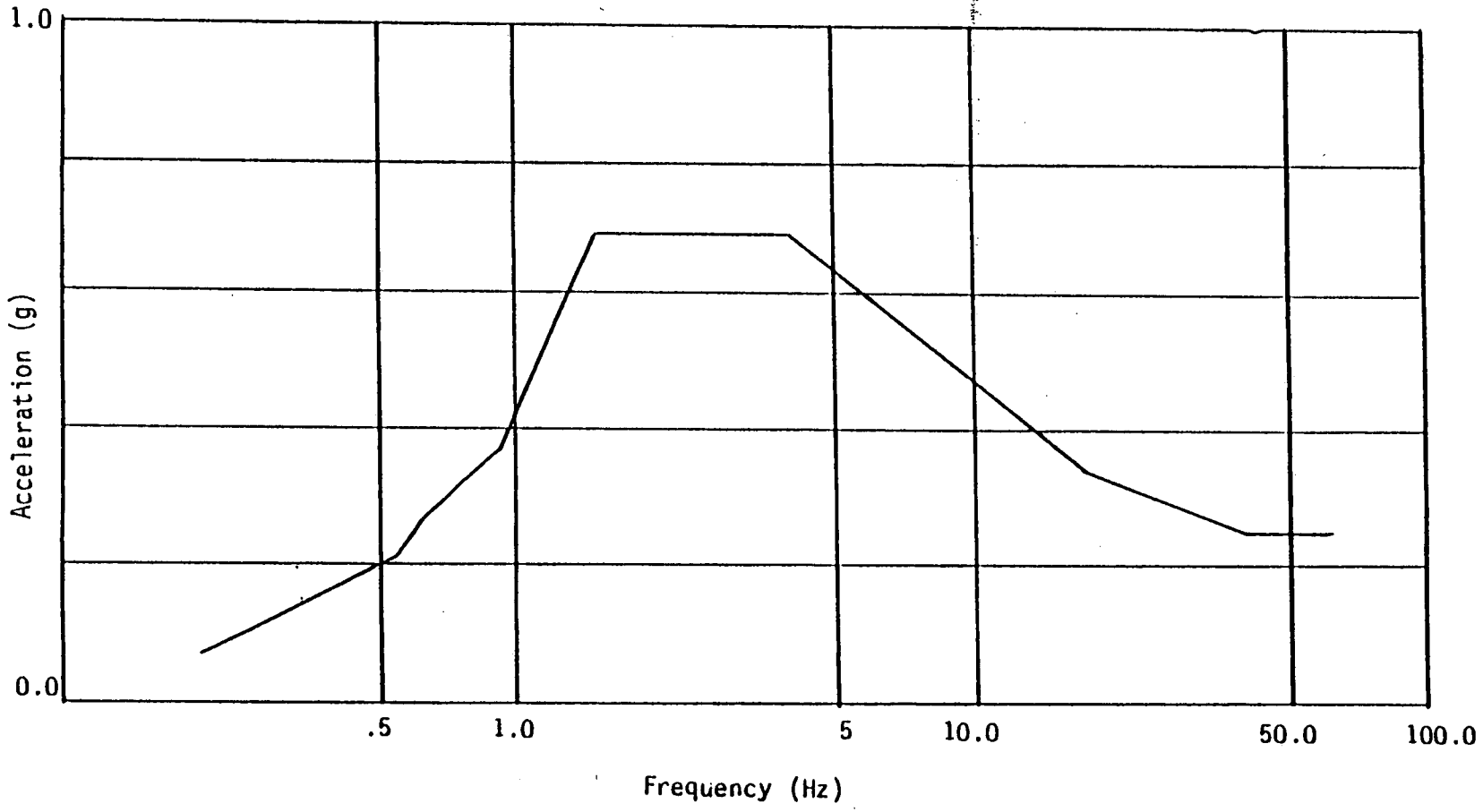

FIGURE 11-2 OBE SPECTRA (2% DAMPING) E-W (HORIZONTAL)

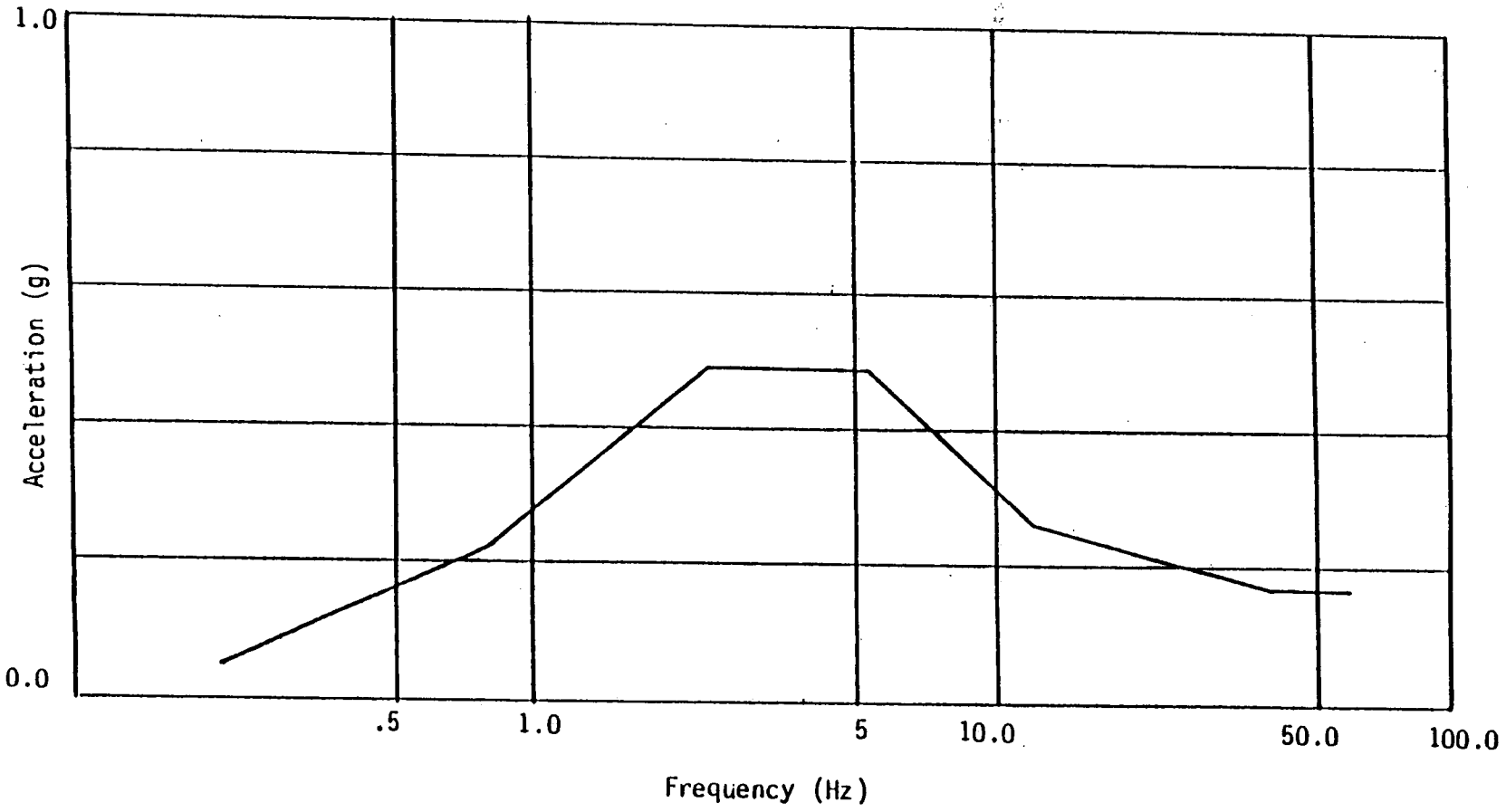

FIGURE 11-3 OBE SPECTRA (2% DAMPING) VERTICAL

TABLE 11-4

6-0-6 NEW SEISMIC

RESULTS FOR FLEXURES

	DISPLACEMENT (mils)			Stress Int (psi)
Angle	Radial	Vertical	Tang.	σ_I
352°	16.69	8.24	20.04	49,637
85°	17.12	9.31	18.89	47,537
124°	17.72	9.62	20.02	50,163
205°	15.87	8.79	21.69	50,792
244°	17.28	9.58	20.36	49,808
325°	16.63	9.12	20.38	50,512

TABLE 11-5

6-0-6 NEW - SEISMIC

RESULTS FOR LOWER BLOCKS

Angle	Displacements (mils) Radial	Vertical	Bolts* σ_I - Preload (psi) 1-8	1/2-13	7/8-9
0°	.20	1.53	679	228	541
60°	.30	1.41	691	196	522
120°	.31	1.73	821	264	611
180°	.22	1.49	678	219	535
240°	.17	1.75	753	279	595
300°	.24	1.77	801	278	614

*Preload = 30,500 psi

12.0 FATIGUE ANALYSIS

The results from the random vibration analysis are rms displacements and forces. These rms values are then applied to the detailed models of the flexures and blocks, to produce rms stresses.

Random vibration stresses in lightly damped structures are typically narrow-band in the frequency domain and Gaussian in the time domain. This means that the structure responds predominantly at a discrete frequency and that the probable stress level at any point in time can be described by the Gaussian or normal distribution function (Figure 12-1). The variable p(z) is the probability that the stress level will be $\sigma(z)$.

$$p(z) = \frac{1}{\sqrt{2\pi}} e^{-z^2/2}$$

$$\sigma(z) = z\sigma_{rms}$$

where

σ_{rms} is the root mean square stress.

Fatigue usage calculations require a knowledge of stress ranges from positive to negative peaks from which cyclic stress amplitudes may be obtained. It is shown in Reference [10] that the amplitudes for a narrow-band Gaussian process have a Rayleigh distribution (Figure 12-2).

For a particular cyclic stress amplitude (σ_i), the ASME curve gives an allowable number of cycles (N_i). If n_i cycles are anticipated at this stress amplitude, then a usage factor (U_i) is defined as follows:

$$U_i = n_i/N_i \qquad (1)$$

Miner's rule is employed to determine the cumulative fatigue damage for a structure subjected to cycles at more than one stress amplitude.

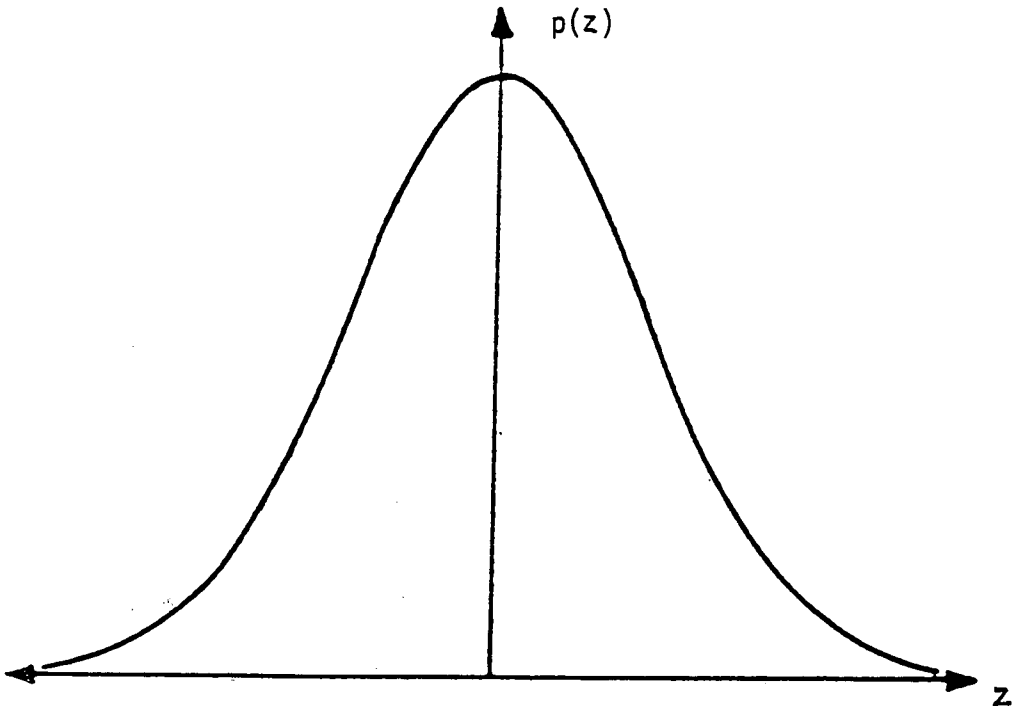

Figure 12-1 GAUSSIAN DISTRIBUTION

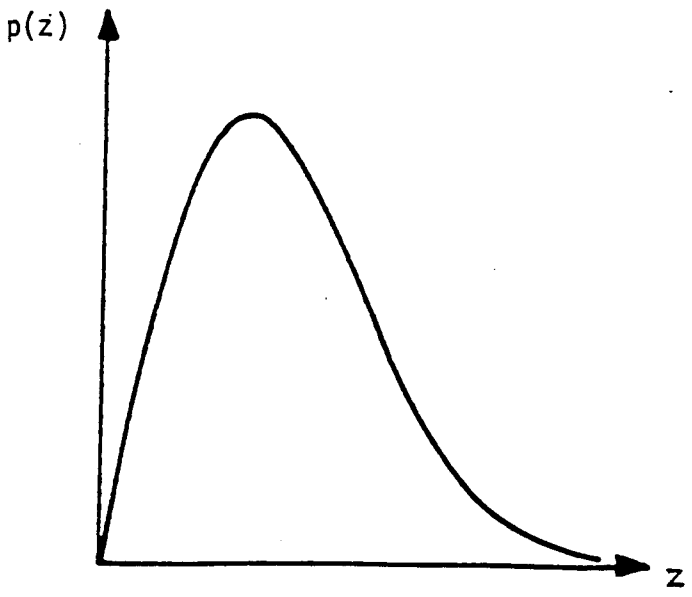

Figure 12-2 RAYLEIGH DISTRIBUTION

$$\sum_i U_i = c$$

The value of c is limited to 1.0 by the ASME Code.

The normalized Rayleigh distribution [10] is as follows:

$$p(z) = ze^{-z^2/2} \qquad z \geq 0$$

The variable p(z) is the probability of an event (stress cycle) occurring with an amplitude of $\sigma(z)$. The distribution of stress amplitudes for a given σ_{rms} is then

$$\sigma(z) = z\sigma_{rms} \qquad (2)$$

The distribution may be divided into arbitrarily thin strips, each of width Δz.

$$z_i = (i\ \Delta z) \quad 0 \leq i \leq \infty$$

$$\sigma_i = z_i\sigma_{rms}$$

If the given total number of cycles is n_{rms}, then the number of cycles (n_i) which will probably occur with amplitudes between ($z_i - \Delta z$) and (z_i) is obtained by integration.

$$n_i = n_{rms} \int_{z_i - \Delta z}^{z_i} g(z)dz$$

where

$$g(z) = az^2 + bz + c$$

The coefficients of g(z) are established in each interval by equating the functions and their derivatives at z_i.

$$g(z_i) = p(z_i)$$

$$g'(z_i) = p'(z_i)$$

$$g''(z_i) = p''(z_i)$$

Thus,

$$a = p''/2$$

$$b = p' - p'' z_i$$

$$c = p - p'z_i + p'' z_i^2/2$$

Performing the integration of the Rayleigh distribution yields the following number of cycles in the ith strip:

$$n_i = n_{rms}\Delta z\{p''(z_i)\Delta z^2/6 - p'(z_i)\Delta z/2 + p(z_i)\} \quad (3)$$

where

$$p(z_i) = z_i e^{-z_i^2/2}$$

$$p'(z_i) = (1 - z_i^2)e^{-z_i^2/2}$$

$$p''(z_i) = (z_i^2 - 3)p(z_i)$$

ASME fatigue curves A and B (Section III Appendices, Figures I-9.2.1 and I-9.2.2) are used in the fatigue analysis of the flexures (Curve A) and bottom block bolts (Curve B).

A computer program was written to calculate the cumulative usage factor given the rms stress and required number of cycles. The maximum value of z used in the fatigue evaluation was 7.0, however, once the number of cycles at any z (equation 3) became less than 1.0, the program was terminated. The following is a brief description of the procedures used in the program:

1) Required input:
   a) Peak rms stress
   b) Required number of cycles
   c) The stress concentration factor which relates the given peak rms stress to the linearized primary plus secondary stress

2) Data specific to this application:
   a) S_m = 29.2 ksi @ 600°F for flexures (ASME Code Case N60-3)
   b) S_m = 25.7 ksi @ 600°F for bottom block bolts (ASME Code Case N60-3)
   c) m = 1.7) for simplified elastic-plastic
      n = 0.3) analysis per ASME Code, Section III, Division 1 NG, paragraph NG-3228.3.

3) The program ramps values of z from 0 to 7.0. The peak stress at any value of z is given by equation (2), and the number of cycles at this peak stress is given by equation (3).

4) The linearized primary plus secondary stress range is computed by

$$P_L + P_B + Q = \frac{\sigma_{peak} \times 2.0}{SCF}$$ where SCF = Stress Concentration Factor.

5) $P_L + P_B + Q$ is then compared to 3.0 S_m per Section NG-3228.3 of the ASME Code to determine the value of K_e. K_e is used as a multiplier for the alternating peak stress used to enter the fatigue curves.

$$K_e = 1.0 \qquad \text{for } S_m \leq 3\ S_m$$

$$= 1.0 + \frac{(1 - n)}{n(m - 1)} \quad \frac{S_n}{3\ S_m} - 1 \qquad \text{for } 3\ S_m < S_n < 3m\ S_m$$

$$= 1/n \qquad \text{for } S_n \geq 3m\ S_m$$

S_n = range of primary plus secondary stress intensity

7) The fatigue curves are interpolated using Lagrangian methods to determine the allowable number of cycles. Curve A is used for the flexures as long as $P_L + P_B + Q < 44$ ksi. If this value is exceeded, Curve B is used. Curve B is also used for the bolts.

8) The cumulative usage factor is determined by equation (1).

Figure 12-3 shows a sample of the output from this program.

SMC O'Donnell RMS Fatigue Evaluation Mon Jul 9 10:15:08 1990

test case

RMS Stress 6.80 Ksi SCF = 1.70 Pl+Pb+Q = 4.00 Ksi

3.0 Sm = 87.60 Ksi N = 0.300 M = 1.700 Req'd Cycles = 1.000E+09

Fatigue Curve used: Austenitic Steels Figures I-9.2.1 & I-9.2.2 Curve A Desig

Sigma	% Prob	Stress	Pl+Pb+Q	Ke	Required Cycles	Allowable Cycles	Usage Factor
0.18	17.2	1.2	1.4	1.00	1.5085E+07	1.0000E+11	0.00
0.35	32.9	2.4	2.8	1.00	4.4126E+07	1.0000E+11	0.00
0.53	45.7	3.6	4.2	1.00	6.9270E+07	1.0000E+11	0.00
0.70	54.8	4.8	5.6	1.00	8.8541E+07	1.0000E+11	0.00
0.88	59.7	6.0	7.0	1.00	1.0078E+08	1.0000E+11	0.00
1.05	60.5	7.1	8.4	1.00	1.0576E+08	1.0000E+11	0.00
1.23	57.8	8.3	9.8	1.00	1.0408E+08	1.0000E+11	0.00
1.40	52.5	9.5	11.2	1.00	9.6980E+07	1.0000E+11	0.00
1.57	45.6	10.7	12.6	1.00	8.6084E+07	1.0000E+11	0.00
1.75	37.8	11.9	14.0	1.00	7.3082E+07	1.0000E+11	0.00
1.93	30.2	13.1	15.4	1.00	5.9507E+07	1.0000E+11	0.00
2.10	23.2	14.3	16.8	1.00	4.6565E+07	1.0000E+11	0.00
2.27	17.1	15.5	18.2	1.00	3.5072E+07	1.0000E+11	0.00
2.45	12.2	16.7	19.6	1.00	2.5455E+07	1.0000E+11	0.00
2.63	8.4	17.9	21.0	1.00	1.7820E+07	1.0000E+11	0.00
2.80	5.6	19.0	22.4	1.00	1.2040E+07	1.0000E+11	0.00
2.97	3.6	20.2	23.8	1.00	7.8572E+06	1.0000E+11	0.00
3.15	2.2	21.4	25.2	1.00	4.9544E+06	1.0000E+11	0.00
3.33	1.3	22.6	26.6	1.00	3.0199E+06	1.0000E+11	0.00
3.50	0.8	23.8	28.0	1.00	1.7799E+06	9.9994E+09	0.00
3.67	0.4	25.0	29.4	1.00	1.0148E+06	1.2087E+07	0.08
3.85	0.2	26.2	30.8	1.00	5.5973E+05	3.4483E+06	0.16
4.03	0.1	27.4	32.2	1.00	2.9877E+05	1.5785E+06	0.19
4.20	0.1	28.6	33.6	1.00	1.5436E+05	9.3280E+05	0.17
4.38	0.0	29.8	35.0	1.00	7.7199E+04	6.8381E+05	0.11
4.55	0.0	30.9	36.4	1.00	3.7381E+04	5.0742E+05	0.07
4.72	0.0	32.1	37.8	1.00	1.7527E+04	3.9984E+05	0.04
4.90	0.0	33.3	39.2	1.00	7959.	3.1862E+05	0.02
5.07	0.0	34.5	40.6	1.00	3500.	2.5592E+05	0.01
5.25	0.0	35.7	42.0	1.00	1491.	2.0710E+05	0.01
5.42	0.0	36.9	43.4	1.00	615.2	1.7259E+05	0.00
5.60	0.0	38.1	44.8	1.00	245.9	1.4532E+05	0.00 *
5.78	0.0	39.3	46.2	1.00	95.23	1.2301E+05	0.00 *
5.95	0.0	40.5	47.6	1.00	35.73	1.0464E+05	0.00 *
6.13	0.0	41.7	49.0	1.00	12.99	8.9314E+04	0.00 *
6.30	0.0	42.8	50.4	1.00	4.576	7.6535E+04	0.00 *
6.47	0.0	44.0	51.8	1.00	1.562	6.5862E+04	0.00 *
				Totals	1.0000E+09		0.89

* Linearized stress exceeded 44.0 Ksi, Curve B used in lieu of Curve A

Figure 12-3

13.0 STRESS CONCENTRATION FACTORS FOR FATIGUE ANALYSIS

The analysis of the bolts for the flexures and bottom blocks computes the linearized stresses for the bolt. In order to complete the fatigue analysis, these linearized stresses have to be multiplied by a stress concentration factor (SCF) in order to obtain the peak stress used to enter the fatigue curves. Per paragraph NG-3232.3(c) of the ASME Code a SCF of 4.0 was used for all bolts.

For the flexures, the situation is reversed. The detailed flexure finite element model (Section 6.0), is used to obtain the peak stress in the flexure. The fatigue evaluation (Section 12.0) requires the comparison of the primary plus secondary linearized stress range $P_L + P_B + Q$. If the SCF for the flexures were known, this linearized value could be obtained from the peak stress as:

$$(P_L + P_B + Q)_{RANGE} = \frac{2.0 * \sigma_{PEAK}}{SCF}$$

In order to determine the SCF of the flexures, the finite element results have to be linearized across the section of the flexure where the peak stress occurs. The peak stress occurs in the web of the flexure. The ANSYS program allows the user an option to determine the equilibrium forces acting on this section. The membrane plus bending stress intensity is computed from these equilibrium forces. The stress concentration factor is then obtained by dividing the peak stress by the linearized value.

14.0 MODEL QUALIFICATION

The results from the random vibration analyses were correlated against actual plant experience to insure accurate results. As a base case for scaling, the SONGS Unit 1 operated for 4.1 EFPY (approximate 50 months) from startup through 1971. After this period, the unit was visually inspected and it was found that none of the flexures were broken. A subsequent inspection at 88 months found four of the six flexures had failed. For purposes of this evaluation, it was assumed that the flexures failed immediately after the fifty-month period. The dominant frequencies of the overall model lie between 6 and 10 Hz. If an average frequency of 8 Hz is used, the fifty-month period results in:

(50 months) (30 days/month) (24 hours/day) (3600 seconds/hour) (8 cycles/sec.) = 1.03×10^9 Cycles

Since the original flexures were preloaded due to thermal expansion, the B Curve on Figure I-9.2.2 of the ASME Code was used for the fatigue evaluation. In addition, the B curve was converted from a design curve to a failure curve by multiplying the stresses by a factor of 2.0. The use of a failure curve is justified since the intent is to determine the most conservative scaling factor. In addition, all other cyclic loading including thermal was ignored, so that the random vibration cycling was considered the only cause of failure. This also provided the most conservative scale factor.

To determine what stress range would cause failure of the flexures, the fatigue program (Section 12) was used iteratively until a fatigue usage factor Of 0.99 was obtained. The results of this run are shown on Table 14-1. The peak stress amplitude is 10,680 psi.

The overall model configuration chosen to match the fifty-month operation was the 6-0-6 case (6 flexures - 0 keys - 6 blocks). The reasons for choosing this case which does not include the radial limiter keys are twofold: (1) the original keys had a hot gap of 15 mils. This value is larger than the calculated displacement at the key locations, and (2) had

TABLE 14-1 SMC O'DONNELL INC.

SMC O'Donnell RMS Fatigue Evaluation Wed Jul 11 20:11:13 1990

Scaling Case for Original Flexure

RMS Stress 10.68 Ksi SCF = 1.30 P1+Pb+Q = 8.22 Ksi

3.0 Sm = 87.60 Ksi N = 0.300 M = 1.700 Req'd Cycles = 1.030E+09

Fatigue Curve used: Austenitic Steels Figures I-9.2.1 & I-9.2.2 Curve B Failure

Sigma	% Prob	Stress	P1+Pb+Q	Ke	Required Cycles	Allowable Cycles	Usage Factor
0.18	17.2	1.9	2.9	1.00	1.5537E+07	1.0000E+11	0.00
0.35	32.9	3.7	5.8	1.00	4.5450E+07	1.0000E+11	0.00
0.53	45.7	5.6	8.6	1.00	7.1348E+07	1.0000E+11	0.00
0.70	54.8	7.5	11.5	1.00	9.1197E+07	1.0000E+11	0.00
0.88	59.7	9.3	14.4	1.00	1.0381E+08	1.0000E+11	0.00
1.05	60.5	11.2	17.3	1.00	1.0893E+08	1.0000E+11	0.00
1.23	57.8	13.1	20.1	1.00	1.0720E+08	1.0000E+11	0.00
1.40	52.5	15.0	23.0	1.00	9.9890E+07	1.0000E+11	0.00
1.57	45.6	16.8	25.9	1.00	8.8667E+07	1.0000E+11	0.00
1.75	37.8	18.7	28.8	1.00	7.5275E+07	1.0000E+11	0.00
1.93	30.2	20.6	31.6	1.00	6.1292E+07	1.0000E+11	0.00
2.10	23.2	22.4	34.5	1.00	4.7962E+07	1.0000E+11	0.00
2.27	17.1	24.3	37.4	1.00	3.6125E+07	1.0000E+11	0.00
2.45	12.2	26.2	40.3	1.00	2.6219E+07	1.0000E+11	0.00
2.63	8.4	28.0	43.1	1.00	1.8354E+07	1.0000E+11	0.00
2.80	5.6	29.9	46.0	1.00	1.2402E+07	1.0000E+11	0.00
2.97	3.6	31.8	48.9	1.00	8.0930E+06	1.0000E+11	0.00
3.15	2.2	33.6	51.8	1.00	5.1031E+06	7.8423E+08	0.01
3.33	1.3	35.5	54.6	1.00	3.1105E+06	1.9042E+07	0.16
3.50	0.8	37.4	57.5	1.00	1.8333E+06	9.0096E+06	0.20
3.67	0.4	39.2	60.4	1.00	1.0452E+06	5.4756E+06	0.19
3.85	0.2	41.1	63.3	1.00	5.7652E+05	3.9162E+06	0.15
4.03	0.1	43.0	66.1	1.00	3.0773E+05	2.9341E+06	0.10
4.20	0.1	44.9	69.0	1.00	1.5899E+05	2.2255E+06	0.07
4.38	0.0	46.7	71.9	1.00	7.9515E+04	1.8496E+06	0.04
4.55	0.0	48.6	74.8	1.00	3.8503E+04	1.6310E+06	0.02
4.72	0.0	50.5	77.6	1.00	1.8053E+04	1.4450E+06	0.01
4.90	0.0	52.3	80.5	1.00	8197.	1.2859E+06	0.01
5.07	0.0	54.2	83.4	1.00	3605.	1.1490E+06	0.00
5.25	0.0	56.1	86.3	1.00	1536.	1.0306E+06	0.00
5.42	0.0	57.9	89.1	1.06	633.6	5.4325E+05	0.00
5.60	0.0	59.8	92.0	1.17	253.3	2.3753E+05	0.00
5.78	0.0	61.7	94.9	1.28	98.09	1.2098E+05	0.00
5.95	0.0	63.5	97.8	1.39	36.80	6.5614E+04	0.00
6.13	0.0	65.4	100.6	1.50	13.38	3.7796E+04	0.00
6.30	0.0	67.3	103.5	1.61	4.713	2.2942E+04	0.00
6.47	0.0	69.2	106.4	1.71	1.609	1.4495E+04	0.00
				Totals	1.0300E+09		0.99

the keys contacted, studies have shown that the wear would be rapid and excessive and that within a short period of time, the keys would cease to be functional.

The maximum unscaled peak stress intensity obtained from the overall and detailed flexure model results is scaled to the peak stress amplitude of Table 14-1 to determine the scale factor for all subsequent runs.

15.0 RESULTS

Three dimensional plots illustrating the finite element results obtained for the flexures are shown in Figures 15-1 through 15-10 for the old design and Figures 15-11 through 15-20 for the new design. The stress results shown are for unit displacements in the radial, vertical and tangential directions as well as for unit rotations. (Rotation about the vertical axis is excluded.)

Several different cases with various combinations of upper flexures and lower support blocks were analyzed to evaluate the new design. The radial limiter keys were not included in any of these cases because of the initial gap at hot condition and the past experience which has shown that they wear rapidly. Excluding the keys thus provides a conservative but realistic assessment. The frequencies and corresponding mode shapes included in the flow-induced vibration analysis for the various cases analyzed are listed in Table 15-1. Following is a discussion of the results for the cases analyzed.

1. Old and New Design (No hydrodynamic mass effect) - 6 Flexures-0 keys - 6 Support Blocks

Both the old and new designs were analyzed without including the effect of the hydrodynamic mass. The purpose here was to provide guidance in selecting the mode shapes when hydrodynamic mass is included in the model but more importantly to provide a comparison of the two designs. Figures showing the mode shapes and corresponding frequencies for the old and new designs are given in Appendix B. The stress results for the flexures and blocks are shown in Tables 15-2 through 15-5. A comparison of stress results shows a definite and significant improvement in the new flexures and bolts.

2. Old Design - 6 Flexures, 0 Keys, 6 Support Blocks

This was the base case that was run to correlate the analysis results to the field data and establish the value of the factor K for use in evaluating the remaining cases. The loads and stresses in the flexures and support block bolts are presented in Tables 15-6 and 15-7. The stresses in the flexure web are illustrated in Figure 15-21.

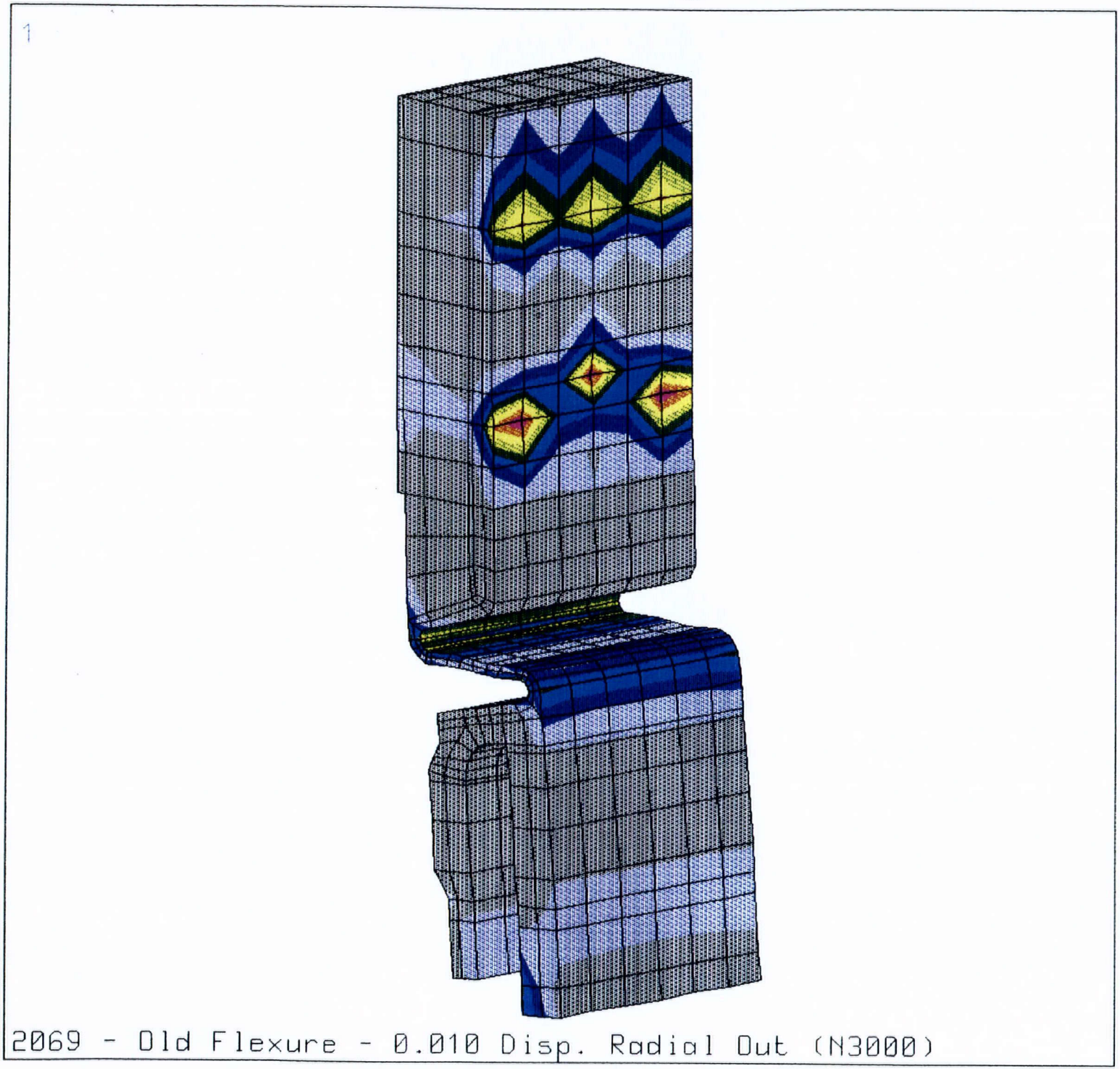
1
ANSYS 4.4
JUL 11 1990
19:01:01
PLOT NO. 6
POST1 STRESS
STEP=1
ITER=10
SI (AVG)
DMX =0.010145
SMN =116.756
SMX =15442
XV =1
YV =0.3
ZV =1
DIST=15.707
XF =65.178
YF =-13.61
PRECISE HIDDEN
116.756
1820
3522
5225
6928
8631
10333
12036
15442
2069 - Old Flexure - 0.010 Disp. Radial Out (N3000)

FIGURE 15-1

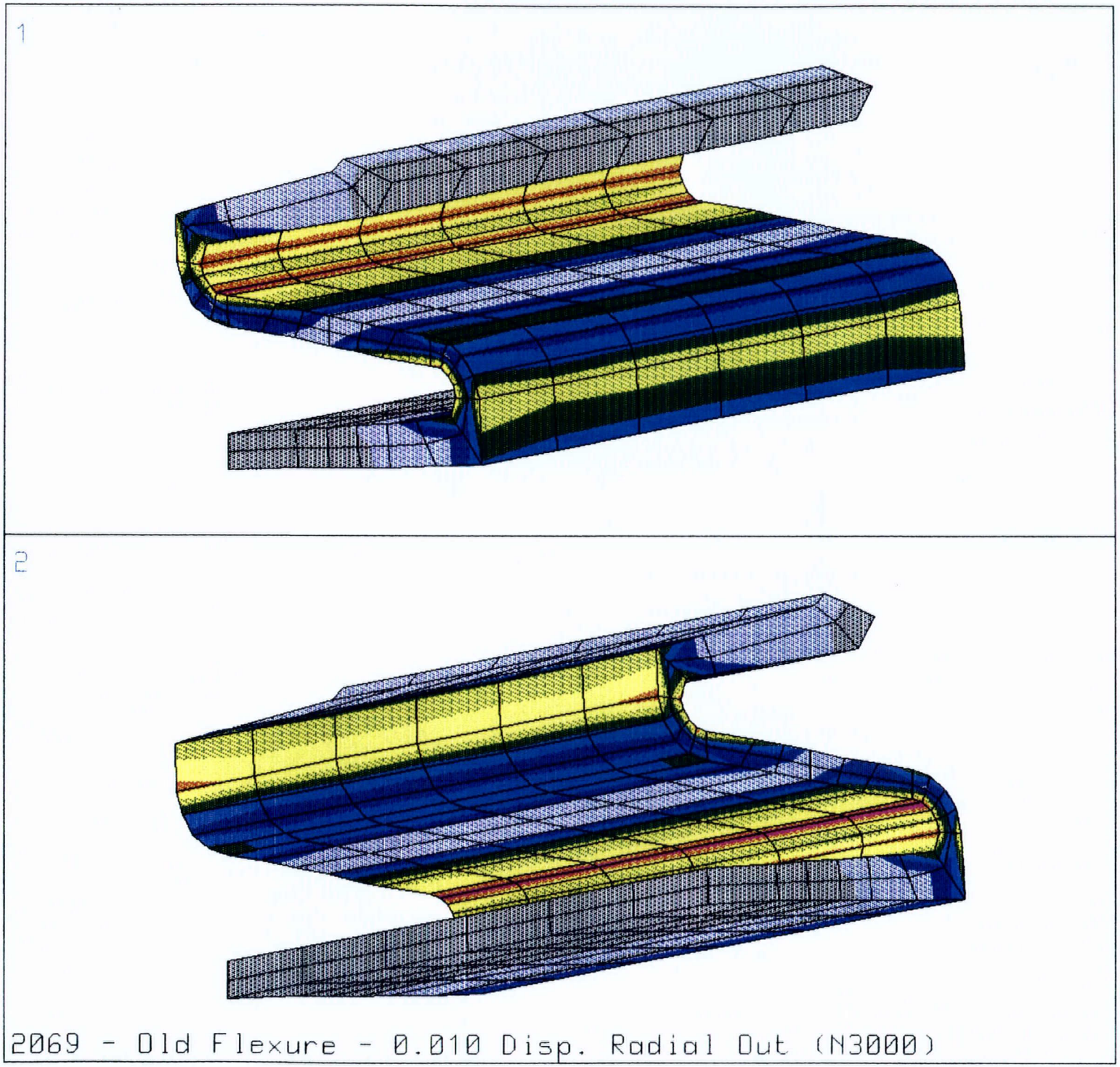
1
2
ANSYS 4.4
JUL 11 1990
18:55:13
PLOT NO. 1
POST1 STRESS
STEP=1
ITER=10
SI (AVG)
DMX =0.005398
SMN =116.756
SMX =10822
XV =1
YV =0.3
ZV =1
DIST=3.254
XF =65.32
YF =-16.756
PRECISE HIDDEN
116.756
1306
2496
3685
4875
6064
7254
8443
10822
2069 - Old Flexure - 0.010 Disp. Radial Out (N3000)

FIGURE 15-2

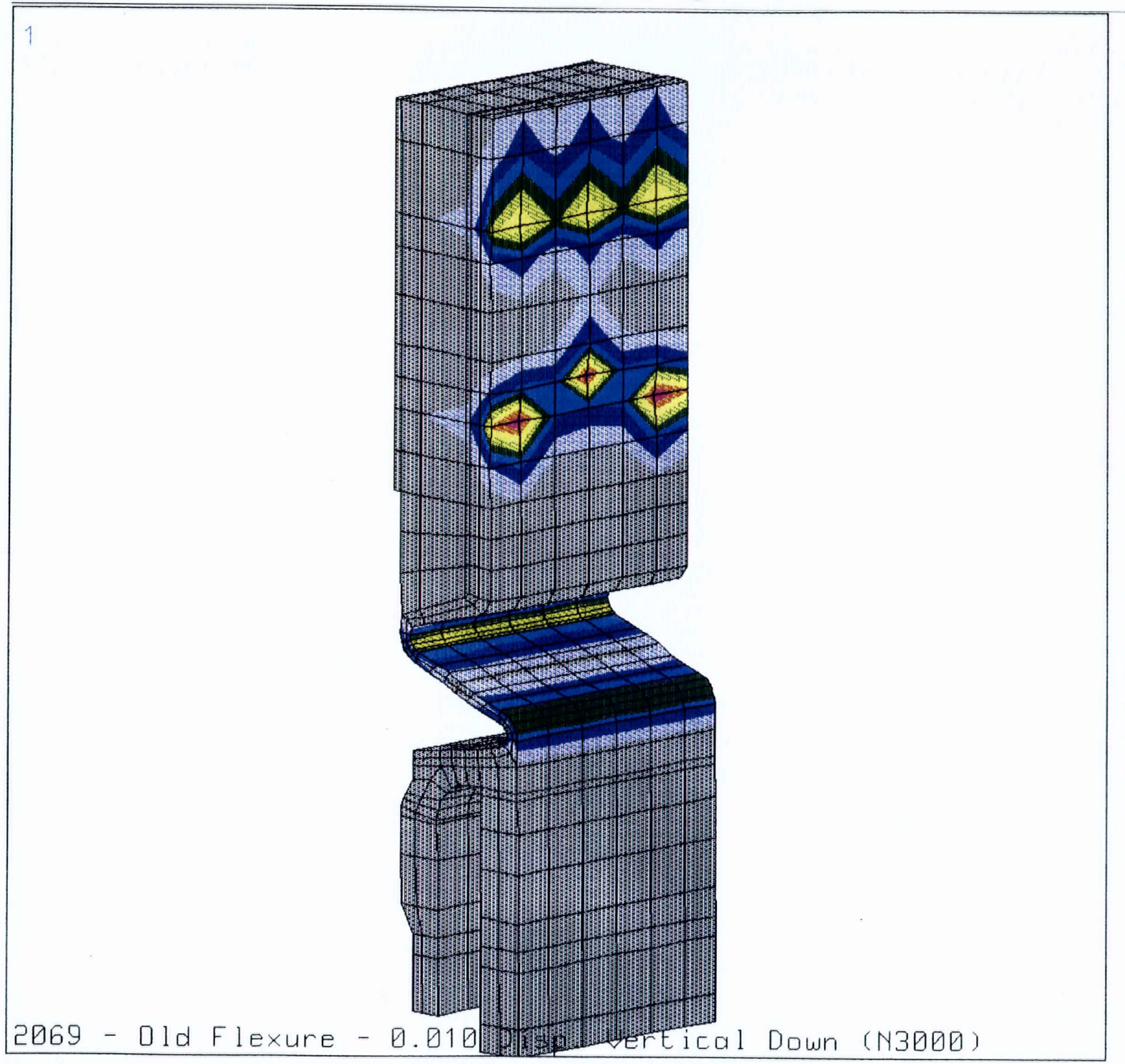
1
ANSYS 4.4
JUL 11 1990
19:02:41
PLOT NO. 7
POST1 STRESS
STEP=2
ITER=10
SI (AVG)
DMX =0.010247
SMN =10.279
SMX =15662
XV =1
YV =0.3
ZV =1
DIST=15.707
XF =65.178
YF =-13.61
PRECISE HIDDEN
10.279
1749
3489
5228
6967
8706
10445
12184
15662
2069 - Old Flexure - 0.010 Disp - Vertical Down (N3000)

FIGURE 15-3

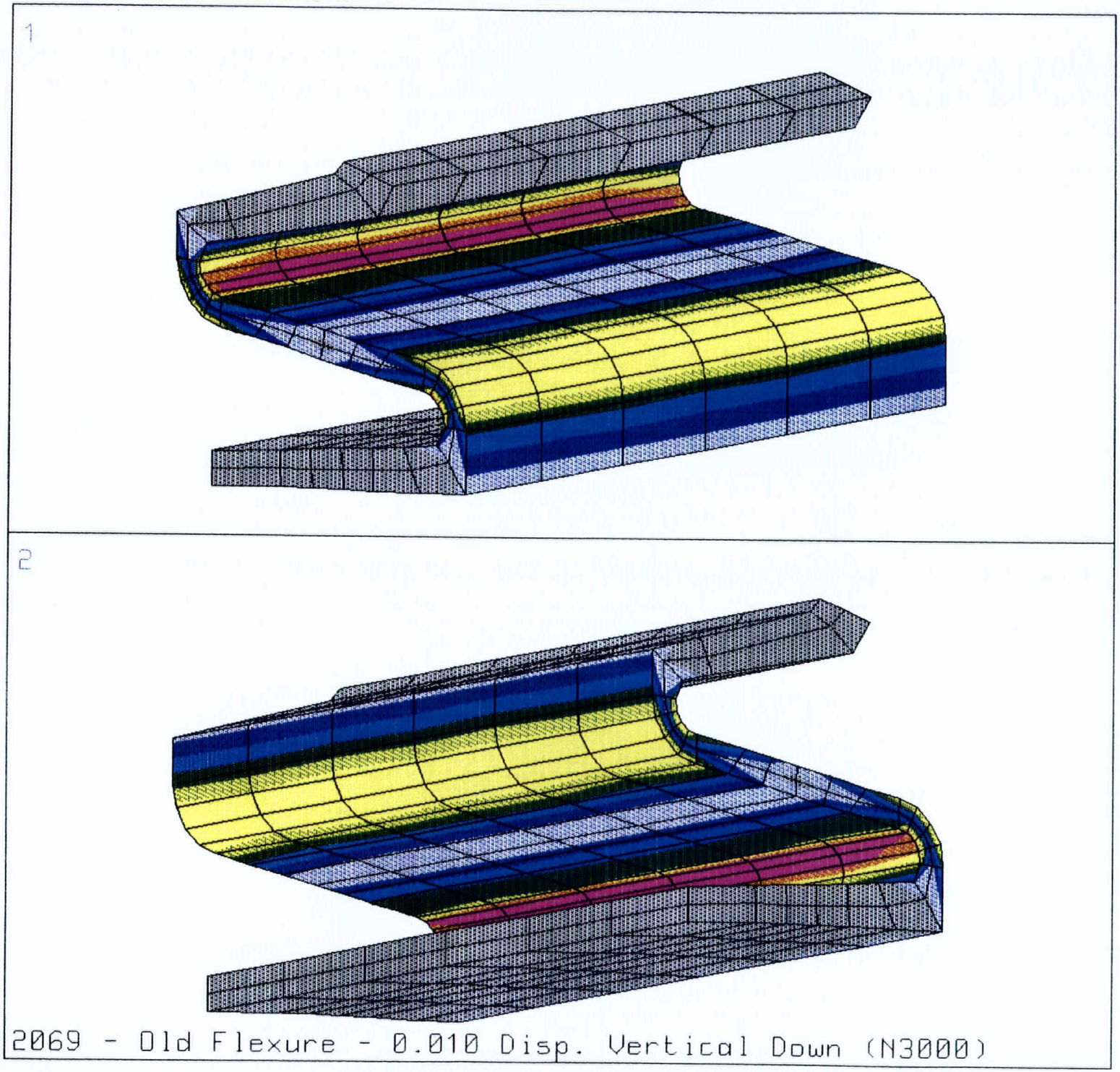
1
2
ANSYS 4.4
JUL 11 1990
18:56:21
PLOT NO. 2
POST1 STRESS
STEP=2
ITER=10
SI (AVG)
DMX =0.010212
SMN =10.279
SMX =10842
XV =1
YV =0.3
ZV =1
DIST=3.254
XF =65.32
YF =-16.756
PRECISE HIDDEN
10.279
1214
2417
3621
4824
6028
7232
8435
10842
2069 - Old Flexure - 0.010 Disp. Vertical Down (N3000)

FIGURE 15-4

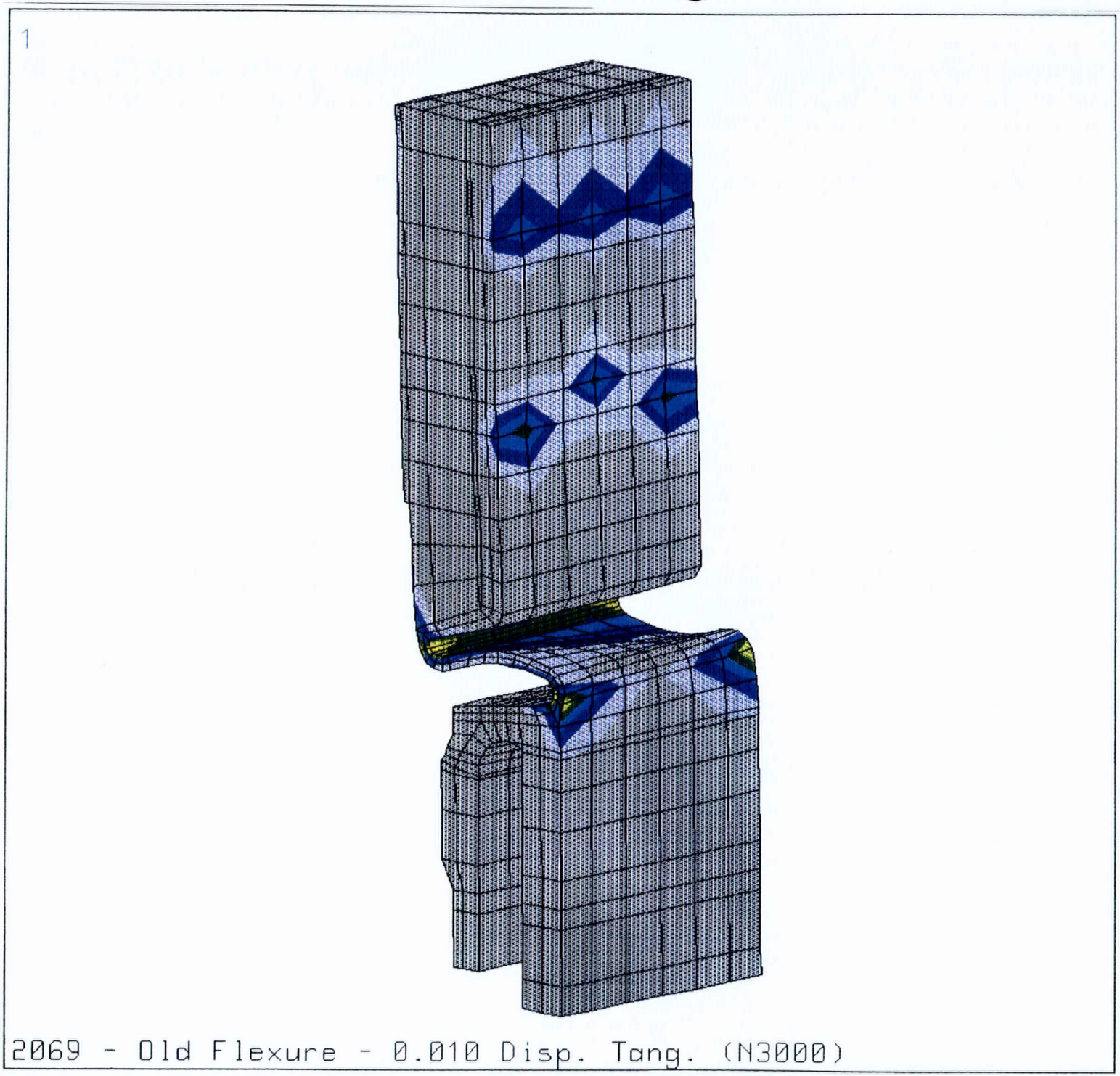
1
ANSYS 4.4
JUL 11 1990
19:04:20
PLOT NO. 8
POST1 STRESS
STEP=3
ITER=10
SI (AVG)
DMX =0.010026
SMN =153.307
SMX =31532
XV =1
YV =0.3
ZV =1
DIST=15.707
XF =65.178
YF =-13.61
PRECISE HIDDEN
153.307
3640
7126
10613
14099
17586
21073
24559
31532
2069 - Old Flexure - 0.010 Disp. Tang. (N3000)

FIGURE 15-5

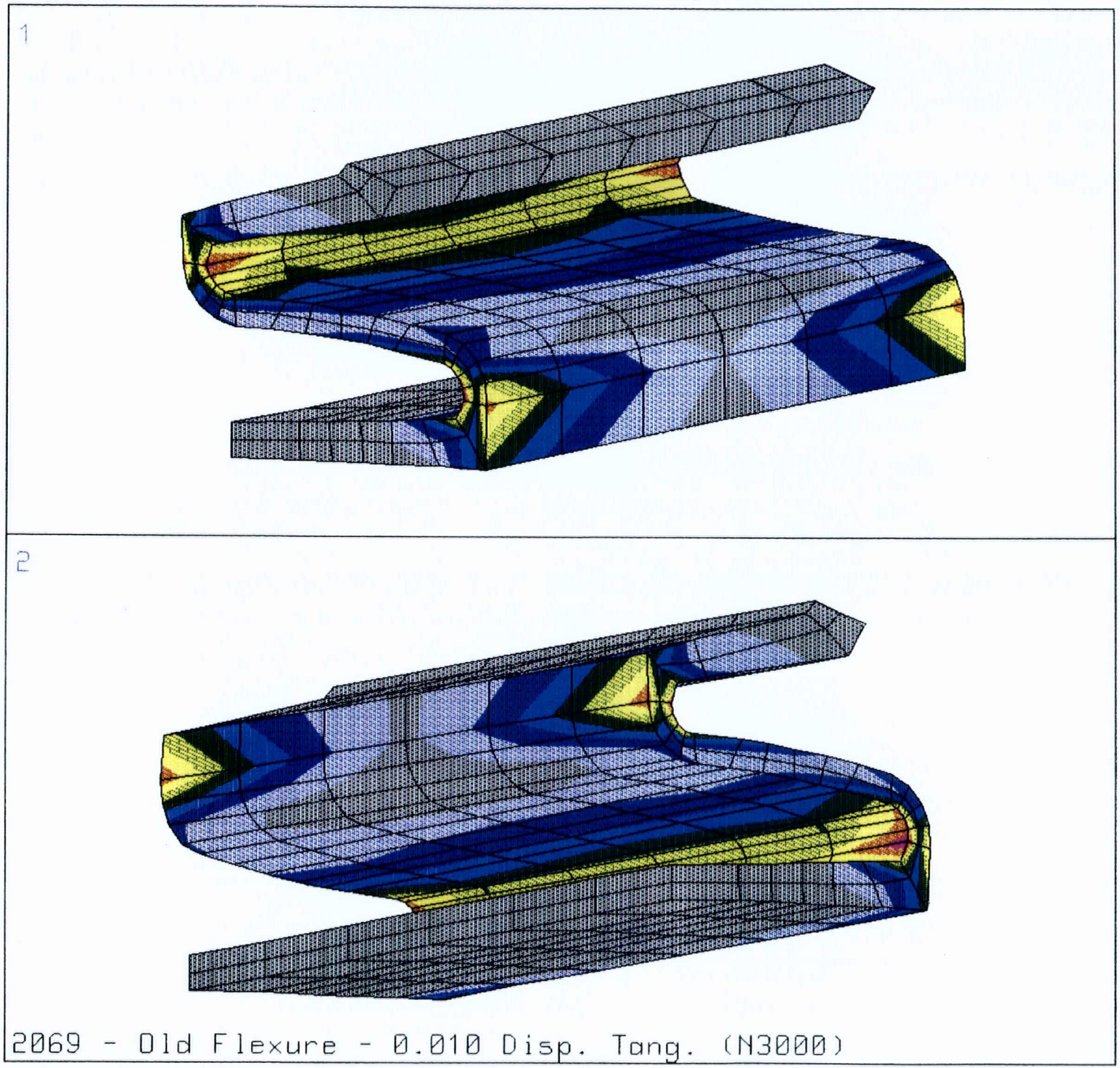
1
2
ANSYS 4.4
JUL 11 1990
18:57:26
PLOT NO. 3
POST1 STRESS
STEP=3
ITER=10
SI (AVG)
DMX =0.009143
SMN =208.24
SMX =25834
XV =1
YV =0.3
ZV =1
DIST=3.254
XF =65.32
YF =-16.756
PRECISE HIDDEN
208.24
3055
5903
8750
11597
14445
17292
20139
25834
2069 - Old Flexure - 0.010 Disp. Tang. (N3000)

FIGURE 15-6

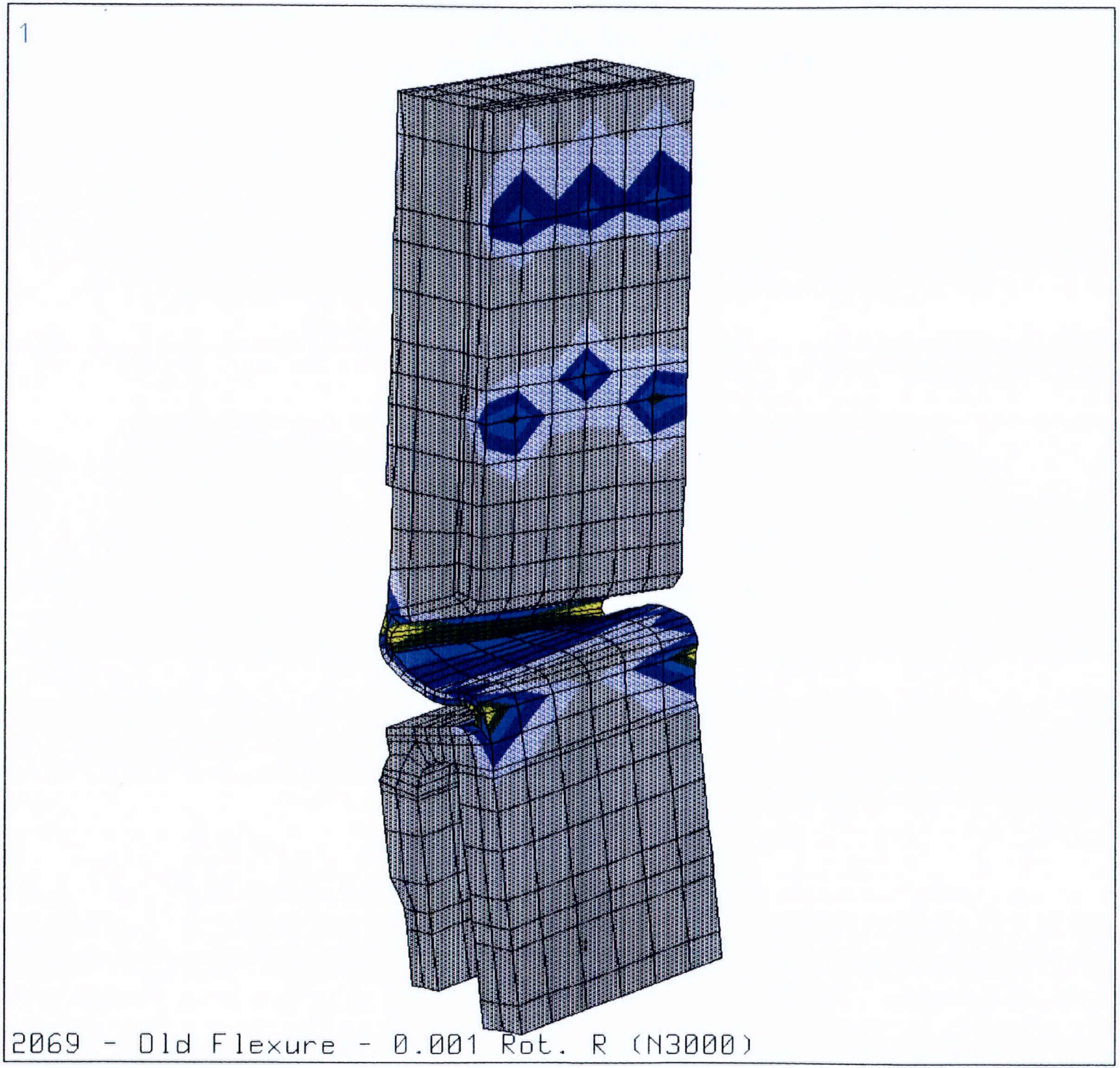
1
ANSYS 4.4
JUL 11 1990
19:06:03
PLOT NO. 9
POST1 STRESS
STEP=4
ITER=10
SI (AVG)
DMX =0.010249
SMN =144.681
SMX =32226
XV =1
YV =0.3
ZV =1
DIST=15.707
XF =65.178
YF =-13.61
PRECISE HIDDEN
144.681
3709
7274
10838
14403
17967
21532
25097
32226
2069 - Old Flexure - 0.001 Rot. R (N3000)

FIGURE 15-7

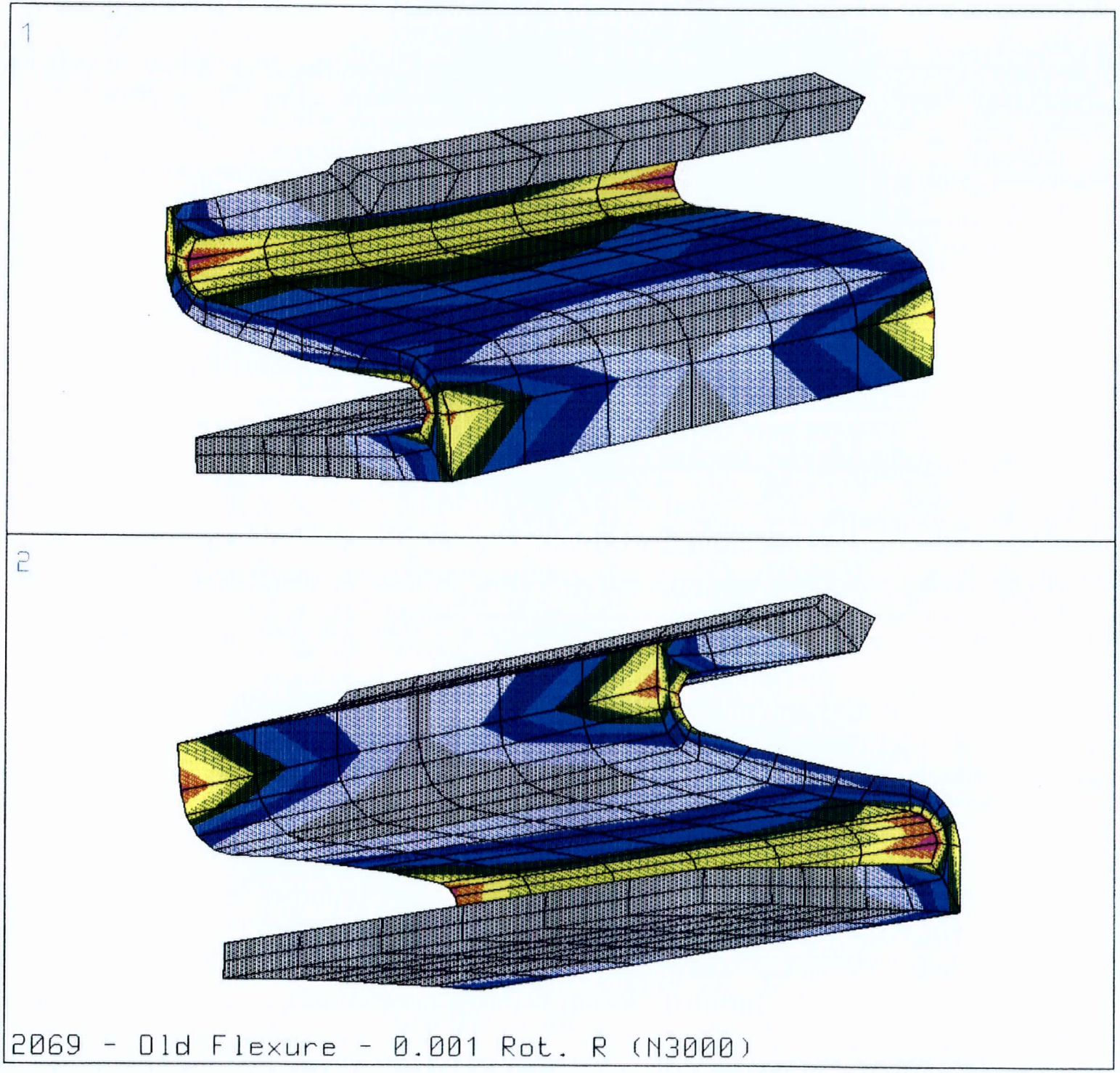
1
2
ANSYS 4.4
JUL 11 1990
18:58:30
PLOT NO. 4
POST1 STRESS
STEP=4
ITER=10
SI (AVG)
DMX =0.010249
SMN =231.696
SMX =26030
XV =1
YV =0.3
ZV =1
DIST=3.254
XF =65.32
YF =-16.756
PRECISE HIDDEN
231.696
3098
5965
8831
11697
14564
17430
20297
26030
2069 - Old Flexure - 0.001 Rot. R (N3000)

FIGURE 15-8

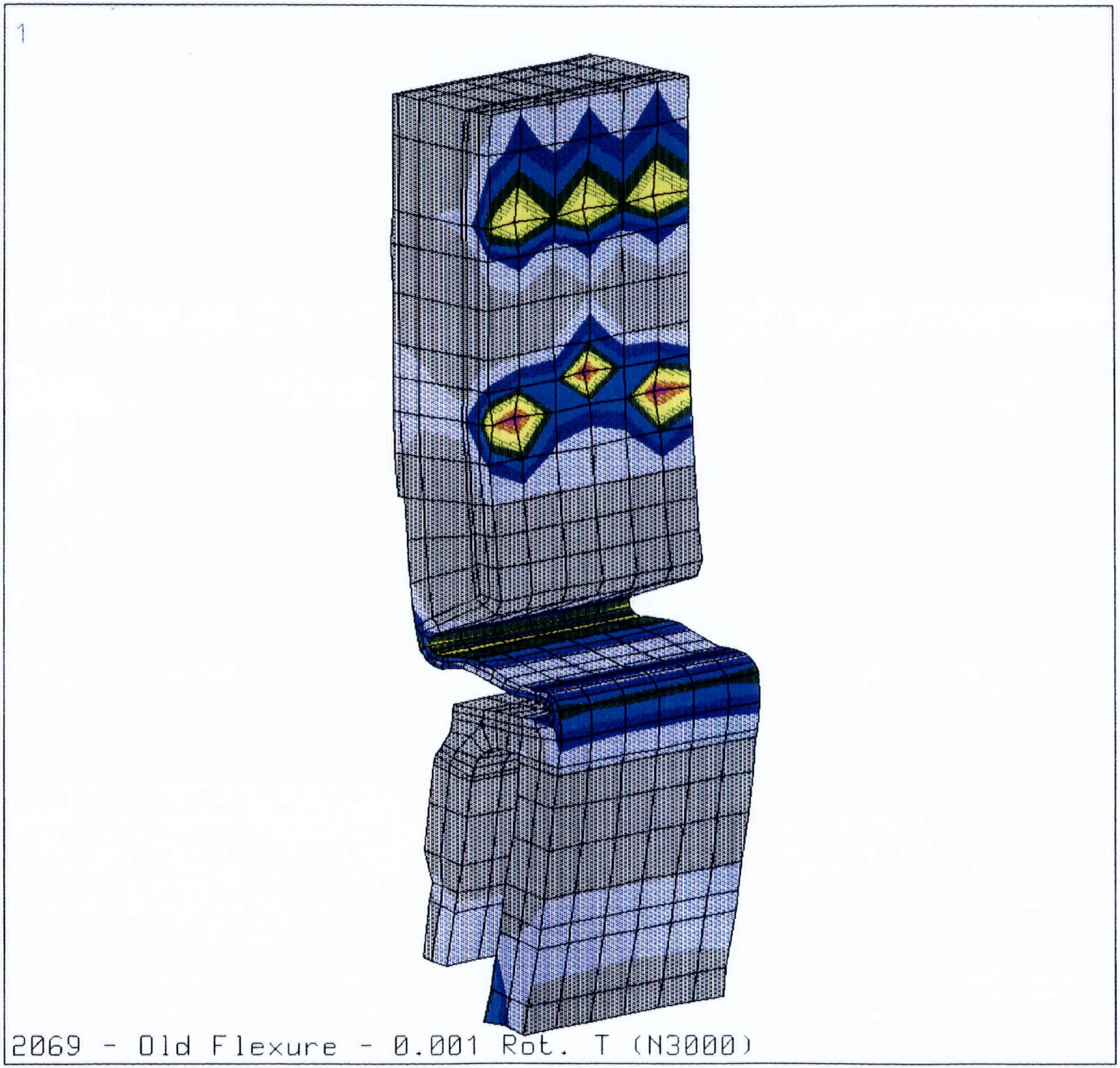
1
ANSYS 4.4
JUL 11 1990
19:07:43
PLOT NO. 10
POST1 STRESS
STEP=5
ITER=10
SI (AVG)
DMX =0.003813
SMN =121.055
SMX =15445
XV =1
YV =0.3
ZV =1
DIST=15.707
XF =65.178
YF =-13.61
PRECISE HIDDEN
121.055
1824
3526
5229
6932
8634
10337
12039
15445
2069 - Old Flexure - 0.001 Rot. T (N3000)

FIGURE 15-9

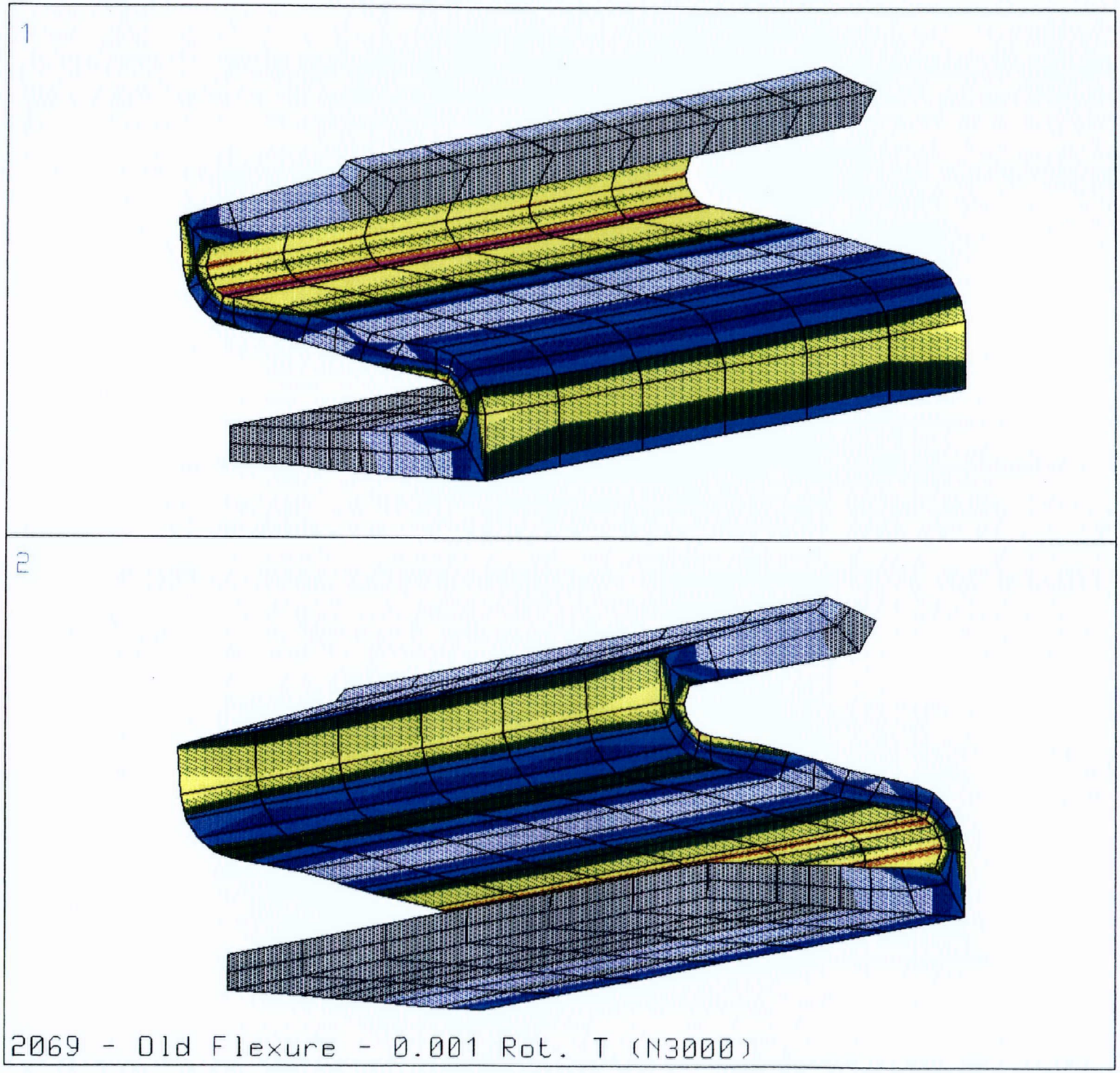
1
2
ANSYS 4.4
JUL 11 1990
18:59:36
PLOT NO. 5
POST1 STRESS
STEP=5
ITER=10
SI (AVG)
DMX =0.003813
SMN =121.055
SMX =11424
XV =1
YV =0.3
ZV =1
DIST=3.254
XF =65.32
YF =-16.756
PRECISE HIDDEN
121.055
1377
2633
3889
5145
6401
7657
8912
11424
2069 - Old Flexure - 0.001 Rot. T (N3000)

FIGURE 15-10

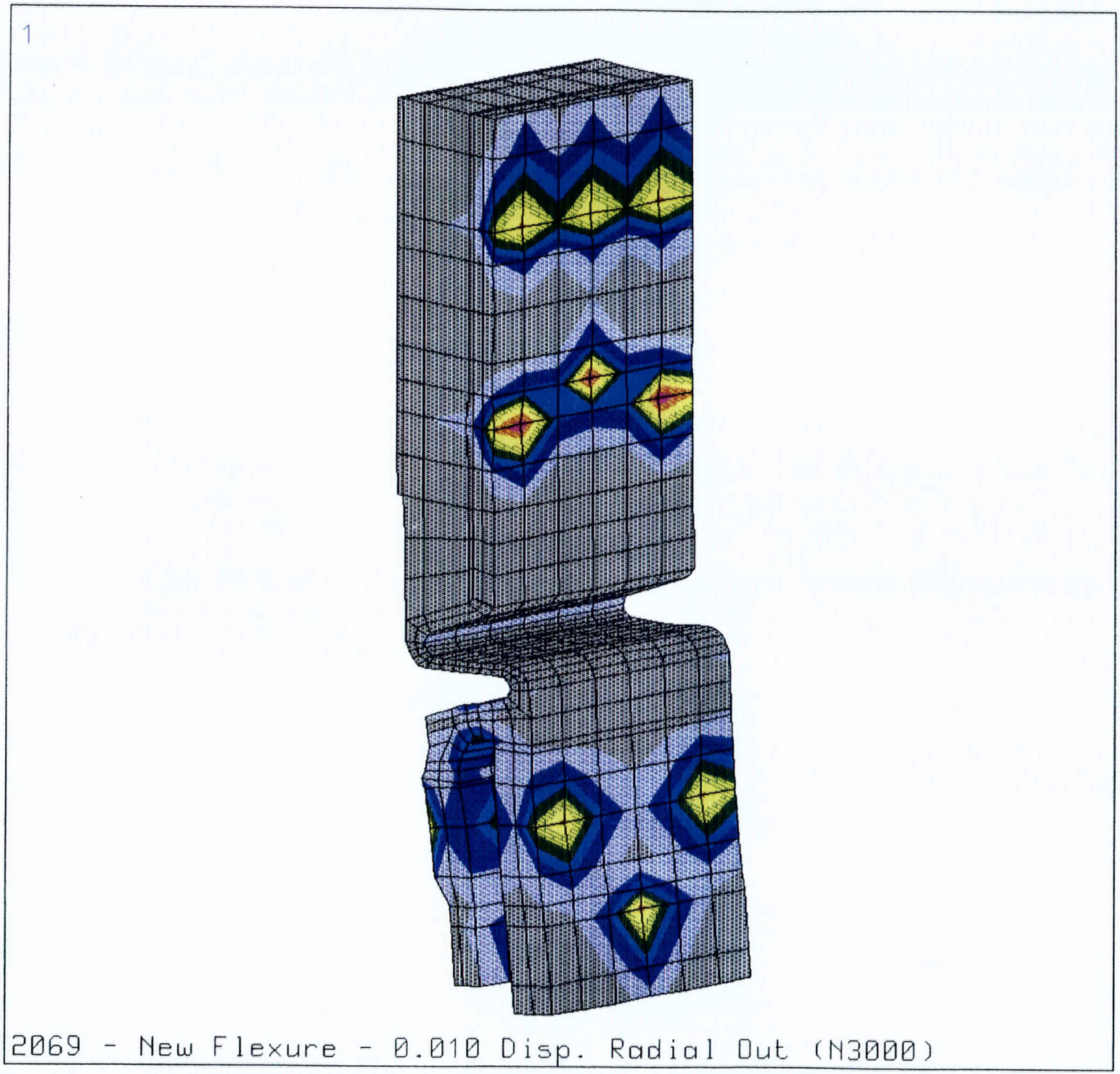
1
ANSYS 4.4
JUL 11 1990
18:03:55
PLOT NO. 6
POST1 STRESS
STEP=1
ITER=10
SI (AVG)
DMX =0.014993
SMN =359.286
SMX =27436
XV =1
YV =0.3
ZV =1
DIST=15.707
XF =65.178
YF =-13.61
PRECISE HIDDEN
359.286
3368
6376
9385
12394
15402
18411
21419
27436
2069 - New Flexure - 0.010 Disp. Radial Out (N3000)

FIGURE 15-11

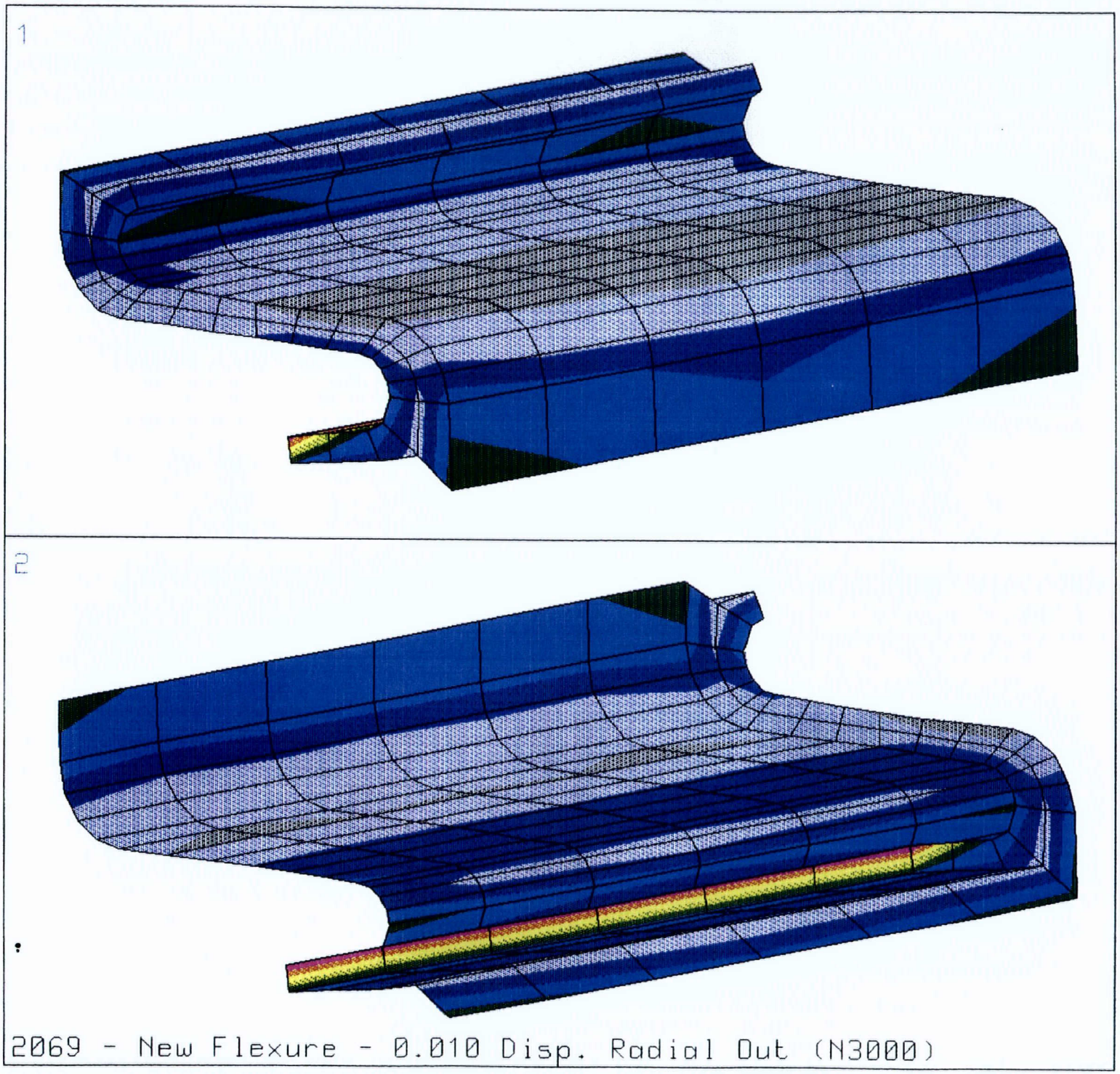
1
2
ANSYS 4.4
JUL 11 1990
17:59:51
PLOT NO. 1
POST1 STRESS
STEP=1
ITER=10
SI (AVG)
DMX =0.003818
SMN =601.342
SMX =7704
XV =1
YV =0.3
ZV =1
DIST=2.505
XF =65.32
YF =-17.015
PRECISE HIDDEN
601.342
1390
2180
2969
3758
4547
5336
6125
7704
2069 - New Flexure - 0.010 Disp. Radial Out (N3000)

FIGURE 15-12

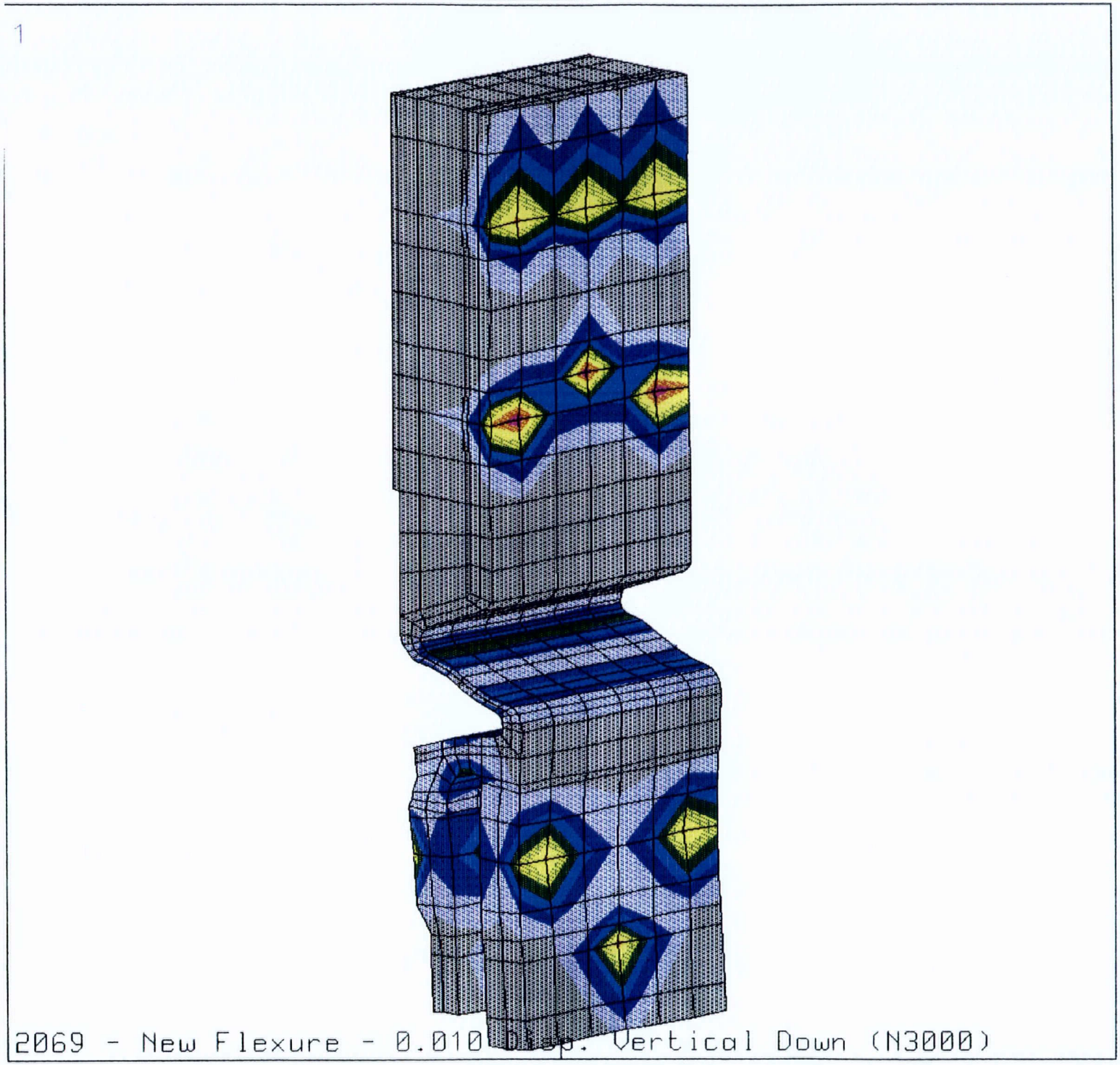
1
ANSYS 4.4
JUL 11 1990
18:05:23
PLOT NO. 7
POST1 STRESS
STEP=2
ITER=10
SI (AVG)
DMX =0.012207
SMN =98.527
SMX =27628
XV =1
YV =0.3
ZV =1
DIST=15.707
XF =65.178
YF =-13.61
PRECISE HIDDEN
98.527
3157
6216
9275
12334
15392
18451
21510
27628
2069 - New Flexure - 0.010 Disp. Vertical Down (N3000)

FIGURE 15-13

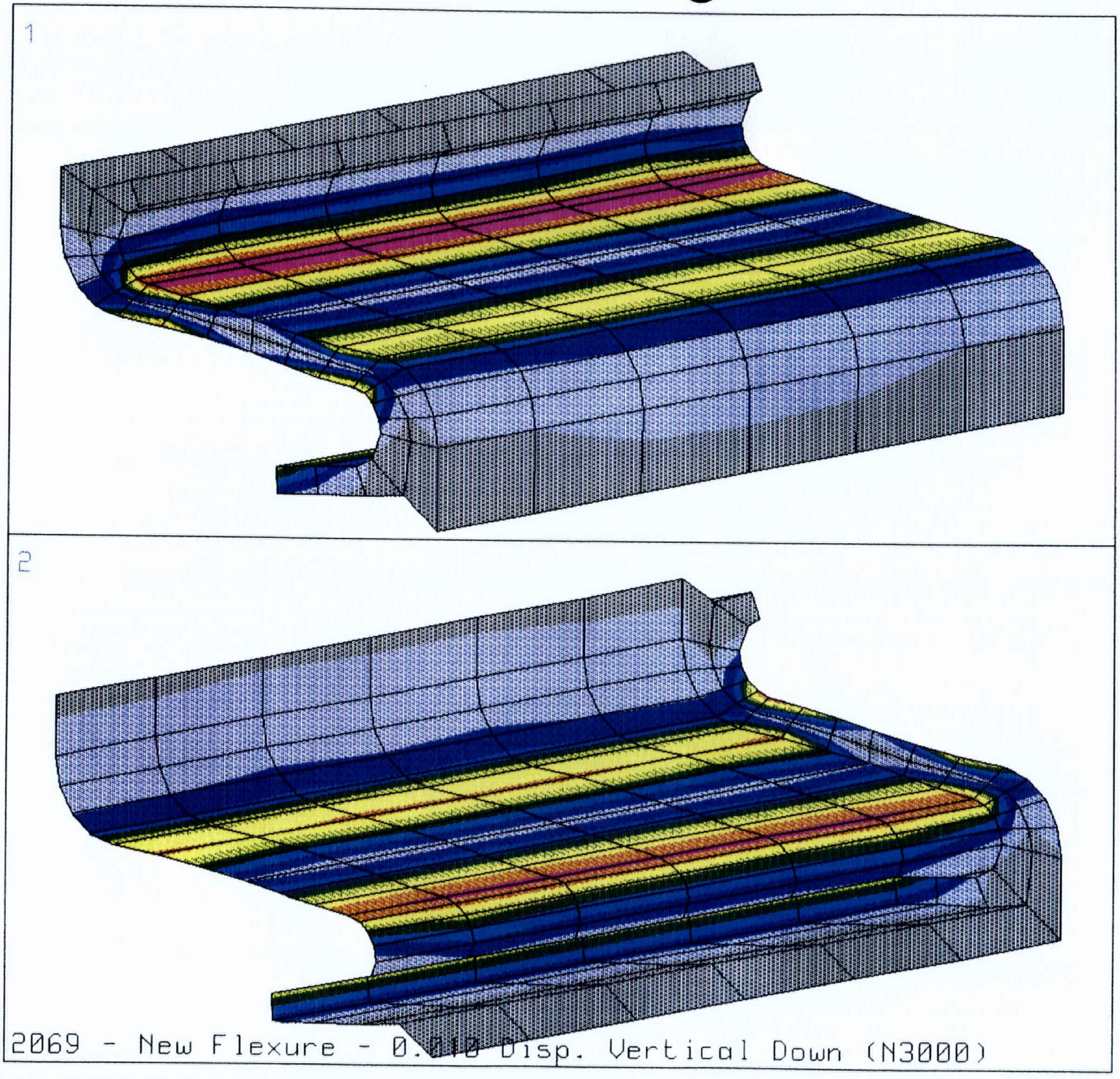
1
2
ANSYS 4.4
JUL 11 1990
18:00:37
PLOT NO. 2
POST1 STRESS
STEP=2
ITER=10
SI (AVG)
DMX =0.009453
SMN =1117
SMX =14204
XV =1
YV =0.3
ZV =1
DIST=2.505
XF =65.32
YF =-17.015
PRECISE HIDDEN
1117
2571
4025
5480
6934
8388
9842
11296
14204
2069 - New Flexure - 0.010 Disp. Vertical Down (N3000)

FIGURE 15-14

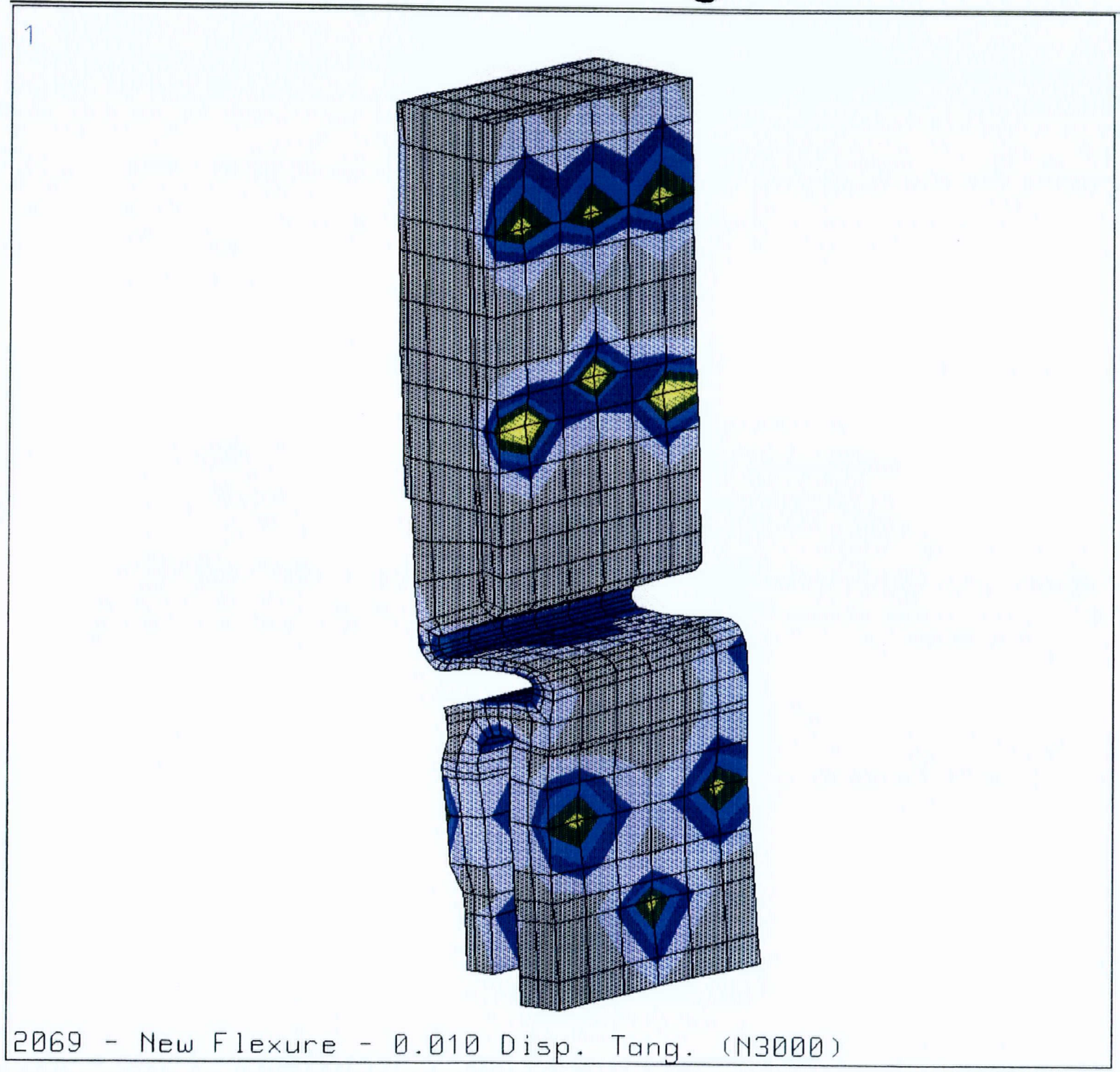
1
ANSYS 4.4
JUL 11 1990
18:06:50
PLOT NO. 8
POST1 STRESS
STEP=3
ITER=10
SI (AVG)
DMX =0.01118
SMN =414.385
SMX =35605
XV =1
YV =0.3
ZV =1
DIST=15.707
XF =65.178
YF =-13.61
PRECISE HIDDEN
414.385
4324
8235
12145
16055
19965
23875
27785
35605
2069 - New Flexure - 0.010 Disp. Tang. (N3000)

FIGURE 15-15

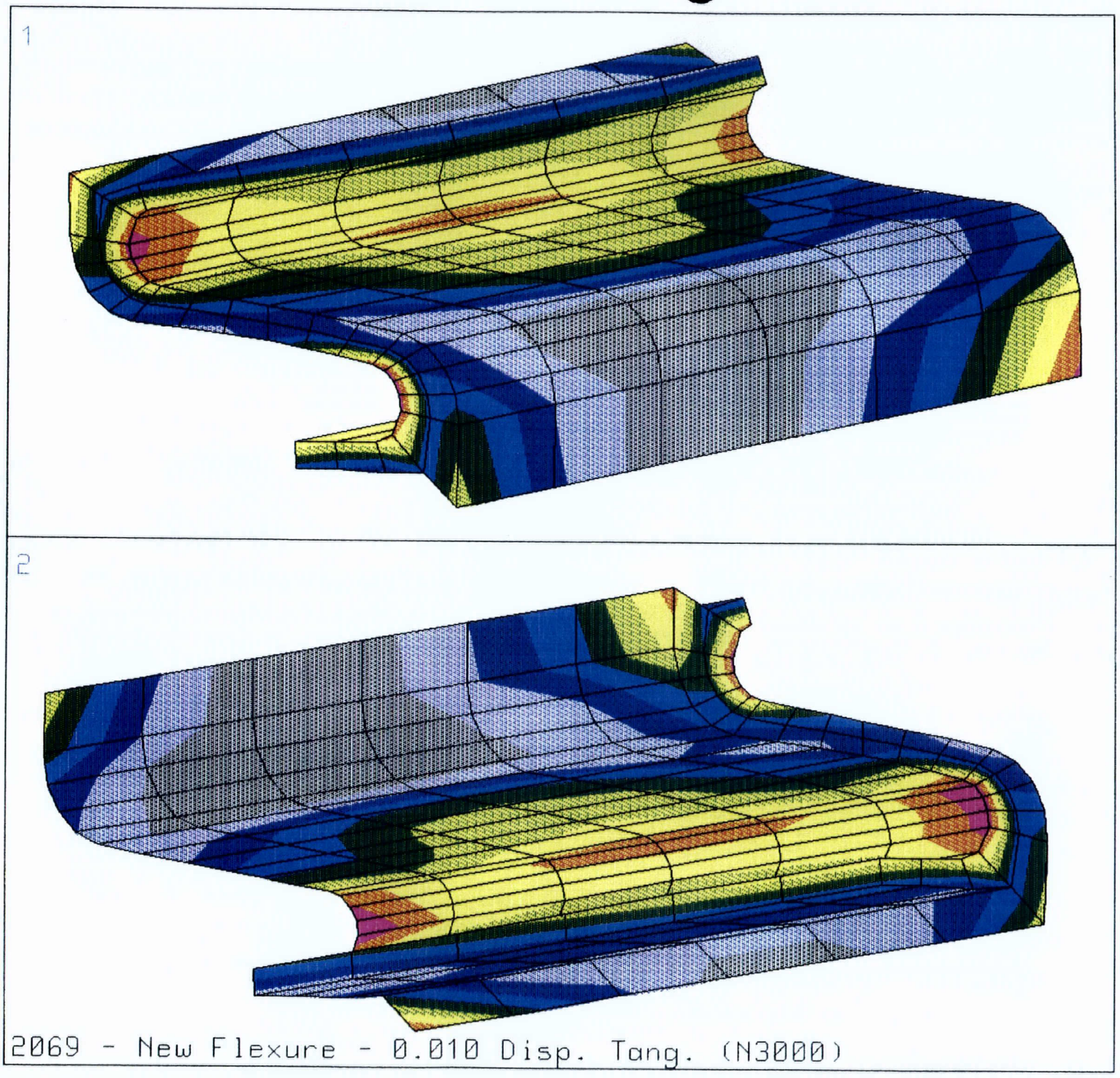
1
2
ANSYS 4.4
JUL 11 1990
18:01:24
PLOT NO. 3
POST1 STRESS
STEP=3
ITER=10
SI (AVG)
DMX =0.00801
SMN =716.875
SMX =14318
XV =1
YV =0.3
ZV =1
DIST=2.505
XF =65.32
YF =-17.015
PRECISE HIDDEN
716.875
2228
3739
5251
6762
8273
9785
11296
14318
2069 - New Flexure - 0.010 Disp. Tang. (N3000)

FIGURE 15-16

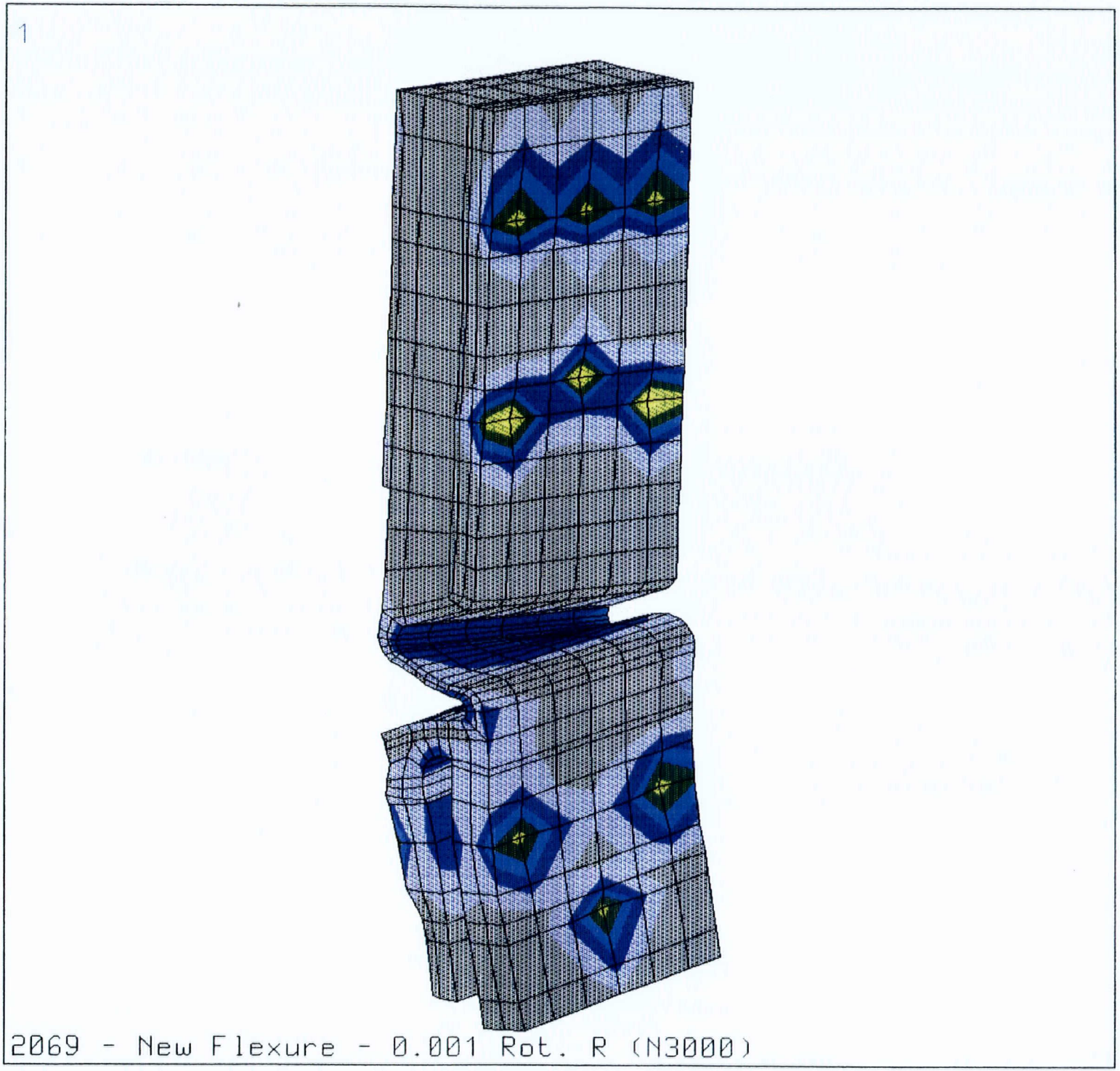
1
ANSYS 4.4
JUL 11 1990
18:08:18
PLOT NO. 9
POST1 STRESS
STEP=4
ITER=10
SI (AVG)
DMX =0.00821
SMN =424.605
SMX =36029
XV =1
YV =0.3
ZV =1
DIST=15.707
XF =65.178
YF =-13.61
PRECISE HIDDEN
424.605
4381
8337
12293
16249
20205
24161
28117
36029
2069 - New Flexure - 0.001 Rot. R (N3000)

FIGURE 15-17

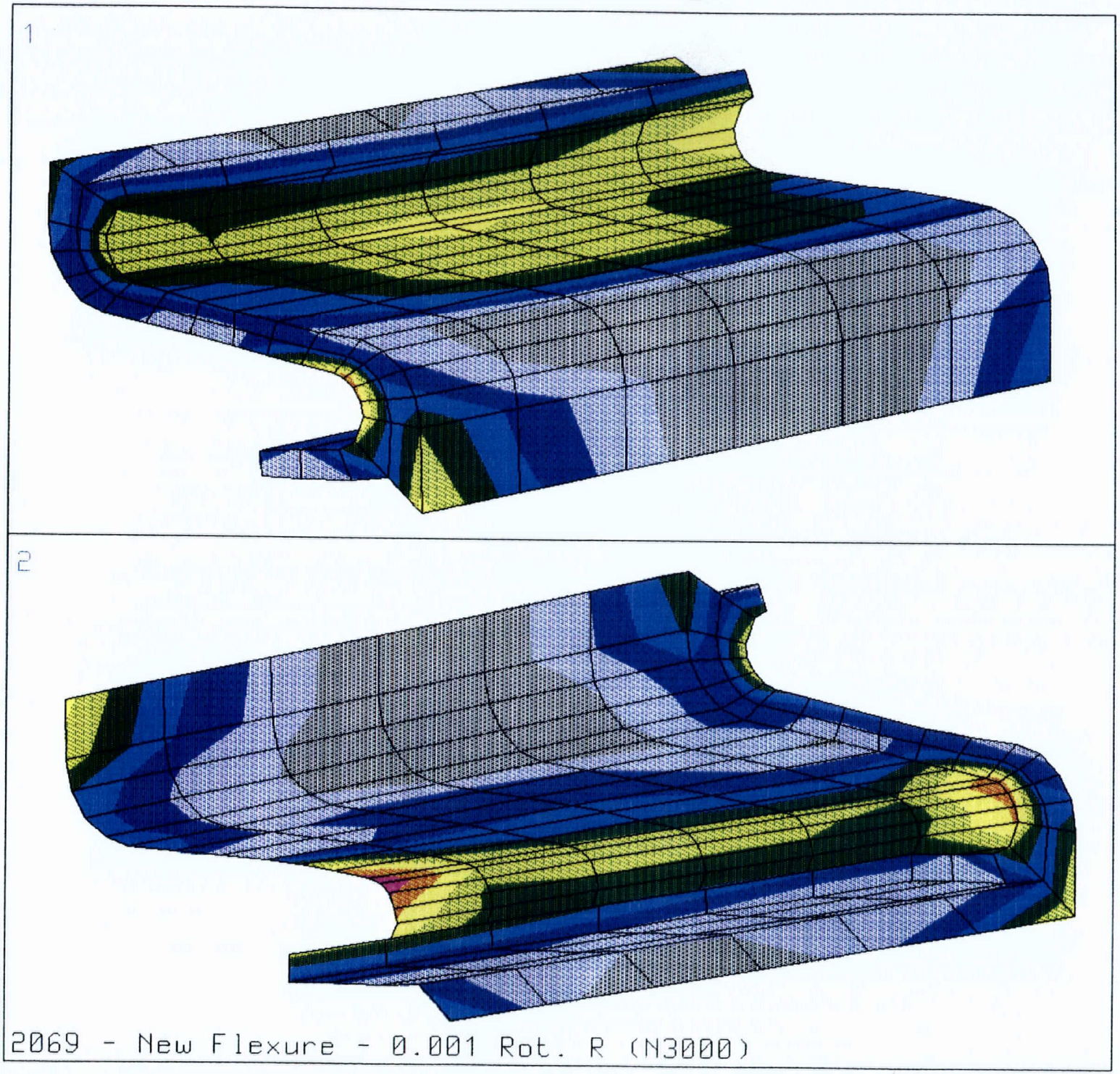
1
2
ANSYS 4.4
JUL 11 1990
18:02:11
PLOT NO. 4
POST1 STRESS
STEP=4
ITER=10
SI (AVG)
DMX =0.00821
SMN =1030
SMX =18176
XV =1
YV =0.3
ZV =1
DIST=2.505
XF =65.32
YF =-17.015
PRECISE HIDDEN
1030
2935
4840
6745
8650
10555
12461
14366
18176
2069 - New Flexure - 0.001 Rot. R (N3000)

FIGURE 15-18

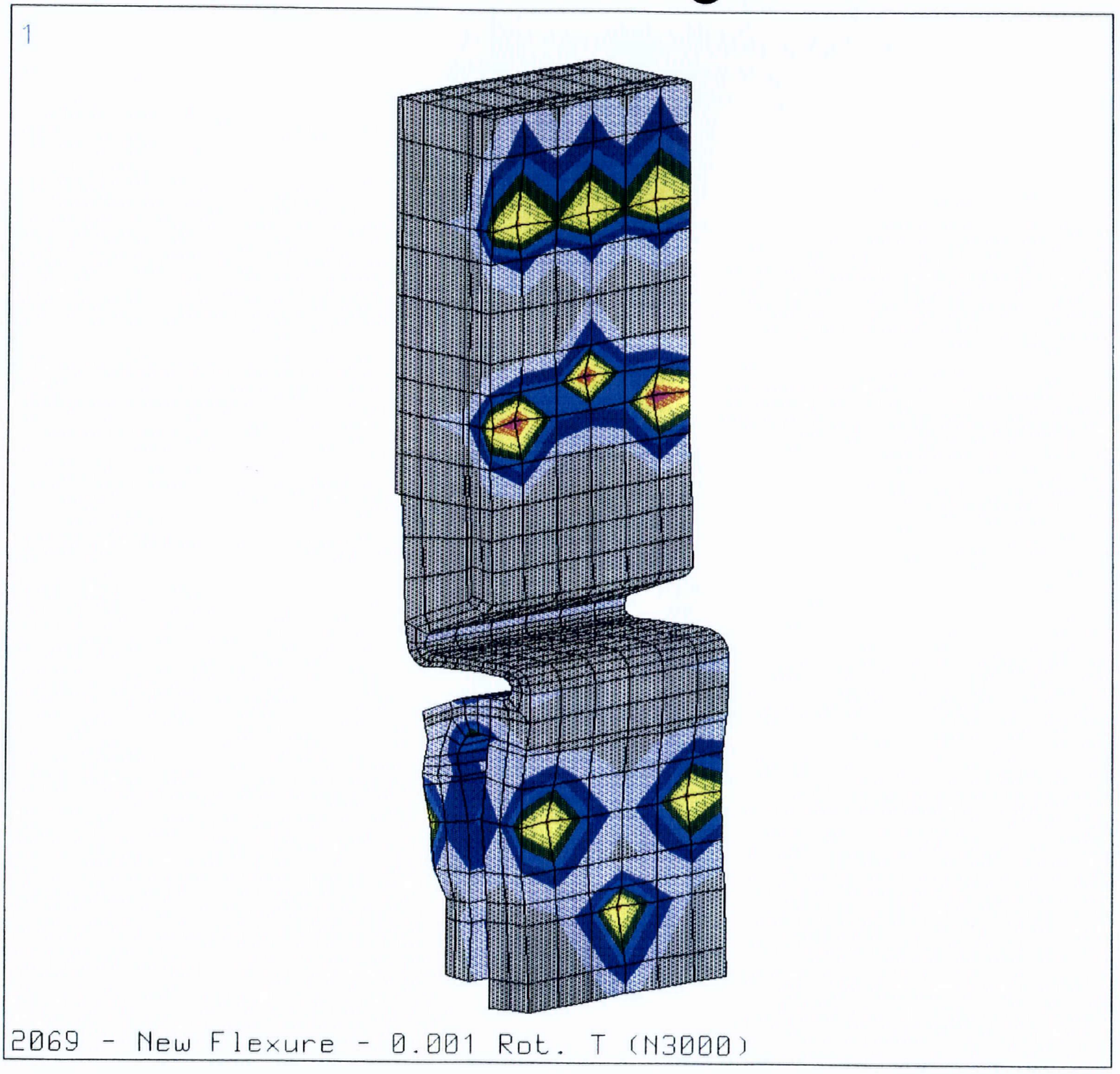
1
ANSYS 4.4
JUL 11 1990
18:09:46
PLOT NO. 10
POST1 STRESS
STEP=5
ITER=10
SI (AVG)
DMX =0.007032
SMN =360.631
SMX =27435
XV =1
YV =0.3
ZV =1
DIST=15.707
XF =65.178
YF =-13.61
PRECISE HIDDEN
360.631
3369
6377
9385
12394
15402
18410
21418
27435
2069 - New Flexure - 0.001 Rot. T (N3000)

FIGURE 15-19

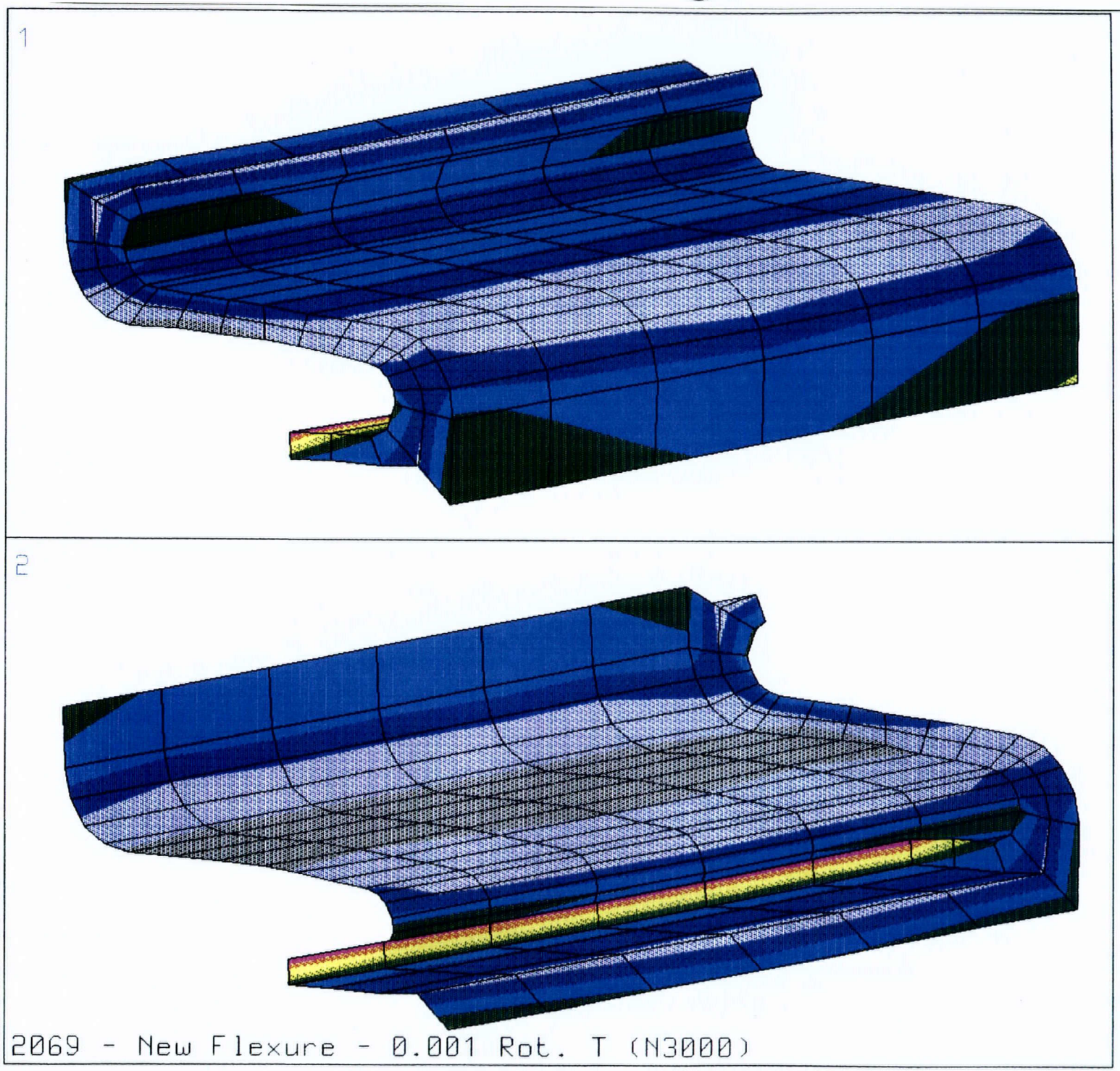
1
2
ANSYS 4.4
JUL 11 1990
18:02:56
PLOT NO. 5
POST1 STRESS
STEP=5
ITER=10
SI (AVG)
DMX =0.001806
SMN =364.853
SMX =7659
XV =1
YV =0.3
ZV =1
DIST=2.505
XF =65.32
YF =-17.015
PRECISE HIDDEN
364.853
1175
1986
2796
3607
4417
5227
6038
7659
2069 - New Flexure - 0.001 Rot. T (N3000)

FIGURE 15-20

TABLE 15-1

FREQUENCIES USED FOR RANDOM VIBRATION ANALYSIS

Case*	Core Barrel Beam Mode	Thermal Shield Beam Mode	Thermal Shield N=2	Thermal Shield N=3
6-0-6 Old	6.00	10.28/11.73	8.06/9.67	13.88/15.40
6-0-6 Old No Hydro-dynamic Mass Effect	16.24/16.67	26.05/26.61	20.50/22.51	43.01/44.32
6-0-6 New	6.01	10.46/12.0	8.36.9.83	13.81/15.50
6-0-6 New No Hydro-dynamic Mass Effect	16.25/16.72	28.35/28.8	21.15/22.17	43.58/44.15
4-0-6 New	6.01	10.37/11.72	7.36/9.44	13.74/15.41
0-0-6 New	6.01	9.96/11.71	8.02/8.69	14.48/15.27

* FLEXURES/KEYS/BLOCKS

TABLE 15-2

6-0-6 OLD (NO HYDRODYNAMIC MASS)

RESULTS FOR FLEXURES

	Displacements (mils)			Stress Intensity
ANGLE	Radial	Vertical	Tang.	σ_I (psi)
21°	5.58	1.67	5.43	14,080
85°	6.22	1.81	5.65	19,210
124°	5.96	1.70	6.18	18,210
205°	5.98	1.87	6.23	16,860
244°	6.48	1.98	5.81	19,460
325°	5.16	1.55	6.40	14,610

TABLE 15-3

6-0-6 OLD (NO HYDRODYNAMIC MASS)

RESULTS FOR BLOCKS

Angle	Displacements (mils)		Forces (Kips)		σ_I - Bolts Preload (psi)		
	Radial	Vertical	Radial	Vertical	3/4-10	1/2-13	7/8-9
0	0.0830	1.4040	1.1	22.8	768	378	3713
60	0.0378	1.4885	0.5	24.2	784	405	3663
120	0.0381	1.5691	0.5	25.5	825	424	3720
180	0.0329	1.5469	0.4	25.2	811	420	3692
240	0.1043	1.7958	1.4	29.2	1089	168	4046
300	0.1311	1.4977	1.7	24.4	844	392	3894

TABLE 15-4

6-0-6 NEW - (NO HYDRODYNAMIC MASS)

RESULTS FOR FLEXURES

Angle	Displacements (mils) Radial	Vertical	Tang.	Stress Int. (psi) σ_I
352°	3.92	1.04	4.53	11,580
85°	4.31	1.21	4.38	11,570
124°	4.35	1.24	4.23	11,590
205°	4.18	1.29	4.47	12,240
244°	4.17	1.29	4.35	11,490
325°	3.71	1.09	4.60	11,900

TABLE 15-5

6-0-6 NEW (NO HYDRODYNAMIC MASS)

RESULTS FOR BLOCKS

	Displacements (mils)		Forces (Kips)		σ_I - Bolts Preload (psi)		
Angle	Radial	Vertical	Radial	Vertical	1-8	1/2-13	7/8-9
0	0.0049	0.9707	0.1	30.1	397	143	291
60	0.0070	0.9985	0.2	31.0	408	146	300
120	0.0060	1.1747	0.1	36.5	474	176	345
180	0.0056	1.0967	0.1	34.0	444	162	323
240	0.0042	1.2073	0.1	37.5	486	183	353
300	0.0057	1.0543	0.1	32.7	428	154	313

TABLE 15-6

6-0-6 OLD

RESULTS FOR FLEXURES

Angle	Displacements (mils) Radial	Vertical	Tang	ROT r	ROT t	Stress Intensity σ_I (psi.)
21	2.4889	0.5129	3.6596	.2515E-03	.1384E-03	7,140
85	2.8276	0.6056	0.9593	.1754E-04	.1974E-03	6,700
124	2.5791	0.5148	2.3446	.7479E-04	.1340E-03	7,206
205	3.2051	0.7157	2.5902	.1420E-03	.1885E-03	8,170
244	3.6252	0.7696	3.1547	.7726E-04	.2390E-03	10,860
325	4.6400	0.9873	2.7727	.1795E-03	.2530E-03	10,370

TABLE 15-7

6-0-6 OLD

RESULTS FOR BLOCKS

Angle	Displacements (mils) Radial	Vertical	Forces (Kips) Radial	Vertical	Bolts σ_I - Preload (psi.) 3/4-10	1/2-13	7/8-9
0	4.6526	0.5008	60.9	8.1	541	188	3089
60	5.9676	0.4710	78.1	7.7	535	182	3077
120	4.9171	0.5162	64.3	8.4	540	194	3073
180	4.6556	0.4438	60.9	7.2	521	180	3016
240	6.0466	0.6962	79.1	11.3	593	227	3239
300	5.3589	0.8326	70.1	13.5	629	252	3364

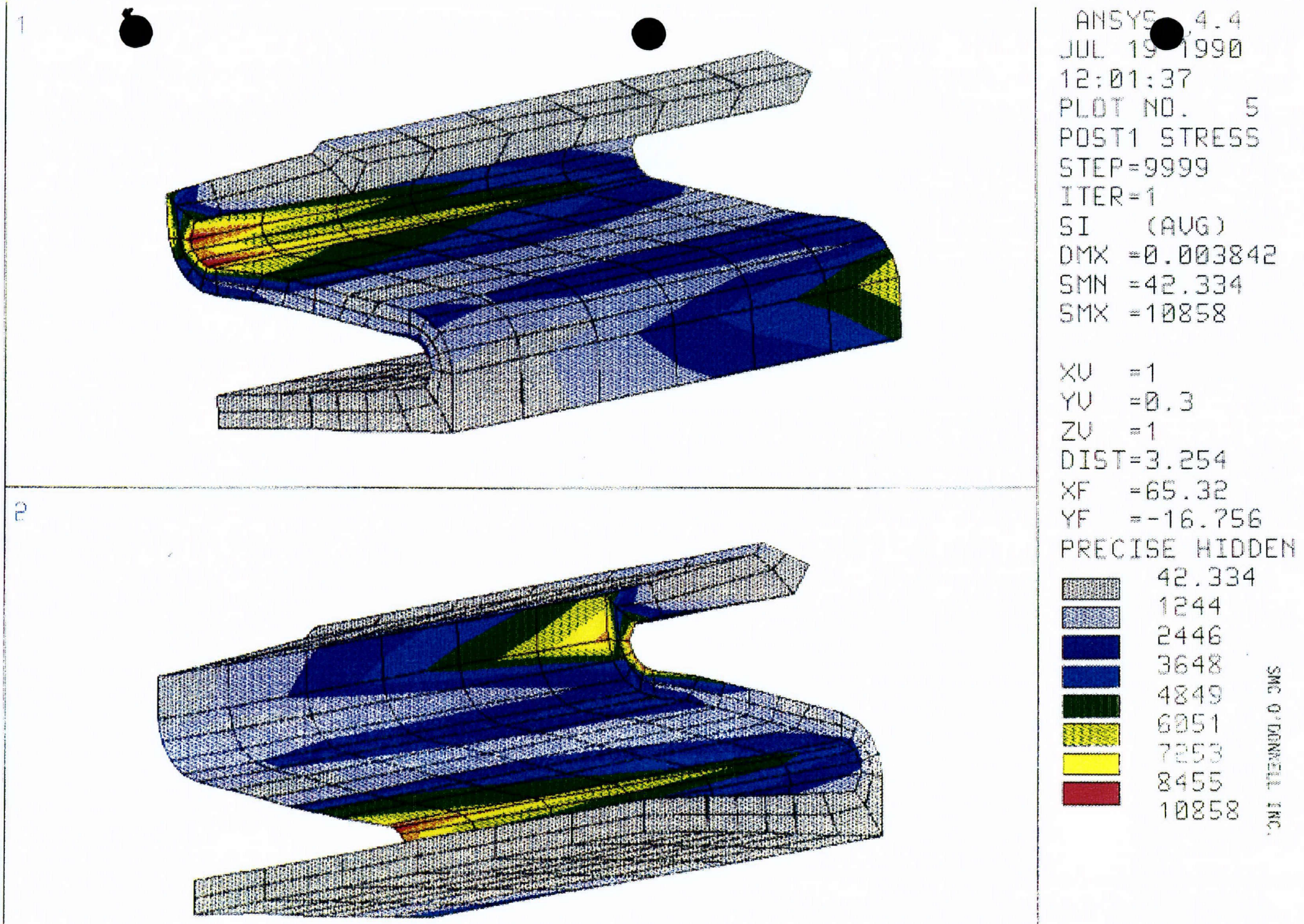

2069 - 6-0-6 - Old Flexure (244 Deg) Combined Modes

FIGURE 15-21

3 New Design - 6 Flexures, 0 Keys, 6 Support Blocks

The results for the new design are given in Tables 15-8 and 15-9. The bolt stresses with a stress concentration factor of 4 meet the limits of the ASME Code Curve B. The 1" bolts in the lower part of the flexure block have a fatigue usage factor of 0.74 considering only 7σ FIV stresses. The intent of these bolts is to close the gap between the flexure forks and thermal shield.

The stresses in the flexure web due to the flow induced vibration are shown in Figure 15-22. The fatigue damage was evaluated using both design and failure Curve A for the thermal and flow induced vibration stresses (4σ) and is given in Table 15-10. The maximum flexure stress based on FIV loads exceeds the design endurance limit. It however meets the fatigue damage limit based on the failure curve for thermal plus 7σ FIV stresses for 15 years of operation.

4. New Design - 4 Flexures, 0 Keys, 6 Support Blocks

This case was analyzed since past history has shown that all flexures do not fail simultaneously but in stages. Such a scenario permits assessment if the unit can be operated for one cycle in this configuration, thereby allowing time to plan for repair and corrective measures. The two highest stressed flexures based on Case 3 above were omitted from this configuration.

The results of this case are given in Tables 15-11 and 15-12. The support block bolt stresses with a stress concentration factor of 4 meet the ASME Code Curve B limits. The flexures meet the failure curve limit for 15 years of operation.

5. New Design - 0 Flexures, 0 Keys - 6 Support Blocks

This hypothetical case was evaluated to assess the functionality in case of no flexures. The results for this case are summarized in Table 15-13. The support block bolts with a stress concentration factor of 4 meet the failure fatigue limit for 15 years of operation.

TABLE 15-8

6-0-6 NEW

RESULTS FOR FLEXURES

Angle	Displacements (mils) Radial	Vertical	Tang	ROT r	ROT t	Stress Intensity σ_I (psi.)	Usage Factor
85	2.6583	0.5330	0.7972	.1031E-04	.1869E-03	4,892	0.04
124	2.2903	0.4758	2.1539	.4663E-04	.1127E-03	5,709	0.04
205	2.9030	0.6272	2.2302	.9319E-04	.1646E-03	7,098	0.04
244	3.6134	0.6640	2.5679	.4129E-04	.2309E-03	8,208	0.11
325	4.0866	0.7493	2.3370	.1138E-03	.2154E-03	8,761	0.26
352	3.2367	0.6057	2.8011	.9309E-04	.1824E-03	8,093	0.09

15 years = 3.78E9 Cycles
Curve A - Failure
Only Considering FIV loads

Additional FIV(POS) + OBE cycles fatigue damage:

39 (OBE + POS) cycles: (50792 + 60977) = 111769 psi → U = 0.155
231 POS cycles: 60977 psi → U = 0.002

TOTAL USAGE = 0.26 + 0.155 + 0.002 = 0.417

TABLE 15-9

6-0-6 NEW

RESULTS FOR BLOCKS

Angle	Displacements (mils) Radial	Vertical	Forces (Kips) Radial	Vertical	Bolts σ_I - Preload (psi.) 3/4-10	1/2-13	7/8-9
0	0.0195	0.3957	0.5	12.3	182	63	149
60	0.0169	0.3902	0.4	12.1	186	63	145
120	0.0119	0.4291	0.3	13.3	200	69	152
180	0.0073	0.4101	0.2	12.7	192	66	143
240	0.0272	0.5445	0.7	16.9	243	82	196
300	0.0413	0.6145	1.0	19.1	220	90	225

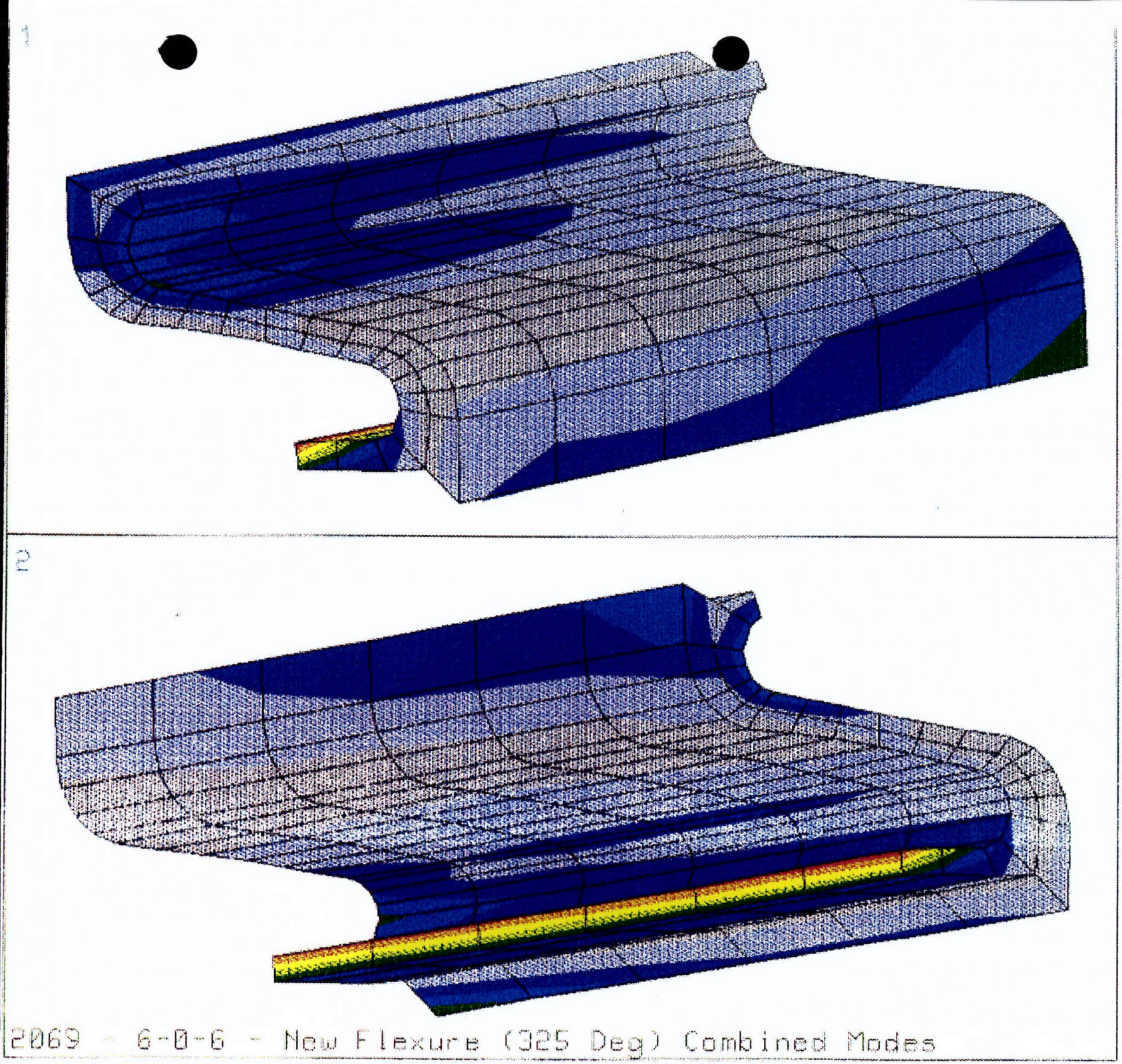

2069 - 6-0-6 - New Flexure (325 Deg) Combined Modes

FIGURE 15-22

TABLE 15-10

FATIGUE USAGE FACTOR FOR THE HIGHEST STRESSED FLEXURE, CASE 6-0-6

THERMAL AND FLOW-INDUCED STRESSES

(S_a)THRM	(POS +OBE)	POS	4σ	$4\sigma + (S_a)$THRM + (POS + OBE)	15 Yrs. Reqd. Thermal Cycles	Usage Design Curve	Usage Failure Curve
30,870	111,769			142,639	1	0.042	0.008
30,870		60,977		91,847	29	0.344	0.048
28,485			35,044	63,529	225	0.078	0.003
26,705			35,044	61,749	75	0.017	0.001
18,325			35,044	53,369	450	0.018	0.000
14,995			35,044	50,039	7185	0.213	0.005
					Σ =	0.712**	0.065*

POS - Pump Over Speed = 1.74 (35044)

* Curve A - Failure

** Curve A - Design

TABLE 15-11

RESULTS FOR FLEXURES

4-0-6 NEW

Angle	Displacements (mils) Radial	Vertical	Tang	ROT r	ROT t	Stress Intensity σ_I (psi.)	Usage Factor
85	3.0871	0.6016	0.8583	1077E-04	.2159E-03	5,580	0.04
124	2.6413	0.5404	2.4854	.5212E-04	.1309E-03	6,573	0.04
205	3.2935	0.7494	3.2551	.1332E-03	.1858E-03	9,050	0.41
352	5.1843	0.8401	3.7089	.3313E-04	.4175E-04	9,323	0.63

15 years = 3.78E9 Cycles
Curve A - Failure
Only Considering FIV loads

TABLE 15-12

4-0-6 NEW

RESULTS FOR BLOCKS

Angle	Displacements (mils) Radial	Vertical	Forces (Kips) Radial	Vertical	σ_I - Bolts Preload (psi.) 1-8	1/2-13	7/8-9
0	0.0184	0.5246	0.4	16.3	235	81	184
60	0.0180	0.4730	0.4	14.7	216	74	169
120	0.0120	0.5103	0.3	15.8	229	80	174
180	0.0069	0.4819	0.2	15.0	218	76	162
240	0.0309	0.8464	0.7	26.3	355	123	278
300	0.0451	0.8432	1.1	26.2	355	121	288

TABLE 15-13

0-0-6 NEW

RESULTS FOR BLOCKS

Angle	Displacements (mils) Radial	Vertical	Forces (Kips) Radial	Vertical	σ_I - Bolts Preload (psi.) 1-8	1/2-13	7/8-9
0	0.0297	0.5839	0.7	18.1	258	88	208
60	0.0253	0.5735	0.6	17.8	254	87	202
120	0.0164	0.5775	0.4	17.9	254	88	196
180	0.0099	0.6998	0.2	21.7	298	106	224
240	0.0389	0.8587	0.9	26.6	360	124	288
300	0.0534	0.8153	1.3	25.3	346	116	286

16.0 SUMMARY OF THE RESULTS

The present analysis was completed as part of an independent third party review of the modified thermal shield support system. The analysis included the core barrel, thermal shield, bottom support blocks, upper flexures and keys limiting radial and tangential displacement of the shield. A random flow-induced vibration analysis was performed together with structural analysis in order to determine stress ranges for fatigue life prediction. Scoping calculations of thermal and seismic stresses were also used to adjust the expected life of the support system.

The existing blocks, flexures and keys will be replaced with new components of modified better design. The new blocks have larger areas. More bolts and dowel pins of larger cross-section areas are used. Flexures without welds are made of higher strength material and the geometry of the flexure is improved to reduce stresses.

The stresses in the flexures and bolts are reduced in comparison with the old design. Fatigue resistance of bolts is also improved by introducing reduced shank design.

The results derived for the modified design are correlated using the existing design performance for the Case 6-0-6 after confirmed 50 months of operation. The analysis results show that for the modified design Case 6-0-6 (where consecutive digits define the number of integral flexures, keys and lower support blocks) the stresses in the lower block bolts meet the limits defined by curve A in the ASME Code for high-cycle fatigue with 15 years of operation.

The maximum stress ranges in the flexures do not meet the endurance limits in the ASME Code. The stresses, however, are lower than the limit defined by the failure high cycle fatigue curve for 15 years of operation.

For the Case 0-0-6 where only the blocks retain their integrity, the bolts meet the failure curve limit for 15 years of operation.

The analysis provided in the present evaluation includes significant margins of conservatism. The model qualification is based on the assumption that the flexure failures occurred after 50 months of operation, while in reality only two flexures failed sometime between 50 months and 88 months of operation. Four flexures were still intact after 88 months. Using a scale factor based on 50 months operation of the old design, thus provides a conservative evaluation of the new design. The effect of thermal transients on the old design was also excluded from model qualification to obtain a conservative scaling factor for the new design. The new design evaluation further takes no credit for the limiter keys. While the keys do wear with time, their wear is a gradual event. Even after they have worn, they provide help to the flexures in case of low probability large radial motion events.

17.0 CONCLUSIONS

The modified system is a significant improvement over the existing design.

The improvements enhance both the strength and fatigue resistance of the system.

The results of analysis indicate that the support system designed by Westinghouse with participation of Bechtel/KWU Alliance and SMC O'Donnell will retain its functionality for 15 years of operation.

In the unlikely event that the number of functional flexures is reduced to four, the operation of the plant can be continued for one cycle until refurbishment can be made.

18.0 REFERENCES

[1] "Thermal Shield Support Degradation in Pressurized Water Reactors," Sweeney, F. J. and Fry, D. N.

[2] "Big Rock Point Vibration Analysis," Corr, J. E., Proceedings, Flow-Induced Vibration, ANL-7685, 1970.

[3] WCAP - 12148, "Engineering Evaluation of the SONGS I Thermal Shield Supports," 1989. (W. - Proprietary)

[4] "Flow-Induced Vibration: Guidelines for Design Diagnosis and Trouble-shooting of Common Power Plant Components," Au-Yang, M. K., J. of Pressure Technology, 107, 1985.

[5] Dynamics of Structures, Hurty, W. C. and Rubinstein, M. F., Prentice - Hall, Inc., 1964.

[6] Flow-Induced Vibrations, R. Blevins, Van Nostrand, 2nd Edition, 1990.

[7] "A Computerized Method for Flow-Induced Random Vibration Analysis of Nuclear Reactor Intervals," Au-Yang, M. K. and Connelly, W. H., Nuclear Eng. and Design, Vol. 42, 1977.

[8] ANSYS Finite Element Code, Swanson Analysis Systems, Inc.

[9] FLOW3D (Flow Science, Inc. Los Alamos, NM).

[10] Random Vibration in Mechanical Systems," Crandall, S. H. and Mark, W. D., Academic Press, 1963.

[11] "RMS Fatigue Curves for Random Vibrations," Brenneman, B. and Talley, J. Q., J. of Pressure Vessel Technology, 1986.

[12] "Structural Response of Reactor Internal Components During Operational Tests," Simonis, J. C., and Thoren, D. E., ASME Special Publications, PVP-39, 1979.

[13] "Dynamic Pressure Inside a PWR - A Study Based on Laboratory and Field Tests Data," Au-Yang, M. K. and Jordan, K. B., Nuclear Eng. and Design, Vol. 58, 1980.

[14] "Response of Reactor Intervals to Fluctuating Pressure Forces," Au-Yang, M. K., Nuclear Eng. and Design, 35, 1975.

[15] "The Effect of Liquids on the Dynamic Motions of Immersed Solids," Fritz, R. J., J. of Engineering for Industry, 1972.

[16] "Normal Mode Solution of Fluid-Coupled Concentric Cylindrical Vessels," Stokey, W. F. and Scavuzzo, R. J., J. of Pressure Vessel Technology, 1978.

[17] "Dynamics of Coupled Fluid-Shells," Au-Yang, M. K., J. of Vibration, Acoustics, Stress and Reliability in Design, 1986.

[18] "Combining Modal Responses and Spatial Components in Seismic Reponse Analysis," USNRC Regulatory Guide, 1.92, 1976.

APPENDIX A

FLOW MODELING AROUND THERMAL SHIELD

S. T. Green and J. C. Simonis
Southwest Research Institute

O'Donnell and Associates requested that Southwest Research (SwRI) perform an analysis of the flow in the annulus between the reactor core barrel and the containment vessel wall of the San Onfree Nuclear Generating Station reactor. This analysis was to include the thermal shield in the lower region of the annulus with the primary objective being to determine the differential pressure acting developed between the inner and outer surface of this shield. This analysis was to include the effects of operating one, two, or three of the feedwater supply pumps.

Geometric Model

The flow field studied in this investigation included only the annular region between the core barrel and the containment vessel. This region extends from the bottom of the thermal shield to the top of the core barrel. Drawings showing this area are presented elsewhere in this report.

The fluid dynamics code, FLOW3D (Flow Science, Inc., Los Alamos, NM) was used to model the flow in this annular region. This code was chosen because of its unique capability to model solid obstacles embedded in the flow field. In this case, the thermal shield suspended in the annular passage is such an obstacle. This computer code also has the ability to simulate sources of mass flow in the computational mesh which was invoked here to model the water flow from the pump inlet piping.

A finite difference mesh was developed to encompass the annular region between the core barrel and the containment vessel walls. The coordinate system for this geometric model is a polar-cylindrical system located at the bottom center of the vessel with the polar axis aligned with the centerline of the vessel. A plan view of the finite difference mesh used for this analysis is shown in Figure A-1. In this and other two-dimensional representations of the flow field, the "X" and "Y" labels refer to the radial ("R") and azimuthal ("θ") coordinate directions, respectively. The "X" axis denotes the $\theta = 0°$ position. The "Z" label refers to the polar coordinate direction.

Referring to Figure A-1, the region between the inner surface of the thermal shield and the core barrel was modeled with 8 computational cells as was the region between the outer thermal shield surface and the containment vessel. The thickness of the thermal shield itself was modeled by 2 computational cells. These cells were blocked to water flow in the area where the shield exists,

but these cells were open to flow in the area above the actual shield. This blockage is indicated in the elevation cross-section of Figure A-2. A developed elevation view of the mesh (i.e., unrolled) is shown in Figure A-3. This clearly shows the nonuniform mesh used in the vertical and circumferential directions. The corresponding developed elevation view of the shield and the location of the pump inlets is shown in Figure A-4.

It should be noted that these figures are taken directly from the graphics post-processor of the FLOW3D code. These are meant to be used as diagnostic tools in performing the computational analysis and are not represented here as engineering drawings of the actual components.

The boundary conditions of the flow field included solid walls at the inner and outer radial surfaces of the mesh. These are the core barrel and containment vessel walls, respectively. A solid wall was used at the top of the mesh to represent the top of the annulus, while a simple "outflow" boundary is used at the bottom of the mesh. There is no real boundary to the flow in the circumferential direction; however, the computational model requires that reflective boundaries be supplied at the minimum and maximum angular positions of the mesh. This ensures that any fluid that exits one side of the mesh enters through the other side in the circumferential direction.

The specification of the inlet water flow required a unique model for this analysis. Referring to the plan view of Figure A-1, the pump inlet pipes are located at 60°, 180°, and 240° from the position marked "1". In the 2-pump configuration, Inlets 1 and 3, at 60° and 240°, respectively, are used to supply water to the flow field. In the 1-Pump case, Pump 2 at 180° is used to supply the water flow to the system.

At first, a mass flow rate transverse to the annulus in the radial direction was specified. The entire inlet flow is directed across thin computational cells and must turn quickly from the radial to the circumferential and downward direction. Because FLOW3D achieves a steady state flow solution only after resolving the initial transient, this inlet flow specification leads to exceedingly small time steps. Indeed, regarding the large pipe diameter of 36" in relation to the annulus gap of 8.25" in that region, it is obvious that the flow actually begins its deflection while still inside the pipe. This effect cannot be resolved with the geometric model employed here and is of little interest to this investigation.

To prevent the excessive computational efforts associated with the feedwater inlet region of the flow field, the inlet flows were modeled as mass sources embedded in the annular gap. These mass sources may be viewed as cylindrical objects coaxial with the inlet pipes which have water uniformly ejecting from their surfaces. Each of these mass sources were specified so as to inject water into the annulus parallel to the annulus walls and away from the simulated pipes. The strength

of each mass source was specified so that 69560 gpm was ejected from the surface of each mass source. In the case of 1- and 2-Pump operation, the appropriate mass source was removed from the model and the entire annulus gap in that particular region was open to flow as dictated by the remaining pump(s). This technique does not properly model the impact and turning of the inlet flow against the core barrel; however, the accurate modeling of this process was not the goal here.

Results

The results of the computational simulation for the 1-pump scenario are summarized in Figures A-5 through A-8. Figures A-5 through A-7 show the results in a two-dimensional θ-z surface at a particular radial position. These color images are taken from the graphical post-processor of FLOW-3D, which uses SI units (meters, Pascals, meters/sec). Figure A-5 is for a surface extending along the entire height of the annulus gap just inside the thermal shield inner surface. The velocity vectors (which are headless) show how the flow spreads away from the feedwater inlet and flows out the bottom of the annulus. Note also that the pressure in the annulus is greatest at the bottom of the flow field. This shows that the pressure drop related to wall friction is not as great as the hydrostatic pressure caused by the force of gravity. Also note that there are some anomalies associated with the graphics processor in the region of the feedwater inlets. These shapes are not real features of the flow field but are caused by the inability of the plotting software to show the true shape of the inlet at the resolution specified by the geometric model.

Figures A-6 and A-7 show similar results only for the region along the inner and outer surfaces of the thermal shield. Because of the difference in gap width between the thermal shield and the other surfaces, the fluid streamlines are markedly different along the inner and outer thermal shield surfaces. Of greater significance, however, is the difference between the pressure on these surfaces. Comparing these two figures, one can see that, just under the feedwater inlet, the pressure at the top of the thermal shield is greater on the inner surface than on the outer surface.

This effect is more clearly observed in Figure A-8 which shows line contours of pressure difference in units of psi. In this figure and other similar figures, a positive pressure difference is oriented radially inward. So, Figure A-8 shows that there is net force at the 180° position oriented toward the center of the vessel and a net force at the 0° position oriented away from the center. These are additive, so there is a strong force oriented along the x-axis and an associated moment about the y-axis.

The results of the 2-pump configuration are summarized in Figures A-9 through A-12. These figures are similar in nature to those for the 1-pump configuration. Figure A-9 clearly shows the interaction of the flow from each of the feedwater inlets along the 180° position. Also, the difference in pressure from the top to the bottom of the flow field is not as severe as in the 1-pump case.

Figures A-10, A-11, and A-12 show that there is still a net pressure difference between the inner and outer thermal shield surfaces. Because there are now two inlets instead of one, the effect of this pressure difference is not as severe for two pumps; however, there is still a net force oriented in the negative x-direction.

Finally, the computational results for the 3-pump configuration are summarized in Figures A-13 through A-16. The color images in A-13, A-14, and A-15 show that the velocity and pressure are highly uniform along most of the thermal shield in the azimuthal direction. It is also interesting to note that the minimum pressure in the annulus is not at the top of the vessel but is located near the top of the thermal shield. This is caused by the interaction and magnitude of the flow from the three feedwater inlets.

There are still pressure variations in the circumferential direction for the 3-pump case along the top of the shield, but these are symmetrically oriented around the thermal shield. This is to be expected because of the symmetry of the feedwater inlets in this case. This symmetry will exist as long as the thermal shield is symmetrically placed and the three flow rates are balanced.

X-Y MESH

	X	Y
NUMBER OF CELLS=	18	20
SMALLEST CELL=	5.556E-03	5.396E-01
LARGEST CELL=	3.175E-02	7.194E-01
MAXIMUM CELL RATIO=	5.714E+00	1.167E+00
	AT CELL 9	AT CELL 3

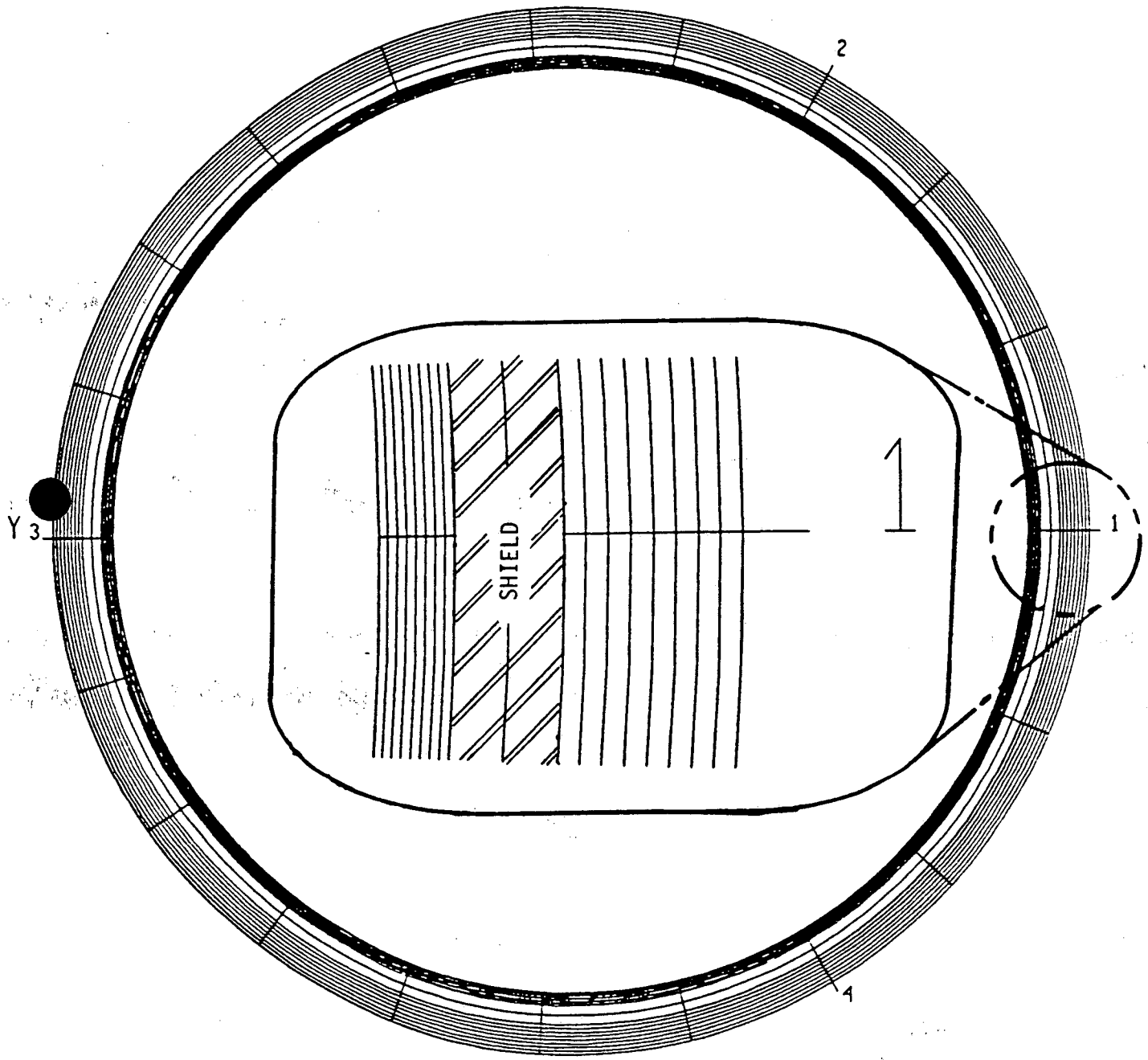

PREP3D 14 32 51 4-Jan-90 TMIT PREP3D VERSION 3, MOD 0, APOLLO-88
O'Donnell Reactor Design - 3 Pump Configuration MASS SOURCE

Figure A-1 Plan View of Mesh

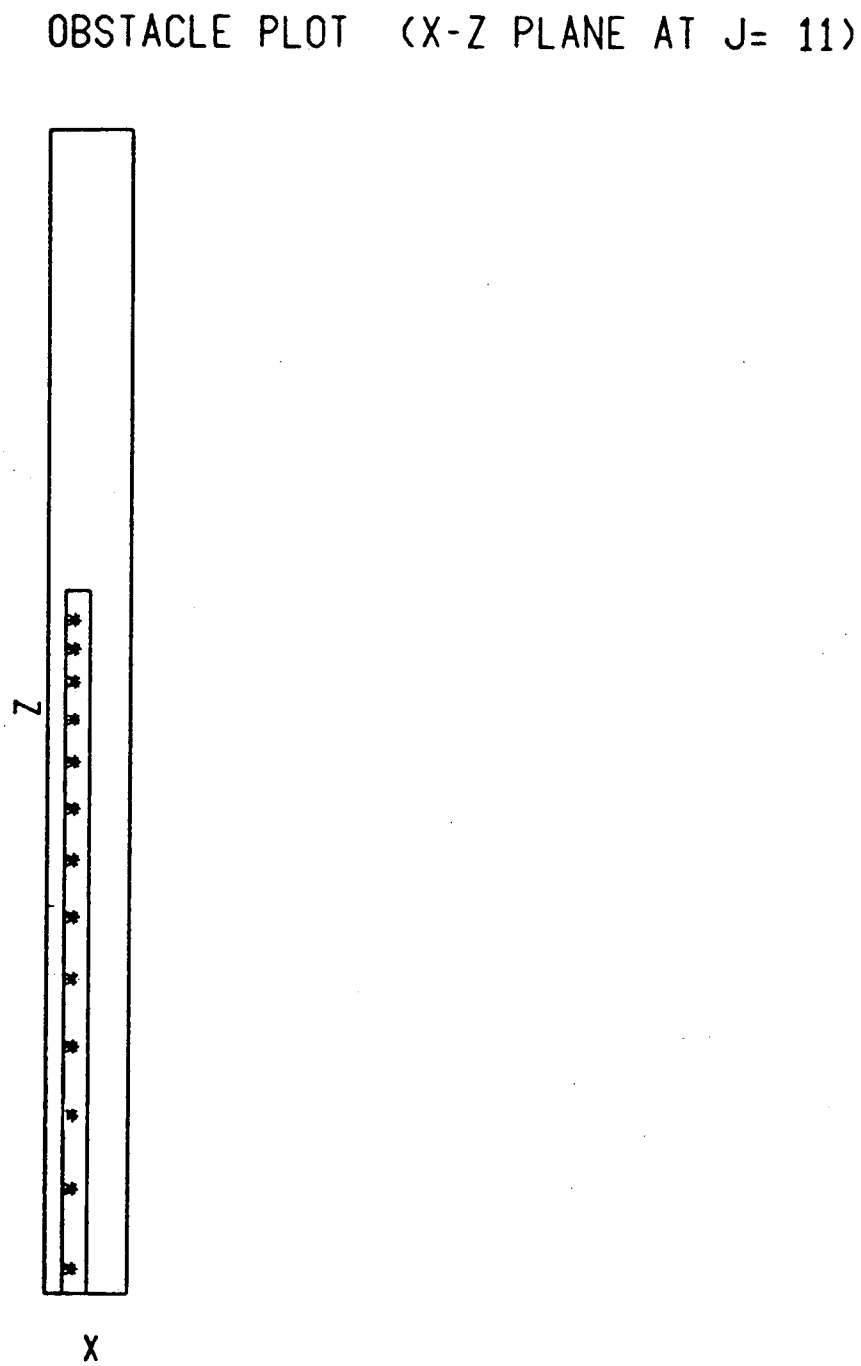

Figure A-2 Cross-Section of Thermal Shield

Y-Z MESH

	Y	Z
NUMBER OF CELLS=	20	23
SMALLEST CELL=	5 396E-01	1 524E-01
LARGEST CELL=	7 194E-01	5 098E-01
MAXIMUM CELL RATIO=	1 167E+00	1 500E+00
	AT CELL 3	AT CELL 16

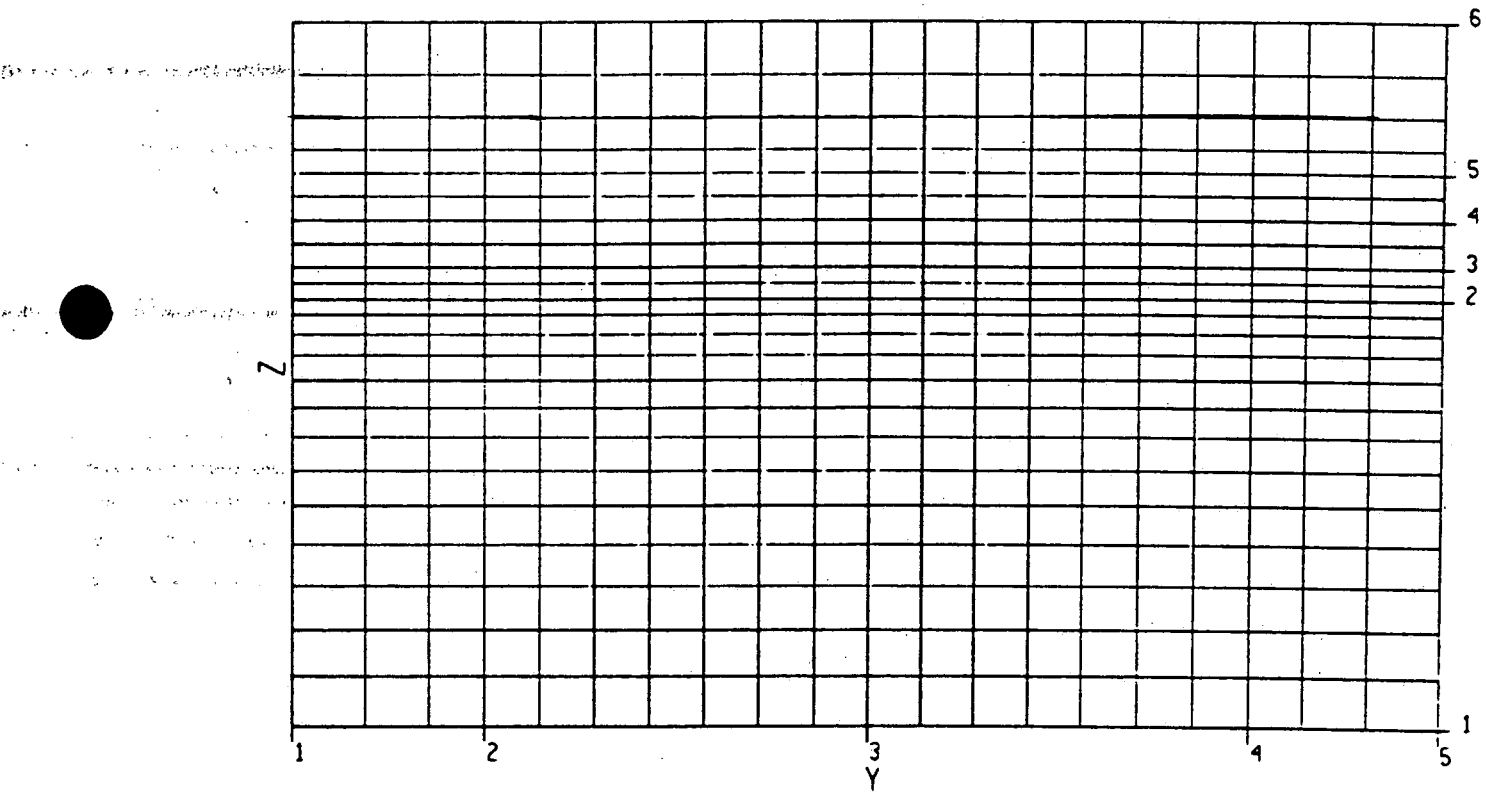

Figure A-3 Developed View of Fluid Mesh

OBSTACLE PLOT (Y-Z PLANE AT I= 10)

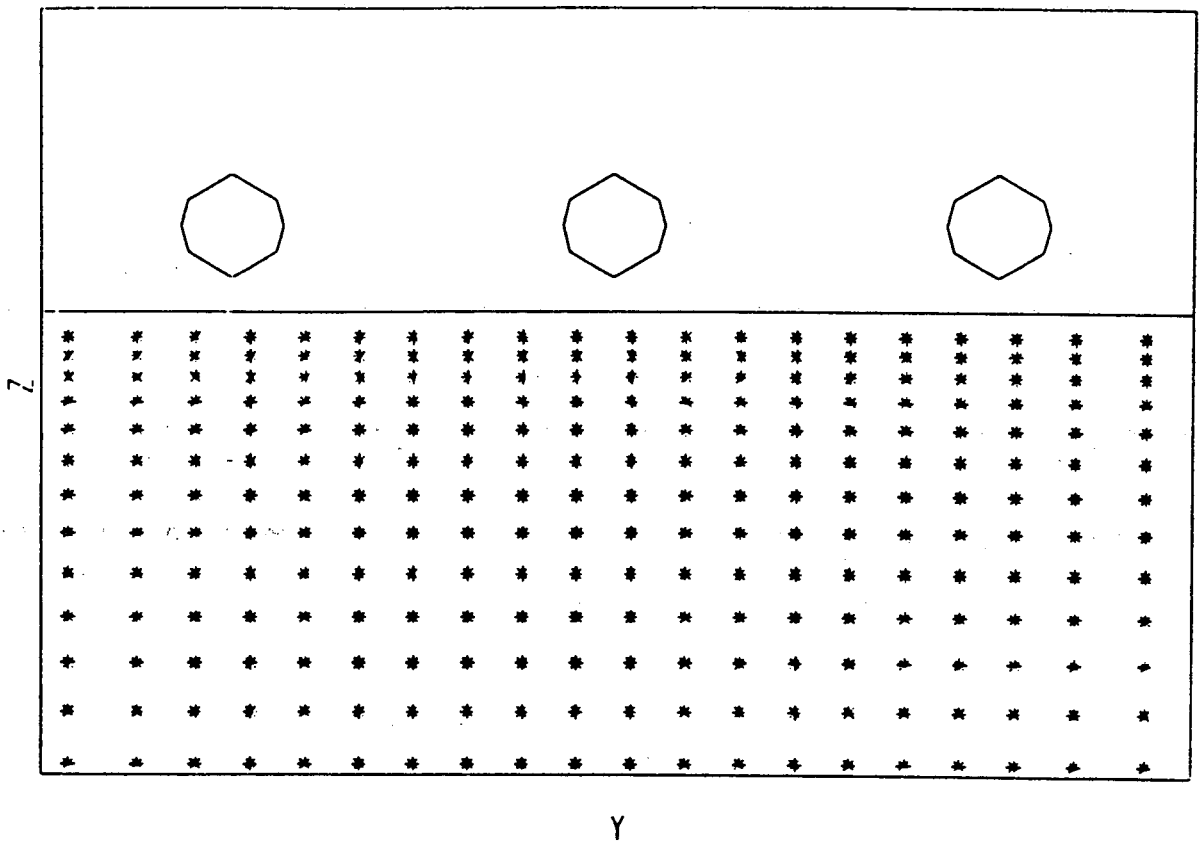

Figure A-4 Developed View of Shield and Inlets

Figure A-5 Complete Pressure and Velocity Fields, Inner Thermal Sheild Surface, 1-Pump Configuration

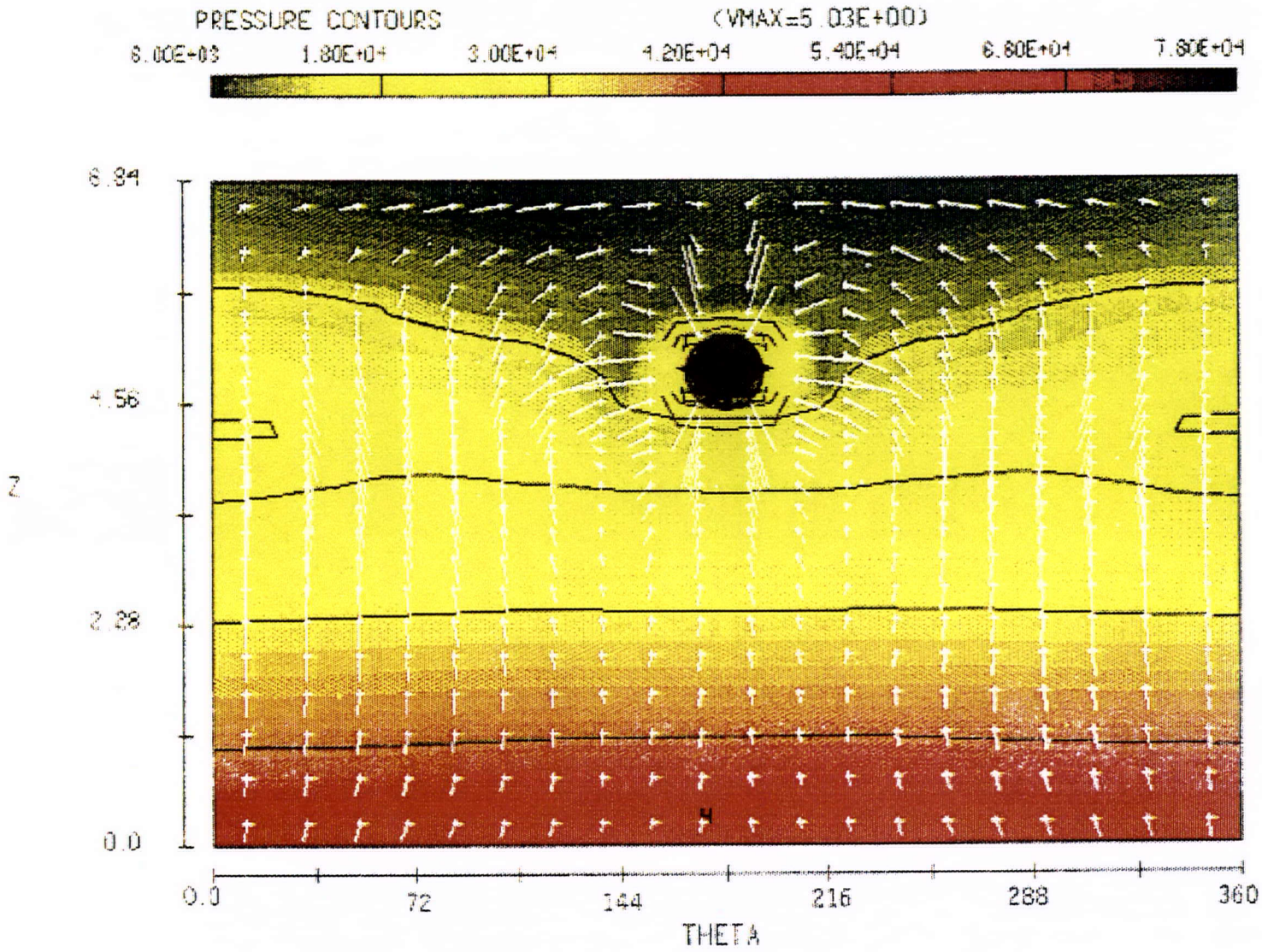

Figure A-7 Pressure and Velocity Fields, Outer Thermal Shield Surface Only, 1-Pump Configuration

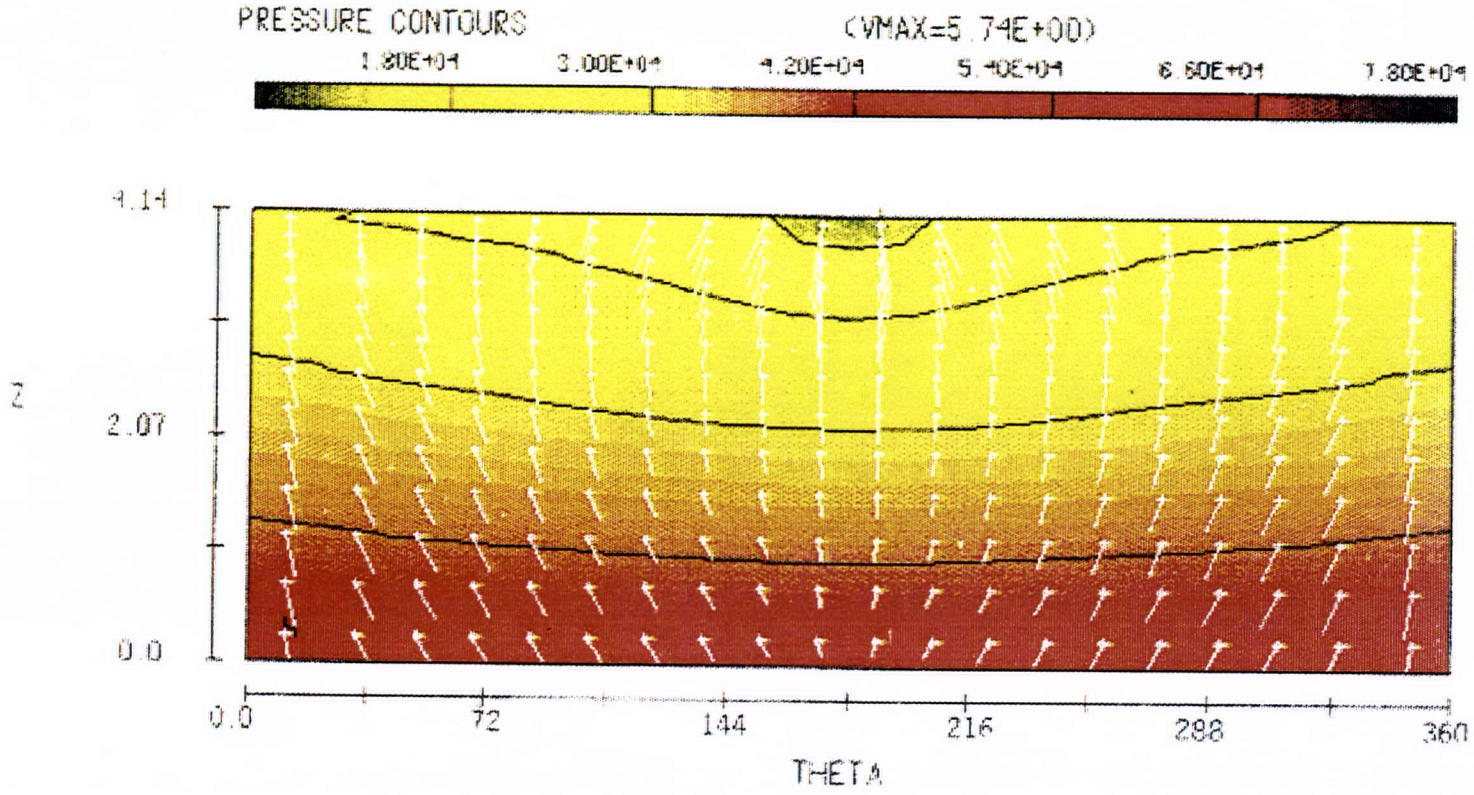

HYDR3D-AP TIME= 4.002E+00 XL= 12
8:26:12 15-Jan-90 PIGY VERSION 2, MOD 0, APOLLO-88
O'Donnell Reactor Design - 1 Pump Configuration MASS SOURCE

Figure A-8

Thermal Shield Pressure Differential
1 – Pump Configuration

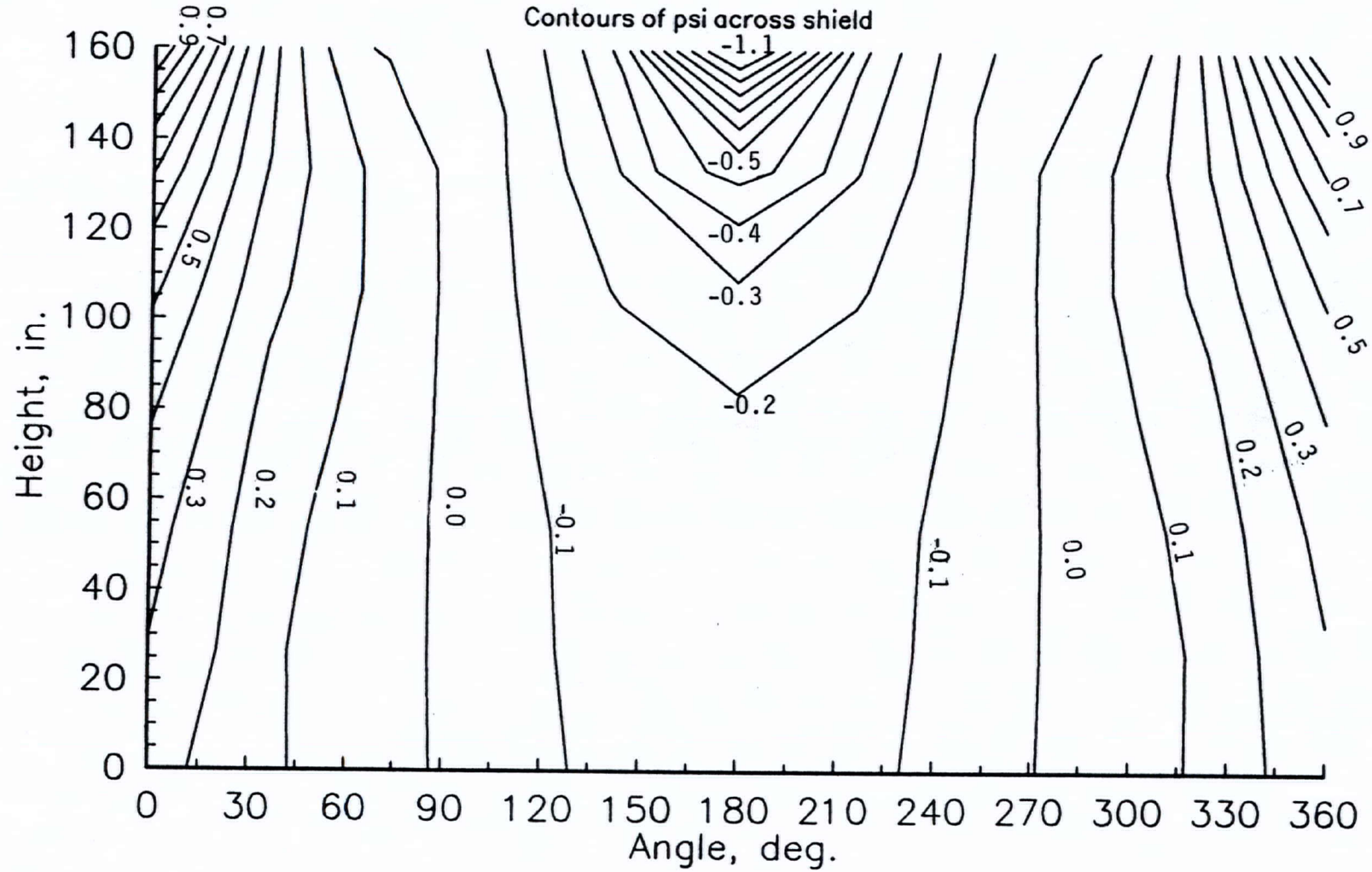

Figure A-9 Complete Pressure and Velocity Fields, Inner Thermal Shield Surface, 2-Pump Configuration

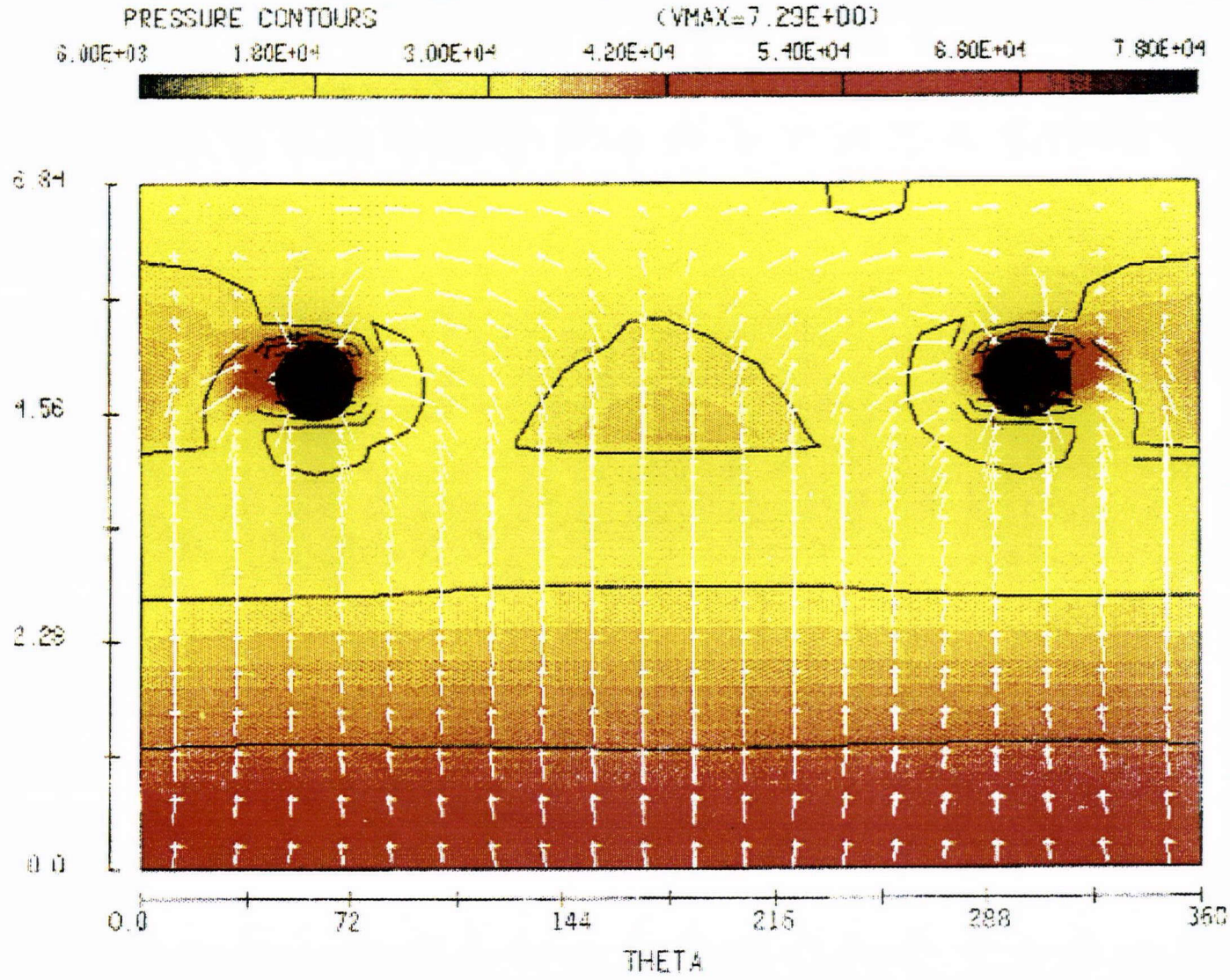

Figure A-10 Pressure and Velocity Fields, Inner Thermal Shield Surface Only, 2-Pump Configuration

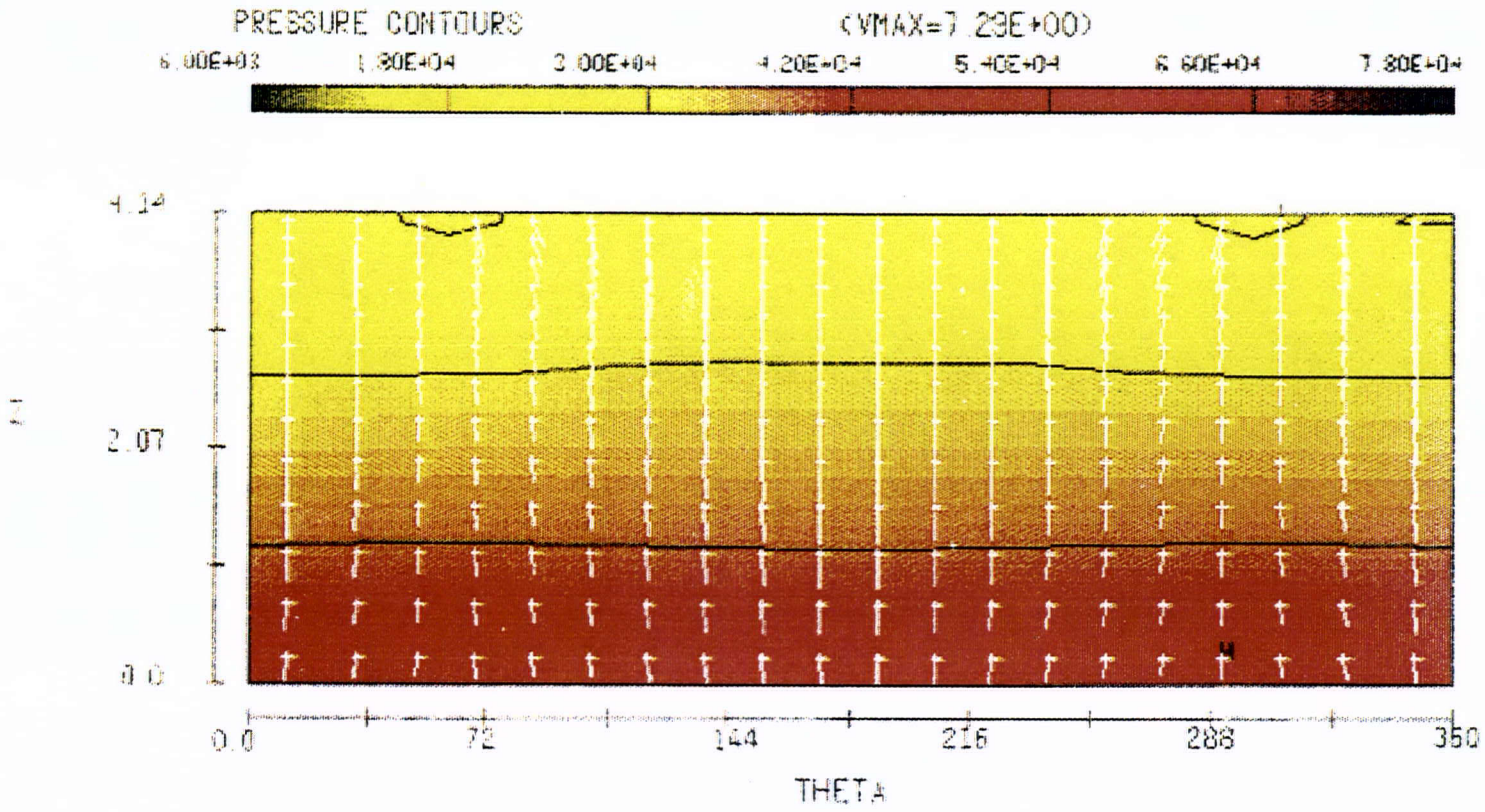

-FLOW3D-4.2 TIME= 2.000E+00 YL= 3
8:44: 3 10-Jan-90 TYPE VERSION 3, MOD 0, APOLLO-SR
O'Donnell Reactor Design - 2 Pump Configuration MASS SOURCE

Figure A-11 Pressure and Velocity Fields, Outer Thermal Shield Surface Only, 2-Pump Configuration

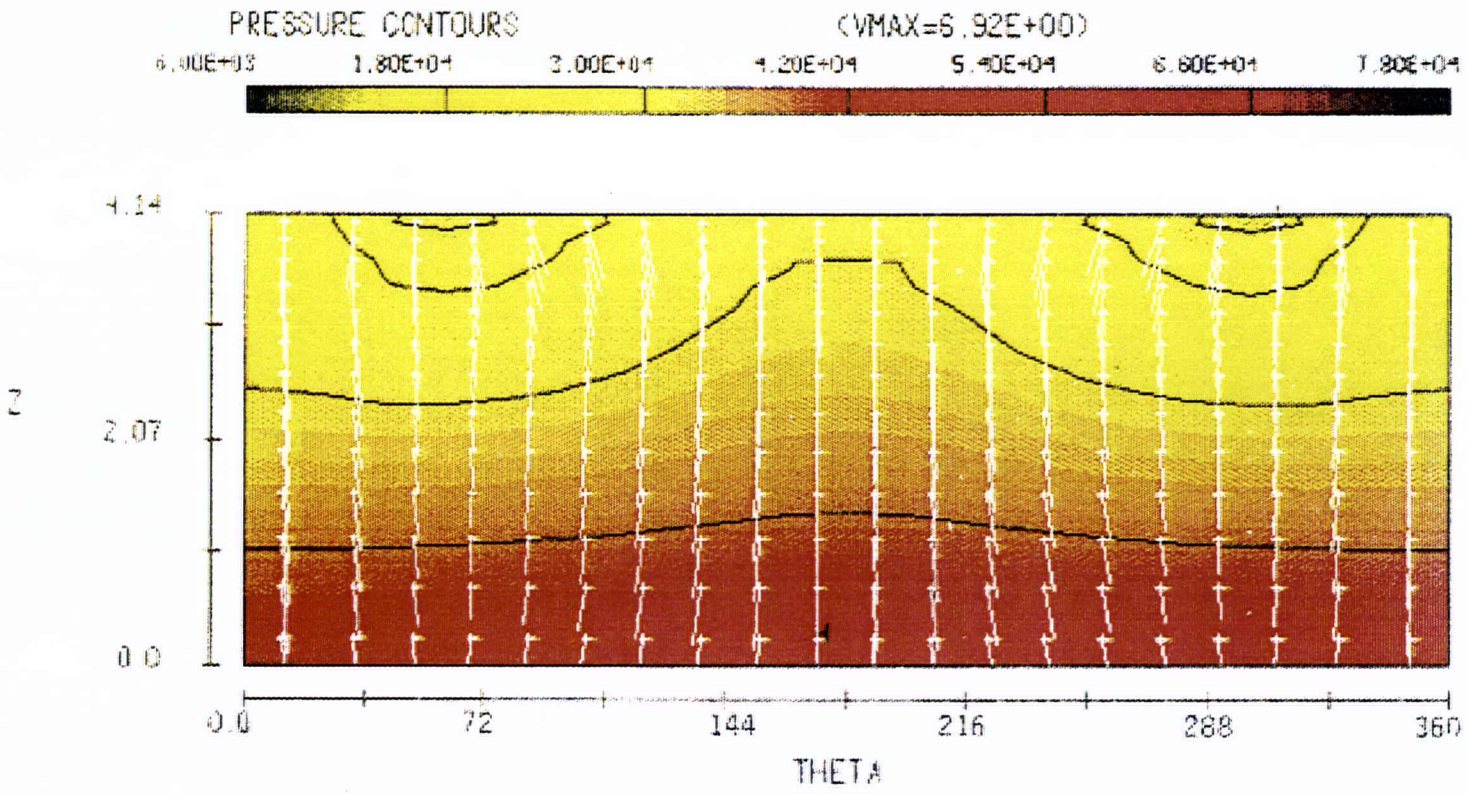

TIME= 2.000E+00 AL= 12
10-Jan-90 TYPE VERSION 3, MOD 0, APOLLO-88
O'Donnell Reactor Design - 2 Pump Configuration MASS SOURCE

Figure A-12

Thermal Shield Pressure Differential
2–Pump Configuration

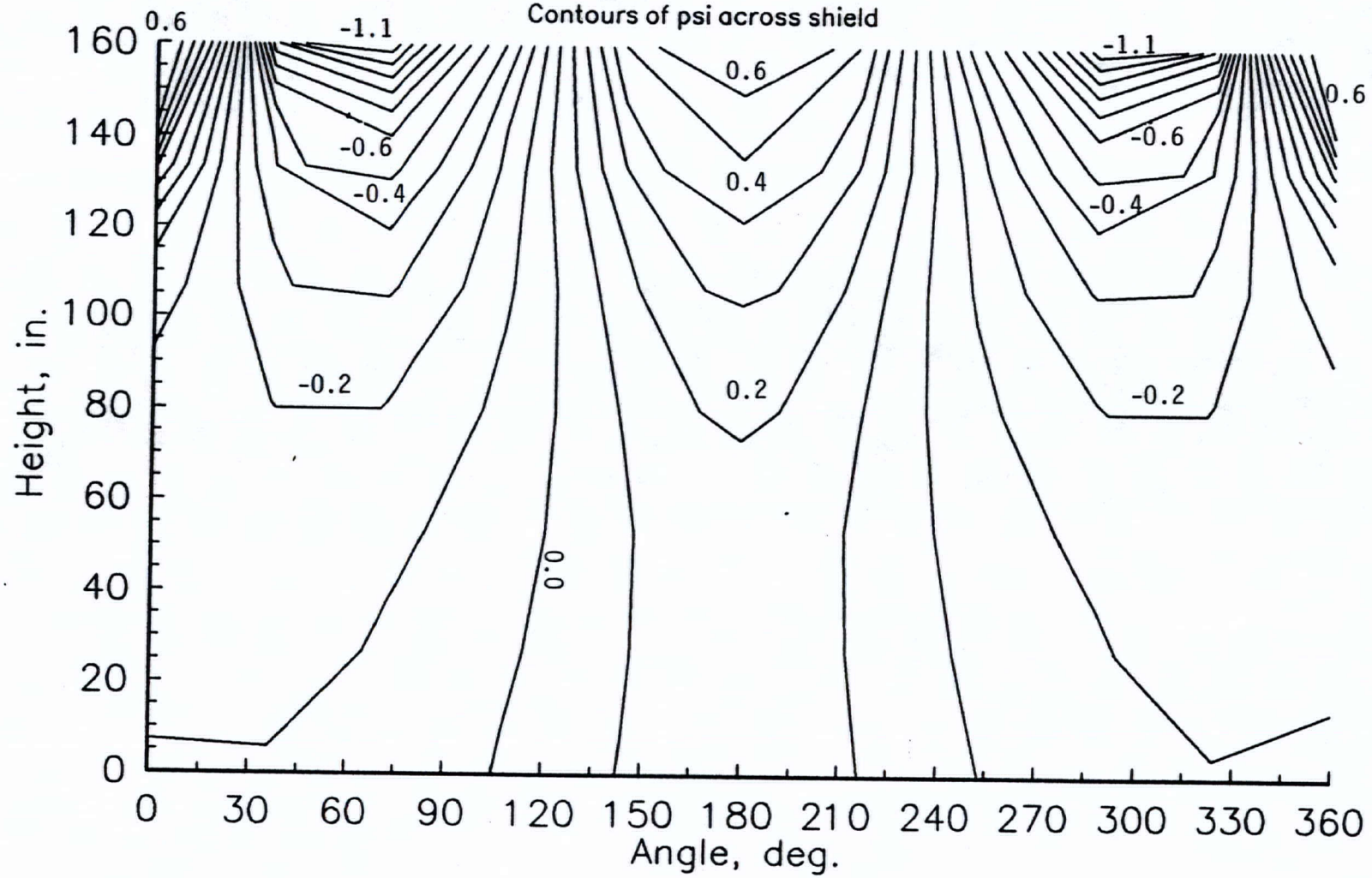

Figure A-13 Complete Pressure and Velocity Fields, Inner Thermal Shield Surface, 3-Pump Configuration

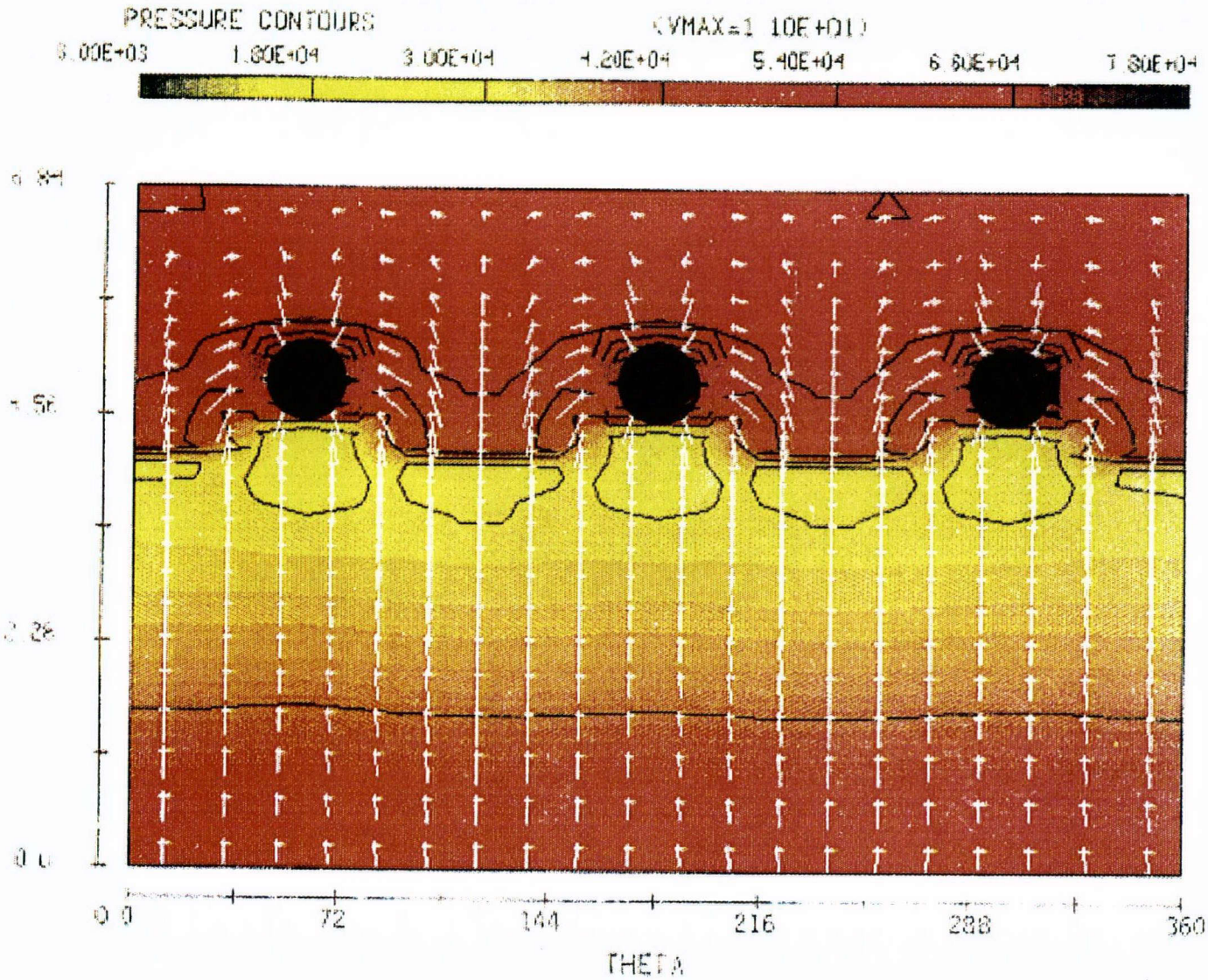

Figure A-14 Pressure and Velocity Fields, Inner Thermal Shield Surface Only, 3-Pump Configuration

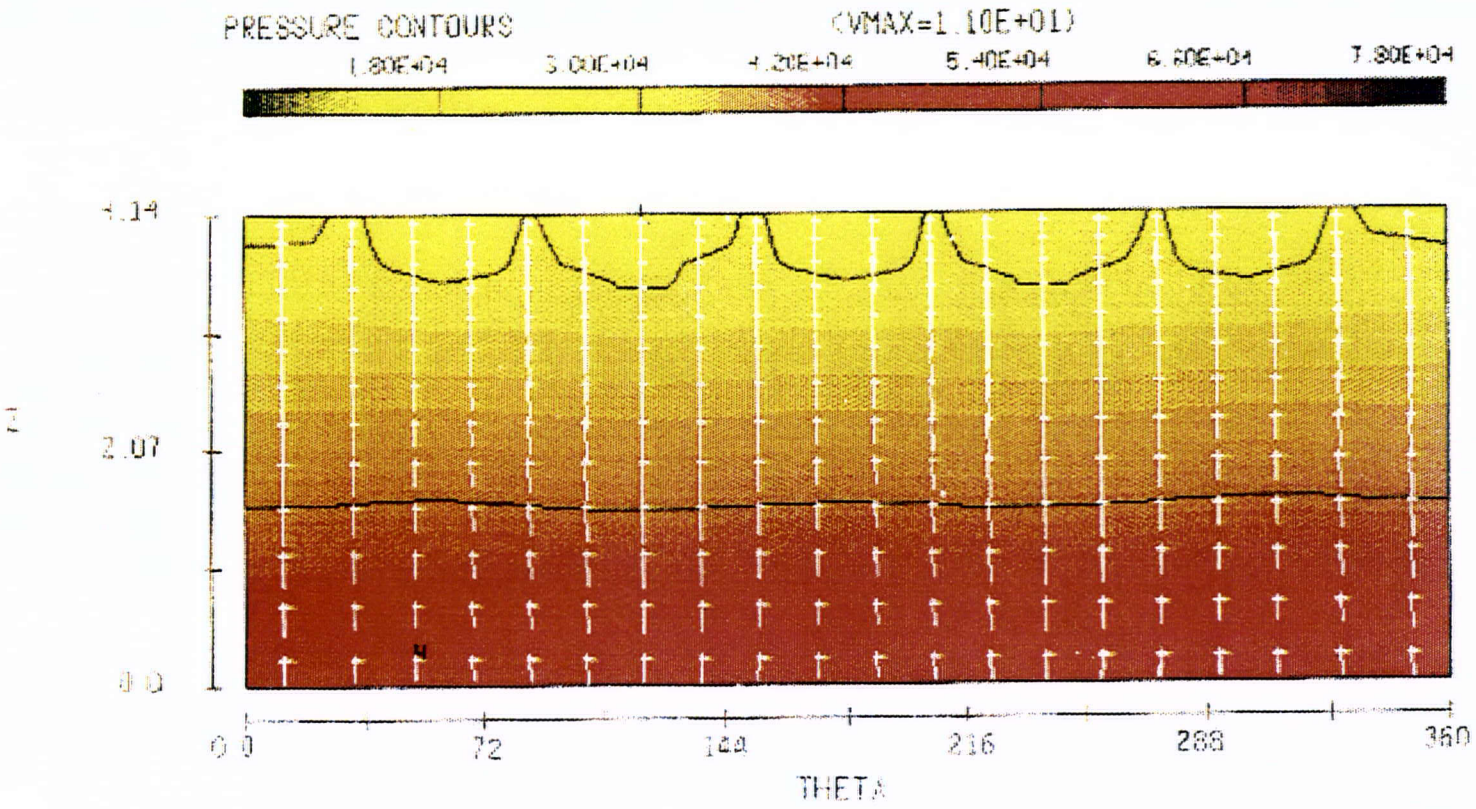

MYDR3D-AP TIME= 3.994E-01 KL= 9
16:42:11 5-Jan-90 ITVL VERSION 3, MOD 0. APOLLO-68
O'Donnell Reactor Design - 3 Pump Configuration MASS SOURCE

Figure A-15 Pressure and Velocity Fields, Outer Thermal Shield Surface Only, 3-Pump Configuration

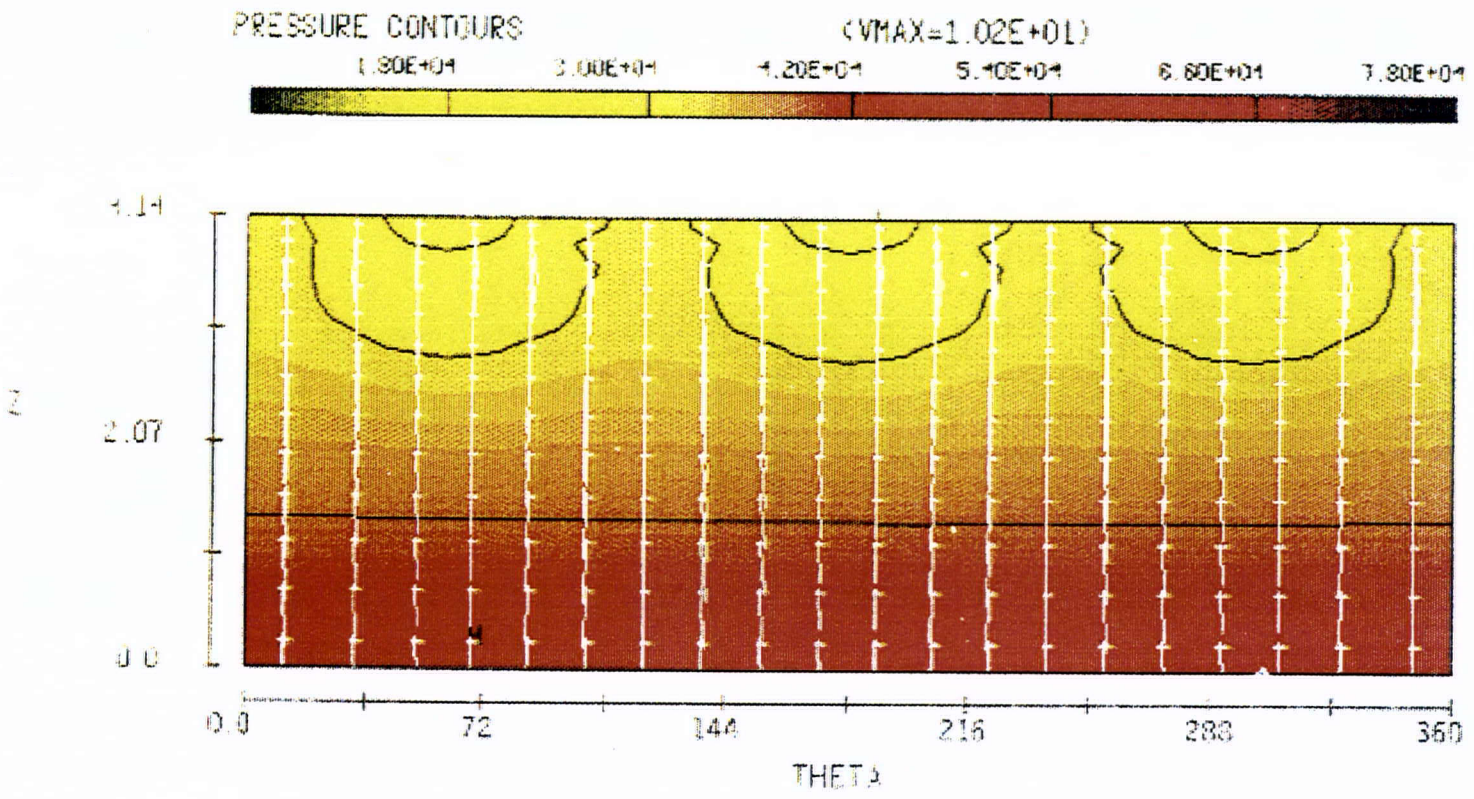

*YORK3D-AP TIME= 3.294E-01 X1= 13
16:42:11 5-Jan-90 ITVL VERSION 3, MOD 0. *POLLO-S3
O'Donnell Reactor Design - 3 Pump Configuration MASS SOURCE

Figure A-16

Thermal Shield Pressure Differential
3–Pump Configuration

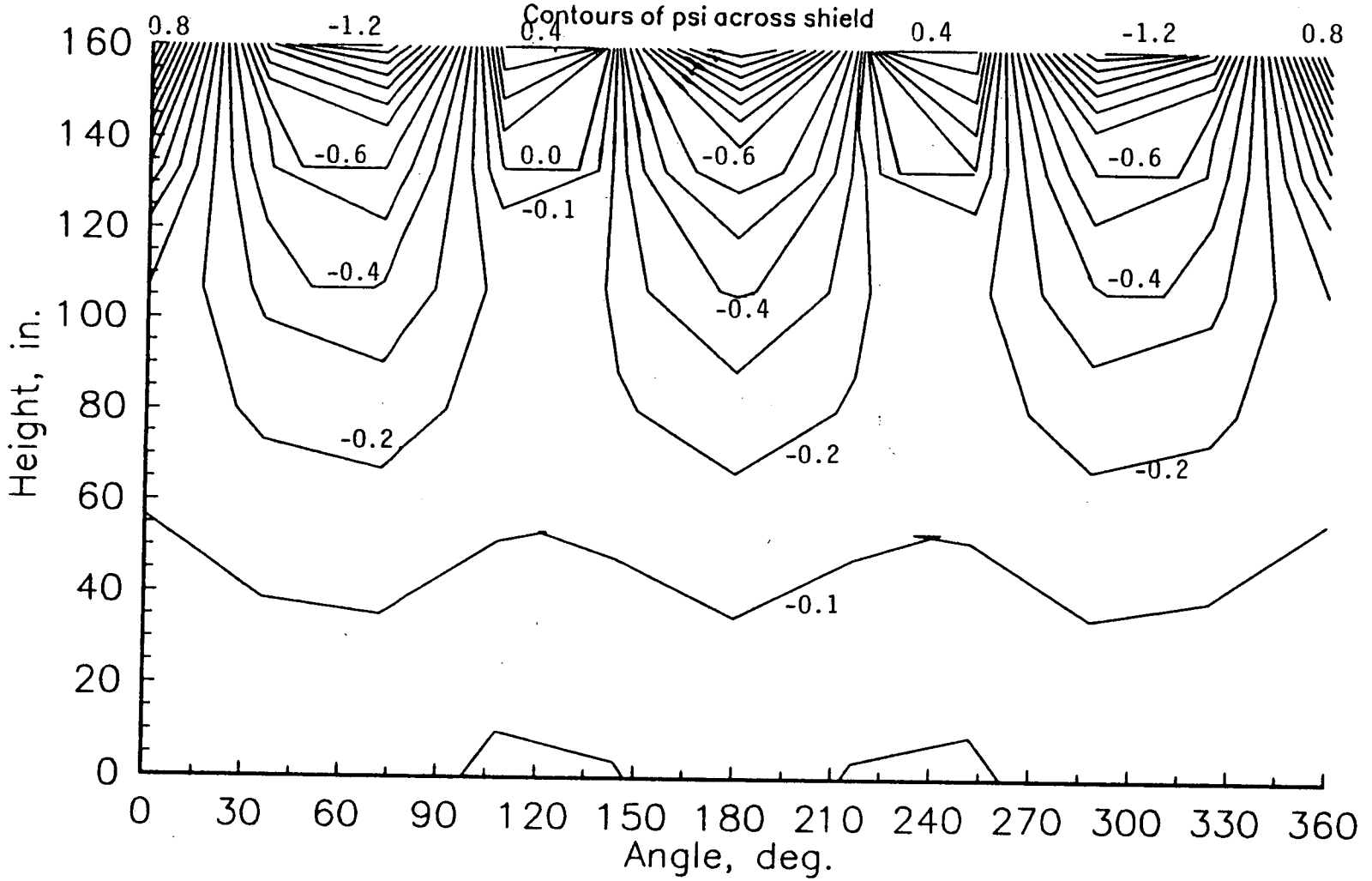

APPENDIX B

MODE SHAPES AND FREQUENCIES FOR OLD AND NEW DESIGNS
WITHOUT HYDRODYNAMIC MASS EFFECT.
(6 FLEXURES – 0 KEYS – 6 SUPPORT BLOCKS)

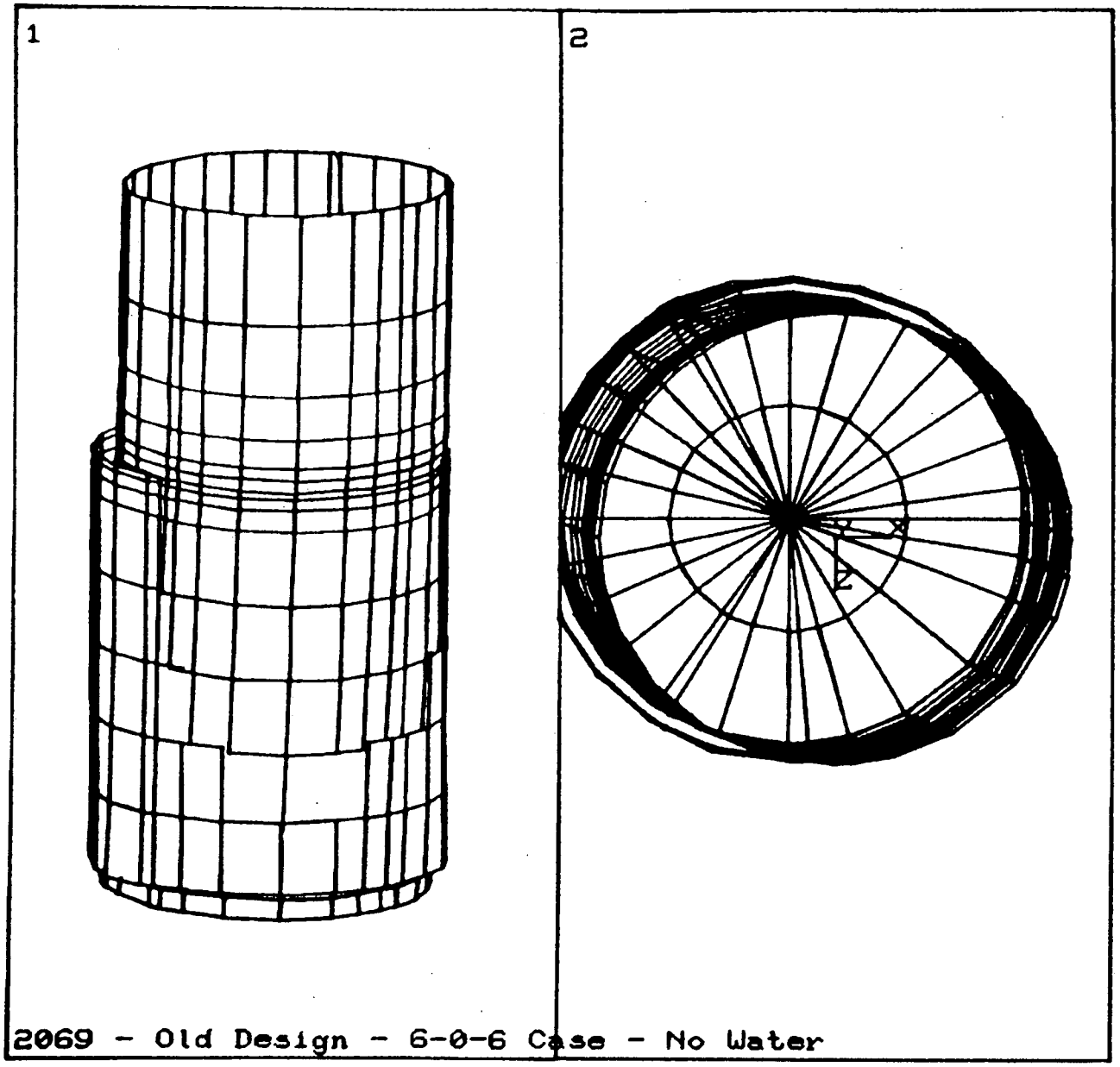

ANSYS 4.4
JUL 9 1990
13:57:05
PLOT NO. 1
POST1 DISPL.
STEP=1
ITER=1
FREQ=16.24
DMX =0.057373

DSCA=356.552
XV =1
YV =0.3
ZV =1
DIST=204.566
YF =-139.535
PRECISE HIDDEN

WIND=2
DSCA=252.12
YV =1
DIST=144.65
YF =-139.535

FIGURE B-1

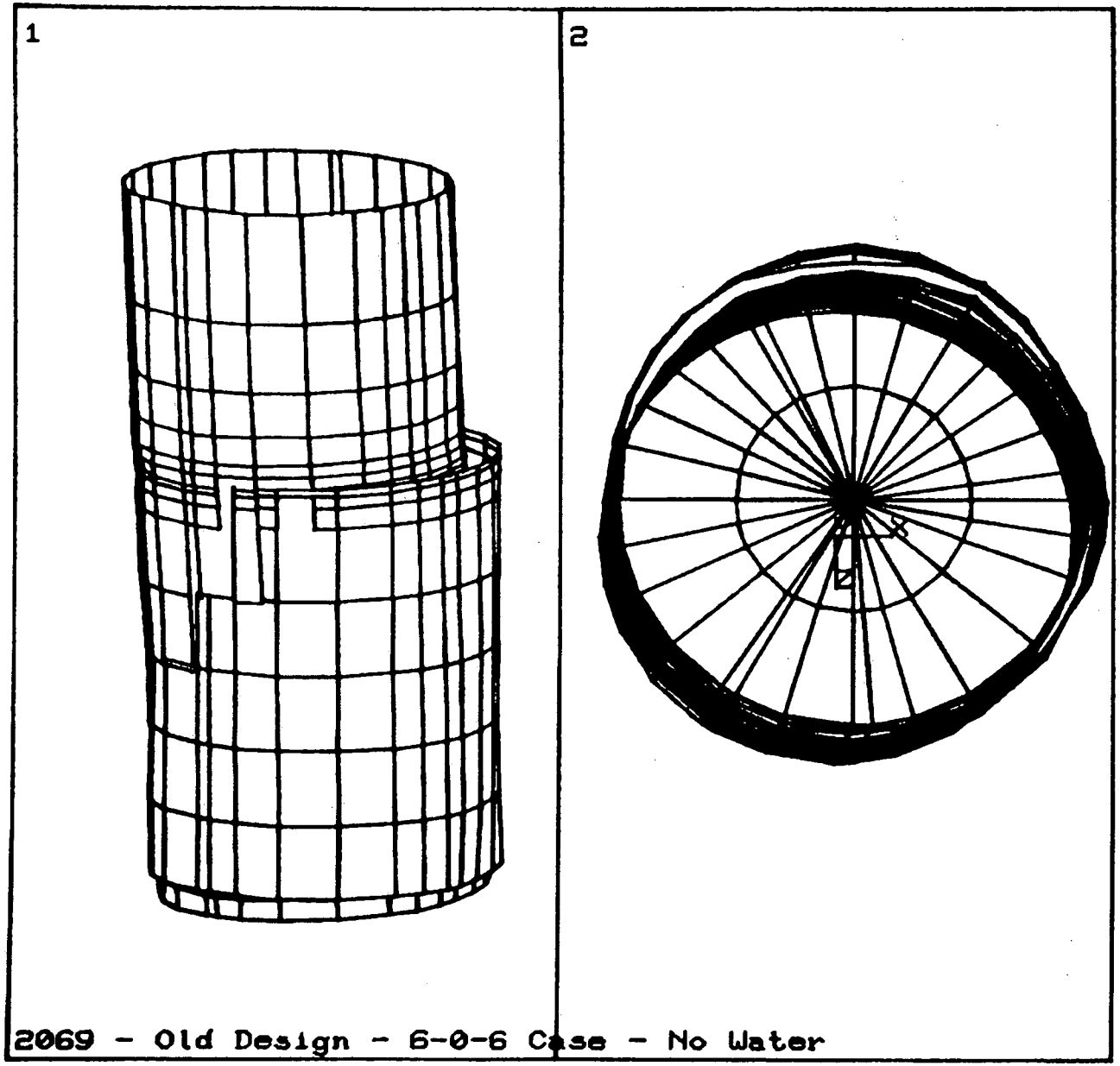
1
2
ANSYS 4.4
JUL 9 1990
13:58:10
PLOT NO. 2
POST1 DISPL.
STEP=1
ITER=2
FREQ=16.672
DMX =0.066025
DSCA=309.833
XV =1
YV =0.3
ZV =1
DIST=204.566
YF =-139.535
PRECISE HIDDEN
WIND=2
DSCA=219.085
YV =1
DIST=144.65
YF =-139.535
2069 - Old Design - 6-0-6 Case - No Water

FIGURE B-2

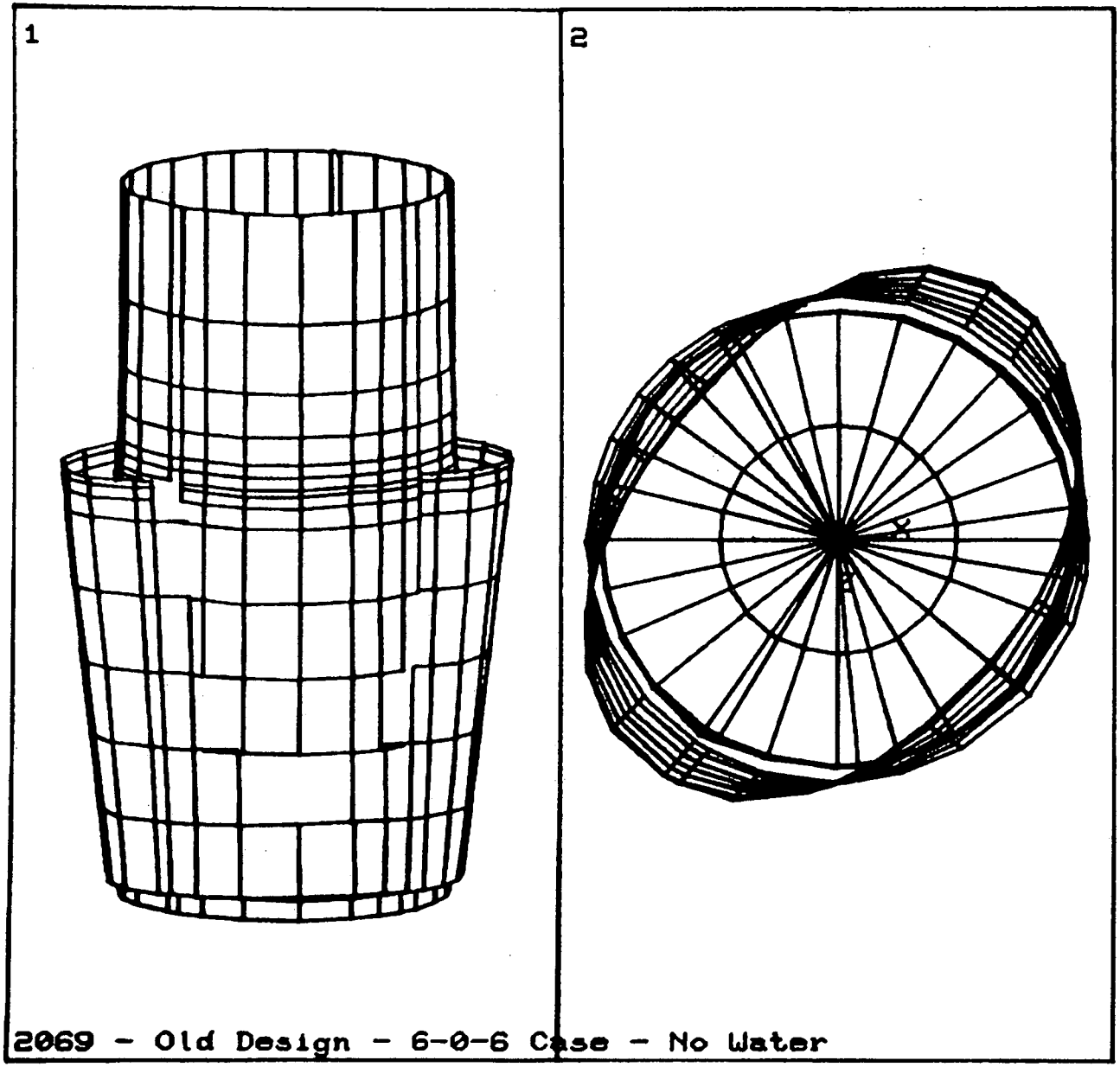
1
2
ANSYS 4.4
JUL 9 1990
14:00:32
PLOT NO. 4
POST1 DISPL.
STEP=1
ITER=4
FREQ=22.513
DMX =0.198036
DSCA=103.297
XV =1
YV =0.3
ZV =1
DIST=204.566
YF =-139.535
PRECISE HIDDEN
WIND=2
DSCA=73.042
YV =1
DIST=144.65
YF =-139.535
2069 - Old Design - 6-0-6 Case - No Water

FIGURE B-4

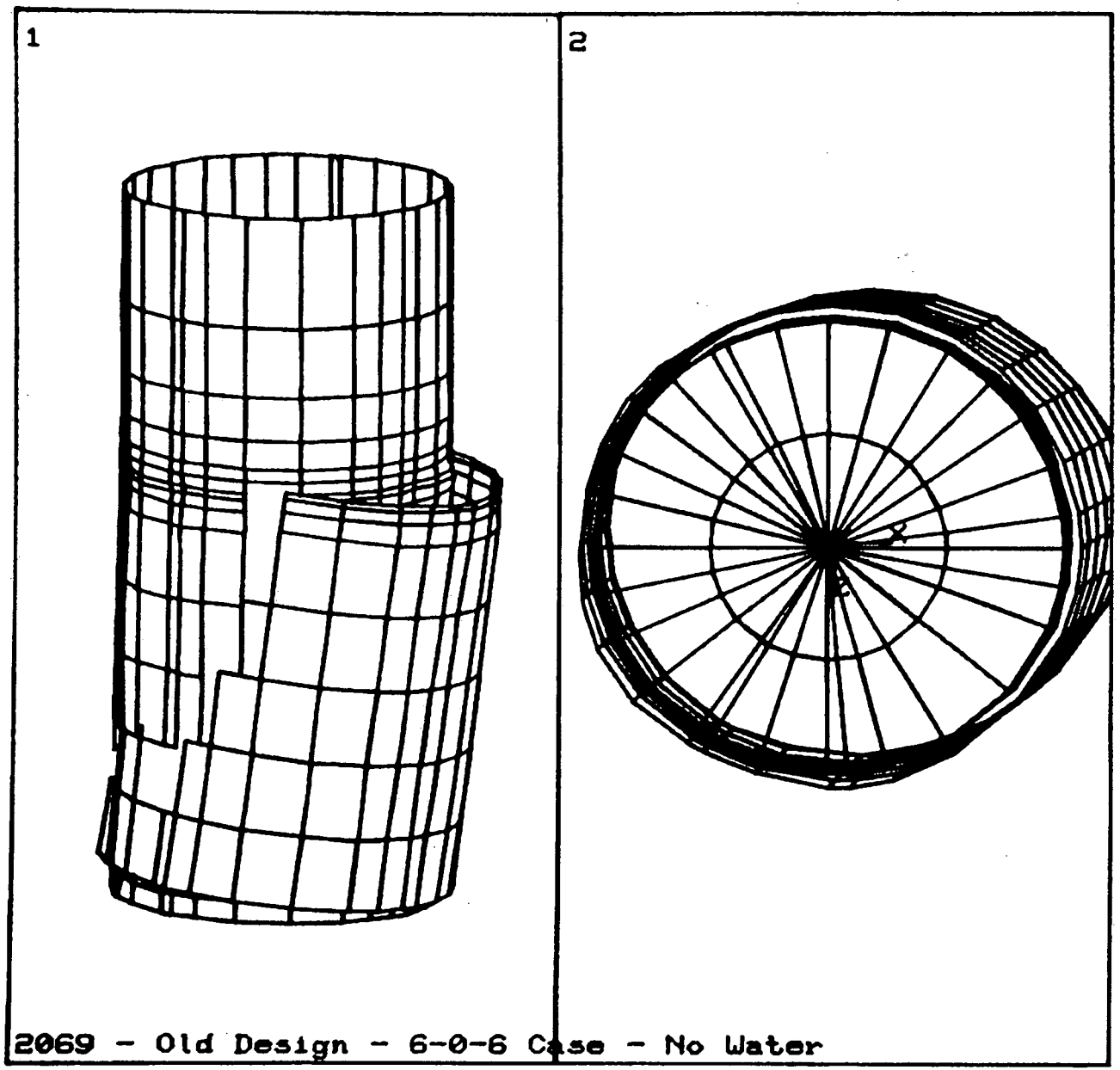
1
2
ANSYS 4.4
JUL 9 1990
14:01:43
PLOT NO. 5
POST1 DISPL.
STEP=1
ITER=5
FREQ=26.045
DMX =0.180757
DSCA=113.172
XV =1
YV =0.3
ZV =1
DIST=204.566
YF =-139.535
PRECISE HIDDEN
WIND=2
DSCA=80.025
YV =1
DIST=144.65
YF =-139.535
2069 - Old Design - 6-0-6 Case - No Water

FIGURE B-5

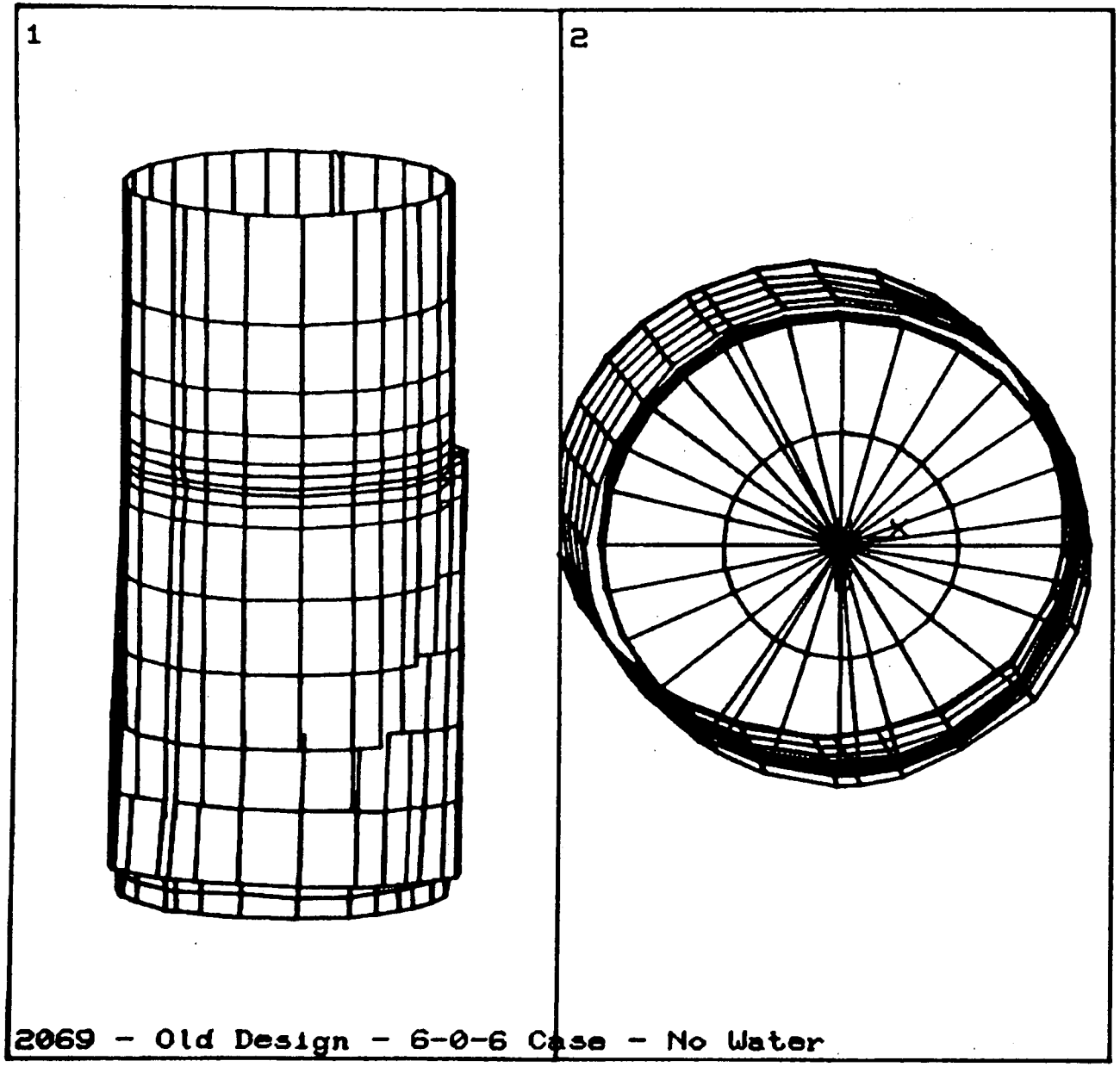
1
2
ANSYS 4.4
JUL 9 1990
14:02:54
PLOT NO. 6
POST1 DISPL.
STEP=1
ITER=6
FREQ=26.611
DMX =0.153167
DSCA=133.557
XV =1
YV =0.3
ZV =1
DIST=204.566
YF =-139.535
PRECISE HIDDEN
WIND=2
DSCA=94.439
YV =1
DIST=144.65
YF =-139.535
2069 - Old Design - 6-0-6 Case - No Water

FIGURE B-6

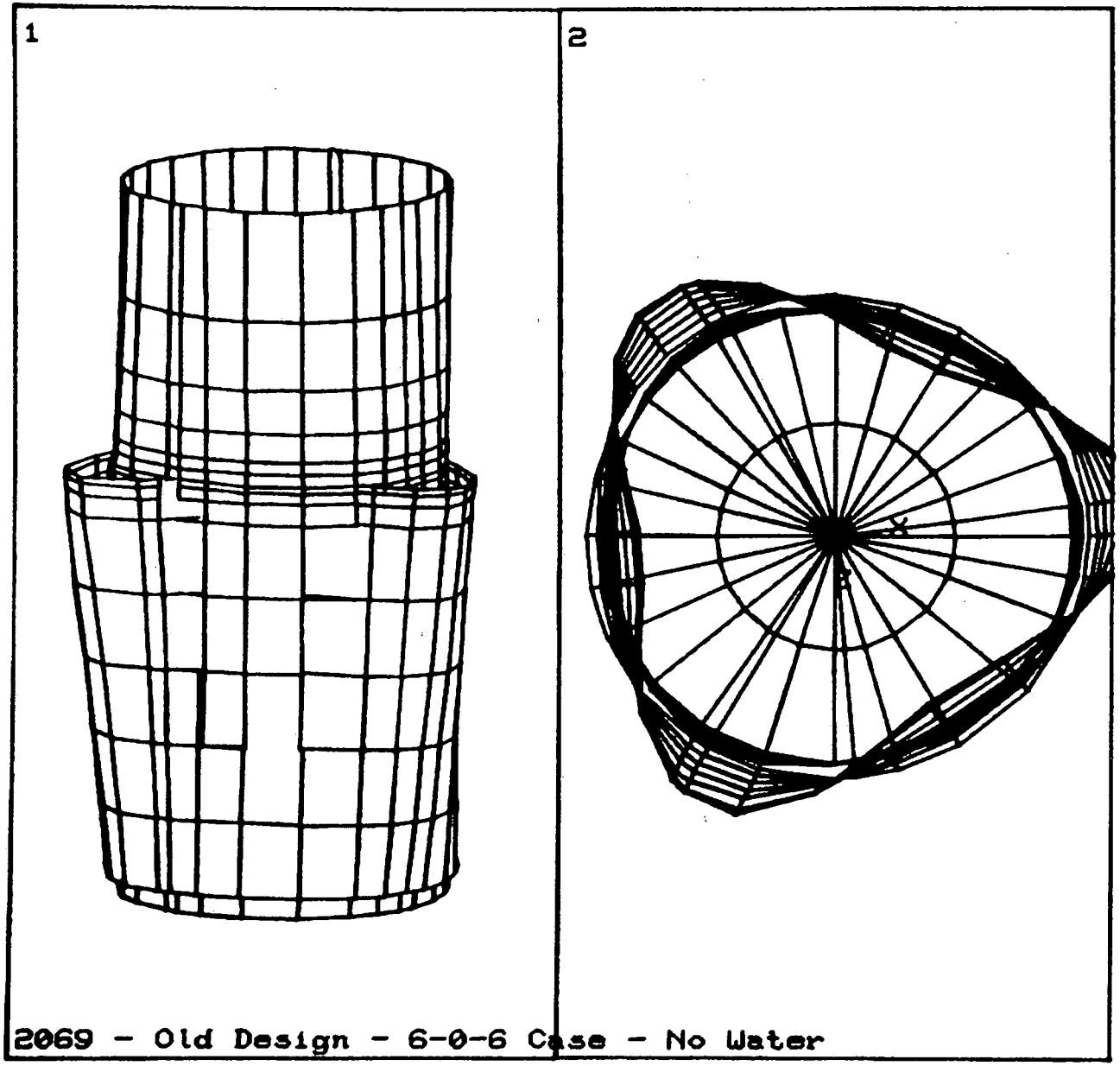
1
2
ANSYS 4.4
JUL 9 1990
14:04:06
PLOT NO. 7
POST1 DISPL.
STEP=1
ITER=7
FREQ=43.014
DMX =0.196543
DSCA=104.082
XV =1
YV =0.3
ZV =1
DIST=204.566
YF =-139.535
PRECISE HIDDEN
WIND=2
DSCA=73.597
YV =1
DIST=144.65
YF =-139.535
2069 - Old Design - 6-0-6 Case - No Water

FIGURE B-7

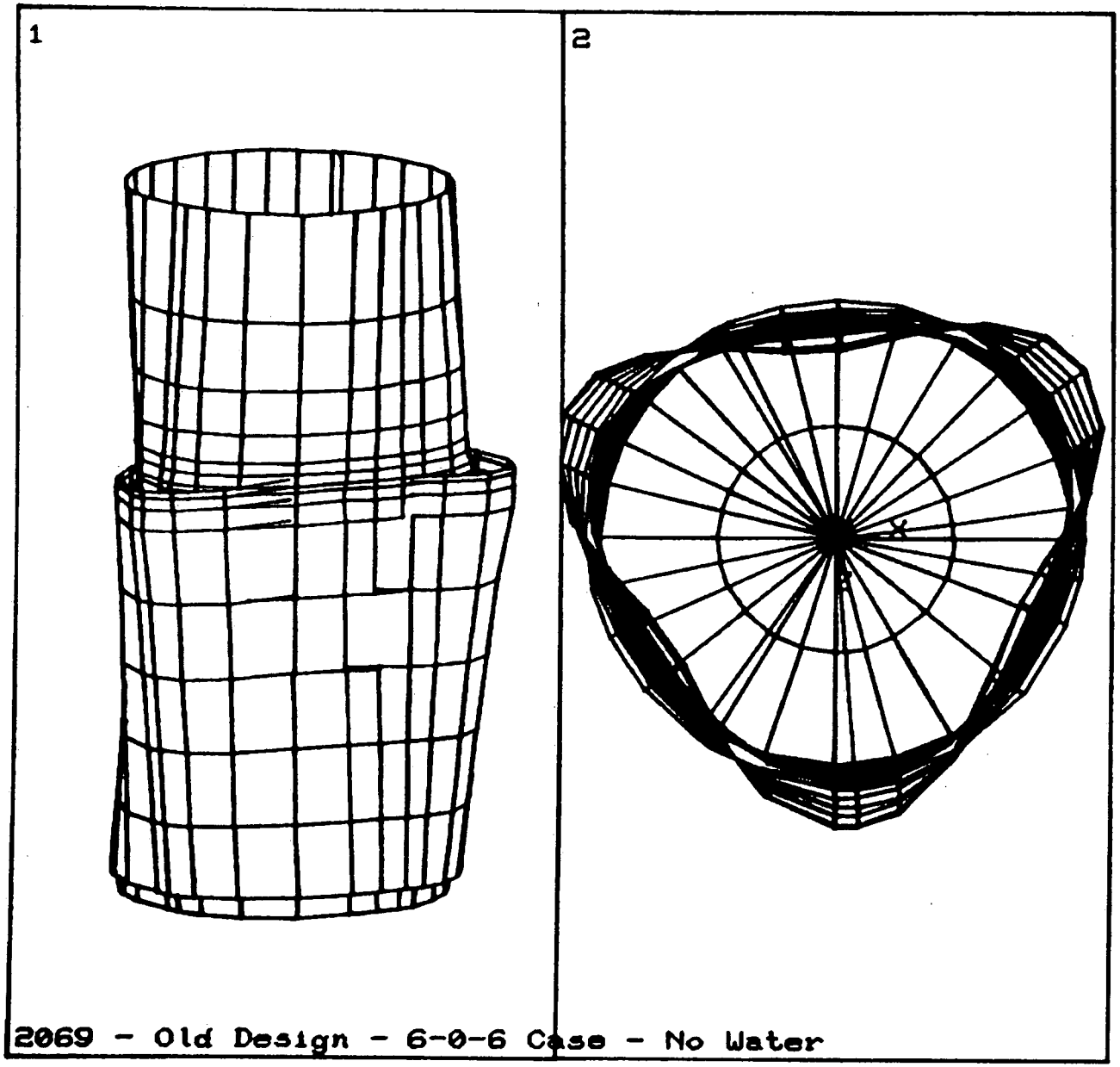
1
2
ANSYS 4.4
JUL 9 1990
14:05:23
PLOT NO. 8
POST1 DISPL.
STEP=1
ITER=8
FREQ=44.322
DMX =0.183382
DSCA=111.552
XV =1
YV =0.3
ZV =1
DIST=204.566
YF =-139.535
PRECISE HIDDEN
WIND=2
DSCA=78.879
YV =1
DIST=144.65
YF =-139.535
2069 - Old Design - 6-0-6 Case - No Water

FIGURE B-8

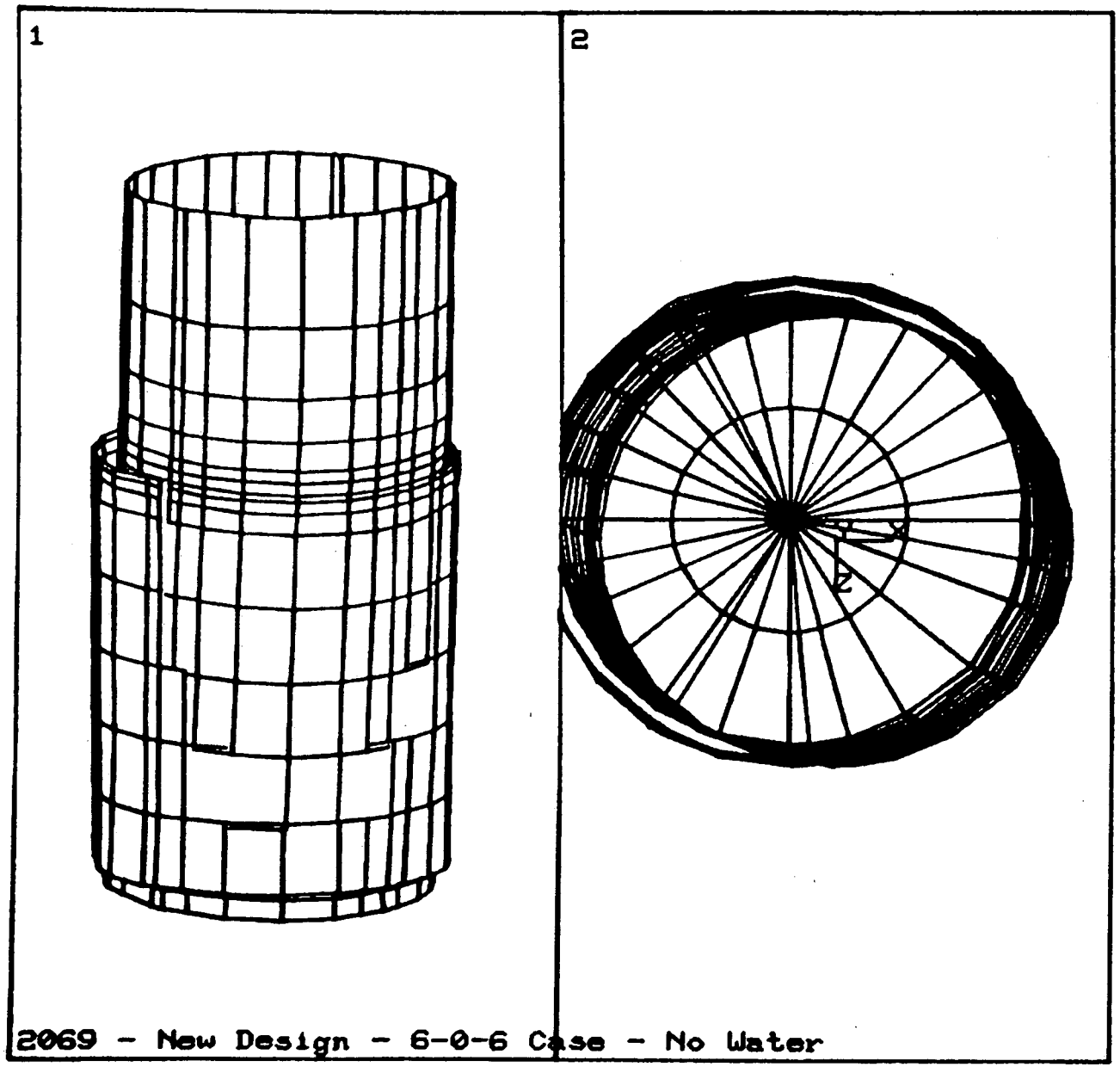
1
2
ANSYS 4.4
JUL 10 1990
08:50:25
PLOT NO. 1
POST1 DISPL.
STEP=1
ITER=1
FREQ=16.251
DMX =0.057692
DSCA=354.583
XV =1
YV =0.3
ZV =1
DIST=204.566
YF =-139.535
PRECISE HIDDEN
WIND=2
DSCA=250.728
YV =1
DIST=144.65
YF =-139.535
2069 - New Design - 6-0-6 Case - No Water

FIGURE B-9

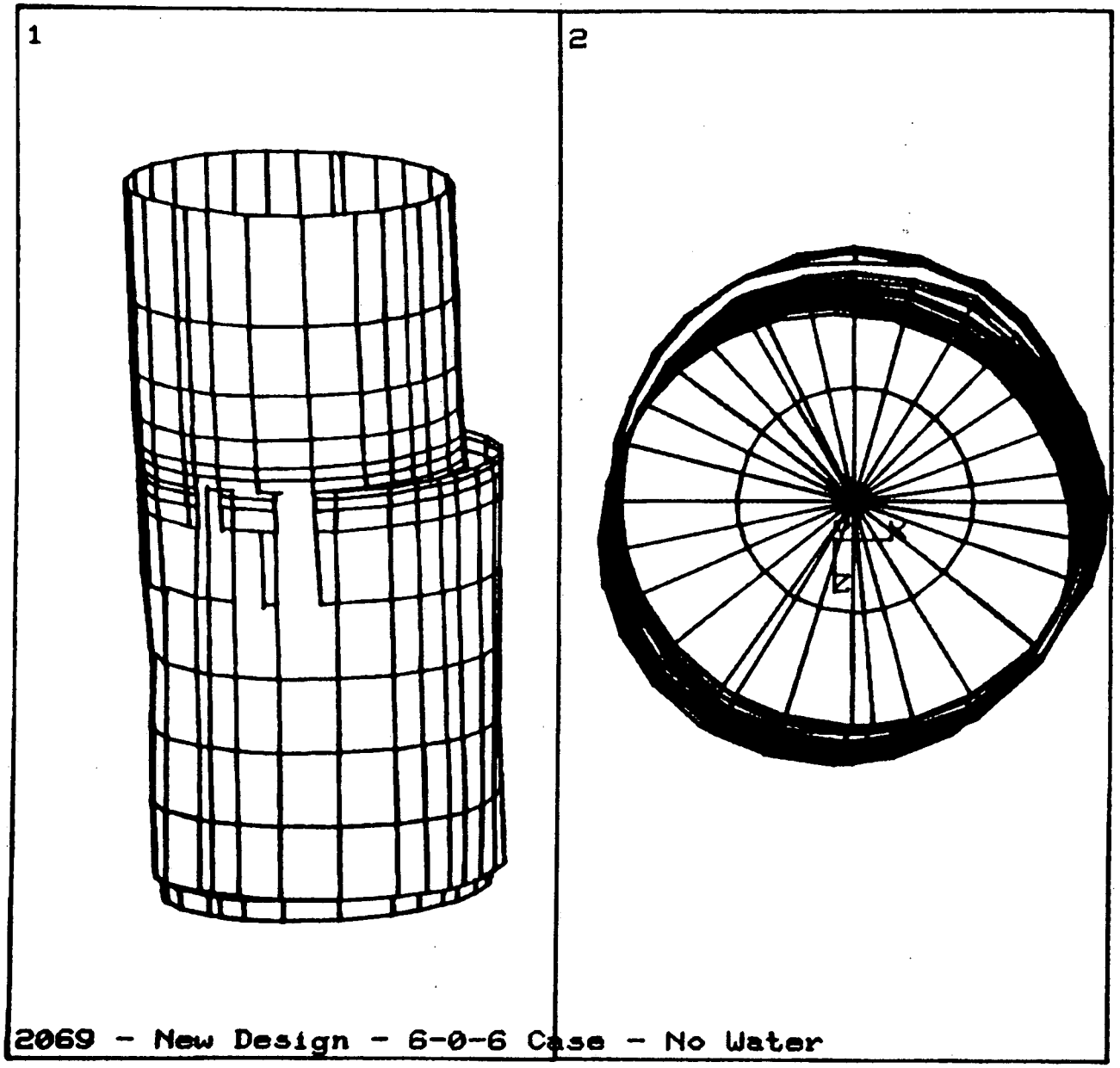
1
2
ANSYS 4.4
JUL 10 1990
08:51:41
PLOT NO. 2
POST1 DISPL.
STEP=1
ITER=2
FREQ=16.722
DMX =0.062628
DSCA=326.639
XV =1
YV =0.3
ZV =1
DIST=204.566
YF =-139.535
PRECISE HIDDEN
WIND=2
DSCA=230.968
YV =1
DIST=144.65
YF =-139.535
2069 - New Design - 6-0-6 Case - No Water

FIGURE B-10

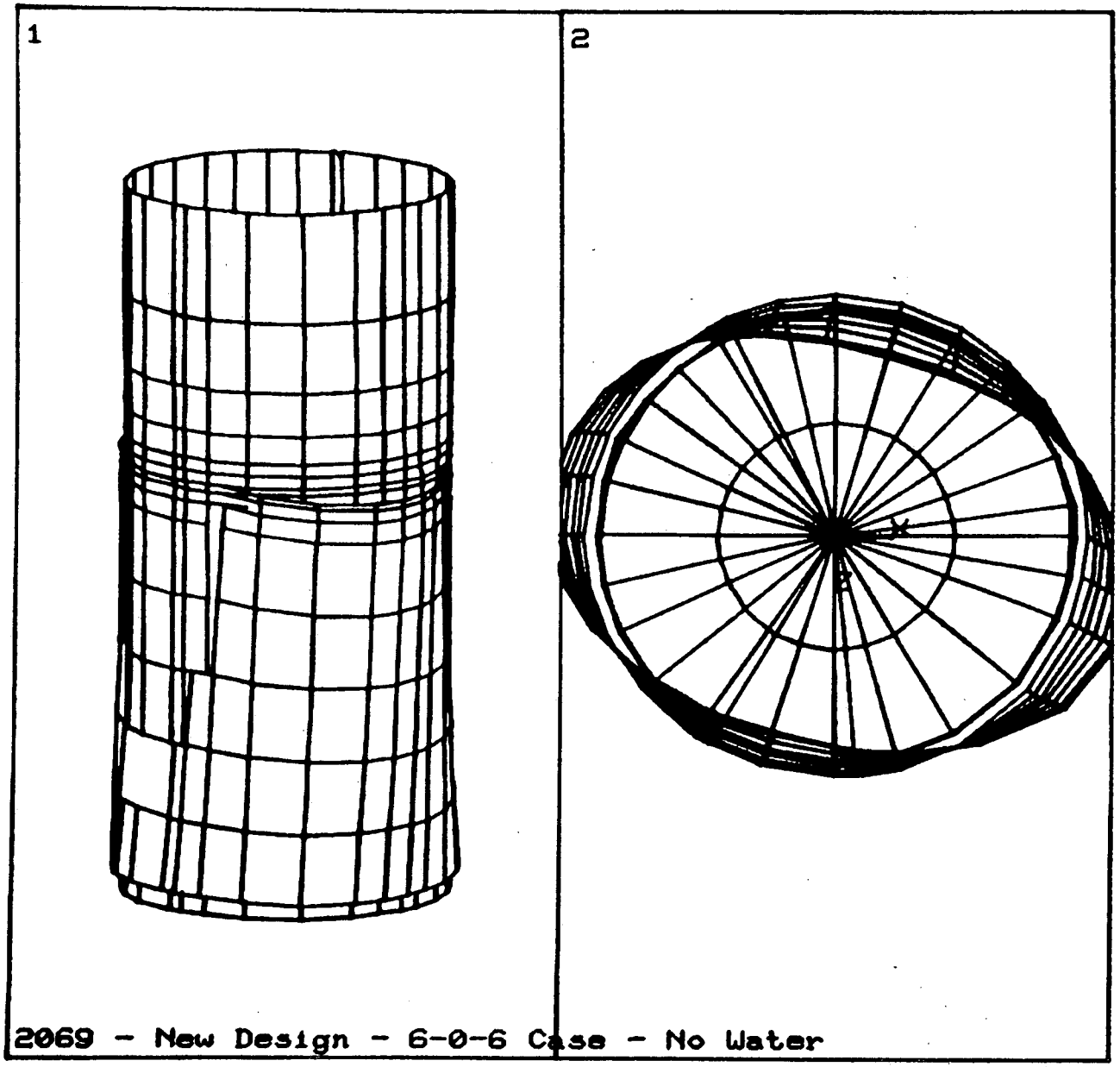
1
2
ANSYS 4.4
JUL 10 1990
08:52:48
PLOT NO. 3
POST1 DISPL.
STEP=1
ITER=3
FREQ=21.147
DMX =0.221662
DSCA=92.287
XV =1
YV =0.3
ZV =1
DIST=204.566
YF =-139.535
PRECISE HIDDEN
WIND=2
DSCA=65.257
YV =1
DIST=144.65
YF =-139.535
2069 - New Design - 6-0-6 Case - No Water

FIGURE B-11

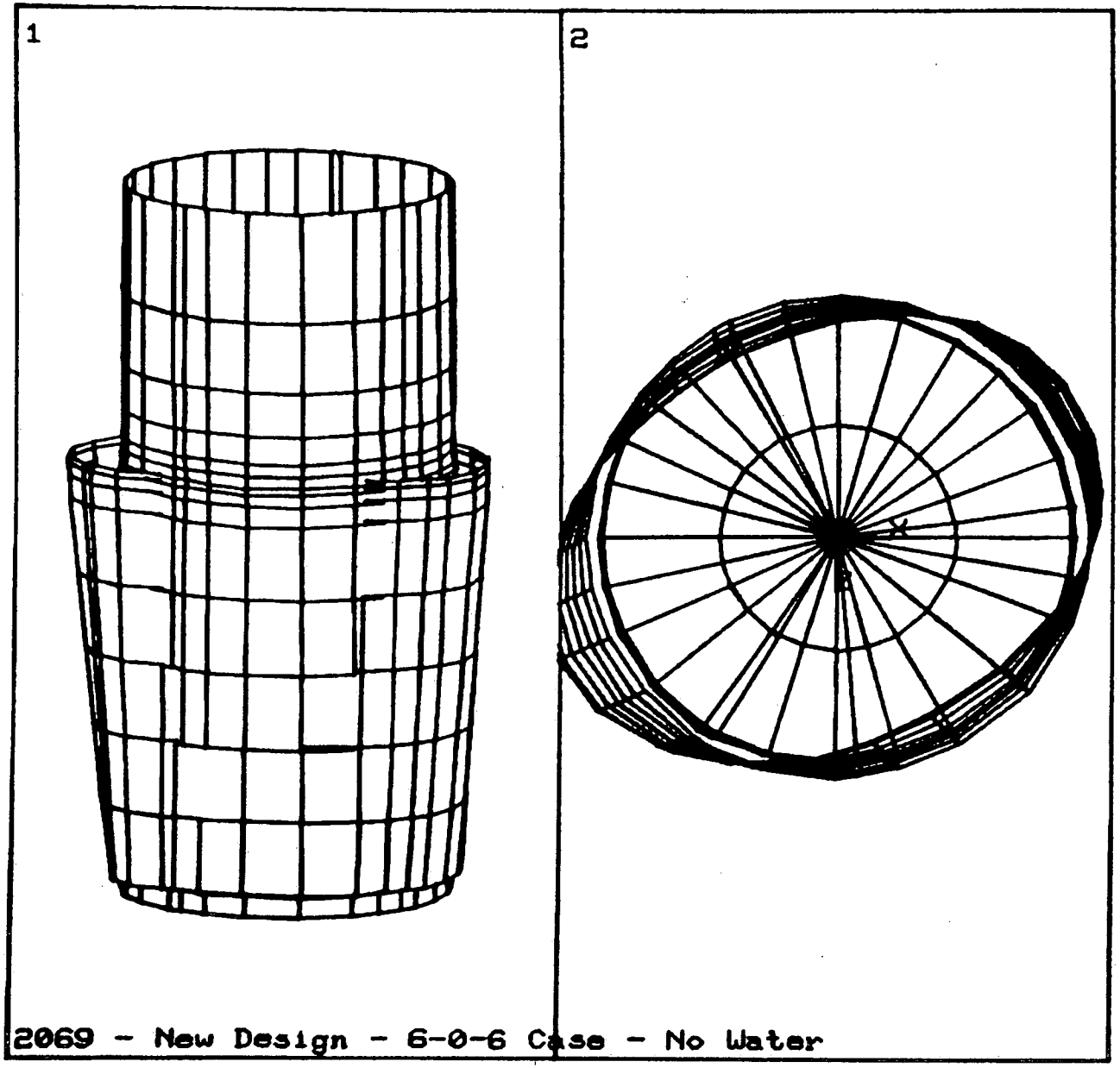
1
2
ANSYS 4.4
JUL 10 1990
08:54:01
PLOT NO. 4
POST1 DISPL.
STEP=1
ITER=4
FREQ=22.174
DMX =0.235448
DSCA=86.884
XV =1
YV =0.3
ZV =1
DIST=204.566
YF =-139.535
PRECISE HIDDEN
WIND=2
DSCA=61.436
YV =1
DIST=144.65
YF =-139.535
2069 - New Design - 6-0-6 Case - No Water

FIGURE B-12

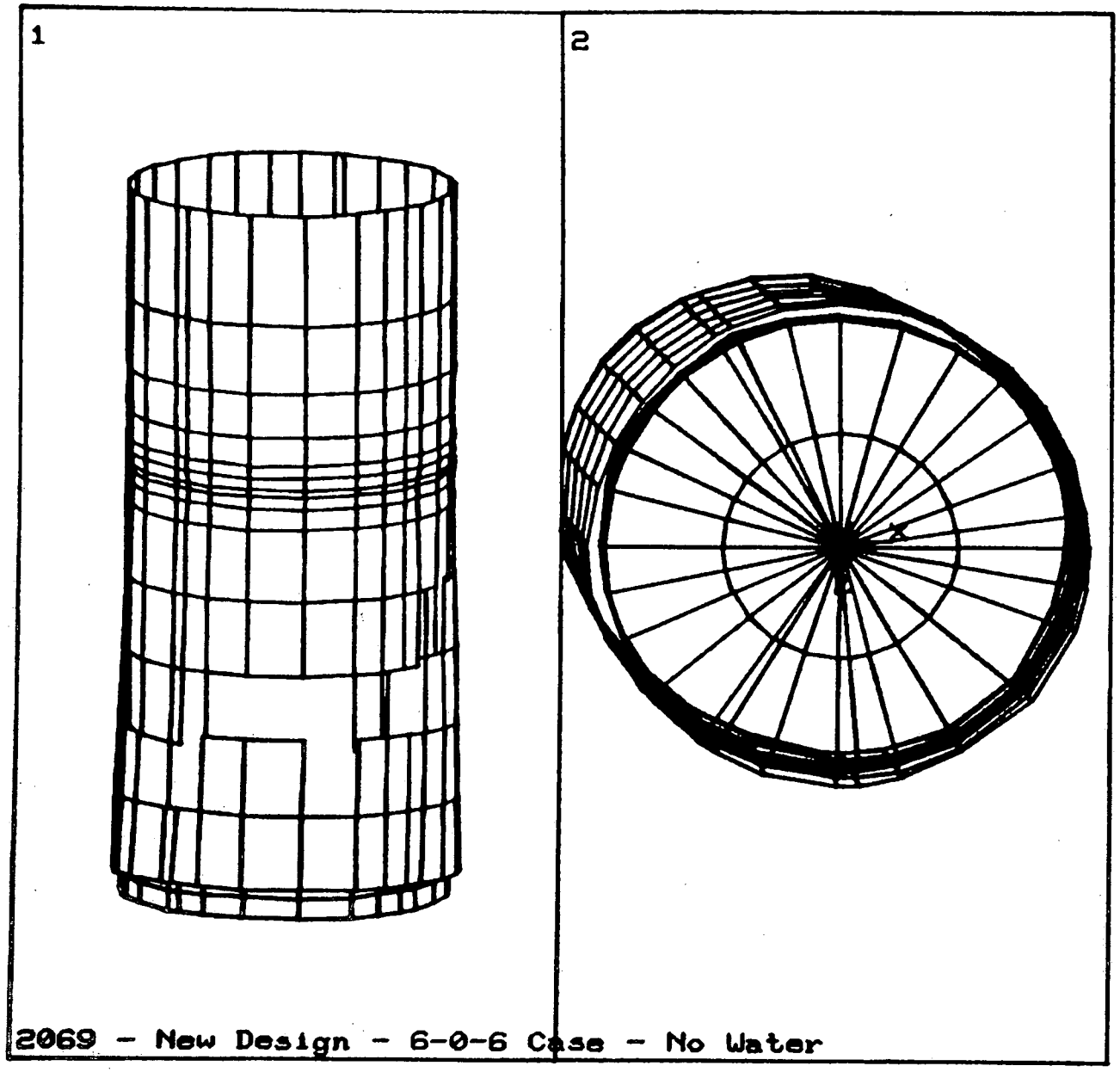
1
2
ANSYS 4.4
JUL 10 1990
08:55:08
PLOT NO. 5
POST1 DISPL.
STEP=1
ITER=5
FREQ=28.345
DMX =0.187495
DSCA=109.105
XV =1
YV =0.3
ZV =1
DIST=204.566
YF =-139.535
PRECISE HIDDEN
WIND=2
DSCA=77.149
YV =1
DIST=144.65
YF =-139.535
2069 - New Design - 6-0-6 Case - No Water

FIGURE B-13

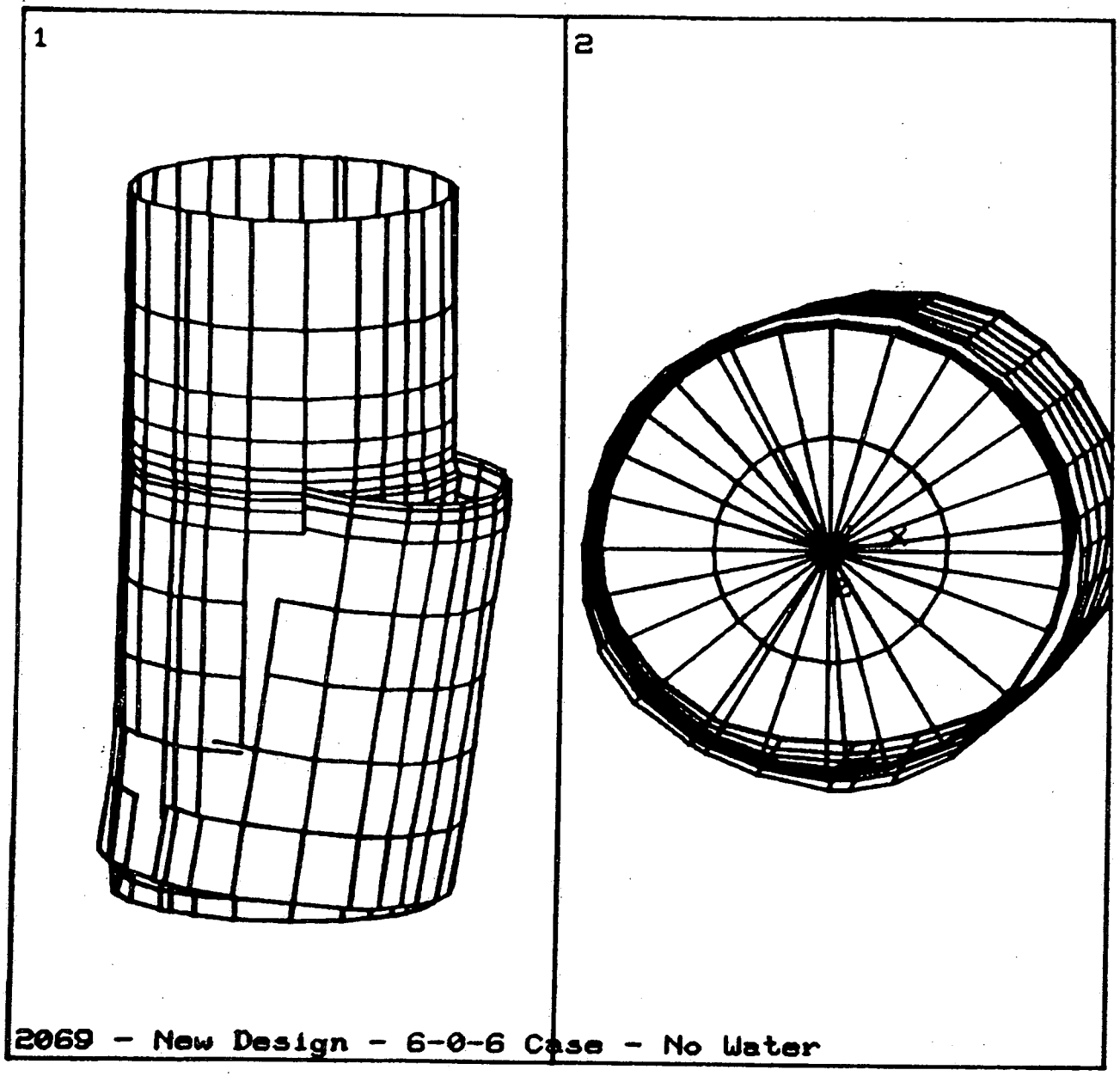
1
2
ANSYS 4.4
JUL 10 1990
08:56:02
PLOT NO. 6
POST1 DISPL.
STEP=1
ITER=6
FREQ=28.8
DMX =0.173114
DSCA=118.168
XV =1
YV =0.3
ZV =1
DIST=204.566
YF =-139.535
PRECISE HIDDEN
WIND=2
DSCA=83.558
YV =1
DIST=144.65
YF =-139.535
2069 - New Design - 6-0-6 Case - No Water

FIGURE B-14

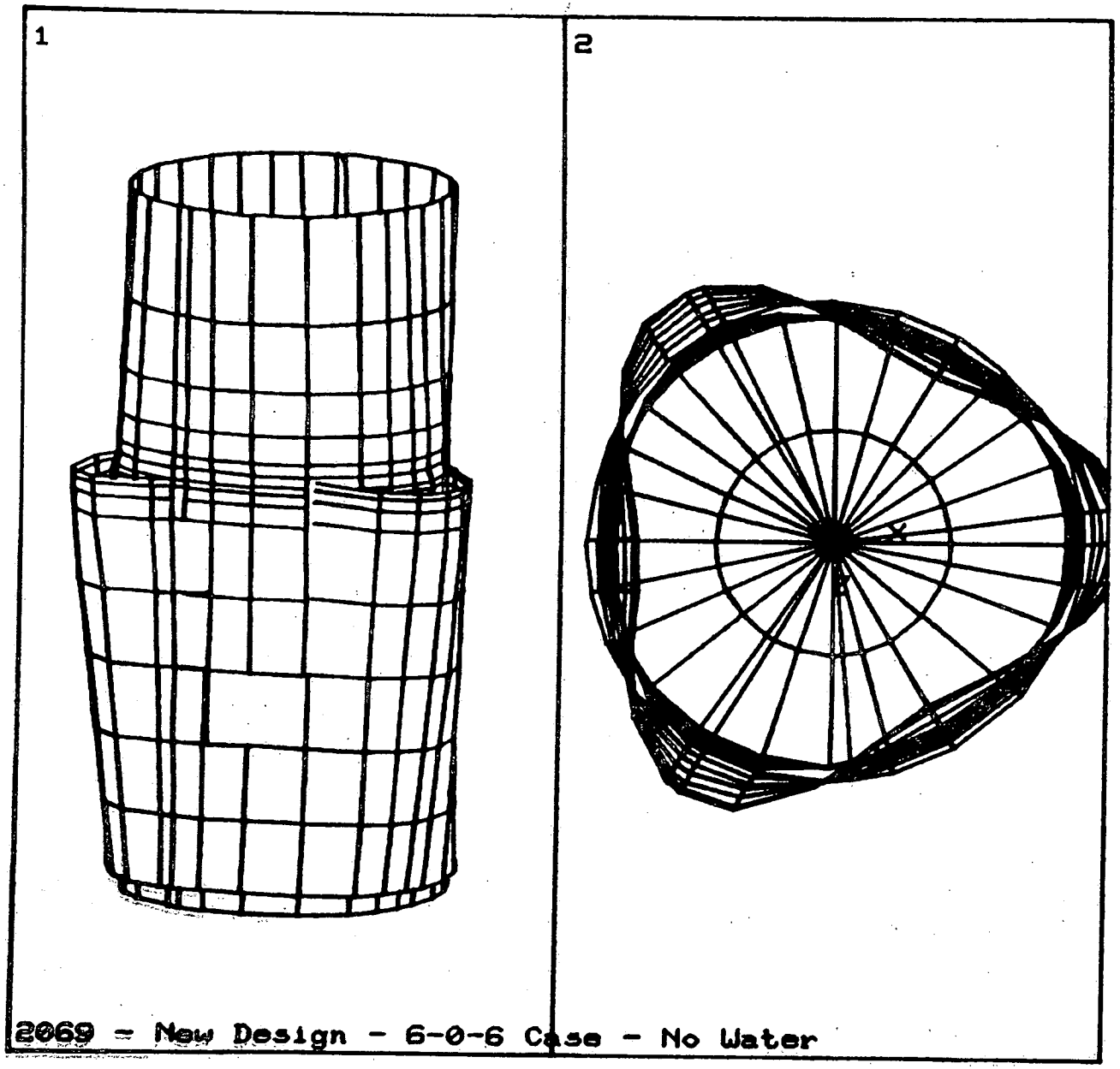

ANSYS 4.4
JUL 10 1990
08:56:48
PLOT NO. 7
POST1 DISPL.
STEP=1
ITER=7
FREQ=43.584
DMX =0.198037

DSCA=103.297
XV =1
YV =0.3
ZV =1
DIST=204.566
YF =-139.535
PRECISE HIDDEN

WIND=2
DSCA=73.042
YV =1
DIST=144.65
YF =-139.535

FIGURE B-15

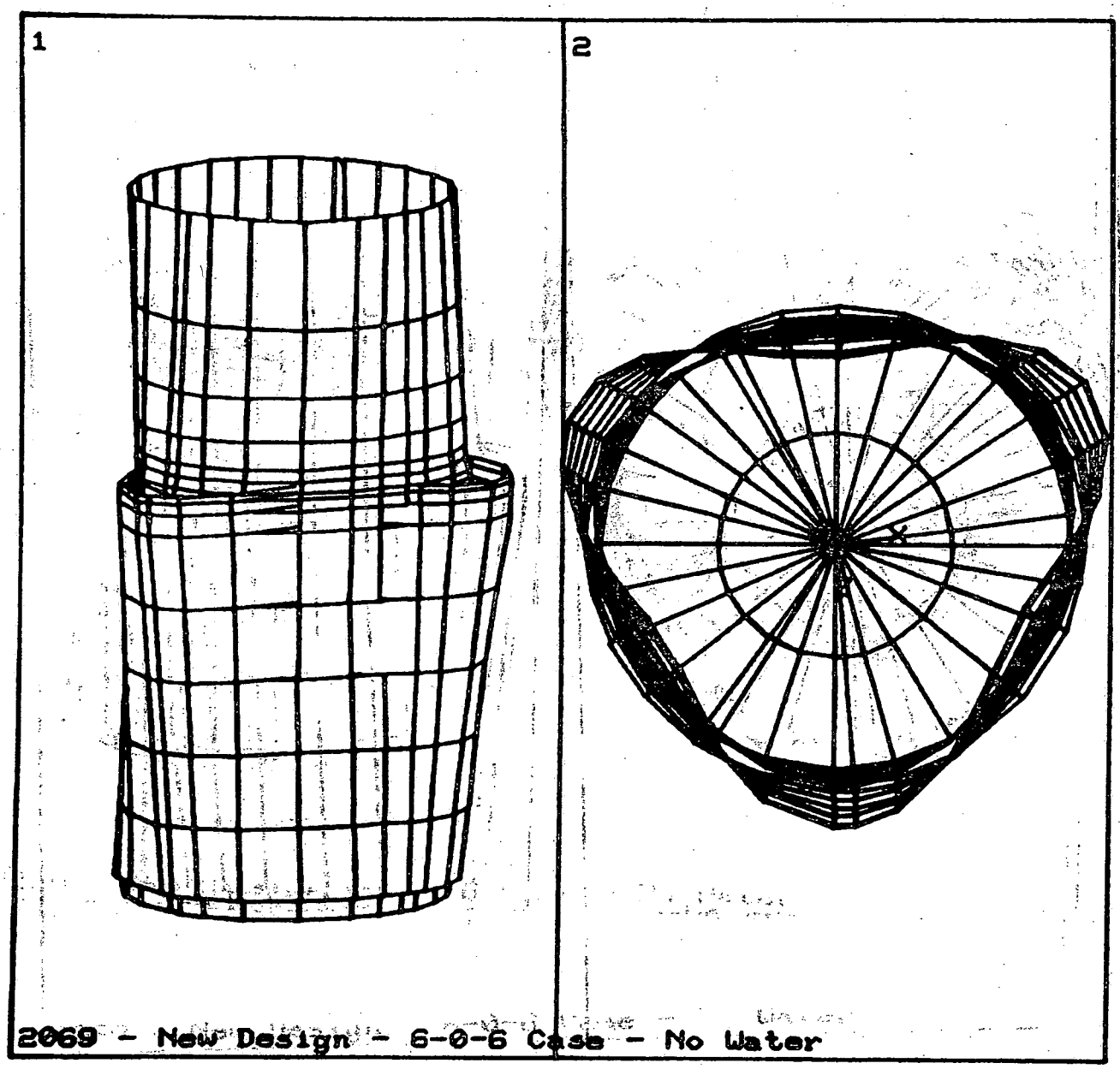
1
2
ANSYS 4.4
JUL 10 1990
08:58:03
PLOT NO. 8
POST1 DISPL.
STEP=1
ITER=8
FREQ=44.147
DMX =0.199904
DSCA=102.332
XV =1
YV =0.3
ZV =1
DIST=204.566
YF =-139.535
PRECISE HIDDEN
WIND=2
DSCA=72.36
YV =1
DIST=144.65
YF =-139.535
2069 - New Design - 6-0-6 Case - No Water

FIGURE B-16